A transsynaptic mechanism regulates glutamate receptor clustering at the *Drosophila* neuromuscular junction

DISSERTATION

zur Erlangung des akademischen Grades des

Doktors der Naturwissenschaften (Dr. rer. nat.)

eingereicht im Fachbereich Biologie, Chemie, Pharmazie

der Freien Universität Berlin

vorgelegt von

Omid Florian Khorramshahi

aus Berlin

Juli 2012

1. Gutachter: PD Dr. Stephan Sigrist
2. Gutachter: Prof. Dr. Dietmar Schmitz

Datum der Disputation: 30.11.2012

Cover image submission for Banovic et al., 2010

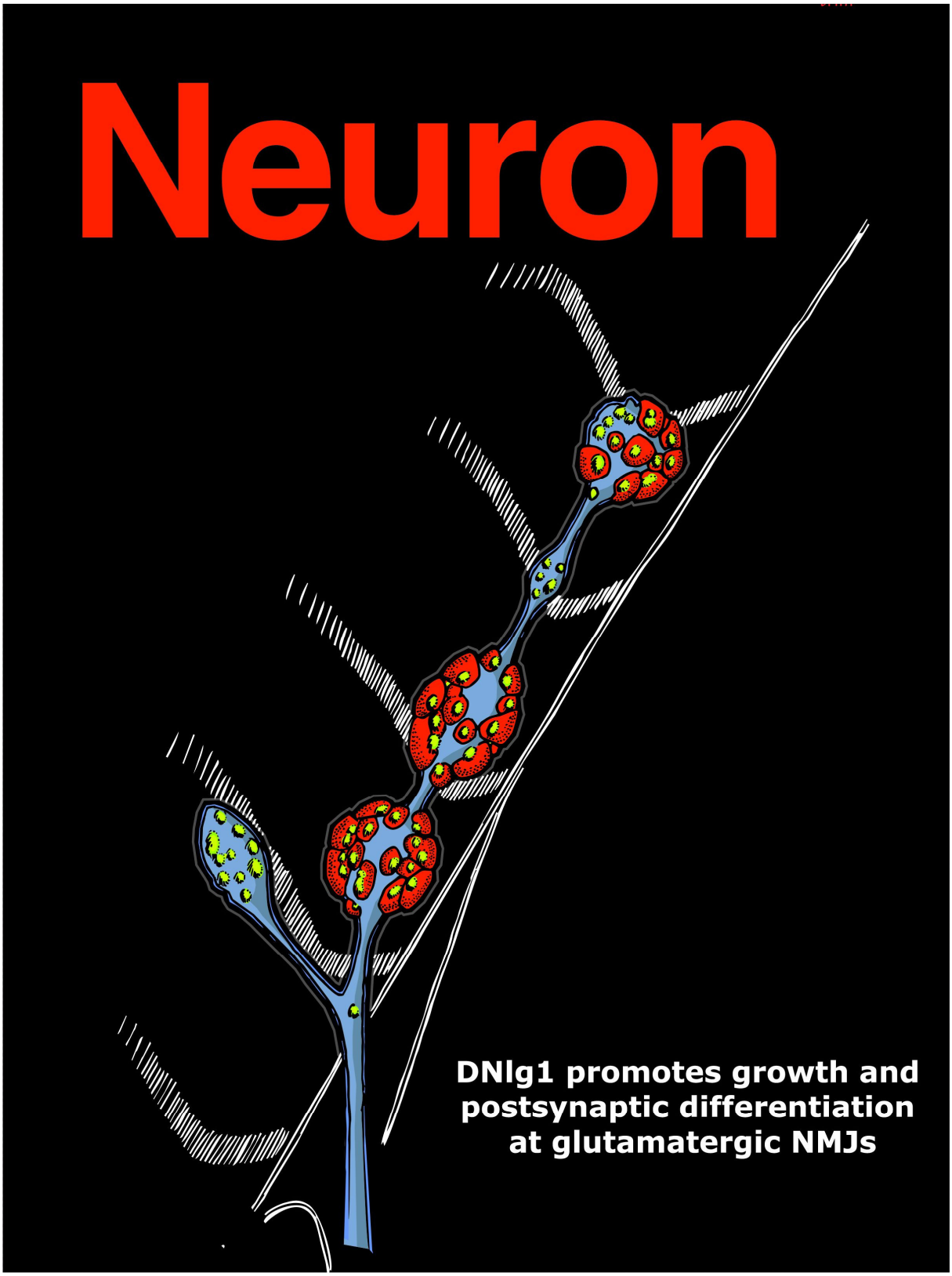

contents

1 general Introduction

1.1 Why do animals have brains?

Every organism's survival depends on its environment, which in most cases underlies constant changes. Therefore, it is crucial for every animal to perceive its dynamic environment and to adapt the behavior accordingly. This perception is created by the constant flow of inputs through the animal's senses and its computation in the central nervous system (CNS). The CNS can generate an appropriate output e.g. a motor pattern which is transmitted to muscles and triggers locomotion; a key feature inherent to all animals.

Most of the computation in the CNS is done by specialized cells: Neurons. Neuronal cells are exclusively specialized for signal processing and propagation. Neurons are among the largest and most complex cells in the body (Kennedy and Ehlers, 2006). These polarized cells receive their input at dendritic trees, integrate all incoming signals at their cell body (neurosoma), and send the output signal as action potentials (APs) along the axon. This intricate geometry allows for complex connections between many neurons via synapses, resulting in the establishment of complex neuronal networks.

A fundamental feature of these networks is (synaptic) plasticity: the ability of their synaptic connections to undergo dynamic changes in strength. Synaptic plasticity is believed to be the cellular substrate of learning and memory, one of the holy grails of modern neuroscience.

There are two types of synapses: chemical and electrical synapses. Electrical synapses consist of intercellular ion channels that build up gap junctions. Ionic signals and small second messenger molecules can quickly pass this cytoplasmic bridge and mediate rapid, bidirectional signal propagation. Electrical synapses thus tightly couple membrane potentials of connected cells and allow for rapid synchronization of small cell ensembles (Hormuzdi et al., 2004).

Most of the synapses in the CNS are chemical synapses which transduce their signal through extracellular secretion of neurotransmitters. Chemical synapses can be further subdivided into excitatory synapses which depolarize the postsynaptic target cell membrane and inhibitory synapses which have a hyperpolarizing effect. The following will focus more on the architecture of excitatory synapses in vertebrates. The second part of the introduction puts this knowledge into context of one model synapse: the neuromuscular junction (NMJ) of *Drosophila melanogaster*.

1.2 The presynaptic terminal: a biological digital-analog converter

A chemical synapse receives its input from action potentials which travel along the axon and invade the presynaptic terminal. Here, the frequency code of APs gets decoded into local Ca^{2+} gradients by voltage-gated Ca^{2+} channels. The influx of Ca^{2+} ions enables Ca^{2+} dependent proteins to fuse synaptic vesicles (SVs) with the presynaptic plasma membrane at specialized regions called the *active zone* (AZ). The presynaptic terminal is packed with SVs and their content (neurotransmitter molecules) dictates if the synapse outputs an excitatory or inhibitory signal.

An averaged 42-nm sized clear-core SV contains about 1500-2000 neurotransmitter molecules which can be either excitatory (e.g. glutamate, Acetylcholine) or inhibitory (e.g. GABA, Glycine). SVs release their full content upon complete fusion (exocytosis) and are therefore the morphological counterpart of the quantal release that was postulated by Katz more than 60 years ago (Haucke, Neher, and Sigrist, 2011; Katz, 1971).

Under the electron microscope, the AZ is clearly visible by its proteinacious cytomatrix (cytoplasmic matrix at the active zone – CAZ) as it appears as an electron-dense structure on the micrographs (Fig. 1a-c). CAZs are a hallmark of matured synapses; they comprise a set of large multidomain proteins and exist in various shapes and sizes in different synapses. In most cases CAZs are closely associated with synaptic vesicles and are therefore suggested to play a role in SV-tethering and synaptic efficacy (Haucke, Neher, and Sigrist, 2011; Zhai and Bellen, 2004).

1.3 Vesicle excocytosis: vesicle tethering and Ca^{2+}-channel clustering as a prerequisite for efficient transmission

Synaptic efficacy is the rate at which APs get encoded into transmitter secretion. Since pore-opening of Ca^{2+}-channels leads to an influx of Ca^{2+} ions, which are rapidly buffered by cytoplasmic buffers, they can only act in a temporally (tens of microseconds) and locally (tens of nanometers) tightly restricted manner, a so called Ca^{2+}-nanodomain (Augustine and Neher, 1992; Pumplin, Reese, and Llinás, 1981). Thus in order to fuse, SVs must be in close proximity to Ca^{2+}-channels. Ca^{2+} ions bind to the Ca^{2+}-sensor synaptotagmin, which in turn facilitates SNARE (soluble N-ethylmaleimide-sensitive factor attachment protein (SNAP)-mediated membrane fusion (Südhof, 2004; Takamori et al., 2006). SNARE proteins are part of the core membrane-fusion (exocytosis) machinery (Jahn, Lang, and Su, 2003; Südhof, 2004).

The CAZ comprises a small set of large multidomain proteins that are directly or indirectly associated with the AZ membrane and provide scaffolds for protein-protein interactions. CAZ components include the giant proteins bassoon and piccolo, Rab6 interacting protein (ELKS/ CAST1), mammalian relatives of the *bruchpilot* (BRP) protein in *Drosophila melanogaster*, liprin and GIT family proteins, Rab3 interacting molecules (RIMs), and the SNARE regulator Munc13 (Haucke, Erwin Neher, and Sigrist, 2011). These scaffold proteins might confer long-term stability by maintaining the position of membrane associated molecules, the exocytic-machinery, and SVs (Wang et al., 2009). The CAZ might hereby also be responsible for a molecular coupling of Ca^{2+} influx with SV fusion. This could be achieved by maintaining spatial proximity of SVs and Ca^{2+} channels (Haucke, Neher, and Sigrist, 2011). Flies with null alleles of BRP for example, show loss of electron dense projections (T-bars) at AZs, a morphological defect that is correlated with impaired clustering of voltage-gated Ca^{2+} channels and with desynchronization of glutamate release (Kittel et al., 2006).

1.4 Vesicle endocytosis

There is a need for recycling of SV proteins and lipids after exocytosis, since the synaptic terminal is able to harbor only a limited number of SVs and transport of SV-proteins from the distant neurosoma is not sufficient to replenish the local pool in time. Thus under prolonged, high frequency stimulations, fused SVs need to be retrieved via endocytosis and form new neurotransmitter-filled SVs to finally participate again in the constant release.

Heuser and Reese were the first to discover an increase in coated SVs after stimulation on ultramicrographs (Heuser and Reese, 1973). Although many details and models of endocytosis are still under debate, many studies come up with one prime model of SV recycling (Fig. 1d): First, SVs fuse with the AZ plasma membrane and flatten out, SV components then diffuse to periactive compartments where adaptor proteins recruit Clathrin to the membrane where SV precursors bud-off. The final fission of the membranes is then mediated by the GTPase Dynamin.

There is overwhelming evidence from many studies that Clathrin- and Dynamin-mediated endocytosis is the major mode of SV recycling (Rizzoli and Jahn, 2007). The strongest arguments derive from experiments where perturbations of Clathrin and Dynamin cause severe defects in SV-recycling , in contrast to other endocytic proteins (Haucke, Neher, and Sigrist 2011).

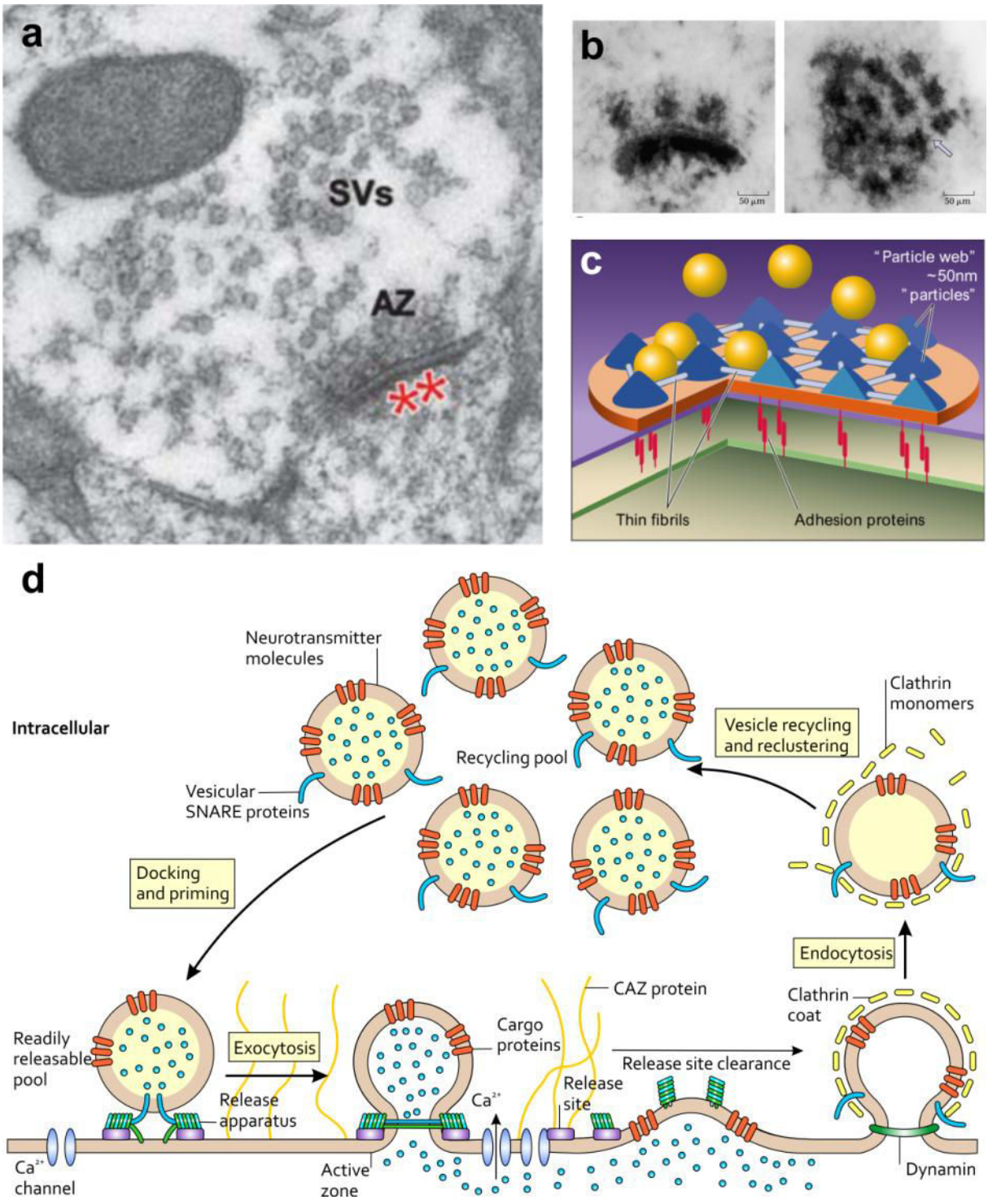

Figure 1: Active zone ultrastructure and model of the synaptic vesicle cycle

(**a**) EM image of synaptic connection between cultured hippocampal neurons. The synapse has many of the classic features of chemical synapses, including a presynaptic bouton containing ~50-nm clear core vesicles, an active zone with electron dense meshwork and docked vesicles, and a prominent electron density (asterisk. (**b**) Electron micrographs of purified active zones from mammalian central nervous system in side view (left) and top view (right). Thin fibris can be seen (arrow) that connects ~50nm particles and hereby builds up the 'particle web'. (**c**) Model of mammalian central synapses. (**d**) Overview of the synaptic vesicle cycle. Docked and primed synaptic vesicles constitute the readily releasable pool. They undergo exocytosis upon Ca^{2+} influx at the active zone. To maintain the availability of release sites they have to undergo clearance. Endocytosis of synaptiv vesicle membrane occurs within the periactive zone. Following clathrin uncoating and neurotransmitter uptake, synaptic vesicles return to the recycling pool. Modified from *Zhai and Bellen* (2004) and *Haucke, Neher, and Sigrist* (2011).

1.5 Mind the gap: transsynaptic interaction through the synaptic cleft

After secretion, neurotransmitter molecules diffuse rapidly into the synaptic cleft and bind to receptors located at the opposed postsynaptic membrane. The efficacy of this process relies heavily on the tight alignment of both opposing cell-membranes, which is controlled by cell adhesion molecules (CAMs). This seems to be achieved by the ability of CAMs to control pre- and postsynaptic organization, while being associated with their opposed binding partners in trans-conformation. CAMs feature a negatively charged transmembrane (TM) domain that enables them to pass the lipid-bilayer of the membrane and allows for transsynaptic interactions.

The powerful ability of CAMs to link pre- and postsynaptic compartments also makes them prime candidates for controlling synaptic strength (Atwood and Karunanithi, 2002) and maintenance. Dissecting the roles in assembly, maturation and function has, however, remained difficult. N-cadherins for example have been reported to play a role in target selection in the *Drosophila* optic neuropil (Prakash et al., 2009), while their vertebrate homologues have rather been associated with synapse maturation and function (Akins and Biederer, 2006).

Other described transsynaptic signaling pathways include IgCAMs, Nephrins, Ephrin ligand-Ephrin receptor interactions, and the Neurexin-Neuroligin pair (Fig. 2a), which all have been shown to regulate synapse formation via bidirectional signaling (Klein, 2009). The complex formed by Neuroligins (Nlgs) and Neurexins (Nrxs) however (Fig. 2b-c) (Ichtchenko et al., 1995), has raised a lot of attention in the past, not only because the molecular asymmetry of their heterophilic binding seems to reflect the asymmetric nature of the synapse perfectly, but also because Neuroligin was the first molecule to be shown to inherit true synaptogenic function in cell culture experiments (Scheiffele et al., 2000; Song et al., 1999).

1.6 The Neurexin-Neuroligin complex

In vertebrates, Neuroligins and Neurexins belong to the best-studied synaptic CAMs with a specific role in synapse formation and function (Dean and Dresbach, 2006; Südhof, 2008). The mammalian genome contains three Nrx genes, each encoding α- and β-proteins from independent promoters, and four Nlg genes which all get extensively spliced to generate a huge variety of Nlg and especially Nrx isoforms (Südhof, 2008).

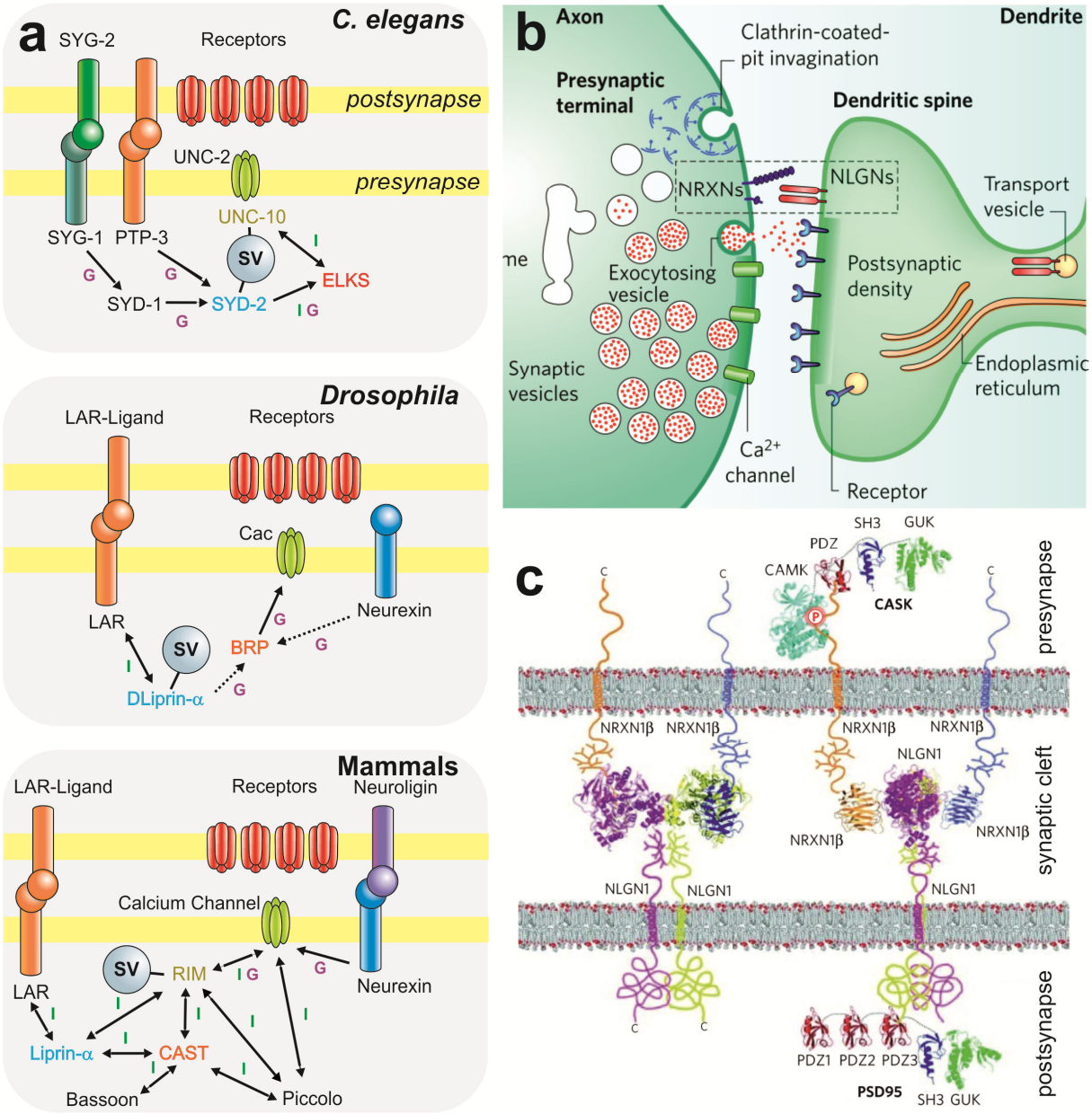

Figure 2: Proteins implicated in synapse assembly

(**a**) A summary of proteins considered to be important for synapse assembly Models for different model organisms are depicted in separated panels. Syd-2/Liprin-α family proteins are highlighted in blue, ELKS/BRP/CAST in red and Unc10/Rim in yellow. The mode of interaction is indicated by letters above the arrows: I = direct physical interaction, G = genetic interaction/ regulation inferred from genetic findings. Dashed lines indicate indirect evidence of interaction from imaging data. (**b**) Architecture of the transsynaptic Neurexin-Neuroligin complex. Sketch of an excitatory synapse with a presynaptic bouton (left), and a postsynaptic spine (right). The putative location of Neurexins (Nrxs/NRXNs) and Neuroligins (Nlgs/NLGNs) is depicted in a dashed box. (**c**) Atomic model of the trans-synaptic complex formed by Nrx1β and Nlg1. The Nrx1β–Nlg1 complex is shown in two orientations: left, en face with the Nrx1β LNS domain on top of the Nlg1 esterase-like domain, to illustrate the Nlg1 dimer; right, in a 90° rotation to illustrate the sideways attachment of the Nrx1β LNS domains to the Nlg1 esterase-like domains. Modified from *Owald and Sigrist* (2009) and *Südhof* (2008).

The transsynaptic Neurexin-Neuroligin complex consists of a postsynaptic Nlg dimer pair which interacts with two single presynaptic Nrx proteins (Fig. 2c) (Araç et al., 2007; Chen et al., 2008; Fabrichny et al., 2007). Nlgs feature an extracellular, catalytically inactive acetylcholinesterase (AChE) – like domain through which Nlgs form constitutive dimers and interact with the extracellular laminin, nectin, sex hormone binding globulin (LNS) domain of Nrx (Ichtchenko et al., 1995; Song et al., 1999). Nlg and Nrx both posses intracellular C termini containing intracellular PDZ-domain binding motifs and pass the membrane with single-pass TM domains. The C termini are thought to be covered with PDZ-domain containing scaffold proteins which in turn can organize the presynaptic release machinery and the postsynaptic receptor complexes (Südhof, 2008).

The Nrx-Nlg complex features all the necessities for controlling the spatiotemporal organization and maturation of a synapse, making them the prototypic CAMs. Synapse formation and specification are also linked to the action of synaptic CAMs, but the disruption of the Nrx-Nlg complex *in vivo* leads to impairments in synaptic properties without completely abolishing synaptic transmission (Chubykin et al., 2007; Missler et al., 2003; Varoqueaux et al., 2006; Wittenmayer et al., 2009). It is therefore not surprising that Nlg and Nrx have been shown to play a role in many non-lethal cognitive diseases, such as schizophrenia and autism spectrum disorders (ASDs), Tourette's syndrome, and learning disability (Südhof, 2008).

1.7 Glutamate receptors

In chemical synapses presynaptically secreted signal molecules get perceived by the postsynaptic partner cells via binding to receptors. In excitatory synapses these receptors will then allow the influx of ions that depolarize postsynaptic membranes. The most common excitatory neurotransmitter in the vertebrate CNS is glutamate which binds to glutamate receptors (GluRs). GluRs are classified as ionotropic or metabotropic glutamate receptors. Metabotropic receptors do not form an ion channel pore as ionotropic receptors do, but are rather indirectly linked with ion-channels e.g. through G-Proteins. Ionotropic GluRs are further classified pharmacologically as AMPA, NMDA-, and kainate-sensitive glutamate receptors.

Each receptor acts in a different time course and plays a distinct role in the CNS. Postsynaptic potentials of metabotropic GluRs are very slow due to the latency of the involved signaling cascade and are generally not involved in direct synaptic transmission. N-methyl-D-aspartate (NMDA)- and kainate-type receptors play roles in slower transmission (10-100 ms) whereas AMPA receptors (AMPARs) play dominant roles in fast synaptic transmission (<10 ms).

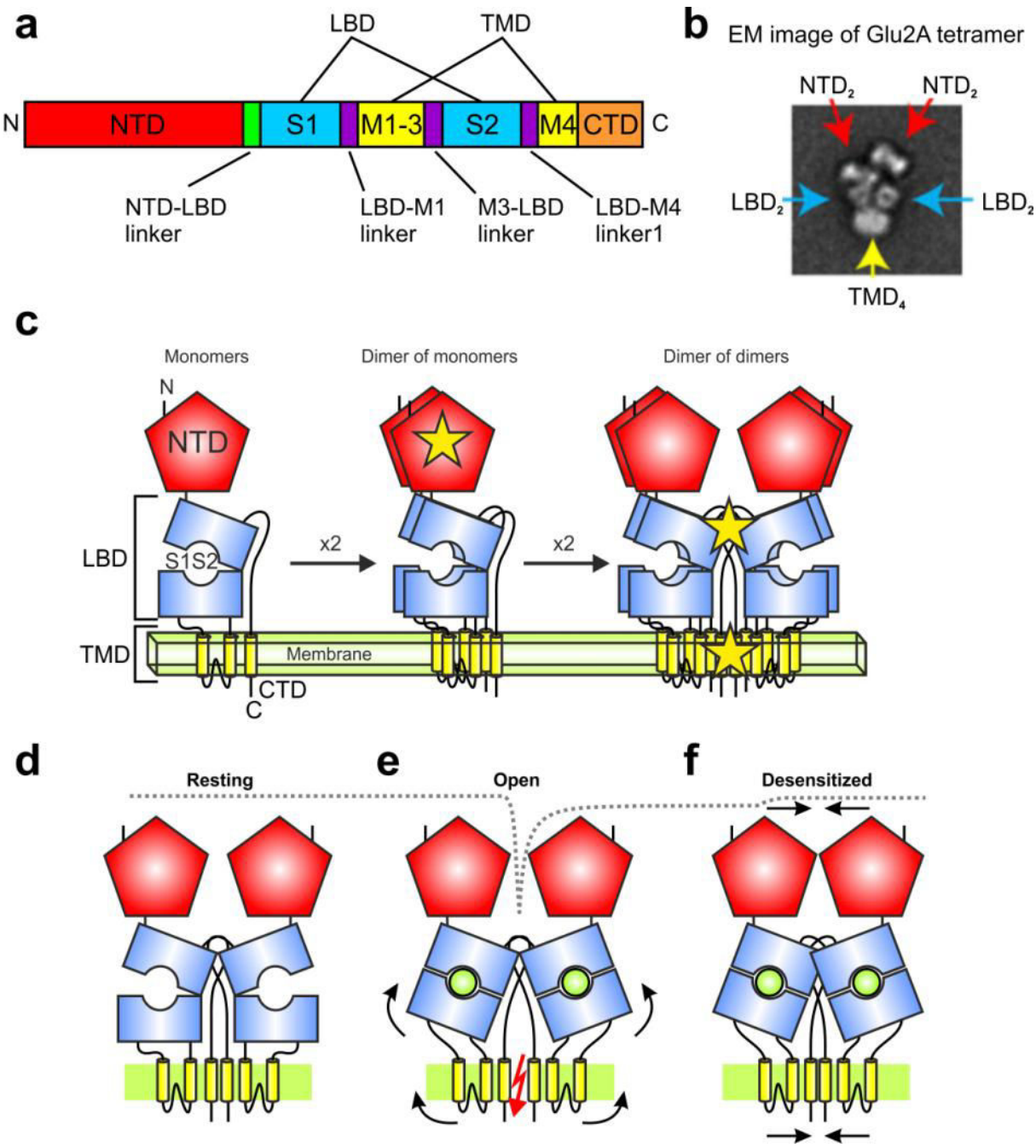

Figure 3: Structure, assembly, and conformational states of AMPA receptor complexes

(**a**) Primary structure of AMPAR subunit. NTD: N-terminal domain, LBD: ligand binding domain, TMD: transmembrane domain, CTD: C-terminal domain. The LBD is made of S1 and S2 subfragments. The TMD contains alpha- helices M1–M4. The linkers between the domains are also indicated. (**b**) EM image of an AMPAR made of homotetrameric GluA2. The position of the domains are depicted with arrows. (**c**) Assembly of AMPAR tetramer in the 'dimer-of-dimer' model. Monomers associate most strongly through NTD-interactions (star in middle Fig.). Dimers undergo secondary dimerization, by interactions of the S2 and TMDs (stars in right Fig.). (**d**-**f**) model for AMPAR activation and desensitization. (**d**) AMPAR in resting state: LDBs are relaxed in absence of ligands and the channel pore is closed. (**e**) Binding of glutamate triggers a conformational change that opens the ion pore (red flash). (**f**) S1S2 remain bound to agonist in a closed-cleft conformation, while subsequent slippage of the dimer interface allows the channel to close again (desensitization). Modified from *Nakagawa* (2010) and *Madden* (2002).

Ionotropic Non-NMDA receptor complexes are tetramers, composed of the subunits (SUs) GluR1-4 (AMPA) and GluR5-7 and KA1-2 (kainate-type) in a homo- or heterooligomeric stochiometry (Fig. 3c)(Madden, 2002; Stern-Bach et al., 1998). Each GluR subunit has an N-terminal extra-cellular amino domain (NTD), a ligand- binding domain (LBD), a channel domain build out of transmembrane domains (TMDs), and an intracellular C-terminal domain (CTD) (Fig. 3a and 3c). The extracellular LBD consists of two polypeptide segments S1 and S2. Three membrane-spanning □-helices (M1, M2 and M3) and a channel pore loop (M2) build up the receptor channel domain (Kumar, Schuck, and Mayer, 2011; Madden, 2002).

The receptor channels are rapidly activated upon glutamate binding, resulting in an opening of the channel pore (Fig. 3d-e)(Robert et al., 2005). This results in an influx of cations, which depolarize the postsynaptic membrane. The pore closes milliseconds later, either because of ligand release or as a result of a conformational change of the receptor into a long-lasting closed, desensitized state with ligands still bound (Fig. 3f).

The next part of this paragraph will focus on the well studied AMPA receptors to illustrate the multitude of translational and post-translational modifications that can apply to any type of GluR.

In AMPA receptors, each subunit gene expresses different subunit isoforms through alternative splicing and RNA editing. Alternative splicing facilitates the exchange of receptor domains, such as the “flip/flop” module near the S2-LBD domain (Sommer et al., 1990). AMPA receptors with the “flip” module desensitize with slower kinetics and are more prominent during early development (Monyer, Seeburg, and Wisden, 1991; Mosbacher et al., 1994). The most prominent RNA editing occurs exclusively in the GluR-B pore loop and converts amino acid codon 589 from glutamine (CAG) to the positively charged arginine (CGG; Q/R site-editing). Channel complexes containing Q/R site-edited GluR-Bs have a linear I/V relationship and low Ca^{2+} permeability that is required for precise NMDA-receptor signaling at synapses at which both GluR types are colocalized (Köhr, 2006).

Phosphorylation of AMPARs results in modulation of receptor properties (Derkach et al., 1999, Soderling et al., 2000) and is considered an important functional readout for signaling pathways associated with synaptic plasticity and learning (Derkach et al., 2007; Lisman and McIntyre, 2001). The GluR1 subunit e.g. harbors two important regulatory phosphorylation sites: serine residue (Ser) 831 and Ser845 in its C terminus. Phosphorylation of Ser831 by calcium/calmodulin (CaM)-dependent protein kinase II (CAMKII) significantly increases single-channel conductance of homomeric GluR1 AMPAs (Derkach, Barria, and Soderling, 1999). This CAMKII-mediated phosphorylation is regarded to be an important contributor of CA-1 hippocampal early phase LTP. Furthermore, protein kinase A (PKA) has been shown to phosphorylate Ser845 which also increases

open probability in GluR1 homomers, although the function of PKA has been mainly implicated in surface and synaptic trafficking of AMPAs (Esteban et al., 2003).

1.8 The postsynaptic density

The postsynaptic membrane contains not only a high density of glutamate receptors, but also associated signaling proteins and cytoskeletal elements, all assembled by a variety of scaffold proteins into an organized structure. EM studies of the postsynapse revealed an electron-dense membrane thickening called the postsynaptic density (PSD) which forms a disk-like shape ~200–800 nm wide and ~30–50 nm thick underneath the postsynaptic membrane (Fig. 4a-c)(Blomberg, Cohen, and Siekevitz, 1977; Cohen et al., 1977). The PSD can be viewed as a membrane-associated mega-organelle that is specialized for postsynaptic signal transduction and processing that can dynamically change its structure and composition during development and in response to synaptic activity (Chung et al. 2000; Okabe, 2007; Walikonis et al., 2000).

Identified proteins in the PSD serve many different roles, from cell surface receptors to cytoplasmic signaling enzymes to the cytoskeletal and scaffold proteins that hold them together. The large diversity of signaling proteins present in the PSD range from protein kinases and phosphatases to small GTPase signaling molecules (Fig. 4d)(Sheng and Hoogenraad, 2007).

Scaffold proteins have been shown to play crucial roles in diverse PSD functions, including: trafficking, anchoring and clustering of GluRs, organizing multiple components into large signaling complexes, and interfacing with and regulating the dynamics of cytoskeletal structures (Sheng and Hoogenraad, 2007). They are the central components of the PSD architecture; their dynamic organization and regulation are directly correlated with the morphology of the PSD.

The most common protein-protein interaction module among PSD scaffold proteins is the PDZ domain. Many of these scaffold proteins are densely packed with multiple copies of PDZ domains and these can interact with small peptide fragments of their targets with weak binding affinities (Fig. 4d)(Zhang and Wang, 2003). Such multi-domain PSD proteins can even assemble to PDZ supramodules that connect multiple PDZ domains in tandem and display novel target-binding properties (Feng et al., 2003; Long, 2003). It was often speculated that the excessive number of PDZ domains in the PSD-scaffold enables the formation of ‘slots’ for various binding partners, such as GluRs, to control their number at the synapse.

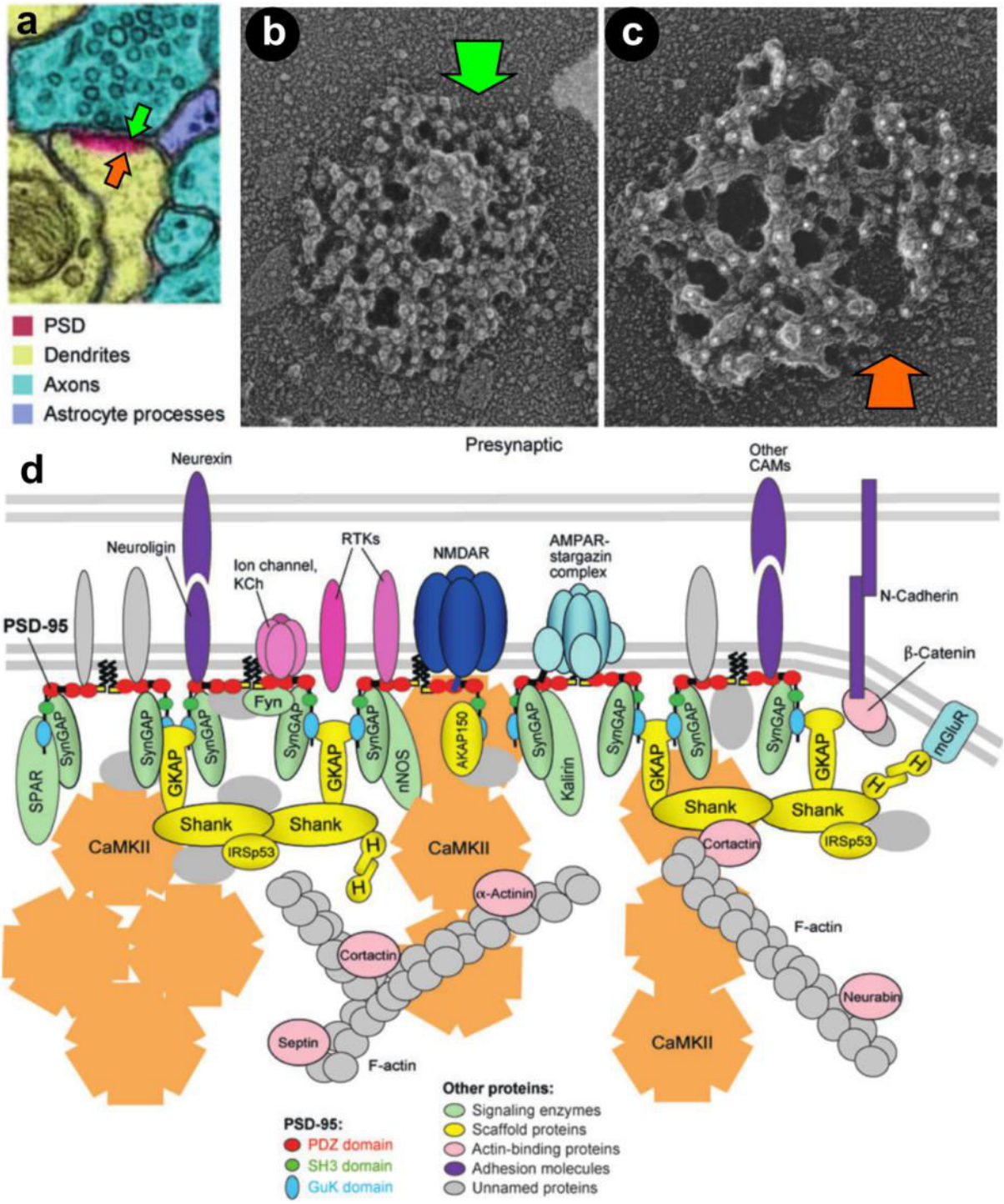

Figure 4: Structure, assembly, and conformational states of AMPA receptor complexes

(**a**) EM image of the CA1 refion of the hippocampus. Morphological features are highlighted in color. The postsynaptic density (PSD) is labeled in magenta. (**b**-**c**) EM Images of purified PSDs. (**b**) The granular surface of the PSD facing the synaptic cleft. (**c**) The convoluted surface, which is oriented towards the cytoplasm. White dots derive from immunogold labeling of the scaffold protein GKAP. (**d**) Schematic diagram of the network of proteins in the PSD. Major families of PSD proteins are shown in approximate stochiometric ratio. PSD-95 is colored in red, other scaffolding molecules in yellow, CAMKII in orange, signaling enzymes in green, actin binding proteins pink. Abbreviations: AKAP150, A-kinase anchoring protein 150 kDa; CAM, cell adhesion molecule; Fyn, a Src family tyrosine kinase; GKAP, guanylate kinase-associated protein; H, Homer; IRSp53, insulin receptor substrate 53 kDa; KCh, K+ channel; mGluR, metabotropic glutamate receptor; nNOS, neuronal nitric oxide synthase; RTK, receptor tyrosine kinases (e.g., ErbB4, TrkB); SPAR, spine-associated RapGAP. Modified from *Sheng and Hoogenraad* (2007).

The major postsynaptic scaffold proteins include PSD-95 (also known as synapse-associated protein 90 (SAP90)), guanylate kinase-associated protein (GKAP), and SH3 and multiple ankyrin repeat domains protein (Shank) families of proteins. PSD-95 binds to GKAP, which interacts with Shank (Kim and Sheng, 2004). This hierarchy is reflected in the laminar sub-structures of the PSD (Chen et al., 2008): the first layer of a PSD mainly contains membrane receptors, ion channels and transmembrane cell-adhesion molecules; the second layer is enriched with scaffold proteins (MAGUK proteins, in particular PSD-95), which are closely coupled to the membrane receptors and ion channels; the third layer is comprised of Shank and GKAP-family proteins, which are linked to MAGUK proteins and are arranged in parallel to the PSD membrane. All these layers form a protein network that appears as a convoluted “mountainous” surface that faces the cytoplasm in the EM (Fig. 4c)(Vinade et al., 2003).

These structures change dynamically to adapt the postsynaptic strength to different activity patterns. A shift in synaptic strength is conducted by changes in the number of synaptic AMPARs, the most common postsynaptic plasticity mechanism. The high mobility of AMPARS appears to be also reflected in their steady state distribution of fixed preparations. There is a non-homogenous distribution of GluRs in the plane of the PSD: NMDARs are highly concentrated in the center, whereas AMPARs densely cluster in the periphery (Choquet and Trille, 2003; Triller and Choquet, 2005). The mobility of GluRs inside the PSD is most likely regulated by the density of PDZ scaffolds that increases towards the centre of the PSD (Chen et al., 2008). This is in line with a model in which AMPARs enter the PSD via lateral diffusion and cluster through the interaction with several PSD proteins, such as protein interacting with C kinase 1 (PICK1) and glutamate receptor interacting protein (GRIP), which interact with the C terminus of various AMPAR subunits (Chung et al., 2000; Li et al., 1999; Malinow and Malenka, 2002; Ziv and Garner, 2001). However, recent studies question the relevance of C-terminal binding to AMPARs as the main regulatory mechanism for immobilization at the PSD and favor an alternative model (Bats, Groc, and Choquet, 2007; Groc and Choquet, 2006). These studies favor a mechanism in which the dense array of PSD-95 proteins in the plane of the PSD membrane is the strongest contributor for GluR clustering, since it is able to bind directly to NMDARs and indirectly to AMPARs via an auxiliary subunit (Bats, Groc, and Choquet 2007; Opazo, Sainlos, and Choquet, 2011; Opazo et al., 2010).

1.9 Auxiliary Subunits control trafficking and gating of Glutamate receptors

In the last decade it became apparent that some AMPARs are bound to transmembrane proteins that serve as auxiliary subunits of the AMPAR complex (Fig. 5a-b) (Nicoll, Tomita, and Bredt, 2006). These proteins are □-subunits of Ca^{2+} channels and define the family of transmembrane AMPAR regulatory proteins (TARPs), which comprise Stargazin (STG), c-3, c-4 and c-8 (Tomita et al., 2003) and c-5, c-7 (Kato et al., 2008; Soto et al., 2009). TARPs are associated with most, but not all, AMPARs early in the synthetic pathway and control their maturation, trafficking and biophysical properties like desensitization kinetics (Fig. 5c) (Nicoll, Tomita, and Bredt, 2006). They were shown to be critical for clustering AMPARs at excitatory synapses through their interaction with PSD-95 (Fig. 5b) (Chen et al., 2000; Schnell et al., 2002), and probably with other MAGUKs (Elias et al., 2006).

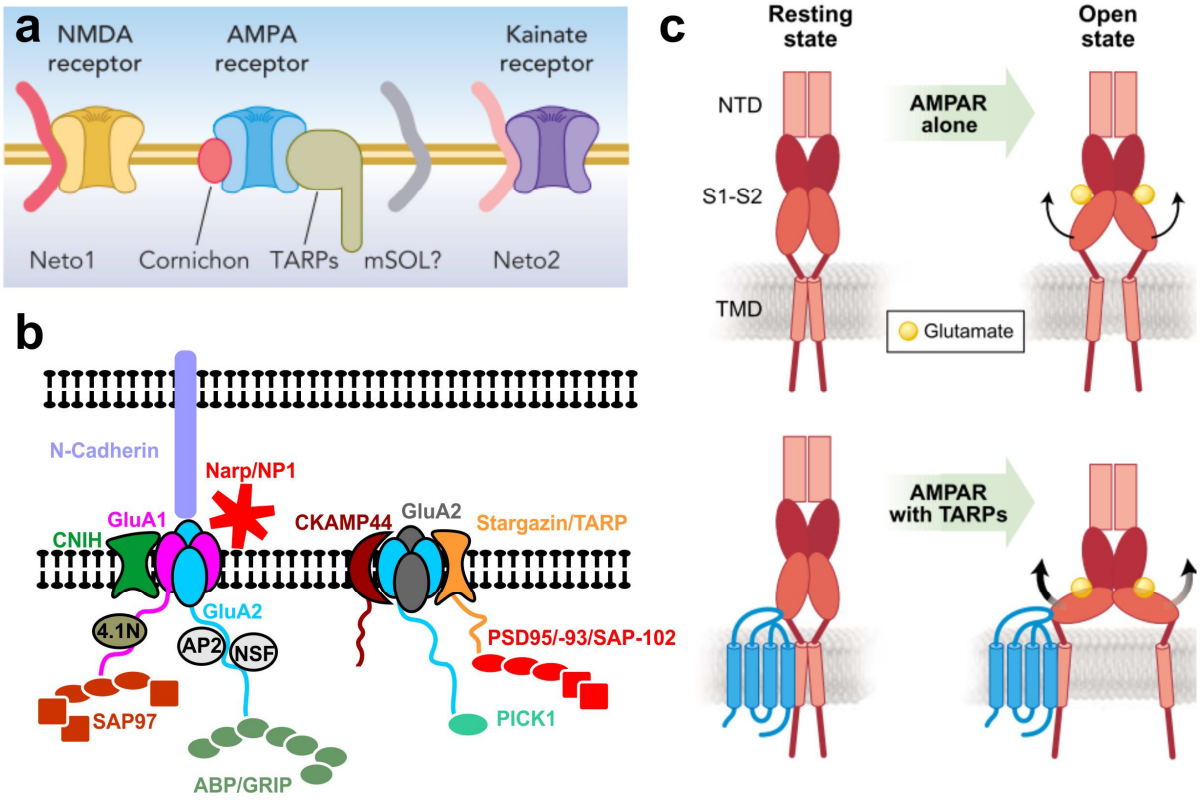

Figure 5: Introduction to interacting proteins of ionotropic glutamate receptors

(**a**) Overview of different iGluRs and their accessory subunits. The NMDAR complex comprises Neto1, the AMPAR complex comprises TARPs and cornichon, and the kainate receptor complex comprises Neto2. The C. elegans AMPAR complex comprises SOL-1, which is a CUB domain-containing protein. If mammalian AMPAR complexes comprise a mammalian homolog of SOL-1 (mSOL) has not been reported so far. Neto1, Neto2, and SOL1 are CUB-domain containing proteins. (**b**) Diagram of the best characterized AMPAR interacting proteins. These pertain to several categories: extracellular proteins (Cadherin and pentraxins), intracellular scaffolds such as PZD domain-containing proteins (PICK, GRIP, PSD-95 and other MAGUKS), as well as others (NSF, AP2, 4.1 N), and families of transmembrane proteins (TARP, CNIH and CKAMP44). (**c**) A model for possible role of TARPs on AMPAR channel opening. Upon glutamate binding, the AMPA LBD closes like a clamshell, which causes channel pore opening. TARPs bind to AMPAR and affect AMPAR channel opening either by inducing more closure of LBD–to–glutamate binding or more efficient coupling of domain closure to pore opening without any change in LBD-closure. Modified from *Tomita* (2010), *Chouquet* (2010), and *Nicoll, Tomita, and Bredt* (2006).

The STG /PSD-95 pair has been shown to specifically immobilize AMPARs at synaptic sites (Schnell et al., 2002). While overexpression of PSD-95 specifically enhances the synaptic AMPAR-mediated response without changing the number of surface AMPAR, the overexpression of STG results in the opposite effect: a selective increase in the number of extrasynaptic AMPARs without changing AMPAR-mediated synaptic currents. Whereas hippocampal neurons of mice mutant for a single TARP show a reduced number of surface AMPARs (Rouach et al., 2005), overexpression of mutated Stargazin unable to bind PSD-95 in cultured hippocampal neurons suppresses AMPAR immobilization at synaptic sites (Bats, Groc, and Choquet, 2007). These findings lead to the conclusion that it needs the presence of both PSD-95 at the PSD and TARPs closely attached to AMPARs for the efficient trafficking and clustering of AMPARs to synaptic sites. Furthermore, TARP-PSD-95 binding has been shown to be regulated by the activity dependent phosphorylation of TARPs (Opazo et al., 2010) and has been linked to synaptic plasticity (Tomita et al., 2005).

Recently, several other unrelated families of transmembrane proteins have been identified to behave as auxiliary AMPAR subunits (Fig. 5a). Cornichon homologues (CNIH) 2 and 3 associate with AMPARs and dramatically increase AMPAR surface expression and slow down their kinetics of deactivation and desensitization (Schwenk et al., 2009). In *C. elegans* SOL-1 has been identified as another AMPAR auxiliary subunit (Zheng, Mellem, Brockie, Madsen, & Maricq, 2004). SOL-1 encodes a CUB-domain transmembrane protein that is required for glutamate receptor GLR-1 currents. In vertebrates CKAMP44 was discovered as a novel brain-specific, single pass transmembrane protein that binds AMPAR and leads to stronger and faster AMPAR desensitization and a slower recovery from desensitization in striking opposition to STG (von Engelhardt et al., 2010).

Recent studies identified auxiliary subunits for NMDARs and Kainate receptors as well (Fig. 5a). Intriguingly, both proteins, Neto1 and Neto2, share a high homology with each other and their two CUB domains are closely related to the CUB domains of SOL-1. Mice mutant for Neto1 exhibit NMDAR-mediated synaptic plasticity and impairment in learning tasks (Ng et al., 2009). Neto2 modulates Kainate receptor kinetics in heterologous cells (Zhang et al., 2009).

2 Introduction to the neuromuscular junction of *Drosophila melanogaster*

2.1 The best studied model synapse: a brief history of 'fruit fly research'

The fruit fly *Drosophila melanogaster* was introduced to the laboratory by Thomas Hunt Morgan at the beginning of the 20th century and has been used ever since as a model organism in many fields of life-science. There are many reasons why research with *Drosophila* has become so popular.

The field of genetics has evolved tremendously in the last decades; in such a way that it has become an integral part of life-science in general. *Drosophila*, due to its small genome (about 13,600 genes (Thompson, 1977)), is perfectly suited for genetic studies and moreover the first experiments with *Drosophila* Thomas Hunt Morgan built the foundation for the field of genetics itself. Thomas Hunt Morgan used the fly to reproduce the experiments done by Gregor Johann Mendel regarding the inheritance of visible features. These led to the discovery of a physical substrate on which these features are ordered in a linear fashion: the chromosomes.

The features of *Drosophila,* which allowed these experiments in the past, are still invaluable for molecular research today:

1.) The short lifecycle of *Drosophila* (Fig. 6a) allowed Morgan to study the offspring of a population in about 2 weeks, which made it feasible to study rules of inheritance over many generations. This same trait, combined with the large catalog of established genetic toolsets (Brand and Perrimon, 1993), allows researchers today to create transgenic flies in a matter of weeks.

2.) The other big advantage of *Drosophila* is its size. It is small enough to be kept in viable populations in small food vials, enabling the handling of many stocks in a single lab; making fruit fly research much more economical than that of larger animals e.g. mice. Adult *Drosophila* flies however, are large enough that many morphological features can be detected with low magnification. This enabled Morgan to score the inheritance of the eye color from his *white* fly what led to the discovery of many other easily visible mutations called *markers*. In combination with *balancer* chromosomes (Thompson, 1977), which enable genetic variants to be kept stable over generations, these tools present an elegant and straightforward way to score and maintain mutations in a *stock*: a stable, propagating population.

These features enabled the realization of large mutagenesis screens which have led to the discovery of many genes involved in cell-patterning and development, which in turn led to the awarding of a Nobel prize in Physiology and Medicine in 1995 to Edeward B. Lewis, Christiane Nüsslein-Vollhart, and Eric F. Wieschaus.

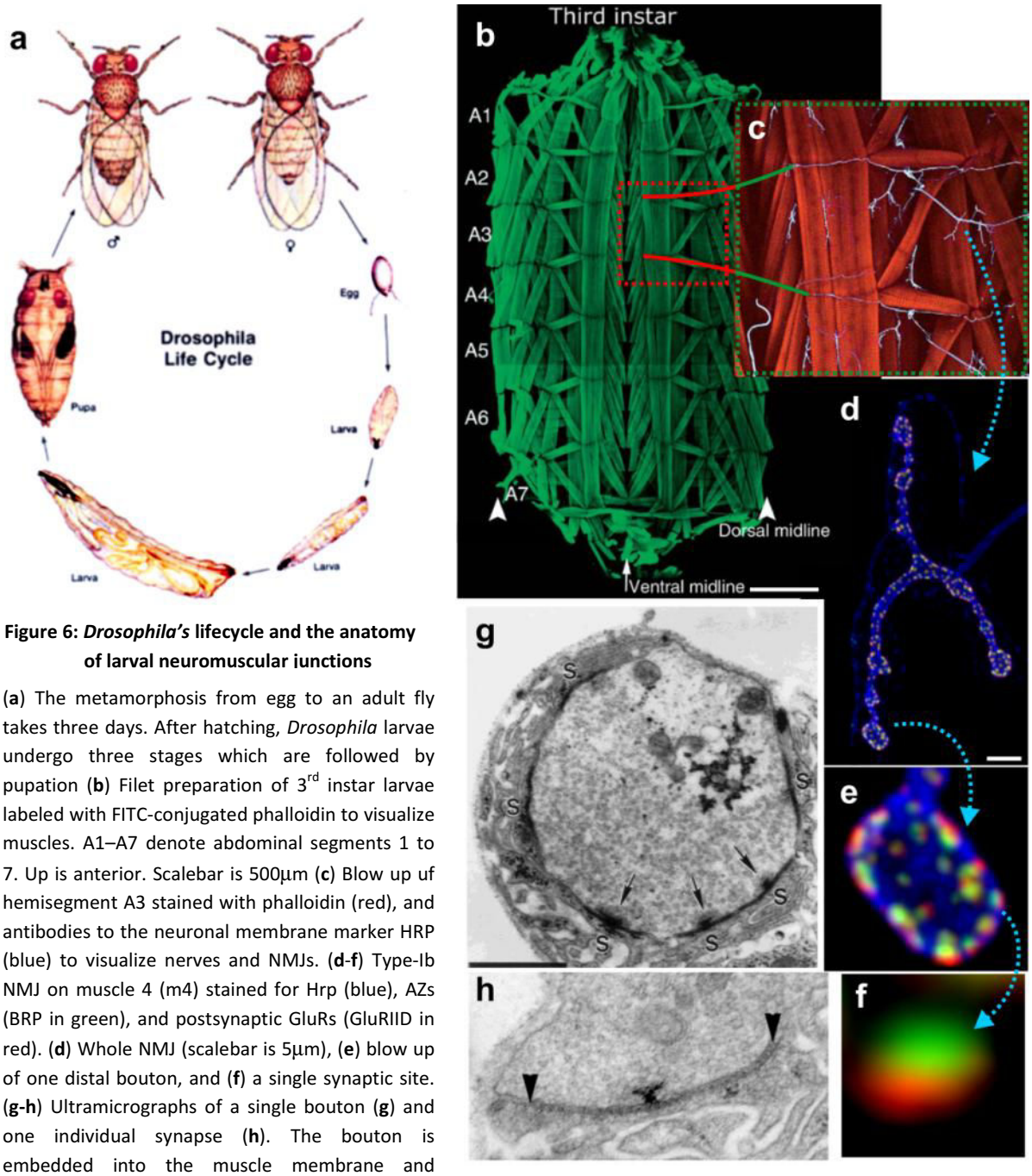

Figure 6: *Drosophila's* lifecycle and the anatomy of larval neuromuscular junctions

(**a**) The metamorphosis from egg to an adult fly takes three days. After hatching, *Drosophila* larvae undergo three stages which are followed by pupation (**b**) Filet preparation of 3rd instar larvae labeled with FITC-conjugated phalloidin to visualize muscles. A1–A7 denote abdominal segments 1 to 7. Up is anterior. Scalebar is 500µm (**c**) Blow up uf hemisegment A3 stained with phalloidin (red), and antibodies to the neuronal membrane marker HRP (blue) to visualize nerves and NMJs. (**d**-**f**) Type-Ib NMJ on muscle 4 (m4) stained for Hrp (blue), AZs (BRP in green), and postsynaptic GluRs (GluRIID in red). (**d**) Whole NMJ (scalebar is 5µm), (**e**) blow up of one distal bouton, and (**f**) a single synaptic site. (**g**-**h**) Ultramicrographs of a single bouton (**g**) and one individual synapse (**h**). The bouton is embedded into the muscle membrane and surrounded by membrane infoldings (SSR depicted with S). Mature AZs are marked by electron dense projections (T-bars depicted with arrows). Scale bar is 1µm. Modified from *International Review Of Biologie* (Volume 75)

In conclusion: *Drosophila* melanogaster has been proven to be an excellent model organism for many genetic studies, but its feasibility does not seem to end here. In the 70s, Jan and Jan utilized the preparations of *Drosophila* larvae to characterize synaptic transmission at the neuromuscular junction (NMJ) (Jan and Jan, 1976). In a few decades the NMJ of *Drosophila* became, arguably, the best model synapse in terms of its molecular organization. Its easy preparation (Fig. 6b) and good accessibility to many electrophysiological and imaging techniques led to the discovery of many genes involved in synapse and neural development.

2.2 *Drosophila's* NMJ: parallels to vertebrate CNS synapses

The NMJ of *Drosophila* has been used as a model for synaptogenesis for over three decades and has several advantages, such as: excellent genetic and optical accessibility, easy preparation and multiple available techniques, and, finally, a tremendous body of previous studies and a well-connected community have made the NMJ one of the most studied synapses today. Most of the NMJs advantages derive from the anatomy of arthropod itself.

Larval *Drosophila* have large muscle fibers to which identifiable neurons project their axons from the ventral nervous system (VNS). Typical for arthropods, *Drosophila's* body features a highly segmented organization. A stereotypic pattern of 30 body wall muscles attached to each abdominal hemi-segment repeats itself in every segment (Fig. 6a-b)(Bate, Landgraf, and Ruiz Gómez Bate, 1999). These muscles are always innervated by the same set of recognizable motor neurons that can be individually identified based on the location in the CNS or the branch pattern on the target muscle (Gramates and Budnik, 1999). A single muscle in *Drosophila* can be multi-innervated by different types of neurons (type-I, type-II and type-III) that present inputs of different modalities on their target. Type-I motoneurons represent the majority of efferent neurons; their glutamatergic release creating strong graduated depolarizations that correlate with the contraction strength of the muscle (Broadie and Bate, 1993; Budnik et al., 1990; Halpern et al., 1989). The axon terminals (Fig. 6d-f), or boutons, of motoneurons are submerged in the muscle and are surrounded by reticular in-vaginations of the muscle membrane, the subsynaptic reticulum (SSR) (Fig. 6g)(Budnik, 1996). These motoneurons can be further subdivided based on their morphology and physiology into type-Ib and type-Is, featuring big and small boutons respectively (Atwood et al., 1993; Hoang and Chiba, 2001; Landgraf et al., 1997). Big type-Ib boutons are 3-5 µm in diameter and possess up to 40 individual junctions, whereas type-Is boutons are significantly smaller (1-3 µm) and harbor less synaptic junctions. In conclusion, the NMJ harbors an ensemble of many presynaptic terminals, which are faced by postsynaptic specializations. In the following we will refer to one of these single synaptic units as an individual synapse (Fig. 6f and 6h).

These features separate the NMJ of *Drosophila* from its cholinergic vertebrate-counterparts and illustrate fundamental morphological and functional properties Arthropod NMJs share with the majority of mammalian CNS neurons (Gramates and Budnik, 1999). These neurons are not only glutamatergic, but they also receive multi-nerve, multi-modal inputs on their dendritic trees, which accumulate in graduated membrane depolarizations on their neurosomata. In contrast, vertebrate muscles are exclusively connected to a single motoneuron, which innervates other muscle fibers as well and forms a functional moto-unit. Vertebrate NMJs are cholinergic and their excitation leads to a uniform response upon which the muscle fiber contracts in a stereotypic manner.

Additionaly, glutamatergic CNS synapses and Arthropod NMJs share a very similar molecular organization with conserved scaffolding proteins, glutamate receptors, and exo/endo-cytic machinery. In this regard it appears as if these glutamatergic synapses share a common ancestor: a prototypic glutamatergic synapse, which makes them far more related than to any other cholinergic synapse.

2.3 Synaptic proteins at the *Drosophila* NMJ

The presynaptic ultrastructure of an individual NMJ synapse in *Drosophila* comprises an AZ with SVs, which is frequently marked by a characteristic shaped CAZ, termed T-bar. In most synapses, SVs cluster in close proximity around the T-bar with a few SVs docked to the plasma membrane (Schoch and Gundelfinger 2006; Zhai and Bellen, 2004). The ELKS family member *bruchpilot* (BRP) has been shown to be a structural component of the T-bar (Fouquet et al., 2009). NMJs mutant for BRP feature synapses devoid of T-bars and de-clustered Ca^{2+}-channels that culminate in severe neurotransmission defects (Hallermann et al., 2010; Wagh et al., 2006).

Another major multidomain protein, important for AZ assembly, is Liprin- (Dai et al., 2006; Kaufmann et al., 2002; Patel et al., 2006). The Liprin-α family is characterized by alpha-helical coiled coil and SAM domains and has been implicated in both pre- and postsynaptic assembly (Spangler and Hoogenraad, 2007). Liprin- binds via DSyd-1 to BRP and mutations in both proteins, Liprin- and Syd-1, cause a decrease in synapse number and abnormal T-bar morphology (Kaufmann et al., 2002; Owald et al., 2010). Live imaging experiments in *Drosophila* larvae showed a sequential assembly of Liprin-α, followed by DSyd-1 that preceded BRP clustering (Fouquet et al., 2009; Owald and Sigrist, 2009). Based on these findings, it was concluded that Liprin- together with Syd-1 is needed for effective nucleation of presynaptic assembly at new membrane spots (Owald et al., 2010; Sigrist and Schmitz, 2011).

Between the pre- and postsynaptic partner cells lies an extracellular matrix that keeps both plasma membranes in tight planar alignment, 10-20 nm apart (Peters, Palay, and Webster, 1991). The pre- and postsynaptic alignment is believed to be controlled by CAMs, but the experimental evidence for the role of CAMs in synaptogenesis in *Drosophila* is scarce. A recent report described the role of the receptor phosphatase DLar that controls, in conjunction with Liprin-, synapse morphogenesis (Kaufmann et al., 2002). The most promising CAM for controlling synaptogenesis, however, is the recently described *Drosophila* Neurexin (DNrx). DNrx has been reported to localize to AZs of NMJs and regulate synapse growth, differentiation, and function (Li et al., 2007). Flies mutants for *dnrx* have a reduced number of boutons and synapses, presynaptic membrane rufflings that cause

detachments of pre- and postsynaptic plasma membranes, and impaired synaptic transmission. Furthermore, accumulations of BRP positive aggregates in the axons of *dnrx* mutants suggest a function of DNrx in synapse assembly (Li et al., 2007). Although it is known from vertebrate studies that Neurexin needs to form heterophilic interactions with postsynaptic Neuroligin to exhibit its synaptogenic function (Scheiffele et al., 2000; Südhof, 2008), there is no study published, prior to the work presented in this thesis, which analyzes Neuroligin function at the *Drosophila* NMJ.

The postsynaptic site contains evolutionary conserved ionotropic glutamate receptors and other ion channels, arranged in the well defined electron-dense meshwork of the PSD (Atwood et al., 1993; Jia et al., 1993). The PSD in *Drosophila* is enriched in signaling molecules and scaffolding proteins that cluster these receptors and are mostly well conserved, too (Kennedy, 1998; Rodesch and Broadie, 2000). Disc Large for example, the homologue of the multidomain scaffolding protein PSD-95, SAP-97, and related, was first identified in *Drosophila* before Dlg-like proteins have emerged as core components at glutamatergic synapses in the vertebrate CNS (Kim & Sheng, 2004).

2.4 Ionotropic glutamate receptors at the *Drosophila* NMJ

The ionotropic glutamate receptors that reside in the PSDs of *Drosophila*'s NMJs are homologous to vertebrate AMPA and Kainate receptors. A single GluR complex appears to be an obligate heteromeric tetramer, consisting of a single subunit of GluRIIC (also known as GluRIII), GluRIID, GluRIIE, and either GluRIIA or GluRIIB (Fig. 7a-b). This notion derives from mutant analysis in which gluRIIC^{null}, gluRIID^{null}, gluRIIE^{null} or gluRIIA^{null}&IIB^{null} mutations lead to embryonic lethality and the loss of any GluR complex-formation at the NMJ (Featherstone et al., 2002; Marrus et al., 2004; Petersen et al., 1997; Qin et al., 2005). In single mutants of gluRIIA and gluRIIB structurally normal synapses with functional GluRs are present, indicating that either subunit is in principle dispensable for the formation of GluR complexes and synapses.

GluR complexes that contain the GluRIIA subunit differ in their transmission properties from complexes that contain GluRIIB (DiAntonio et al., 1999). GluRIIB complexes desensitize about 10 times more rapidly than GluRIIA complexes while displaying identical single-channel amplitudes (Fig. 7c-e) (DiAntonio et al., 1999). Intracellular current-clamp recordings demonstrated that larvae lacking the GluRIIA subunit show a lower postsynaptic response to single vesicle fusions (quantal size) than gluRIIB^{null} mutants. Though this may also be attributable to differences in receptor density, it is more likely that a subset of GluRIIB complexes desensitizes before opening, which translates into a reduced synaptic current (DiAntonio et al., 1999; Heckmann and Dudel, 1997).

It was therefore concluded that GluRIIA complexes account for most of the synaptic current in *wildtype* animals.

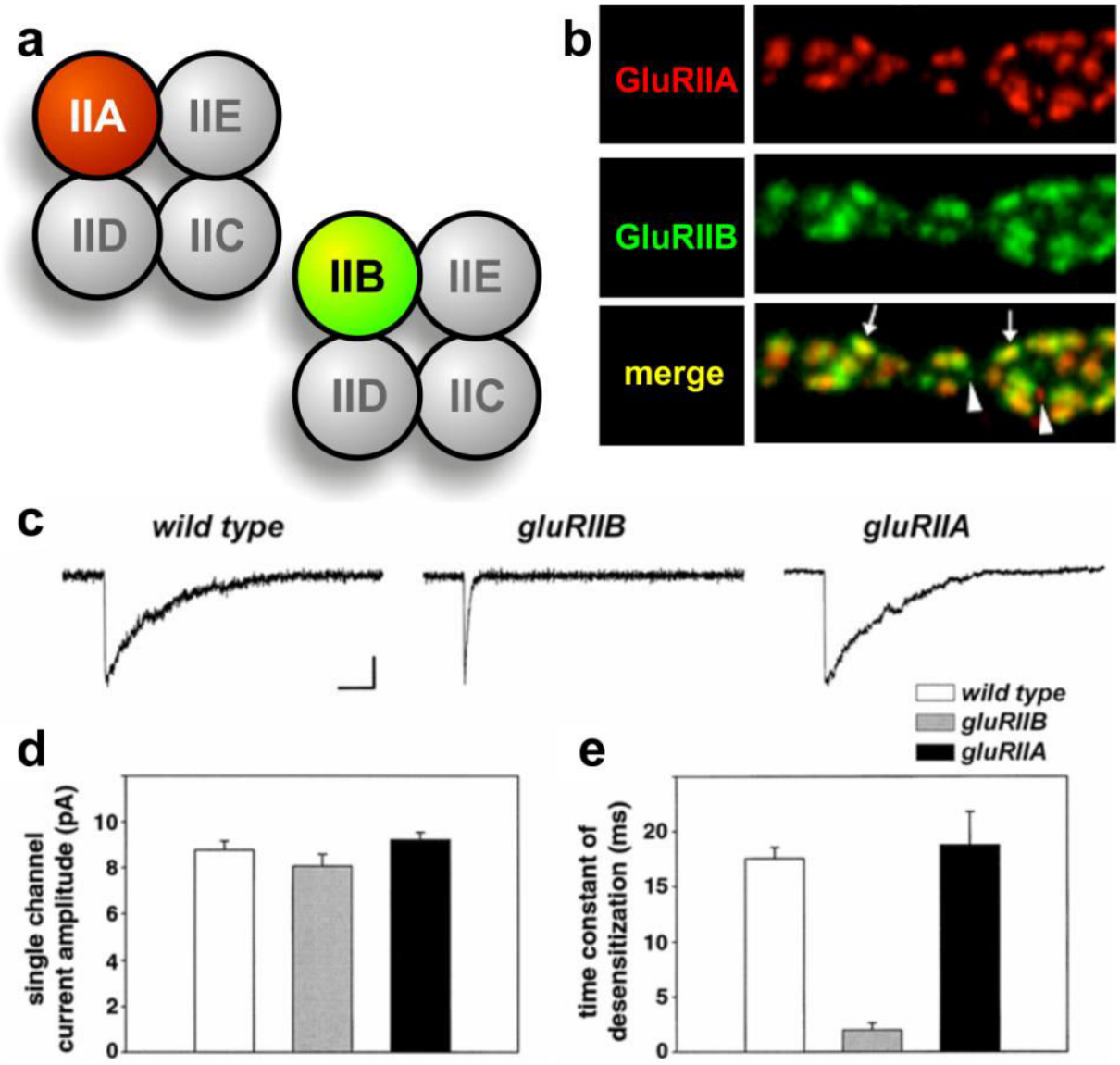

Figure 7: Localization and physiology of iGluRs at the NMJ of *Drosophila*

(**a**) Stochiometry of hetero-tetrameric GluR complexes at the NMJ. Two different complexes are thought to assemble here, incorporating GluRIIC (IIC), GluRIID (IID), and GluRIIE (IIE) together with either GluRIIA (IIA) or GluRIIB (IIB). (**b**) Both complexes coexisted, but do not fully overlap at single PSDs. Small nascent PSDs (arrowheads) are either dominated by GluRIIA (red) or by GluRIIB (green), whereas mature PSDs (arrows) show a balance of both receptor types. (**c**) Evoced junctional current (EJC) traces of outside-out patches from larval muscle membrane of *wildtype* NMJs and gluRIIA^{null}IIB^{null} mutants expressing gluRIIA or gluRIIB. Traces show average responses to rapid application of 10mM glutamate. (**d**) Single channel amplitudes do not differ in all three groups. (**e**) The time constant of desensitization, however, is significantly increased in gluRIIB expressing (thus gluRIIA^{null} mutants) ($p < 0.005$). Calibration 10msec, 5pA. Modified from *Schmid et al.,* (2008) and *DiAntonio et al.,* (1999).

Mutant analysis of *gluRIIA* and *gluRIIB* genes also revealed compensatory changes that nicely illustrate the plastic potential of the NMJ. For example, gluRIIA^{null} mutants exhibit decreased synaptic current, which was partially compensated by an increase in quantal content (DiAntonio et al., 1999). Retrograde mechanisms led to structural alterations of the presynaptic terminal, such as a change to more complex T-bars, which contributed for an increase in presynaptic release (Davis et al., 1998; Reiff et al., 2002).

Furthermore, GluR expression levels are able to control the number of synapses forming at the NMJ. Overexpression of the GluRIIA subunit at *wildtype* synapses triggers the formation of additional boutons, which corresponded with an increase of synapses per NMJ and an enhancement of the junctional signal transmission (Sigrist et al., 2002). Conversely, such a strengthening of the NMJ can be suppressed by genetic downregulation of GluRIIA or upregulation of GluRIIB expression (Sigrist et al., 2002). Thus, in terms of synaptic plasticity, these two glutamate receptor subunits show antagonistic effects.

The molecular mechanisms for subunit-specific GluR anchoring at *Drosophila's* NMJ under physiological conditions are widely unknown. Recent publications, however, examine the requirement of Dlg, the *Drosophila* PSD-95 homologue, for the stabilization of GluRIIB complexes (Chen and Featherstone 2005) and show that Coracle, a homologue of the mammalian Band 4.1N protein, is responsible for effective clustering of GluRIIA complexes at the PSD (Chen et al., 2005). While other molecular factors regulating glutamate receptor localization at the *Drosophila* NMJ still need to be defined, a deep understanding of the dynamics of receptor clustering requires a detailed description of the synapse development under physiological conditions (DiAntonio, 2006).

The transparency of larval body wall muscles enables the application of imaging techniques to follow the spatio-temporal assembly of fluorescent tagged proteins in living intact animals (*in vivo*). To utilize this feature, the Sigrist lab has made an effort to developed devices to anaesthetize *Drosophila* larvae and genetic tools to address the rates of GluR turnover and incorporation throughout NMJ development. Hereby, genomic constructs of GluRIIA and GluRIIB were fused to a fluorescent protein and tested for their functionality (Rasse et al., 2005; Schmid et al., 2008). These tagged GluRIIA and GluRIIB complexes are physiologically indistinguishable from their endogenous counterparts and rescue larval lethality of gluRIIA^{null}&IIB^{null} mutants (Rasse et al., 2005). Furthermore, the sub-synaptic localization and protein expression levels of fluorescent-tagged GluR subunits are comparable to untagged GluRs (Rasse et al., 2005; Schmid et al., 2008).

Consecutive imaging studies could show that the formation and growth of individual synapses directly correlates with the entry of GluRIIA complexes from diffuse extra-synaptic pools (Rasse et al.,

2005). This study also revealed that the entry of GluRIIA into postsynaptic receptor fields preceded the presynaptic assembly of BRP (Rasse et al., 2005), which in turn has been shown to correlate with the formation of T-bars (Fouquet et al., 2009). These studies were followed by studies that compared the incorporation of GluRIIA and GluRIIB complexes during development (Schmid et al., 2008). It turned out that the majority of small nascent PSDs start out with a GluRIIA-rich composition and acquire both GluR types over time. The overall incorporation dynamic, measured with fluorescence recovery after photobleaching (FRAP) experiments, appeared uniform over the whole population of the synapses for GluRIIB complexes. However, the incorporation of GluRIIA differed between individual synapses suggesting a strong regulation of this subunit. To determine whether GluRIIA containing complexes are regulated by presynaptic activity, the researchers turned to genetic tools to inhibit presynaptic evoked release. Under these conditions a higher proportion of synapses showed GluRIIA-FRAP, which correlated with an increase in the relative number of newly incorporated GluRIIA complexes (Schmid et al., 2008). The authors could additionally show that this activity-dependent regulation is functional at the level of individual synapses. By utilizing presynaptically expressed fluorescently tagged BRP fragments (BRP^{short}) it could be shown that with increasing levels of BRP^{short}, the absolute incorporation of GluRIIA decreased (Schmid et al., 2008). These data imply that the accumulation of GluRIIA is reduced as soon as an efficient accumulation of BRP, a sign for efficient presynaptic release, occurs at the AZ during synaptic maturation.

Drosophila Neuroligin 1 promotes growth and postsynaptic differentiation at glutamatergic neuromuscular junctions

by

Daniel Banovic[1,*], Omid Khorramshahi[2,*], David Owald[2], Carolin Wichmann[2,3], Tamara Riedt[1,4], Wernher Fouquet[2], Rui Tian[2], Stephan J. Sigrist[2,§], and Hermann Aberle[1,§]

[1] University of Münster, Institute for Neurobiology, Badestrasse 9, 48149 Münster, Germany
[2] Freie Universität Berlin, Institute for Biology/Genetics, Takustr. 6, 14195 Berlin, Germany
[3] present address European Neuroscience Institute Göttingen, Grisebachstr. 5, 37077 Göttingen, Germany
[4] present address University of Bonn, Department of Hematology/Oncology, Medical Center III, Wilhelmstrasse 35-37, 53111 Bonn, Germany
* contributed equally
§ corresponding authors
H.A., tel: +49-251-8328479; e-mail: aberleh@uni-muenster.de
S. J. S., tel: +49-30-838-56940; e-mail: stephan.sigrist@fu-berlin.de

Running title: *Drosophila* Neuroligin 1 regulates synapse assembly

Keywords: *Drosophila*, neuromuscular junction, neuroligin, neurexin, DNlg1, DNrx, synapse assembly, active zone, glutamate receptor field.

Abstract

Precise apposition of pre- and postsynaptic domains is a fundamental property of all neuronal circuits. Experiments *in vitro* suggest that Neuroligins and Neurexins function as key regulatory proteins in this process. In a genetic screen, we recovered several mutant alleles of *Drosophila neuroligin 1* (*dnlg1*) that cause a severe reduction in bouton numbers at neuromuscular junctions (NMJs). In accord with reduced synapse numbers, these NMJs show reduced synaptic transmission. Moreover, lack of postsynaptic DNlg1 leads to deficits in the accumulation of postsynaptic glutamate receptors, scaffold proteins, and subsynaptic membranes, while increased DNlg1 triggers ectopic postsynaptic differentiation via its cytoplasmic domain. DNlg1 forms discrete clusters adjacent to postsynaptic densities. Formation of these clusters depends on presynaptic *Drosophila* Neurexin (DNrx). However, DNrx binding is not an absolute requirement for DNlg1 function. Instead, other signaling components are likely involved in DNlg1 transsynaptic functions, with essential interactions organized by the DNlg1 extracellular domain but also by the cytoplasmic domain.

Introduction

Synapses are specialized membrane contacts between pre- and postsynaptic cell compartments that are connected by cell-cell adhesion proteins, which regulate the assembly and maturation of synapses (Yamagata et al., 2003; Washbourne et al., 2004). Different classes of synaptic adhesion proteins have been identified, including members of the immunoglobulin superfamily, Eph/Ephrins, Cadherins and the Neurexin/Neuroligin families (Dalva et al., 2007; Takeichi, 2007). A typical transsynaptic complex is formed by the heterophilic interaction of presynaptic Neurexins and postsynaptic Neuroligins (Dean and Dresbach, 2006). Neuroligins (Nlgs) are encoded by four independent genes in rodents and five genes in humans (Ichtchenko et al., 1995; Lise and El-Husseini, 2006). Nlgs possess a catalytically-inactive acetylcholinesterase-like domain, which interacts with presynaptic Neurexins (Nrxs) (Ichtchenko et al., 1996; Arac et al., 2007; Fabrichny et al., 2007). Both Nrxs and Nlgs contain C-terminal, intracellular PDZ domain-binding motifs believed to recruit scaffolding proteins for organization of either the presynaptic release machinery or postsynaptic neurotransmitter receptors, respectively (Ushkaryov et al., 1992; Missler et al., 2003; Dean and Dresbach, 2006). Therefore, the interaction of Nrxs with Nlgs has the potential to assemble a large transsynaptic complex that mediates the precise apposition of pre- and postsynaptic membranes.

Neuroligins localize to postsynaptic regions and, when expressed in non-neuronal cells, induce co-cultured neurons to form presynaptic specializations onto the non-neuronal cell (Song et al., 1999; Scheiffele et al., 2000). In support for a central role in the formation of synaptic contacts, overexpression of Nlgs in cultured neurons increases not only the number and density of synapses but also synaptic function (Chih et al., 2005; Levinson et al., 2005; Sara et al., 2005; Chubykin et al., 2007). Conversely, knock-down of Neuroligins by RNA interference leads to a reduction of synapse numbers (Chih et al., 2005), suggesting a role for Nlgs in synapse formation and/or stability. Mice that are triply deficient in Nlgs 1-3 die immediately after birth due to respiratory failure, likely as a consequence of reduced synaptic transmission in the brain stem centers controlling respiration (Varoqueaux et al., 2006). Unexpectedly, however, brain cyto-architecture and synapse density were not visibly altered, indicating that Nlgs are dispensable for the initial formation of synapses in vivo and rather control synaptic function. The differentiation and maturation of central synapses in the brain is technically difficult to analyze at the single synapse level and particularly might be subject to compensatory regulations. It would thus be desirable to also explore the function of Nlgs in synaptic differentiation/maturation and its relation to Nrxs at a genetically accessible and comparatively simple synaptic terminal.

In a large-scale, unbiased mutagenesis screen for genes that regulate synaptic terminal growth in *Drosophila*, we isolated mutations in a *neuroligin* homolog (*dnlg1*) resulting in neuromuscular junctions (NMJs) with strongly reduced numbers of synaptic boutons. NMJ *in vivo* imaging showed that the structural defects in *dnlg1* mutants are due to a deficit in bouton addition but not to subsequent deficits in bouton stability. DNlg1 is specifically expressed and functionally required at the postsynaptic side of NMJs, forming discrete clusters adjacent to, but not overlapping with, glutamate receptor clusters. Lack of DNlg1 provoked severe deficits in postsynaptic differentiation, with individual active zones or even entire boutons lacking postsynaptic glutamate receptor fields. The phenotypes identified by this analysis might be valuable for the further mechanistic analysis of Neuroligin-mediated signaling and might shed light on Neuroligin-associated diseases, such as autism (Jamain et al., 2003; Laumonnier et al., 2004).

Results

Mutations in *Drosophila neuroligin 1* identified by an unbiased screen for NMJ morphology defects

Drosophila NMJs consist of chains of synaptic boutons. Each bouton contains 30-40 individual transmitter-release sites, or synapses (Atwood et al., 1993; Jia et al., 1993). Synapses comprise a presynaptic active zone (AZ) apposed by an individual postsynaptic density (PSD) (Collins and DiAntonio, 2007). During postembryonic development, synaptic terminals of neuromuscular junctions (NMJs) gain in complexity, and the number of synaptic boutons increases dramatically in order to provide enough neurotransmitter for the growing muscle fibers (Lnenicka and Mellon, 1983). The expansion of NMJs is also subject to activity-dependent mechanisms (Griffith and Budnik, 2006; Collins and DiAntonio, 2007).

In a forward genetic screen for genes that regulate the growth of NMJs (Aberle et al., 2002) using EMS (ethyl methanesulfonate) as a chemical mutagen, we identified a complementation group of eight mutants with NMJs clearly smaller than normal (Fig. 1A-C). Using chromosomal deficiencies, meiotic recombination, and single nucleotide polymorphisms, we mapped the mutations to the annotated gene CG31146 (Drysdale, 2008). The protein encoded by CG31146 displays strong homology to vertebrate Neuroligins (Fig. 1D). We therefore named this locus *Drosophila neuroligin 1* (*dnlg1*), owing to the presence of three additional *neuroligin* family genes in the *Drosophila* genome (Suppl. Fig. S1) (Biswas et al., 2008).

The dnlg1 locus is localized at the cytological position 84D11-84D12 of the third chromosome. The previously isolated *dnlg1* cDNA clone RE29404 encompassed 5996 bps, including an unusually long 5' UTR (765 bps) (Stapleton et al., 2002). Sequencing of RT-PCR products derived from total embryonic RNA confirmed the annotated gene model (Fig. 1D). The only difference we found was an alternative splice site in the 5' UTR, which removes nucleotides 106-315 of exon 1 in roughly 50% of the *dnlg1* transcripts but has no effect on the coding region or the proposed translational start site in exon 2 (Fig. 1D).

The cDNA encoded a transmembrane protein of 1354 amino acids (Fig. 1E). The extracellular domain of DNlg1 contains a N-terminal signal peptide and an acetylcholinesterase-like domain (Fig. 1E). Similar to known Neuroligins, this domain is likely to be enzymatically non-functional, as the catalytic triad S-E-H of acetylcholinesterases is changed to S-E-M (S366, E495, M609) in DNlg1 (Gilbert and Auld, 2005). The cytoplasmic domain contains a PDZ-domain binding motif at the very C-terminus.

We sequenced the coding region and identified several EMS-induced point mutations in our *dnlg1* alleles (Y189H in K1809; K242Stop in I960; L319 splice site mutation in H324; L849Q in F1109; C934Stop in H703) (Fig. 1E). Any transheterozygous combination between these alleles was viable.

Lack of *dnlg1* results in a severe reduction of bouton numbers at neuromuscular junctions

We quantified morphometric parameters of mutant NMJs in different alleles. The number of synaptic boutons (measured on muscle pair 1/9 and normalized to the combined muscle surface area) was reduced by approximately 50% in any mutant allele combination tested (5.3±0.2 boutons per 10^4 µm^2 muscle area in wild-type versus 2.4±0.1 in *dnlg1*^{I960}/Df(3R)Dsx29 mutants (n=40, ±SEM)) (Fig. 1F). The reduction in bouton number was not a secondary consequence of fewer synaptic branches, as terminal axon branching was not affected (data not shown). However, when we calculated the average number of boutons normalized to synaptic branch length (Fig. 1G), bouton density on muscles 1/9 was significantly decreased in *dnlg1* mutants (1.4±0.1 boutons in *dnlg1*^{I960}/Df(3R)Dsx29 per 10 µm branch length versus 2±0.1 boutons in wild-type versus (n=40, ±SEM)). We also measured the average diameter of the largest bouton within a given NMJ (Fig. 1H). The bouton diameter on muscles 1/9 was slightly but significantly increased in *dnlg1* mutants (6.4±0.1 µm in wild-type versus 7.6±0.1 in *dnlg1*^{I960}/Df(3R)Dsx29 mutants (n=40, ±SEM)).

To create an undisputable null allele we took advantage of piggyBac elements containing FRT sites and generated three excision alleles (*dnlg1*$^{ex1.9}$; *dnlg1*$^{ex2.3}$; *dnlg1*$^{ex3.1}$; Fig. 1D). In *dnlg1*$^{ex3.1}$, the entire open reading frame of *dnlg1* is eliminated. Combinations of these excision alleles in trans to the EMS-induced alleles *dnlg1*^{I960} and *dnlg1*^{H324} led to unambiguously small NMJs (Fig. 1F-1H). Thereby, *dnlg1*$^{ex3.1}$ homozygous mutant junctions were not smaller than EMS-allele combinations (Fig. 1F-1H). Thus, among the EMS alleles, *dnlg1*^{I960} and *dnlg1*^{H324} represent very strong hypomorphic alleles or most likely null alleles. In conclusion, elimination of *dnlg1* function leads to a severe loss of synaptic boutons at NMJs of mature *Drosophila* larvae.

NMJs of *dnlg1* mutants initially form but lack bouton addition throughout development

NMJs normally form during stages 16-17 of embryonic development. To visualize embryonic NMJs, we used an antibody against the *Drosophila* vesicular glutamate transporter DVGLUT (Mahr and Aberle, 2006). Size and shape of developing NMJ terminals was similar in wild-type and *dnlg1* mutant embryos (Suppl. Fig. S2). Thus, initial formation of synaptic terminals seems to proceed

normally in the absence of DNlg1. During subsequent larval stages, however, NMJs appeared smaller in *dnlg1* mutants. This phenotype *per se* might be due to reduced addition of synaptic boutons or, alternatively, due to increased retraction of established boutons. To distinguish between these possibilities, we observed NMJ development directly by imaging NMJs on dorsal muscles 1/9 in living larvae using the postsynaptic marker CD8-GFP-Sh (Zito et al., 1999) (Fig. 1I-1L). Wild-type NMJs generally expand during larval development, with only a small fraction of synaptic branches (17.5%, n=25 hemisegments) not growing (Fig. 1I-1J). In *dnlg1* mutants, the percentage of non-growing branches was significantly increased (74.6%, n=30 hemisegments) (Fig. 1K-1L). Even when growth did occur, it never reached the size observed at wild-type NMJs. Importantly, none of the terminals present in first instar larvae retracted (Fig. 1K-1L). Even single and isolated boutons remained throughout the larval instars, indicating that NMJ stability was not affected. Thus, DNlg1 is required for effective addition of synaptic boutons at developing NMJ terminals.

Neurotransmission at *dnlg1* mutant NMJs is reduced in accord with reduced synapse numbers

Does the loss of synaptic boutons lead to a reduction in neurotransmitter release? Usually, the number of synaptic boutons scales with the number of individual synapses present per NMJ terminal. In fact, when we quantified individual release sites opposed to glutamate receptor fields on muscle 6 using antibodies directed against the active zone protein Bruchpilot (BRP) and the glutamate receptor subunit IID (GluRIID) (Featherstone et al., 2005; Qin et al., 2005; Wagh et al., 2006), their number was strongly reduced in *dnlg1* mutants (Fig. 2A) (502±24 synapses in controls (n=9) compared to 219±8 in $dnlg1^{I960}/dnlg1^{H324}$ mutants (n=9); $p<0.0001$). We wondered whether this would be reflected in reduced neurotransmission. Thus, we first examined both the spontaneous and the evoked release using intracellular recordings at 1 mM Ca^{2+} concentrations. Compared to control third instar larvae, the evoked excitatory junctional currents (eEJC) from NMJs innervating muscles 6/7 were reduced by nearly 50% in *dnlg1* mutants (Fig. 2B) (68±5 nA in controls (n=9) versus 37±5 nA in $dnlg1^{I960}/dnlg1^{H324}$ mutants (n=12); p=0.0016). The eEJC amplitudes were reduced to a similar extent when measured at 0.5 mM extracellular Ca^{2+} concentration (Fig. 2C) (20±2 nA in controls (n=9) compared to 10±1 nA in $dnlg1^{I960}/dnlg1^{H324}$ mutants (n=11); p=0.0009). At the same time, the amplitude of spontaneous miniature excitatory junctional currents (mEJC) appeared unchanged at mutant NMJs (Fig. 2D) (0.86±0.03 nA in controls (n=14) compared to 0.86±0.05 nA in $dnlg1^{I960}/dnlg1^{H324}$ mutants (n=16); p=0.9). The mEJC frequency showed a trend towards smaller values in mutant cells, however this trend was statistically not significant (1.9±0.2 Hz in controls (n=14) compared to 1.5±0.2 Hz in $dnlg1^{I960}/dnlg1^{H324}$ mutants (n=16); p=0.17). Thus, our

electrophysiological analysis indicates that *dnlg1* mutant NMJ terminals release less neurotransmitter per action potential. This reduction seems proportional to the reduction of synapses present at these terminals (compare Fig. 2A and 2B). As we also did not observe any changes in functional parameters such as Ca^{2+} dependence of release, the structural reduction in the number of release sites seems to be responsible for the reduction in transmitter release, while the synapses remaining at *dnlg1* mutant NMJs appear largely functional.

Defects of postsynaptic differentiation at *dnlg1* mutant boutons

To investigate possible pre- or postsynaptic differentiation defects we performed light microscopic analysis of *dnlg1* mutant terminals. First, the presynaptic vesicle protein Synaptotagmin (Syt) and cytoskeleton marker Ankyrin 2 (Ank2) (Koch et al., 2008) were stained together with CD8-GFP-Sh, which marks the subsynaptic reticulum (SSR) (Fig. 3A-3D). The SSR consists of membranous invaginations of the muscle plasma membrane and surrounds the postsynaptic glutamate receptor fields. Notably, we found many areas where apparently mature presynaptic boutons, as highlighted by the accumulation of Syt and Ank2, were not opposed by CD8-GFP-Sh signals (compare arrows in Fig. 3D). Quantified, 46% of NMJs on muscles 1/9 possessed obvious postsynaptic differentiation defects, compared to only 5% in control larvae (n=20). These mismatches did not include the entire branch because a majority of boutons still maintained close apposition of the pre- and postsynaptic membranes. Rather, mismatches affected a subset of boutons, regardless of whether they were localized in proximal or distal branch regions. These results indicate that a fraction of fully differentiated presynaptic boutons face a postsynaptic site that lacks SSR.

To discriminate assembly deficits from secondary stabilization defects, we performed *in vivo* live imaging of *dnlg1* mutant terminals expressing a BRP-fragment highlighting presynaptic active zones (Schmid et al., 2008) together with the postsynaptic marker CD8-GFP-Sh (Fig. 3E-3F). Growing boutons normally contain active zones, T-bars, synaptic vesicles, and are surrounded by SSR membranes (Zito et al., 1999) (Fig. 3E). In contrast, a subset of presynaptic boutons in *dnlg1* mutants continuously added active zone material but failed to differentiate an apposing postsynaptic domain, as indicated by the complete lack of the CD8-GFP-Sh signal (arrows in Fig. 3F). The number of unapposed BRP spots increased over time (t=0h: 7.39±0.71; t=12h: 9.06±1.34; t=24h: 10.88±1.23 BRP spots per bouton lacking SSR membranes (n=9 boutons on muscles 1/9)). Overall, the lack of postsynaptic SSR reflects a genuine inability to assemble postsynaptic structures at *dnlg1* boutons.

Glutamate receptor accumulation defects in the absence of DNlg1

Next, we asked whether apart from the SSR defects the accumulation of postsynaptic proteins – particularly of postsynaptic glutamate receptors (GluRs) – would be affected. We subjected control (Fig. 4A, 4C) and *dnlg1* mutant terminals (Fig. 4B, 4D-4G) to an extensive immunohistochemical analysis. Normally, the active zone marker BRP localizes opposite glutamate receptor clusters at mature NMJs (Fig. 4A and 4C). At *dnlg1* mutant NMJs, however, we could readily identify presynaptic areas that lacked postsynaptic domains, as indicated by BRP-positive punctae not opposed by glutamate receptors (arrows in Fig. 4B, 4D-4E). Frequently, individual active zones or groups of active zones lacking GluRs were present (arrows in Fig. 4D-4E). "Orphan" boutons, i.e. differentiated presynaptic boutons entirely lacking postsynaptic GluRs, occurred with a frequency of about 8% of *dnlg1* mutant boutons, but were not found in control NMJs (Fig. 4H). The severity and frequency of these phenotypes were independent of the *dnlg1* alleles used and were also observed in $dnlg1^{H703}$, which contains a stop codon in the cytoplasmic domain, suggesting that this domain plays an important role in the assembly of PSDs (Suppl. Fig. S3). Other postsynaptic markers, namely the PSD marker Pak and the SSR marker Spectrin, were absent in orphan boutons as well (Suppl. Fig. S4). Thus, DNlg1 seems to promote the accumulation of postsynaptic glutamate receptors as well as SSR differentiation at neuromuscular terminals.

Electron micrographs reveal synaptic membrane detachments and postsynaptic differentiation defects

At the fly NMJ, synapses are characterized by planar, 100-500 nanometer wide appositions of pre- and postsynaptic membranes (Fig. 5A, arrowheads) decorated by T-bars. Lateral to synapses, bouton membranes are not entirely aligned in parallel, but rather form punctate contacts. In electron micrographs, we found that presynaptic active zones still formed in *dnlg1* mutant boutons (arrowheads in Fig. 5B). Mutant active zones contained T-bars and clustered synaptic vesicles. Synaptic vesicles were present at roughly normal size and density, with large vesicle diameters in slightly higher numbers than normal (35.31±0.25 nm in controls (n=410 vesicles) versus 36.88±0.55 nm in $dnlg1^{I960}/dnlg1^{H324}$ mutants (n=362 vesicles); p=0.0049, students t-test)).

Notably, we observed a subset of mutant boutons with a reduction in the thickness of the SSR. In fact, the relative SSR area was significantly reduced in *dnlg1* NMJs (wild-type 2.22±0.34, n=19; $dnlg1^{I960}/dnlg1^{H324}$ 1.27±0.16, n=26; p=0.0083, students t-test) (Fig. 5G). In extreme cases, boutons appeared to be in "direct contact" with the contractile filaments (arrowheads in Fig. 5C).

Importantly, however, even at places without SSR, active zones were still present and maintained the tight apposition of pre- and postsynaptic membranes, indicating that synapse formation *per se* appeared not to be affected (Fig. 5C). Thus, molecular and ultrastructural data agree that the differentiation of postsynaptic domains is affected in *dnlg1* mutants. Surprisingly, even at places where postsynaptic SSR differentiation largely failed, basic aspects of synapse formation seemed to proceed.

Postsynaptic DNlg1 clusters localize adjacent to glutamate receptor fields

Where is DNlg1 expressed to regulate bouton addition and postsynaptic differentiation? To answer this question, we first performed *in situ* hybridization experiments. Antisense probes synthesized from clone RE29404 recognized endogenous *dnlg1* transcripts in somatic muscles (Fig. 6A-6B), whereas sense probes did not. We first detected expression at late stage 12 in a subset of myoblasts, the progenitor cells of body wall muscles. At stage 14, most myoblasts expressed *dnlg1* (Fig. 6A). At the end of embryogenesis, *dnlg1* was also expressed in the dorsal pharyngeal muscles and the ring gland. We were unable to detect any expression in the central nervous system (arrowhead in Fig. 6B).

To investigate the subcellular distribution of DNlg1, we raised a polyclonal antiserum against a C-terminal peptide (see Experimental Procedures). The affinity-purified antiserum clearly highlighted NMJs in wild-type larvae (Fig. 6C-6D). In contrast, NMJs in *dnlg1* mutants were not stained and only background signals remained, demonstrating the specificity of the antibody (Fig. 6E-6F). For unequivocally demonstrating postsynaptic expression, endogenous DNlg1 was downregulated specifically either on the pre- or postsynaptic side using transgene-mediated RNA interference (RNAi) in combination with the UAS/Gal4 system (Brand and Perrimon, 1993; Dietzl et al., 2007). While presynaptic expression using elav-Gal4 did not interfere with the antibody signal at NMJs (Fig. 6G-6H), expression in postsynaptic muscles using mef2-Gal4 completely abolished the DNlg1 clusters, confirming that they are of postsynaptic origin (Fig. 6I-6J).

Does the position of the postsynaptic DNlg1 spots relate to postsynaptic marker proteins? We stained NMJs with anti-DNlg1 and anti-GluRIID antibodies and found that DNlg1 was expressed in a spotted pattern adjacent to GluR fields (Fig. 6K-6L). Quantification showed that 69±9% of all PSDs were associated with discrete DNlg1 spots (n=1425 PSDs). We detected a similar distribution of the DNlg1 spots relative to presynaptic active zones (visualized with anti-BRP antibodies) (Fig. 6M-6N), consistent with a very high degree of AZ to PSD coordination in this system (Schmid et al., 2008).

Thus, DNlg1 is specifically expressed in postsynaptic muscle cells and accumulates at NMJs, in a location adjacent to PSDs.

Postsynaptic DNlg1 is needed for effective addition of synaptic boutons at developing NMJ terminals

The specific clustering of DNlg1 adjacent to but not within PSDs might define a novel postsynaptic compartment at *Drosophila* NMJs. To test whether DNlg1 is functionally required at these postsynaptic sites we attempted to eliminate *dnlg1* expression in selected tissues using RNAi. As mentioned above, all allelic combinations (early stop codons or full deletions) invariably resulted in unusually small NMJs, showing a 50% reduction in overall bouton numbers. To define the relevant cell compartment for DNlg1 function, we first triggered RNAi in neurons or muscles of wild-type larvae. Presynaptic knock-down of DNlg1 (using elav-Gal4) altered neither the size of NMJs (Suppl. Fig. S5) nor the staining of DNlg1 at NMJs (Fig. 6G-6H). In contrast, when *dnlg1* function was eliminated in muscles (using mef2-Gal4), NMJ size was drastically reduced (Suppl. Fig. S5). This is in line with the elimination of DNlg1 staining at NMJs upon knock-down of DNlg1 in muscles (Fig. 6I-6J).

We also tested for tissue-specific functions in genetic rescue experiments (Fig. 7). For this purpose, we expressed a wild-type *dnlg1* cDNA in muscles or neurons in *dnlg1* mutant backgrounds. To increase detection sensitivity, we labeled DNlg1 with GFP in a juxta-membrane position, as this location is predicted not to interfere with protein function (Dresbach et al., 2004; Wittenmayer et al., 2009) (Fig. 7A). Full-length DNlg1-GFP, when expressed with mef2-Gal4 in a mutant background, rescued the small terminal phenotype back to control levels (Fig. 7E and 7K). In contrast, expression of DNlg1-GFP in all postmitotic neurons using elav-Gal4 did not substantially improve the synaptic phenotype of *dnlg1* mutants (Fig. 7D and 7K). Thus, DNlg1 is not only expressed in muscle fibers, but its functional expression within fibers is also required for effective formation of synaptic boutons at developing and maturing NMJs.

Lack of the cytoplasmic domain of DNlg1 provokes strong dominant-negative effects

We next created transgenic lines expressing deletion constructs of DNlg1 based on DNlg1-GFP to isolate the domains important for DNlg1 function (Fig. 7A). First, a construct lacking the extra-cellular domain but retaining the transmembrane and cytoplasmic domains (DNlg1-GFP$^{\Delta extra}$) was overexpressed under control of mef2-Gal4 specifically in muscles. While DNlg1-GFP$^{\Delta extra}$ localized to

NMJs, it had no effect on NMJ morphology (Fig. 7I and 7L). In addition, DNlg1-GFP$^{\Delta extra}$ expression in muscles of *dnlg1* mutants did not substantially rescue the null mutant phenotypes (Fig. 7F and 7K). Notably, however, DNlg1-GFP$^{\Delta cyto}$ (Fig. 7A) lacking the cytoplasmic domain provoked very small NMJs when expressed in wild-type muscles (Fig. 7J and 7L). In fact, NMJs were even slightly smaller than in the null phenotypes (Fig. 7C). When expressed in a *dnlg1* mutant background, DNlg1-GFP$^{\Delta cyto}$ not only failed to rescue the number of synaptic boutons and the size of NMJs but also produced NMJs even smaller than in null mutants (compare Fig. 7C with 7G). Likely, DNlg1-GFP$^{\Delta cyto}$ can still attach to signaling partners via its extracellular and/or transmembrane region (because it effectively localizes to NMJs). Due to the lack of its cytoplasmic domain, we suppose it renders these complexes non-functional, in effect acting as a dominant-negative protein. Since only DNlg1-GFP was able to rescue the mutant phenotype, we conclude that both the extracellular and the cytoplasmic domain appear to be essential for DNlg1 signaling.

Ectopic postsynaptic differentiation triggered by increased amounts of DNlg1

While expressing DNlg1-GFP, we found further evidence that DNlg1 is important for postsynaptic assembly. Apart from type I NMJ innervations, larval muscles also receive innervation by thin diameter type II terminals (Hoang and Chiba, 2001). While normally these lack SSR, and hence typical postsynaptic markers of type I boutons such as CD8-GFP-Sh or Discs large (Dlg), they can be labeled with anti-HRP antibodies (Jia et al., 1993). Notably, after muscle expression of DNlg1-GFP, we noticed not only an increase of DNlg1 intensity at NMJs but also that type II terminals normally negative for the SSR marker Dlg now show Dlg expression (Fig. 7N). Similarly, we could detect low levels of the glutamate receptor subunit GluRIIC, normally confined to type I boutons, at type II terminals (data not shown). This effect was specific to DNlg1, as it was not observed after expression of the synaptic adhesion protein Fasciclin II (Grenningloh et al., 1991) (Fig. 7M). While DNlg1-GFP$^{\Delta cyto}$ localized to type II terminals, obviously due to the lack of its cytoplasmic domain, it failed to recruit Dlg (Fig. 7O). In contrast, DNlg1-GFP$^{\Delta extra}$ did not localize to type II terminals and consequently type II boutons lacked Dlg (Fig. 7P). However, DNlg1-GFP$^{\Delta extra}$ accumulated in cytoplasmic granulae in muscle fibers that contained Dlg (Fig. 7P) and GluRs (data not shown), suggesting that the cytoplasmic domain is tightly associated with these markers. Thus, DNlg1, when over-expressed, is able to ectopically recruit postsynaptic marker proteins to a terminal normally not undergoing such a differentiation, again pointing towards a rate-limiting role of this protein for postsynaptic differentiation.

Presynaptic DNrx is essential for effective clustering of postsynaptic DNlg1

Binding of Neurexin via an ectodomain-ectodomain interaction is suggested to be important for Neuroligin function. Thus, we wanted to compare the *dnrx* and *dnlg1* mutant phenotypes directly and introduced the CD8-GFP-Sh marker into the *dnrx* mutant background (Fig. 8A-8C) (Li et al., 2007; Zeng et al., 2007). Most NMJs in *dnrx* mutants were visibly smaller (Fig. 8B), confirming previous observations (Li et al., 2007). Compared to various amorphic *dnlg1* alleles, however, NMJ size was less affected in *dnrx* mutants (Fig. 8C). Quantitatively, bouton numbers on muscles 1/9 were reduced by 53% in *dnlg1* but only 36% at *dnrx* mutants terminals (27.3±1.1 boutons in wild-type, 12.7±0.6 boutons in $dnlg1^{l960}$/Df(3R)Dsx29, and 17.5±0.8 boutons in $dnrx^{241}$/Df(3R)Exel6191 (n=40, ±SEM)) (Fig. 8E; Suppl. Fig. S6). To test for a possible genetic interaction, we also produced *dnrx*, *dnlg1* double mutants. These double mutants were adult viable as was each single mutant. NMJs in *dnrx, dnlg1* double mutants were indistinguishable from *dnlg1* single mutants (Fig. 8D). Thus, further loss of *dnrx* does not add onto the bouton formation defects present in *dnlg1* mutants (Fig. 8E; Suppl. Fig. S6).

In another series of experiments, we overexpressed untagged, full-length DNlg1 at levels significantly higher than DNlg1-GFP (Suppl. Fig. S7). This reduced NMJ size in wild-type larvae, probably by interfering with endogenous DNlg1 complexes (Fig. 8F). This dominant-negative effect was, however, not observed when we overexpressed DNlg1 in the *dnrx* mutant background (Suppl. Fig. S7). To further test for a possible involvement of DNrx in DNlg1 function we introduced a point mutation into DNlg1, $DNlg1^{D356R}$, which by inference from mammalian data should abolish the binding to DNrx (Reissner et al., 2008). In contrast to the unmodified version, $DNlg1^{D356R}$ overexpression in wild-type muscles did not visibly alter the structure of NMJs (both DNlg1 and $DNlg1^{D356R}$ were expressed from the same chromosomal integration site to ensure equal expression levels) (Fig. 8G). When expressed in a *dnlg1* mutant background, $DNlg1^{D356R}$ significantly rescued the NMJ phenotype (Fig. 8I). Thus, these data imply that DNrx binding via its ectodomain is not an absolute prerequisite for DNlg1 function, but rather promotes DNlg1 function.

To further compare *dnrx* and *dnlg1* mutants, we wondered whether *dnrx* mutants also display pre- and postsynaptic apposition defects. We therefore stained *dnrx* mutant NMJs with anti-BRP and anti-GluRIID antibodies. In contrast to *dnlg1* mutant NMJs (Fig. 4), entire boutons or individual AZs lacking GluRs were not observed in *dnrx* mutants, confirming previous observations (data not shown, Li et al., 2007). Upon closer analysis, however, we recognized that postsynaptic receptor fields appeared irregular and often enlarged in both *dnlg1* and *dnrx* mutants (Suppl. Fig. S8). In fact, quantification after 3D reconstruction (see Suppl. Experimental Procedures) showed that the

integrated GluR intensities per PSD were significantly increased in both *dnlg1* and *dnrx* mutants (Suppl. Fig. S8). Again, this effect was qualitatively similar but quantitatively milder in *dnrx* than in *dnlg1* mutants.

Further similarities were also revealed by our ultrastructural analysis of *dnlg1* mutant boutons. In control animals, active zone membranes were aligned in parallel and showed hardly any ruffles in the synaptic membranes (Fig. 5D). In contrast, in *dnlg1* mutants, we found an atypical number of shallow ruffles (arrows in Fig. 5E) in active zones (1.88±0.21 ruffles per active zone in $dnlg1^{I960}/dnlg1^{H324}$ compared to only 0.22±0.07 in wild-type larvae ($p<0.005$, students t-test)) (Fig. 5H). The average distance of the ruffles to the center of the T-bar was not significantly altered (wild-type 144.43±23.92 nm, $n_{ruffles}=15$, $n_{AZ}=73$; $dnlg1^{I960}/dnlg1^{H324}$ 158.97±10.12, $n_{ruffles}=87$, $n_{AZ}=52$; $p=0.57$; students t-test) (Fig. 5I). Notably, *dnrx* mutant active zones were shown previously to display similar ruffles in active zones (Li et al., 2007; Zeng et al., 2007). However, for *dnlg1* NMJs, similar but even more pronounced invaginations were readily observed (arrows in Fig. 5F). Thus, mutations in *dnlg1* result in certain deficits of presynaptic assembly, obviously in a transsynaptic manner, with defects again being similar but apparently stronger than found for *dnrx*.

Due to these phenotypic similarities, DNlg1 might work in a related context, where DNrx promotes but is not absolutely required for DNlg1 signaling. Similar to DNlg1 (Fig. 6M-6N), DNrx was reported to cluster in discrete patches close to but not overlapping with presynaptic active zones (Li et al., 2007). To perform co-labeling experiments, we created a GFP-tagged version of DNrx and expressed this in presynaptic motoneurons of *dnrx* mutants. Endogenous DNlg1 and DNrx-GFP frequently were found in apposing spots on both sites of the synapse (Fig. 8L). Thus, we asked whether presynaptic DNrx might be needed for effective clustering of postsynaptic DNlg1. In fact, clusters of DNlg1 adjacent to active zones were drastically reduced at *dnrx* mutant NMJs (Fig. 8N). Similarly, presynaptic (but not postsynaptic) RNAi downregulating DNrx expression prevented DNlg1 clustering (Suppl. Fig. S7). Thus, presynaptic DNrx is required for effective accumulation of DNlg1 at a compartment adjacent to PSDs. However, the fact that the *dnrx* phenotype is clearly weaker than the *dnlg1* phenotype indicates that not all DNlg1 signaling and thus protein seems to be lost in absence of presynaptic DNrx. Collectively, as *dnrx* phenotypes appear qualitatively similar but not of the same severity as *dnlg1* phenotypes, clustering of DNlg1 via presynaptic DNrx seems to promote DNlg1 signaling, but does not seem to be an absolute requirement for it.

Discussion

Neuroligins (Nlgs) are generally considered to play an important role in the establishment of fully functional neuronal circuits (Varoqueaux et al., 2006; Hoon et al., 2009). Nlgs bind Neurexins (Nrxs) (Ichtchenko et al., 1995; Sudhof, 2008), and both proteins are sufficient to induce synapse formation in cultured cells (Scheiffele et al., 2000; Graf et al., 2004). Major issues, however, concerning the precise role of Nlgs for synapse formation, maturation, and maintenance have therefore remained open and are actively discussed (Sudhof, 2008). These aspects include whether Nlgs can execute actual synaptogenic functions or are restricted to maturation and/or maintenance of synapses. To what extent functions of Nlgs can be reduced to retrograde signaling via Nrxs is another question.

Drosophila Neuroligin functions in the developmental addition of synaptic boutons

Here, in an unbiased EMS mutagenesis screen, we identify a *Drosophila* Neuroligin family protein, DNlg1. Null mutations in *Drosophila dnlg1* dramatically reduced the number of synaptic boutons (Fig. 1). Consistent with a reduction in terminal size, the number of the remaining synapses per NMJ was similarly reduced. Electrophysiological analysis suggested that the reduction in synapses provoked a similar reduction in the amount of neurotransmitter released per action potential. In contrast to findings in mice, where electrophysiological but no structural abnormalities were observed in *nlg* triple mutants (Varoqueaux et al., 2006), the functional defects at *Drosophila* NMJs seem to be a consequence of the structural defects.

Notably, DNlg1 is not required for the initial formation of synaptic terminals *per se*, as NMJs form on all muscles of *dnlg1* mutant animals, with an apparently normal timing (Suppl. Fig. S2). In addition, approximately 50% of the synapses are still present and largely functional, also at later stages. DNlg1, however, is required for effective addition of synaptic boutons during NMJ development and growth. We performed extended *in vivo* imaging of synaptic terminals at wild-type and mutant NMJs (Zito et al., 1999; Rasse et al., 2005; Schmid et al., 2008), finding that the *dnlg1* phenotype clearly reflects a genuine inability to effectively add new synaptic boutons to a synaptic terminal but does not arise as a secondary deficit in the stability of previously assembled boutons (Fig. 1). Thus, the inability to add new boutons, identified as the hallmark of this complementation group in the unbiased screen, leads to the reduction of NMJ size at the end of larval development. The reduction in bouton numbers also correlated with a reduction in the total number of synapses per NMJ. Establishment of a direct causal relation awaits further genetic dissection of DNlg1 signaling. Clearly, however, DNlg1 is not absolutely essential, as residual boutons still form. Thus, DNlg1 might be

regarded more as a regulatory factor rather than an essential building block of synapses, consistent with its localization adjacent to but not overlapping with PSDs labeled by GluRs.

DNlg1 functions in postsynaptic differentiation

Assembly of the postsynaptic apparatus did not take place for a significant fraction of boutons and individual synapses, while the accumulation of presynaptic markers was essentially normal. Again, we used live imaging to demonstrate a genuine postsynaptic assembly deficit, as boutons lacking SSR differentiation develop and continuously add presynaptic BRP-positive active zones without signs of presynaptic dedifferentiation (Fig. 3). It thus appears that DNlg1 coordinates the formation of the postsynaptic compartment at the larval NMJ, including the proper localization of GluR clusters and the formation of the SSR and PSDs. We previously showed that a genetically induced lack of GluR complexes interferes with formation of the SSR (Schmid et al., 2006). Thus, an inability to target, transport and/or maintain GluRs sufficiently might be at the center of the postsynaptic differentiation/maturation deficits.

The links between bouton defects and individual active zone deficits remain to be addressed. Mutations in *dnlg1* affected NMJs both at the single bouton level and the single synapse level, but affected these synaptic structures only partially. On the other hand, increased DNlg1 levels were able to trigger molecular aspects of postsynaptic differentiation even at type II boutons, emphasizing the rate-limiting character DNlg1 can play for assembly processes in this system. The partial character of these phenotypes is not due to residual DNlg1 activities in our alleles because a deletion allele with the entire *dnlg1* open reading frame removed resulted in the very same phenotypes. Pathways operating in parallel and/or upstream of DNlg1 and related differentiation processes need to be addressed in future analyses. Our EM analysis showed that planar appositions between presynaptic active zone membranes and postsynaptic membranes, a hallmark of synapse formation, still formed in bouton regions where the postsynaptic assembly largely failed (indicated by a lack of SSR). Thus, consistent with genetic analysis in mammals, at least some fundamental aspects of synapse formation - likely involving the deposition of specific cell adhesion proteins at both pre- and postsynaptic membrane - continue in *dnlg1* mutants.

Structure-function analysis of DNlg1 - relation to Neurexin function

The prominent *in vivo* phenotype that we report for a Nlg-family protein allowed the first mechanistic analysis of this important gene family at the Drosophila NMJ. All evidence, particularly functional rescue analysis, conclusively demonstrated that DNlg1 operates in the postsynaptic muscle compartment. When overexpressed, DNlg1 lacking the cytoplasmic domain (DNlg1-GFP$^{\Delta cyto}$) displayed a drastic dominant negative phenotype. As DNlg1-GFP$^{\Delta cyto}$ was effectively targeted to the NMJ, it appears plausible that it still incorporates into DNlg1 signaling complexes but abrogates their functionality. Thus, apart from ectodomain-mediated interactions to proteins other than DNrx, the cytoplasmic domain seems also essential for the role of DNlg1 complexes in addition of presynaptic boutons. The cytoplasmic interactions of DNlg1 most likely consist of physical links to submembrane scaffold proteins. This is true, at least in part, for Neuroligin-2, which connects to the postsynaptic density proteins gephyrin and collybistin at GABAergic and glycinergic synapses (Poulopoulos et al., 2009). At vertebrate excitatory synapses, similar interactions to postsynaptic scaffolding proteins such as PSD-95 support Nlg function (Irie et al., 1997; Levinson et al., 2005). The fact that DNlg1-GFP$^{\Delta extra}$ (ectodomain deleted) is still localized to type I NMJ terminals and triggers ectopic clusters of postsynaptic proteins further underlines the role of the cytoplasmic domain in mediating protein-protein interactions. Thus, while future mechanistic analysis should also include expression of similar constructs under physiological expression levels, screening for interactions with the loss and gain of function phenotypes is warranted.

Interaction with presynaptic Neurexins is thought to be of prime importance for Nlg function (Sudhof, 2008). However, depending on the assay and context studied, results that conflict with this hypothesis are reported (Ko et al., 2009b). In preliminary cell aggregation and immoprecipitation experiments we were unable to detect direct interaction between DNrx and DNlg1 (data not shown). It thus remains to be shown that DNlg1 interacts with DNrx directly. In principle, DNrx and DNlg1 could be part of larger complexes that might also comprise *Drosophila* homologs of an alternative postsynaptic Neurexin receptor, called LRRTM2 (de Wit et al., 2009; Ko et al., 2009a). Irrespective of the exact nature of the protein-protein interactions, we here present evidence that presynaptic *Drosophila* Neurexin promotes DNlg1 function but is not an absolute prerequisite for it. First, whilst some aspects of the *dnlg1* phenotype are similar to *dnrx* mutant terminals (reduction of bouton numbers, ruffles in active zone, irregular receptor fields), they all are quantifiably less pronounced. Second, the most extreme phenotype (entire boutons lacking postsynaptic differentiation) was absent at *dnrx* terminals. Third, the severity of the *dnlg1* phenotype did not increase upon simultaneous elimination of DNrx, consistent with the idea that both proteins regulate a similar biological process or that DNrx functions are fully mediated via DNlg1.

Endogenous DNlg1 forms discrete clusters close to but not identical with PSD regions. In fact, loss of presynaptic *dnrx* severely reduced the numbers of DNlg1 clusters. DNrx and DNlg1 clusters often appear apposed at corresponding pre- and postsynaptic sites, perhaps defining a new synaptic "compartment". The DNlg1 ectodomain together with the transmembrane region seems to be sufficient for the assembly of DNlg1 clusters, while active signaling seems to depend on the cytoplasmic domain. Neurexin-binding might contribute to this ectodomain-mediated integration, as the dominant-negative effect of DNlg1 overexpression could be suppressed by either blocking DNrx binding by a point mutation or by expressing it in a *dnrx* mutant background (Fig. 8). Taken together, our data imply that presynaptic Neurexin binding promotes accumulation of Neuroligin clusters at the postsynaptic membrane. Loss of this Neurexin-binding activity weakens but does not eliminate Neuroligin signaling.

Experimental Procedures

Genetics

The *dnlg1* alleles F1109, G998, H324, H453, H703, I960, K1132, and K1809 were isolated in an EMS mutagenesis screen (Aberle et al., 2002) employing CD8-GFP-Sh flies (Zito et al., 1999). The *dnlg1* excision alleles were generated by deleting the genomic DNA between two insertion elements carrying FRT-sites (*dnlg1*$^{ex1.9}$ (PBacf00735 and PBacf00756), *dnlg1*$^{ex2.3}$ (PBacf00756 and PXPd00812), *dnlg1*$^{ex3.1}$ (PBacf00735 and PXPd00812)). UAS-FasII, mef2-Gal4, and elav-Gal4 were kind gifts of C. Goodman. OK6-Gal4 has been described (Aberle et al., 2002). The UAS-*dnlg1*-IR RNAi lines (ID42616, ID104209) were obtained from the VDRC stock center (Dietzl et al., 2007). Genetic analysis of *dnrx* was performed using the excision allele *dnrx*^{241} (Li et al., 2007). *dnrx dnlg1* double mutants were generated by meiotic recombination and verified by PCR and complementation analysis. All deficiency lines were ordered from the Bloomington or Harvard stock centers. As wild-type control strains, *w*^{1118} or *w*^{1118};; CD8-GFP-Sh were used.

Cloning and molecular analysis of *dnlg1* and *dnrx*

The EMS induced point mutations formed a complementation group and were mapped to *dnlg1* using available deficiencies, meiotic recombination and single nucleotide polymorphisms. Df(3R)Antp17, Df(3R)dsx29, Df(3R)D7, Df(3R)D6, Df(3R)dsx11 failed to complement the *dnlg1*^{I960} allele, whereas Df(3R)Antp1, Df(3R)Exel614, Df(3R)roe, Df(3R)Scx4 did complement. The *dnlg1* alleles were sequenced on both strands (see Suppl. Experimental Procedures). A full-length *dnlg1* cDNA clone (RE29404) was obtained from DGRC (Stapleton et al., 2002). The *dnlg1* cDNA was used to synthesize three different digoxigenin-labeled sense and antisense probes (Roche) using T3 and T7 polymerases (Ambion). *In situ* hybridizations were performed according to standard protocols (Tautz and Pfeifle, 1989).

Full length DNlg1-GFP was generated by insertion of EGFP between amino acids A865 and L866 (see Suppl. Experimental Procedures). The pUAST-*dnlg1*-GFP vector was used as a template to generate *dnlg1*-GFP$^{\Delta cyto}$ (aa 1 - 865, followed by EGFP) and *dnlg1*-GFP$^{\Delta extra}$ (aa 1 - 741 was deleted and replaced by a cassette containing a signal peptide from rat CD2 followed by 10 myc tags). DNrx-GFP was generated by PCR using cDNA clone LP14275 (Stapleton et al., 2002). EGFP was inserted between amino acids N1748 and T1749 (see Suppl. Experimental Procedures).

Site-directed mutagenesis was performed using the QuickChange XL kit (Stratagene). The D356R exchange corresponds to the mutation D271R in rat Nlg1 (Reissner et al., 2008). All DNlg1 constructs were first subcloned into the entry vector pENTR of the gateway cloning system (Invitrogen) and then transferred into the pUAST*attB* expression vector. DNlg1 transgenic fly strains were generated based on the ϕC31-mediated integration system using the landing site at the cytological position 68E (Bischof et al., 2007).

Antibody production and immunohistochemistry

For the DNlg1 antibody, a rabbit polyclonal serum was raised (Seqlab) against a synthetic peptide (C-QQFQPAPGRSITTNI) representing amino acids 1340-1354 of DNlg1. Wandering third instar larvae were dissected in PBS and fixed for 15 min in 3.7% formaldehyde. Larval fillets were stained as described (Beuchle et al., 2007). Dilutions of primary antibodies used: rabbit anti-Ank2-XL 1:1000 (Koch et al., 2008), rabbit anti-DVGLUT (Mahr and Aberle, 2006), rabbit anti-GluRIIC and GluRIID 1:1000 (Qin et al., 2005), mouse anti-Bruchpilot 1:100 (Wagh et al., 2006), anti-HRP conjugated to Cy5 1:200 (Dianova), mouse anti-Synaptotagmin 1:20 (clone 3H2), and mouse anti-Dlg (clone 4F3; kind gifts of C. Goodman). Fluorescently labeled secondary antibodies conjugated to Alexa488, Alexa568, or Alexa647 (Invitrogen) were diluted 1:1000. Mounted larvae were examined using a LSM510 (Zeiss) confocal laser scanning microscope. DNlg1-Signals were quantified by acquiring 16 Bit confocal images (TCS SP5, Leica Mircosystems) of type Ib boutons (see Suppl. Experimental Procedures for details). For the quantification of GluRIID receptor field size, confocal image stacks (TCS SP5, Leica Microsystem) were analyzed using ImageJ and Bitplane Imaris 6.15 (see Suppl. Experimental Procedures).

Analysis of NMJs

The number of synaptic boutons (type Ib + Is) was quantified on dorsal muscles 1/9 in abdominal segments A3 of intact CD8-GFP-Sh third instar larvae. The approximate muscle surface area was calculated by measuring the width and length of each fiber. Bouton density was defined as the number of boutons per synaptic branch length. Bouton diameter was determined for the largest bouton on muscles 1/9 by measuring the diameter crosswise followed by averaging of the two values.

For *in vivo* imaging, first instar larvae were transferred into a drop of 70% Glycerol/PBS and immobilized by an adequate cover slip. Larvae were transferred singly on yeasted fruit agar plates for recovery and imaging at the third instar stage. Growing synaptic branches were distinguished from non-growing branches by the addition of at least one bouton to a branch present at the LI stage. In vivo imaging of BRP-short-Strawberry (Schmid et al., 2008) was performed as described (Rasse et al., 2005).

Electrophysiology and electron microscopy

TEVC recordings were performed as previously described (Owald et al., 2010). All recordings were performed on muscle 6 of male third instar larvae (segments A2 and A3) in HL3 (70 mM NaCl, 5 mM KCl, 20 mM $MgCl_2$, 10 mM $NaHCO_3$, 5 mM trehalose, 115 mM sucrose, 5 mM Hepes, and 1 mM or 0.5 mM $CaCl_2$, pH 7.2). For electron microscopy, conventional room temperature embedding was performed as described previously (Fouquet et al., 2009).

Acknowledgements

We thank Corey Goodman, David Featherstone, Nicholas Harden, the Bloomington Drosophila Stock Center, the VDRC Stock Center, the Harvard Exelixis Collection, the Developmental Studies Hybridoma Bank, and the *Drosophila* Genome Research Center for providing fly stocks and reagents. We would also like to thank Elke Naffin, Christine Quentin, Franziska Zehe, Anastasia Stawrakakis, and Madeleine Brünner for excellent technical assistance. We are grateful to Christian Klämbt, Bernd Goellner, David Featherstone, and Andrew Plested for discussions and critical comments on the manuscript. This work was supported by grants from the Deutsche Forschungsgemeinschaft to S.J.S. (Exc 257, SFB 665) and H.A. (Ab116/3-2).

References

Aberle, H., Haghighi, A.P., Fetter, R.D., McCabe, B.D., Magalhaes, T.R., and Goodman, C.S. (2002). wishful thinking encodes a BMP type II receptor that regulates synaptic growth in Drosophila. Neuron *33*, 545-558.

Arac, D., Boucard, A.A., Ozkan, E., Strop, P., Newell, E., Sudhof, T.C., and Brunger, A.T. (2007). Structures of neuroligin-1 and the neuroligin-1/neurexin-1 beta complex reveal specific protein-protein and protein-Ca2+ interactions. Neuron *56*, 992-1003.

Atwood, H.L., Govind, C.K., and Wu, C.F. (1993). Differential ultrastructure of synaptic terminals on ventral longitudinal abdominal muscles in Drosophila larvae. J. Neurobiol. *24*, 1008-1024.

Beuchle, D., Schwarz, H., Langegger, M., Koch, I., and Aberle, H. (2007). Drosophila MICAL regulates myofilament organization and synaptic structure. Mech. Dev. *124*, 390-406.

Bischof, J., Maeda, R.K., Hediger, M., Karch, F., and Basler, K. (2007). An optimized transgenesis system for Drosophila using germ-line-specific phiC31 integrases. Proc. Natl. Acad. Sci. U. S. A. *104*, 3312-3317.

Biswas, S., Russell, R.J., Jackson, C.J., Vidovic, M., Ganeshina, O., Oakeshott, J.G., and Claudianos, C. (2008). Bridging the synaptic gap: neuroligins and neurexin I in Apis mellifera. PLoS One *3*, e3542.

Brand, A.H., and Perrimon, N. (1993). Targeted gene expression as a means of altering cell fates and generating dominant phenotypes. Development *118*, 401-415.

Chih, B., Engelman, H., and Scheiffele, P. (2005). Control of excitatory and inhibitory synapse formation by neuroligins. Science *307*, 1324-1328.

Chubykin, A.A., Atasoy, D., Etherton, M.R., Brose, N., Kavalali, E.T., Gibson, J.R., and Sudhof, T.C. (2007). Activity-dependent validation of excitatory versus inhibitory synapses by neuroligin-1 versus neuroligin-2. Neuron *54*, 919-931.

Collins, C.A., and DiAntonio, A. (2007). Synaptic development: insights from Drosophila. Curr. Opin. Neurobiol. *17*, 35-42.

Dalva, M.B., McClelland, A.C., and Kayser, M.S. (2007). Cell adhesion molecules: signalling functions at the synapse. Nat. Rev. Neurosci. *8*, 206-220.

de Wit, J., Sylwestrak, E., O'Sullivan, M.L., Otto, S., Tiglio, K., Savas, J.N., Yates, J.R., 3rd, Comoletti, D., Taylor, P., and Ghosh, A. (2009). LRRTM2 interacts with Neurexin1 and regulates excitatory synapse formation. Neuron *64*, 799-806.

Dean, C., and Dresbach, T. (2006). Neuroligins and neurexins: linking cell adhesion, synapse formation and cognitive function. Trends Neurosci. *29*, 21-29.

Dietzl, G., Chen, D., Schnorrer, F., Su, K.C., Barinova, Y., Fellner, M., Gasser, B., Kinsey, K., Oppel, S., Scheiblauer, S*., et al.* (2007). A genome-wide transgenic RNAi library for conditional gene inactivation in Drosophila. Nature *448*, 151-156.

Dresbach, T., Neeb, A., Meyer, G., Gundelfinger, E.D., and Brose, N. (2004). Synaptic targeting of neuroligin is independent of neurexin and SAP90/PSD95 binding. Mol. Cell. Neurosci. *27*, 227-235.

Drysdale, R. (2008). FlyBase : a database for the Drosophila research community. Methods Mol. Biol. *420*, 45-59.

Fabrichny, I.P., Leone, P., Sulzenbacher, G., Comoletti, D., Miller, M.T., Taylor, P., Bourne, Y., and Marchot, P. (2007). Structural analysis of the synaptic protein neuroligin and its beta-neurexin complex: determinants for folding and cell adhesion. Neuron *56*, 979-991.

Featherstone, D.E., Rushton, E., Rohrbough, J., Liebl, F., Karr, J., Sheng, Q., Rodesch, C.K., and Broadie, K. (2005). An essential Drosophila glutamate receptor subunit that functions in both central neuropil and neuromuscular junction. J. Neurosci. *25*, 3199-3208.

Fouquet, W., Owald, D., Wichmann, C., Mertel, S., Depner, H., Dyba, M., Hallermann, S., Kittel, R.J., Eimer, S., and Sigrist, S.J. (2009). Maturation of active zone assembly by Drosophila Bruchpilot. J. Cell Biol. *186*, 129-145.

Gilbert, M.M., and Auld, V.J. (2005). Evolution of clams (cholinesterase-like adhesion molecules): structure and function during development. Front. Biosci. *10*, 2177-2192.

Graf, E.R., Zhang, X., Jin, S.X., Linhoff, M.W., and Craig, A.M. (2004). Neurexins induce differentiation of GABA and glutamate postsynaptic specializations via neuroligins. Cell *119*, 1013-1026.

Grenningloh, G., Rehm, E.J., and Goodman, C.S. (1991). Genetic analysis of growth cone guidance in Drosophila: fasciclin II functions as a neuronal recognition molecule. Cell *67*, 45-57.

Griffith, L.C., and Budnik, V. (2006). Plasticity and second messengers during synapse development. Int. Rev. Neurobiol. *75*, 237-265.

Hoang, B., and Chiba, A. (2001). Single-cell analysis of Drosophila larval neuromuscular synapses. Dev. Biol. *229*, 55-70.

Hoon, M., Bauer, G., Fritschy, J.M., Moser, T., Falkenburger, B.H., and Varoqueaux, F. (2009). Neuroligin 2 controls the maturation of GABAergic synapses and information processing in the retina. J. Neurosci. *29*, 8039-8050.

Ichtchenko, K., Hata, Y., Nguyen, T., Ullrich, B., Missler, M., Moomaw, C., and Sudhof, T.C. (1995). Neuroligin 1: a splice site-specific ligand for beta-neurexins. Cell *81*, 435-443.

Ichtchenko, K., Nguyen, T., and Sudhof, T.C. (1996). Structures, alternative splicing, and neurexin binding of multiple neuroligins. J. Biol. Chem. *271*, 2676-2682.

Irie, M., Hata, Y., Takeuchi, M., Ichtchenko, K., Toyoda, A., Hirao, K., Takai, Y., Rosahl, T.W., and Sudhof, T.C. (1997). Binding of neuroligins to PSD-95. Science *277*, 1511-1515.

Jamain, S., Quach, H., Betancur, C., Rastam, M., Colineaux, C., Gillberg, I.C., Soderstrom, H., Giros, B., Leboyer, M., Gillberg, C., and Bourgeron, T. (2003). Mutations of the X-linked genes encoding neuroligins NLGN3 and NLGN4 are associated with autism. Nat. Genet. *34*, 27-29.

Jia, X.X., Gorczyca, M., and Budnik, V. (1993). Ultrastructure of neuromuscular junctions in Drosophila: comparison of wild type and mutants with increased excitability. J. Neurobiol. *24*, 1025-1044.

Ko, J., Fuccillo, M.V., Malenka, R.C., and Sudhof, T.C. (2009a). LRRTM2 functions as a neurexin ligand in promoting excitatory synapse formation. Neuron *64*, 791-798.

Ko, J., Zhang, C., Arac, D., Boucard, A.A., Brunger, A.T., and Sudhof, T.C. (2009b). Neuroligin-1 performs neurexin-dependent and neurexin-independent functions in synapse validation. EMBO J. *28*, 3244-3255.

Koch, I., Schwarz, H., Beuchle, D., Goellner, B., Langegger, M., and Aberle, H. (2008). Drosophila ankyrin 2 is required for synaptic stability. Neuron *58*, 210-222.

Laumonnier, F., Bonnet-Brilhault, F., Gomot, M., Blanc, R., David, A., Moizard, M.P., Raynaud, M., Ronce, N., Lemonnier, E., Calvas, P.*, et al.* (2004). X-linked mental retardation and autism are associated with a mutation in the NLGN4 gene, a member of the neuroligin family. Am. J. Hum. Genet. *74*, 552-557.

Levinson, J.N., Chery, N., Huang, K., Wong, T.P., Gerrow, K., Kang, R., Prange, O., Wang, Y.T., and El-Husseini, A. (2005). Neuroligins mediate excitatory and inhibitory synapse formation: involvement of PSD-95 and neurexin-1beta in neuroligin-induced synaptic specificity. J. Biol. Chem. *280*, 17312-17319.

Li, J., Ashley, J., Budnik, V., and Bhat, M.A. (2007). Crucial role of Drosophila neurexin in proper active zone apposition to postsynaptic densities, synaptic growth, and synaptic transmission. Neuron *55*, 741-755.

Lise, M.F., and El-Husseini, A. (2006). The neuroligin and neurexin families: from structure to function at the synapse. Cell. Mol. Life Sci. *63*, 1833-1849.

Lnenicka, G.A., and Mellon, D., Jr. (1983). Changes in electrical properties and quantal current during growth of identified muscle fibres in the crayfish. J Physiol *345*, 261-284.

Mahr, A., and Aberle, H. (2006). The expression pattern of the Drosophila vesicular glutamate transporter: A marker protein for motoneurons and glutamatergic centers in the brain. Gene Expr. Patterns *6*, 299-309.

Missler, M., Zhang, W., Rohlmann, A., Kattenstroth, G., Hammer, R.E., Gottmann, K., and Sudhof, T.C. (2003). Alpha-neurexins couple Ca2+ channels to synaptic vesicle exocytosis. Nature *423*, 939-948.

Owald, D., Fouquet, W., Schmidt, M., Wichmann, C., Mertel, S., Depner, H., Christiansen, F., Zube, C., Quentin, C., Korner, J.*, et al.* (2010). A Syd-1 homologue regulates pre- and postsynaptic maturation in Drosophila. J. Cell Biol. *188*, 565-579.

Poulopoulos, A., Aramuni, G., Meyer, G., Soykan, T., Hoon, M., Papadopoulos, T., Zhang, M., Paarmann, I., Fuchs, C., Harvey, K.*, et al.* (2009). Neuroligin 2 drives postsynaptic assembly at perisomatic inhibitory synapses through gephyrin and collybistin. Neuron *63*, 628-642.

Qin, G., Schwarz, T., Kittel, R.J., Schmid, A., Rasse, T.M., Kappei, D., Ponimaskin, E., Heckmann, M., and Sigrist, S.J. (2005). Four different subunits are essential for expressing the synaptic glutamate receptor at neuromuscular junctions of Drosophila. J. Neurosci. *25*, 3209-3218.

Rasse, T.M., Fouquet, W., Schmid, A., Kittel, R.J., Mertel, S., Sigrist, C.B., Schmidt, M., Guzman, A., Merino, C., Qin, G.*, et al.* (2005). Glutamate receptor dynamics organizing synapse formation in vivo. Nat. Neurosci. *8*, 898-905.

Reissner, C., Klose, M., Fairless, R., and Missler, M. (2008). Mutational analysis of the neurexin/neuroligin complex reveals essential and regulatory components. Proc. Natl. Acad. Sci. U. S. A. *105*, 15124-15129.

Sara, Y., Biederer, T., Atasoy, D., Chubykin, A., Mozhayeva, M.G., Sudhof, T.C., and Kavalali, E.T. (2005). Selective capability of SynCAM and neuroligin for functional synapse assembly. J. Neurosci. *25*, 260-270.

Scheiffele, P., Fan, J., Choih, J., Fetter, R., and Serafini, T. (2000). Neuroligin expressed in nonneuronal cells triggers presynaptic development in contacting axons. Cell *101*, 657-669.

Schmid, A., Hallermann, S., Kittel, R.J., Khorramshahi, O., Frolich, A.M., Quentin, C., Rasse, T.M., Mertel, S., Heckmann, M., and Sigrist, S.J. (2008). Activity-dependent site-specific changes of glutamate receptor composition in vivo. Nat. Neurosci. *11*, 659-666.

Schmid, A., Qin, G., Wichmann, C., Kittel, R.J., Mertel, S., Fouquet, W., Schmidt, M., Heckmann, M., and Sigrist, S.J. (2006). Non-NMDA-type glutamate receptors are essential for maturation but not for initial assembly of synapses at Drosophila neuromuscular junctions. J. Neurosci. *26*, 11267-11277.

Song, J.Y., Ichtchenko, K., Sudhof, T.C., and Brose, N. (1999). Neuroligin 1 is a postsynaptic cell-adhesion molecule of excitatory synapses. Proc. Natl. Acad. Sci. U. S. A. *96*, 1100-1105.

Stapleton, M., Liao, G., Brokstein, P., Hong, L., Carninci, P., Shiraki, T., Hayashizaki, Y., Champe, M., Pacleb, J., Wan, K*., et al.* (2002). The Drosophila gene collection: identification of putative full-length cDNAs for 70% of D. melanogaster genes. Genome Res. *12*, 1294-1300.

Sudhof, T.C. (2008). Neuroligins and neurexins link synaptic function to cognitive disease. Nature *455*, 903-911.

Takeichi, M. (2007). The cadherin superfamily in neuronal connections and interactions. Nat. Rev. Neurosci. *8*, 11-20.

Tautz, D., and Pfeifle, C. (1989). A non-radioactive in situ hybridization method for the localization of specific RNAs in Drosophila embryos reveals translational control of the segmentation gene hunchback. Chromosoma *98*, 81-85.

Ushkaryov, Y.A., Petrenko, A.G., Geppert, M., and Sudhof, T.C. (1992). Neurexins: synaptic cell surface proteins related to the alpha-latrotoxin receptor and laminin. Science *257*, 50-56.

Varoqueaux, F., Aramuni, G., Rawson, R.L., Mohrmann, R., Missler, M., Gottmann, K., Zhang, W., Sudhof, T.C., and Brose, N. (2006). Neuroligins determine synapse maturation and function. Neuron *51*, 741-754.

Wagh, D.A., Rasse, T.M., Asan, E., Hofbauer, A., Schwenkert, I., Dürrbeck, H., Buchner, S., Dabauvalle, M.C., Schmidt, M., Qin, G*., et al.* (2006). Bruchpilot, a protein with homology to ELKS/CAST, is required for structural integrity and function of synaptic active zones in Drosophila. Neuron *49*, 833-844.

Washbourne, P., Dityatev, A., Scheiffele, P., Biederer, T., Weiner, J.A., Christopherson, K.S., and El-Husseini, A. (2004). Cell adhesion molecules in synapse formation. J. Neurosci. *24*, 9244-9249.

Wittenmayer, N., Korber, C., Liu, H., Kremer, T., Varoqueaux, F., Chapman, E.R., Brose, N., Kuner, T., and Dresbach, T. (2009). Postsynaptic Neuroligin1 regulates presynaptic maturation. Proc. Natl. Acad. Sci. U. S. A. *106*, 13564-13569.

Yamagata, M., Sanes, J.R., and Weiner, J.A. (2003). Synaptic adhesion molecules. Curr. Opin. Cell Biol. *15*, 621-632.

Zeng, X., Sun, M., Liu, L., Chen, F., Wei, L., and Xie, W. (2007). Neurexin-1 is required for synapse formation and larvae associative learning in Drosophila. FEBS Lett. *581*, 2509-2516.

Zito, K., Parnas, D., Fetter, R.D., Isacoff, E.Y., and Goodman, C.S. (1999). Watching a synapse grow: noninvasive confocal imaging of synaptic growth in Drosophila. Neuron *22*, 719-729.

Figure legends

Fig. 1:

Mutations in *Drosophila neuroligin 1* (*dnlg1*) cause smaller neuromuscular junctions (NMJs).

(A-C) Confocal micrographs of NMJs labeled with the postsynaptic marker CD8-GFP-Sh. (A) Wild-type NMJs on dorsal muscle pairs 1/9 (upper arrow) and 2/10 (lower arrow). (B) NMJs on muscles 1/9 and 2/10 are clearly smaller in $dnlg1^{I960}/dnlg1^{H324}$ mutant larvae. (C) Larvae transheterozygous for an excision allele and an EMS allele ($dnlg1^{ex2.3}/dnlg1^{I960}$) show a similar NMJ phenotype.

(D-E) Genomic locus of *dnlg1* (CG31146). (D) Exons are color coded according to the protein domains they encode. Positions of insertion elements, and dimensions of resulting excisions are indicated. Combining ex1.9 and ex3.1 specifically removes only *dnlg1*. (E) The *dnlg1* locus encodes a 1354 aa protein comprising a signal peptide (SP), an acetylcholinesterase-like domain (AChE), a transmembrane domain (TMD) and a C-terminal PDZ domain-binding motif. The EMS induced point mutations in the respective alleles are indicated. SSM indicates a splice site mutation.

(F-H) Morphometric analysis of *dnlg1* mutant NMJs on muscles 1/9. (F) Quantification of the bouton number adjusted to the muscle surface area in wild-type and several *dnlg1* mutant genotypes, as indicated. (G) Quantification of bouton number per 10 µm synaptic branch length. Bouton density is decreased in *dnlg1* mutants. (H) Quantification of the average diameter of the largest bouton in a given terminal. Data shown are means ± SEM; n=40 hemisegments; asterisks: $p \leq 0.001$ (Mann-Whitney-U-Test).

(I-J) Identified wild-type NMJs innervating muscles 1/9 imaged at the first (I) and third (J) instar stage in the same animal. Synaptic boutons are constantly added to existing synaptic branches (identified by numbered arrowheads).

(K-L) NMJs on dorsal muscles 1/9 of a $dnlg1^{I960}$ mutant larva at the first (K) and third (L) instar stage. Very few boutons are added.

Scale bars: 50 µm (A), 20 µm (I-J). See also Suppl. Figs S1 and S2.

Fig. 2:

Fewer synapses and reduced evoked excitatory current amplitudes at *dnlg1* mutant NMJs.

(A) Synapse numbers are strongly reduced in *dnlg1* mutants. Synapses on muscle 6 of control (black) and *dnlg1*^{I960}/*dnlg1*^{H324} mutant (grey) larvae were labeled with anti-BRP and anti-GluRIID antibodies. Synapses were counted using Imaris software.

(B-D) Electrophysiological analysis of control and *dnlg1* mutant NMJs on muscles 6/7 of third instar larvae. (B) Left panel shows representative traces of the amplitudes of evoked excitatory junctional currents (eEJC; in nA) at 1 mM extracellular Ca^{2+} concentration. Right panel: Bar graphs of mean eEJC amplitudes. (C) Bar graphs of mean eEJC amplitudes at 0.5 mM extracellular Ca^{2+} concentration. (D) Left panel shows representative traces of miniature excitatory junctional currents (mEJC). Right panel: Bar graphs of mean values of mEJC amplitudes. Controls: CD8-GFP-Sh/mef2-Gal4, CD8-GFP-Sh; mutants: CD8-GFP-Sh, mef2-Gal4, *dnlg1*^{H324} /CD8-GFP-Sh, *dnlg1*^{I960}. Error bars: SEM. Asterisks: $p \leq 0.01$ (Mann-Whitney-U-Test).

Fig. 3:

Fully differentiated presynaptic boutons are not apposed by postsynaptic specializations in *dnlg1* mutants.

(A-D) Wild-type NMJs on muscles 1/9 (A, C) compared to *dnlg1*^{I960}/Df(3R)Dsx29 mutant NMJs (B, D). The overviews (A, B) highlight the presynaptic markers Synaptotagmin (Syt, green) and Ankyrin 2 (Ank2, red), and the postsynaptic marker CD8-GFP-Sh (blue). Boxed regions are enlarged. (C) Synaptotagmin labels synaptic vesicles accumulating in presynaptic boutons. Ankyrin 2 forms a cytoskeletal lattice that is typically unfolded in major boutons. CD8-GFP-Sh reveals the outline of the postsynaptic subsynaptic reticulum. Merged images show that postsynaptic regions are normally strictly opposed to presynaptic boutons at wild-type NMJs. (D) Fully differentiated presynaptic regions of *dnlg1* mutant NMJs not apposed by postsynaptic domains (compare arrows in (D)).

(E-F) *In vivo* image of identified NMJs in wild-type and *dnlg1*^{I960}/*dnlg1*^{H324} mutant third instar larvae at two different time points. Active zones are labeled with a fluorescently tagged fragment of BRP (BRP-short-Strawberry, green) and SSR membranes with CD8-GFP-Sh (red). (E) At control NMJs, all BRP-positive puncta develop in the postsynaptic zone within a 24h time interval. (F) Imaging of *dnlg1* mutant NMJs within a 24h time interval reveals continuous clustering of presynaptic active zone material in boutons lacking postsynaptic markers (arrows in (F)).

Scale bars: 30 µm (A), 10 µm (C), and 5 µm (E).

Fig. 4:

Misalignment of presynaptic transmitter release sites and postsynaptic glutamate receptor fields in *dnlg1* mutants.

(A-B) Wild-type (A) and *dnlg1*$^{ex1.9}$*/dnlg1*$^{ex2.3}$ mutant (B) NMJs stained with antibodies recognizing neuronal plasma membrane (HRP), active zone marker Bruchpilot (BRP), and glutamate receptor subunit GluRIID. The merged image in (B) shows presynaptic AZs not apposed to postsynaptic receptor fields (arrows).

(C-G) Wild-type (C) and *dnlg1* mutant boutons (D-G) triple labeled with antibodies recognizing BRP, GluRIID, and HRP. In *dnlg1*$^{ex1.9}$*/dnlg1*$^{ex2.3}$ mutant boutons, a subset of AZs are not apposed by corresponding glutamate receptors (arrows in (D) and (E)). Orphan boutons, presynaptic boutons entirely lacking postsynaptic GluRs, occur only in *dnlg1* mutants, irrespective of the alleles used (*dnlg1*$^{ex1.9}$*/dnlg1*$^{ex2.3}$ in (F), *dnlg1*^{I960}*/dnlg1*^{H324} in (G)).

(H) Quantification of orphan boutons and AZs unapposed by receptor fields in controls and two allelic *dnlg1* combinations. While orphan boutons are not found in controls, approximately 8.2% of presynaptic boutons on muscle 4 completely lack apposed GluRs in *dnlg1*^{I960}/*dnlg1*^{H324} mutants. Unapposed AZs occurred with a frequency of 15.7%.

Scale bar in (B): 5 µm. See also Suppl. Figs. S3 and S4.

Fig. 5:

Electron micrographs reveal postsynaptic differentiation defects and synaptic membrane detachments in *dnlg1* mutant boutons.

(A-C) Electron micrographs of control (A) and *dnlg1*^{I960}/*dnlg1*^{H324} (B-C) boutons on muscle 6. Active zones with T-bars are marked (arrowheads). (C) Active zone (arrowheads) not surrounded by SSR but facing contractile muscle filaments.

(D-F) Active zones in wild-type (D) and *dnlg1*^{I960}/*dnlg1*^{H324} mutant (E-F) boutons. Active zones are characterized by parallel alignment and close apposition of pre- and postsynaptic membranes

(arrowheads). (E-F) Presynaptic plasma membranes frequently detach from the dense material in the synaptic cleft forming membrane ruffles (arrows). Scale bars 500 nm (C), 200 nm (F).

(G-I) Quantification of ultrastructural parameters in control (w^{1118}, black) and $dnlg1^{I960}/dnlg1^{H324}$ (grey) NMJs. (G) The relative SSR area is reduced in *dnlg1* mutants. (H) The number of membrane ruffles in active zones is strongly increased in *dnlg1* mutants (I) The distance of these ruffles to the center of the T-bar is unchanged. Error bars: SEM, asterisks: p≤0.01 (students t-test).

Fig. 6:

DNlg1 localizes in discrete spots adjacent to postsynaptic glutamate receptors.

(A-B) *In situ* hybridizations labeling *dnlg1* mRNA in wild-type embryos at stage 14. (A) Lateral view showing *dnlg1* expression in differentiating myoblasts (arrow). (B) Ventral view showing expression in developing muscle fibers (arrow) but not in the ventral nerve cord (arrowhead: ventral midline).

(C-J) Confocal micrographs of NMJs (muscle 4) labeled by CD8-GFP-Sh and anti-DNlg1 staining. (C-D) DNlg1 antiserum recognizes a punctate pattern at wild-type but not at $dnlg1^{I960}$/Df(3R)Dsx29 mutant NMJs (E-F). (G-H) Control NMJs expressing UAS-*dnlg1*-IR in all postmitotic neurons using elav-Gal4. DNlg1 is still expressed and NMJs appear normal. (I-J) NMJs of a wild-type larva expressing UAS-*dnlg1*-IR specifically in muscles using mef2-Gal4. The postsynaptic RNAi effect abolishes the expression of DNlg1 and provokes smaller NMJs.

(K-L) Wild-type NMJs stained with anti-DNlg1 and anti-GluRIID antibodies. DNlg1 shows a punctate pattern (L) that is adjacent to postsynaptic glutamate receptors (inset in (K)). (M-N) Control NMJs stained with anti-DNlg1 and anti-BRP antibodies. Postsynaptic DNlg1 punctae (N) localize adjacent to presynaptic BRP punctae (inset in (M)).

Scale bars: 50 µm (A), 20 µm (C), 5 µm (M). See also Suppl. Fig. S5.

Fig. 7:

DNlg1 is functionally required in muscles and induces the differentiation of postsynaptic domains.

(A) Schematic representation of N- and C-terminal deletion constructs of DNlg1-GFP.

(B-G) Genetic rescue experiments. Compared to *dnlg1*^{I960}/*dnlg1*^{H324} mutants (C), expression of DNlg1-GFP under control of elav-Gal4 failed to rescue the NMJ phenotypes (D). Postsynaptic expression, however, using mef2-Gal4, rescued NMJ size (E). Both DNlg1-GFP$^{\Delta extra}$ and DNlg1-GFP$^{\Delta cyto}$ failed to rescue *dnlg1* mutant NMJs when expressed in muscles (F-G). All rescue experiments were performed in *dnlg1*^{I960}/*dnlg1*^{H324} mutants expressing the CD8-GFP-Sh transgene.

(H-J) Overexpression of DNlg1-GFP (H) and DNlg1-GFP$^{\Delta extra}$ (I) in muscles of wild-type larvae using a recombinant mef2-Gal4, CD8-GFP-Sh line had no effect on NMJ size. (J) Expression of DNlg1-GFP$^{\Delta cyto}$ under control of mef2-Gal4 strongly inhibited synaptic growth.

(K-L) Quantification of bouton numbers at NMJs on muscles 1/9 in rescue (K) and overexpression (L) experiments of the indicated genotypes. Bouton numbers in control and *dnlg1*^{I960}/*dnlg1*^{H324} mutant larvae are shown for comparison. Error bar: SEM; n.s.: not significant; asterisks (**): p≤0.01 (Mann-Whitney-U-Test).

(M-P) The cytoplasmic domain of DNlg1 recruits Dlg, a marker for the postsynaptic SSR that normally surrounds type I but not type II boutons. Fasciclin II (M), DNlg1-GFP (N), DNlg1-GFP$^{\Delta cyto}$ (O), and DNlg1-GFP$^{\Delta extra}$ (P) were expressed in muscles using mef2-Gal4. NMJs were stained with anti-HRP, anti-Dlg, and either anti-DNlg1 (M) or anti-GFP (N-P) antibodies. Type II boutons are visualized by HRP. (M) The synaptic adhesion protein FasII is unable to recruit Dlg into type II boutons (arrows). (N) DNlg1-GFP accumulates at type I and type II boutons and ectopically recruits Dlg into type II boutons (arrows). (O) DNlg1-GFP$^{\Delta cyto}$ is also expressed at type II boutons but fails to recruit Dlg (arrows). (P) DNlg1-GFP$^{\Delta extra}$ enriches at type I but not type II boutons, and is found in cytoplasmic granulae also positive for ectopic Dlg (arrows).

Scale bars: 50 µm (B), 10 µm (M).

Fig. 8:

Role of DNrx for DNlg1 signaling.

(A-D) Comparison of NMJs on muscles 1/9 in wild-type CD8-GFP-Sh (A), *dnrx*^{241}/Df(3R)Exel6191 (B), *dnlg1*^{I960}/*dnlg1*^{H324} (C), and *dnlg1*^{I960}, *dnrx*^{241}/*dnlg1*^{H324}, Df(3R)Exel6191 (D) mutant larvae. Compared to wild-type controls, NMJ size is reduced in *dnlg1* and *dnrx* mutant larvae, while bouton spacing is affected only in *dnlg1* mutants. NMJ size is not further decreased in *dnlg1 dnrx* double mutants.

(E) Quantification of bouton numbers (muscles 1/9) in the indicated genotypes. Error bars: SEM, n.s.: not significant, asterisks (***): p≤0.001 (Mann-Whitney-U-Test).

(F-G) Overexpression of full-length DNlg1 at high levels using mef2-Gal4 induces a dominant-negative NMJ phenotype, with bouton numbers clearly reduced (F). Overexpression of a DNlg1 construct carrying a point mutation predicted to abolish DNrx-binding does not reduce the size of NMJs (G). Both constructs were expressed from in the same genomic insertion site. For quantification see (J).

(H-I) Genetic rescue experiments using mef2-Gal4 to express full-length DNlg1 at high levels improves but does not fully rescue the *dnlg1* mutant phenotype (H). The mutant NMJ phenotype, however, is fully rescued by the construct carrying the D356R point mutation (I). For quantification see (K).

(L) Presynaptic DNrx-GFP, expressed in motoneurons of $dnrx^{241}$/Df(3R)Exel6191 mutants using OK6-Gal4, localizes in apposition to postsynaptic DNlg1 clusters. NMJs were stained with anti-GFP and anti-DNlg1 antibodies.

(M-N) Endogenous DNlg1 fails to cluster adjacent to postsynaptic glutamate receptor fields in the absence of DNrx. NMJs in wild-type (M) and $dnrx^{241}$/Df(3R)Exel6191 mutants (N) stained with anti-GluRIID and anti-DNlg1 antibodies. Postsynaptic DNlg1 clusters are no longer observed.

Scale bar: 50 µm (A). See Suppl. Figs. S6-S8.

Figure 1.) Banovic et al., 2010

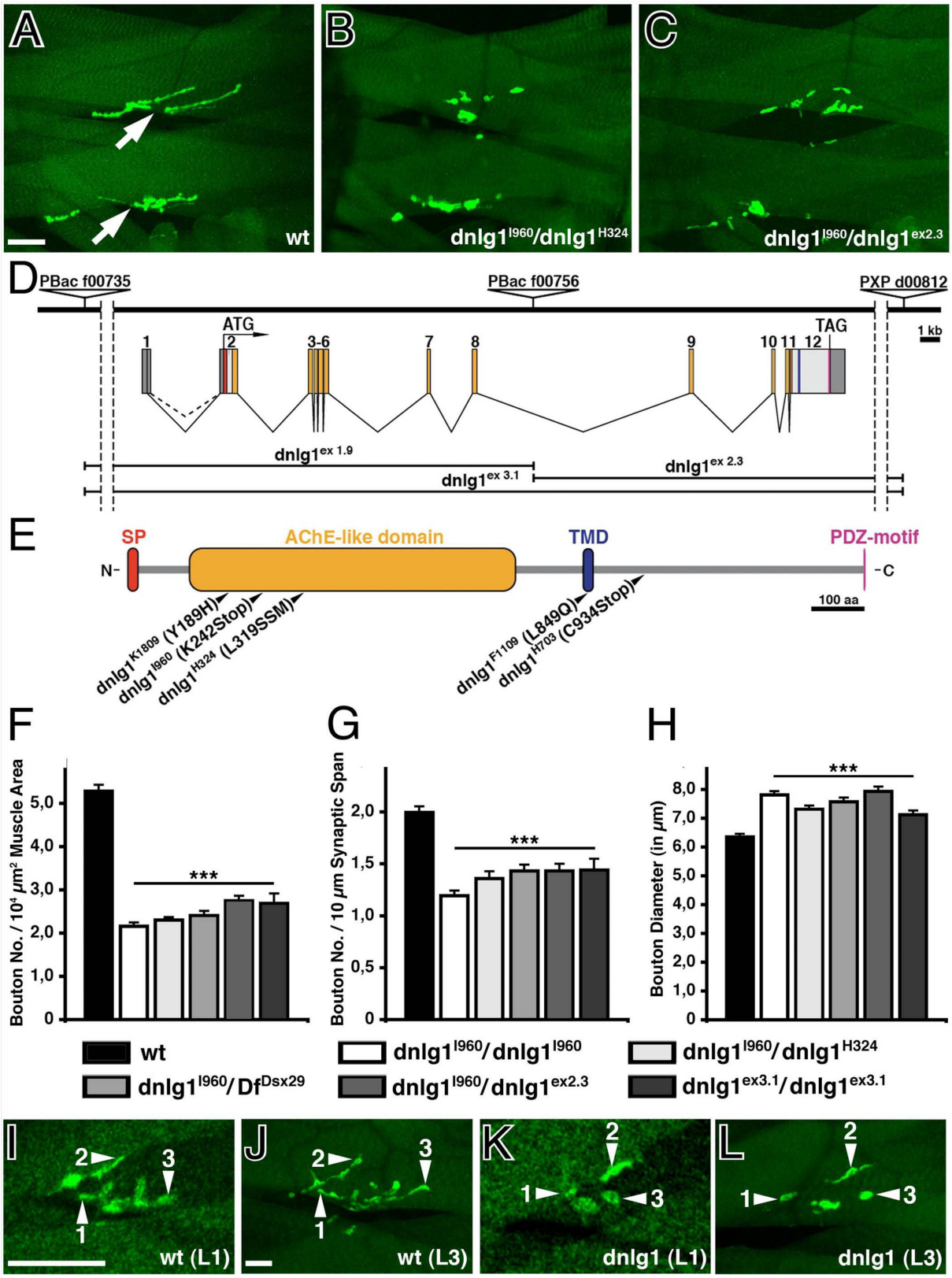

Figure 2.) Banovic et al., 2010

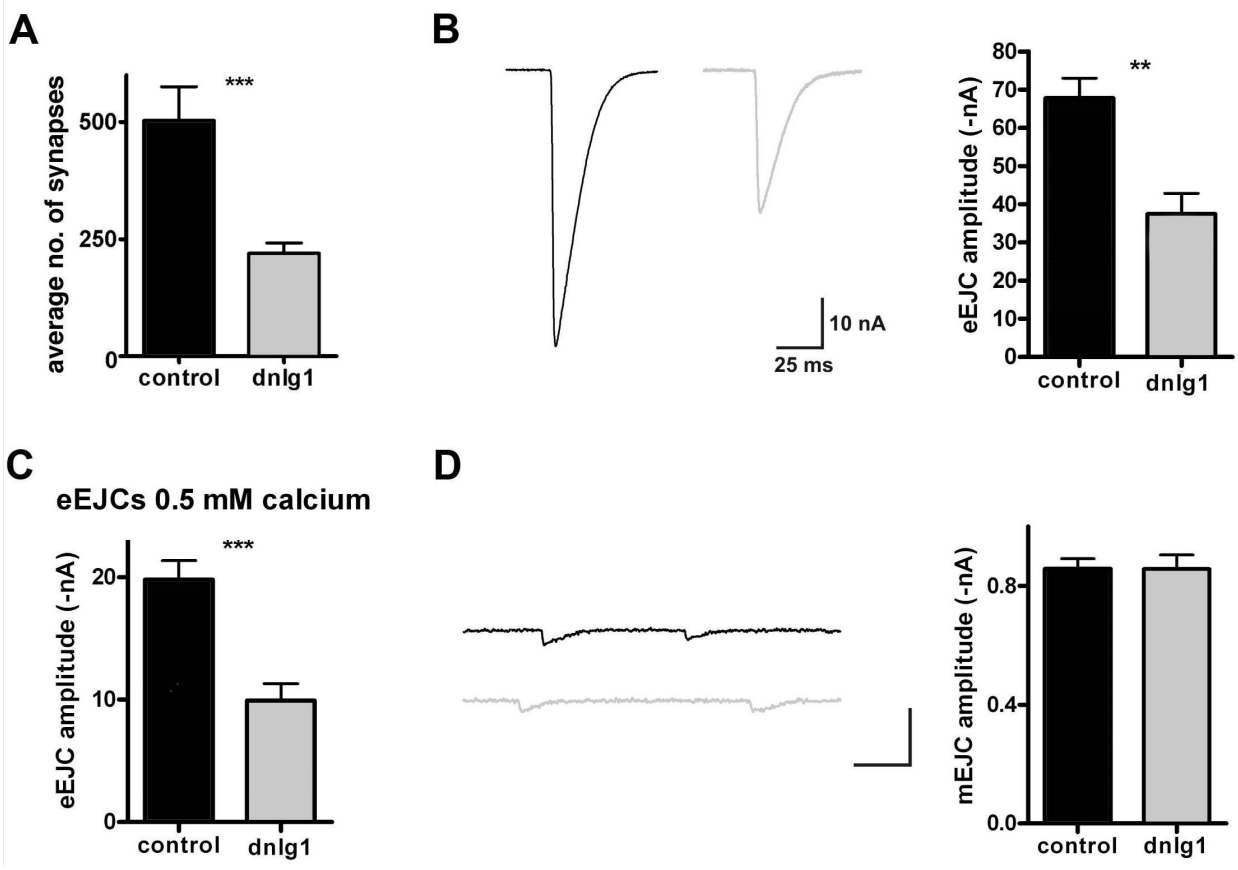

Figure 3.) Banovic et al., 2010

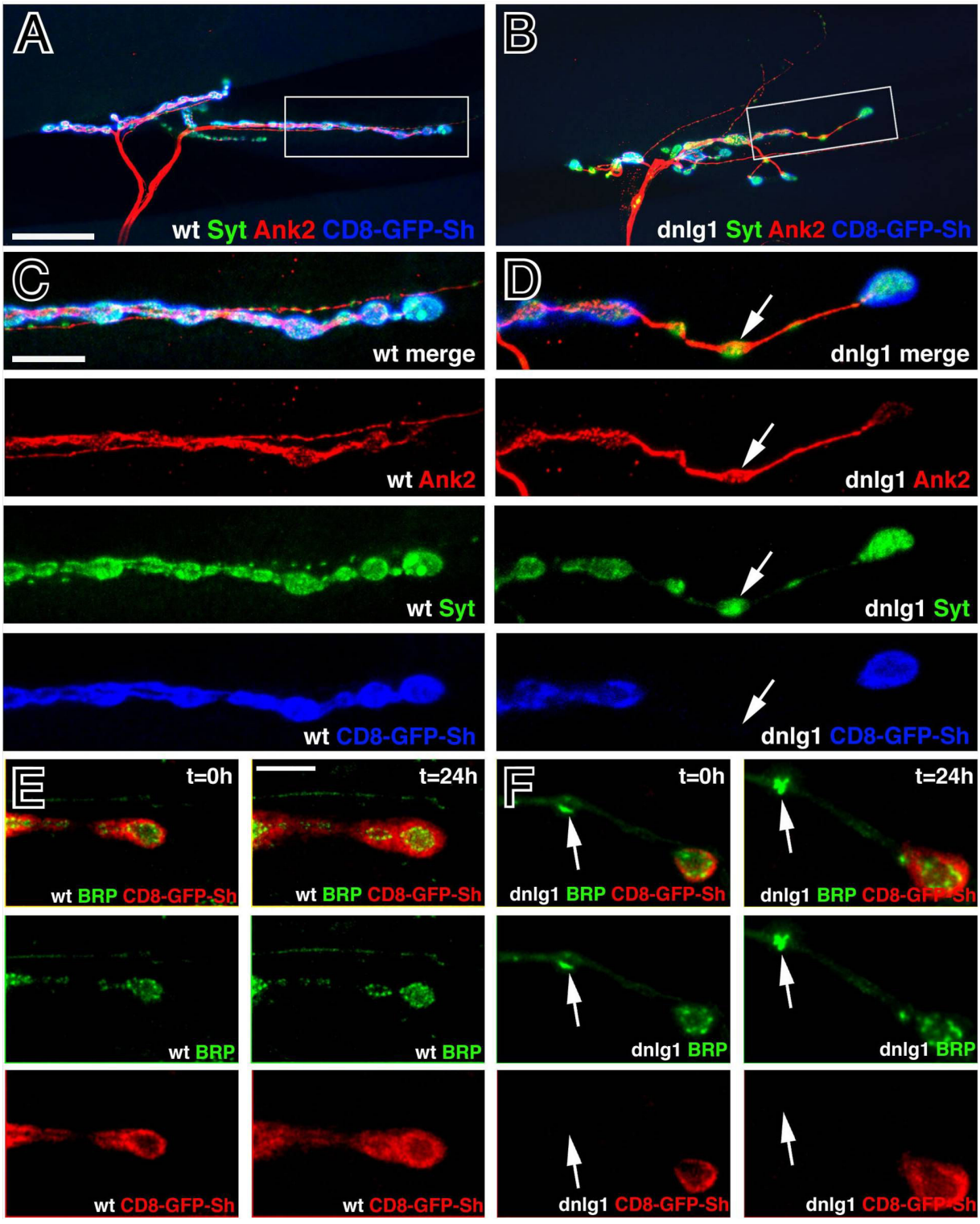

Figure 4.) Banovic et al., 2010

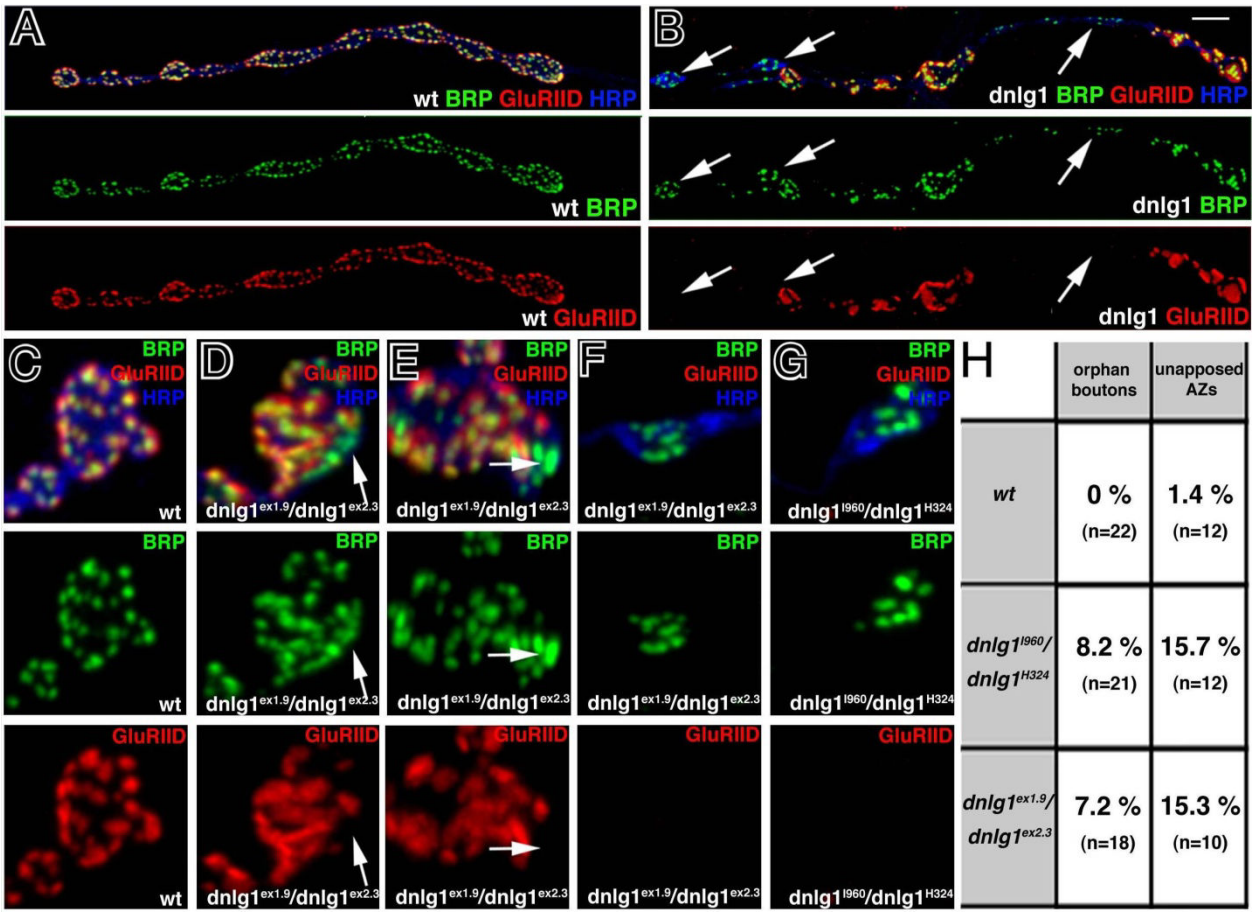

	orphan boutons	unapposed AZs
wt	0 % (n=22)	1.4 % (n=12)
dnlg1^{I960}/ dnlg1^{H324}	8.2 % (n=21)	15.7 % (n=12)
dnlg1$^{ex1.9}$/ dnlg1$^{ex2.3}$	7.2 % (n=18)	15.3 % (n=10)

Figure 5.) Banovic et al., 2010

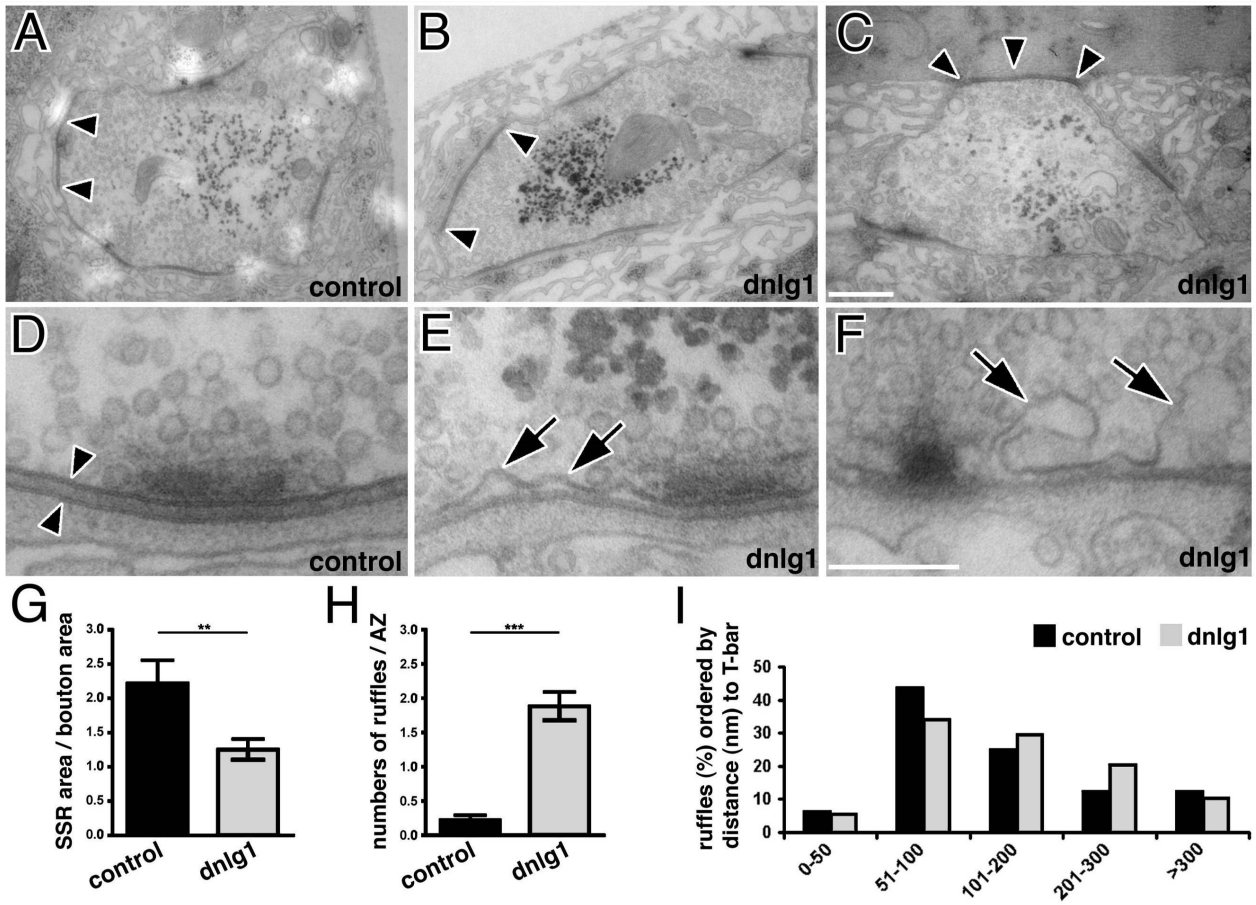

Figure 6.) Banovic et al., 2010

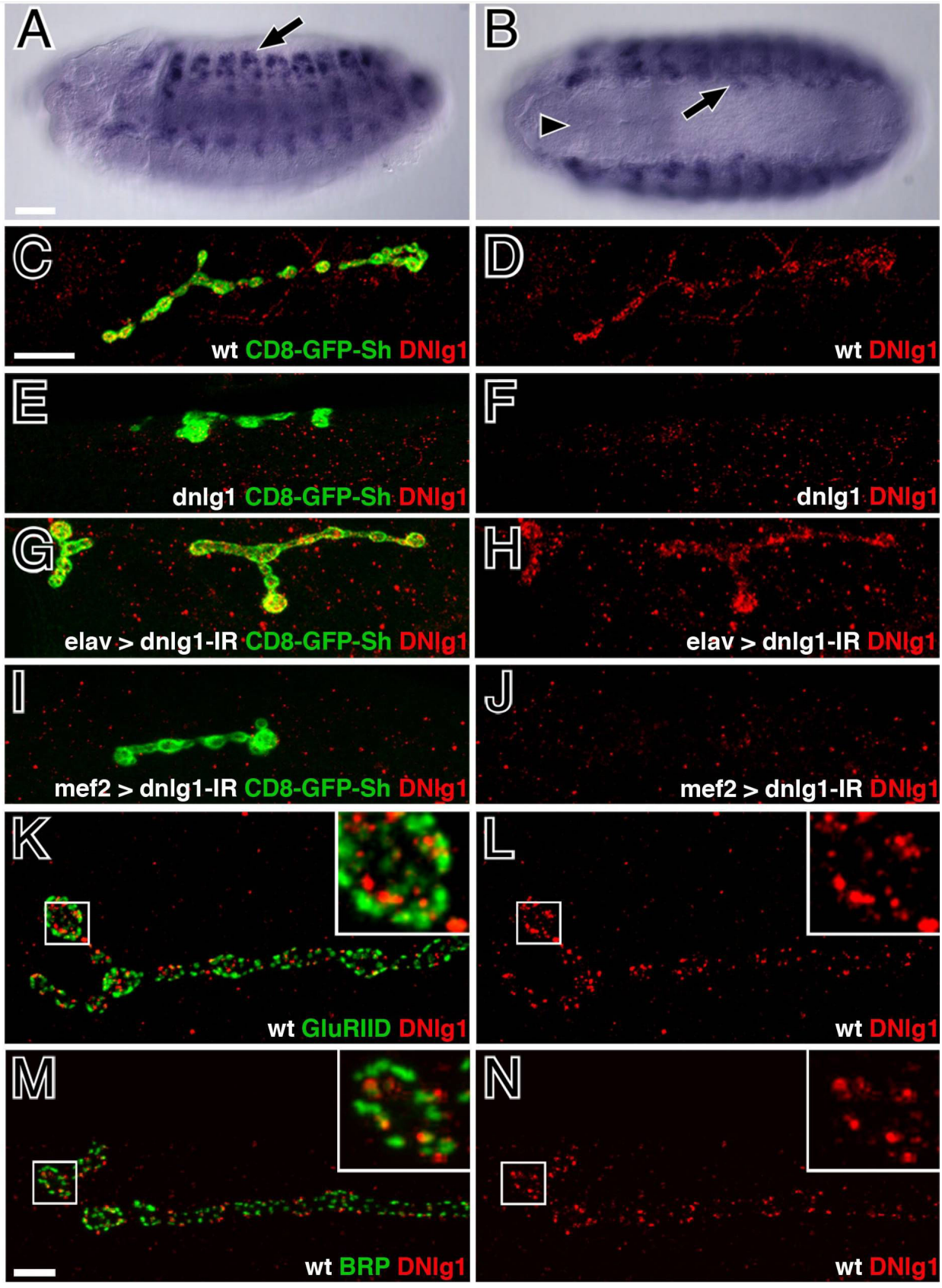

Figure 7.) Banovic et al., 2010

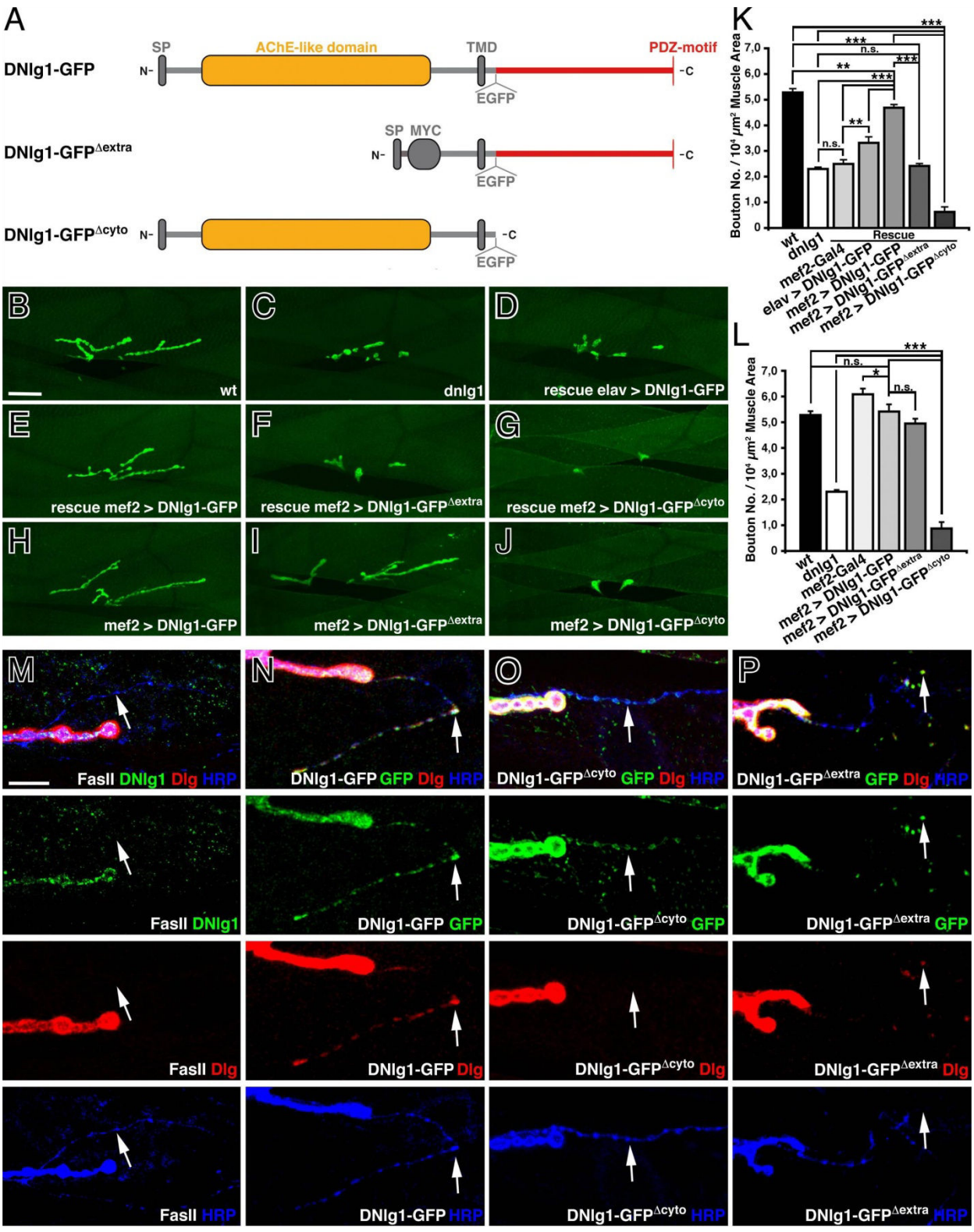

Figure 8.) Banovic et al., 2010

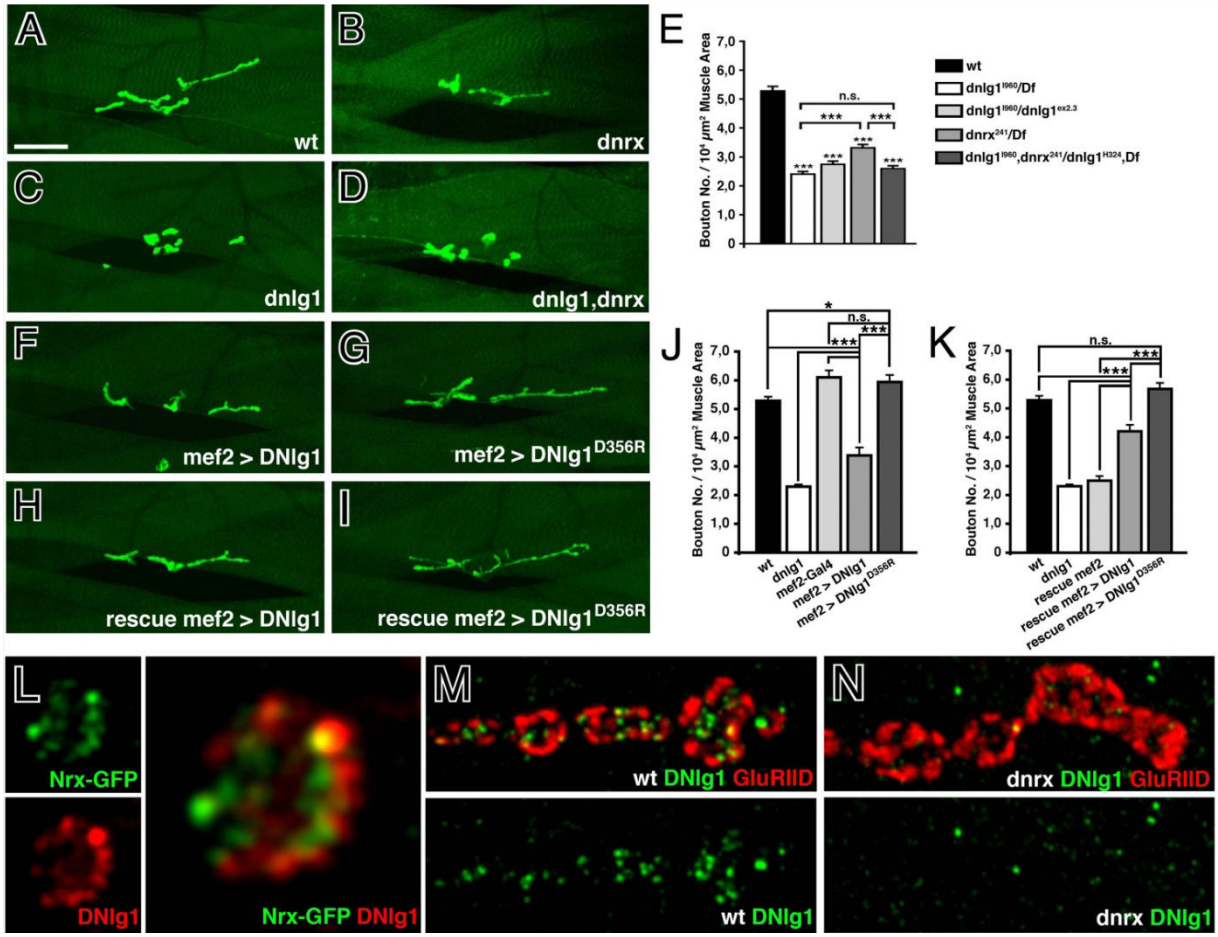

Supplemental Information

Supplemental Figures

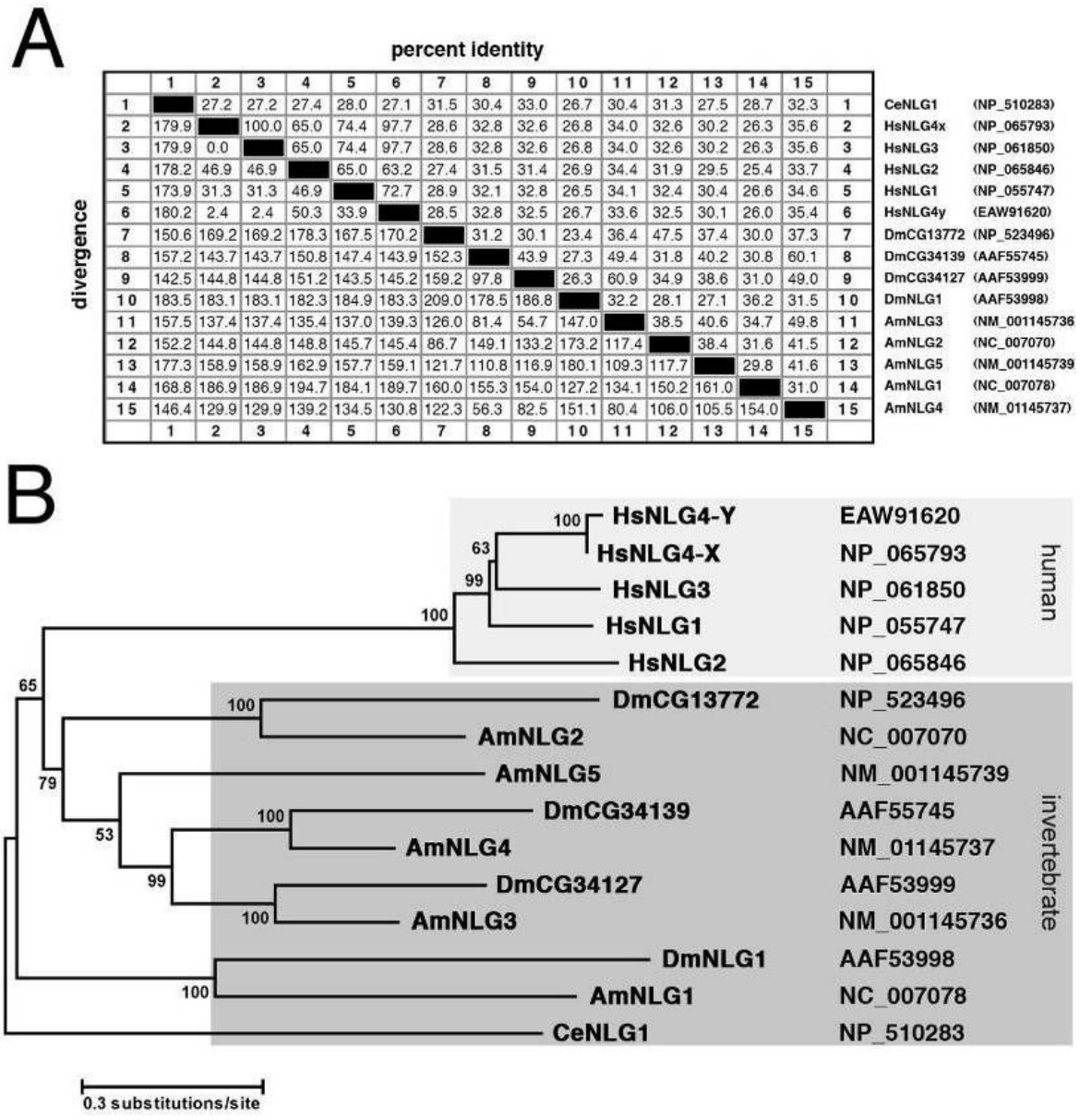

Supplemental Fig. S1

Evolutionary relationship between Neuroligin proteins from vertebrates and invertebrates. (A) Pairwise alignment of the indicated Neuroligin sequence pairs from human, *Drosophila*, *Apis* and *Caenorhabditis* Neuroligin proteins using ClustalW. The overall identity of DNlg1 to

human Nlgs ranged from 26.5-26.8%, showing that it was difficult to assign a specific human ortholog. The divergence and percent identity across the entire protein sequence are shown. The GenBank accession numbers are indicated.

(B) Phylogenetic analysis of human, Drosophila, Apis and Caenorhabditis Neuroligin protein sequences (adapted from Biswas et al., 2008). Drosophila DNlg1 is most closely related to AMNLG1 in the honeybee. Invertebrate Neuroligins share a common ancestor with vertebrate Neuroligins. The phylogenetic tree represents evolutionary distances of Nlg homologs as number of amino acid substitution per site and was generated using MEGA4 software (Tamura et al., 2007). The bootstrap confidence values are indicated as percentages along the branches. Protein sequences are labeled with species names and GenBank accession numbers. Abbreviations: *Homo sapiens* (Hs), *Apis mellifera* (Am), *Caenorhabditis elegans* (Ce), *Drosophila melanogaster* (Dm).

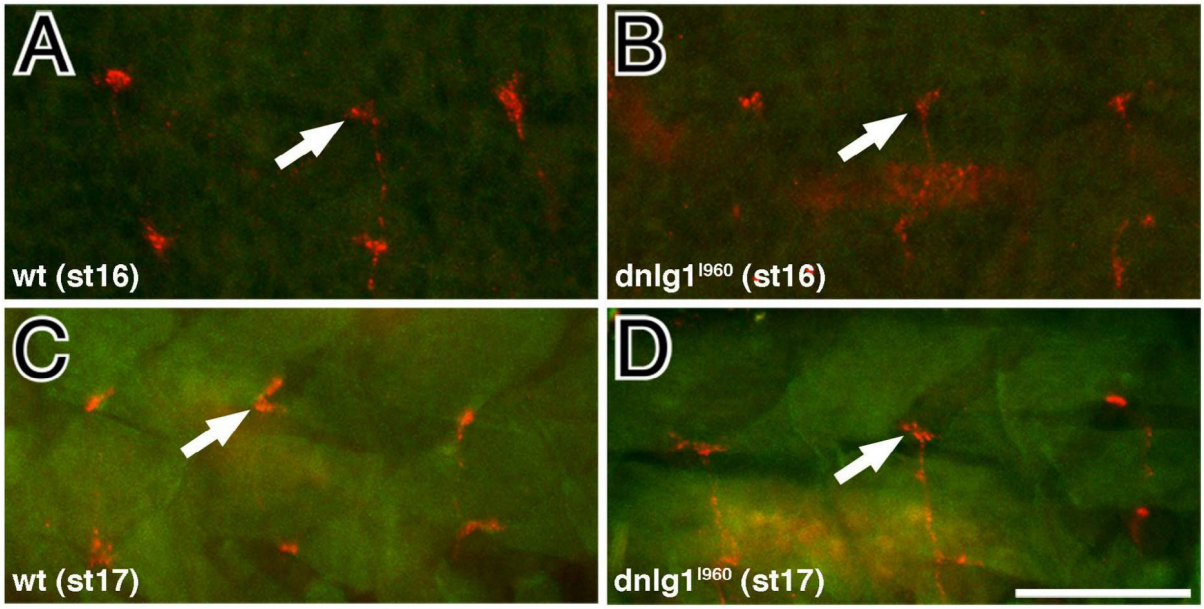

Supplemental Fig. S2

dnlg1 mutant terminals initially form and appear indistinguishable in shape and size from wild-type NMJs. (A-D) Confocal micrographs of developing NMJs on dorsal muscles 1/9 (arrows) in wild-type (A and C) and *dnlg1* mutant (B and D) embryos at stage 16 (A and B) and stage 17 (C and D). NMJs were labeled with anti-DVGLUT antibodies (red). Muscles were labeled with anti-GFP (green) because muscle expression of the CD8-GFP-Sh marker does not label NMJs at this stage. Scale bar: 50 µm. wt: CD8-GFP-Sh; mutant: *dnlg1*^{I960}/*dnlg1*^{I960} carrying CD8-GFP-Sh in the background.

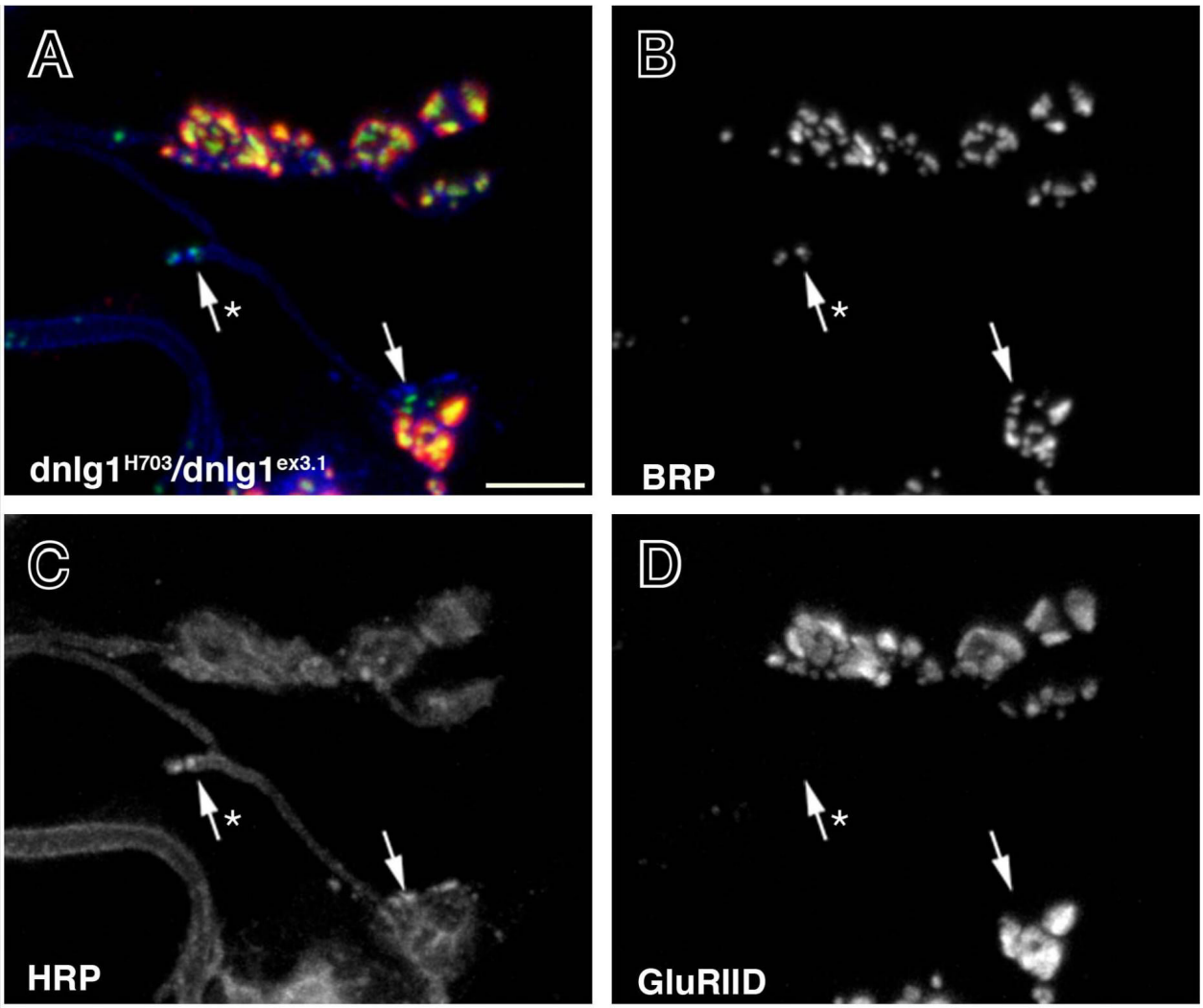

Supplemental Fig. S3

dnlg1^{H703} mutant NMJs exhibits postsynaptic assembly defects typical for all dnlg1 alleles indicating an important function of the cytoplasmic domain in the assembly of PSDs. *dnlg1*^{H703} encodes for a truncated DNlg1 lacking large parts of the cytoplasmic domain but retaining the transmembrane domain due to a premature stop codon.

(A-D) Confocal micrographs of a *dnlg1*^{H703}/*dnlg1*$^{ex3.1}$ mutant NMJ of a third instar larvae stained for the active zone marker BRP (B, green), the neuronal membrane marker HRP (C, blue), and the glutamate receptor subunit GluRIID (D, red). All images are merged in (A). Arrows highlight boutons that contain presynaptic active zones but lack opposing PSDs. Scale bar: 5 µm.

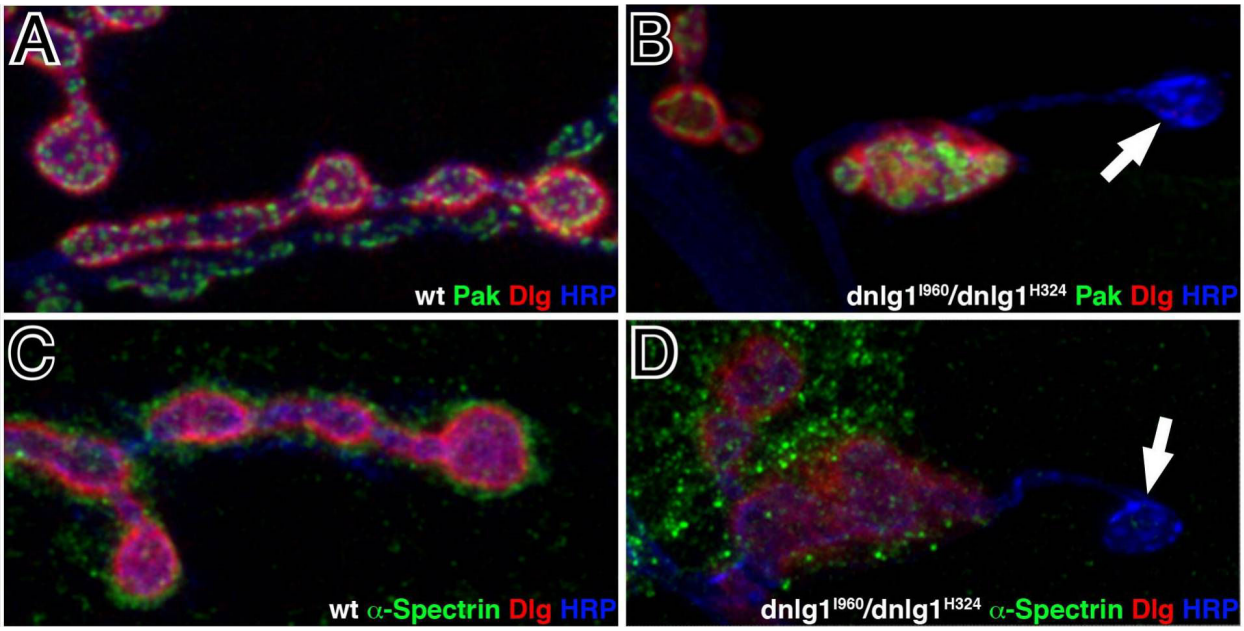

Supplemental Fig. S4

Orphan boutons at *dnlg1* mutant NMJs lack various postsynaptic markers.

(A-D) Confocal micrographs of NMJs on the dorsal side of muscle 4 in wild-type (A, C) and *dnlg1* mutant (B, D) third instar larvae. All NMJs are stained for the SSR marker Dlg (red), the neuronal membrane marker HRP, and either co-stained for the postsynaptic marker Pak (A-B, green) or α-Spectrin (C-D, green). Arrows in (B) and (C) point to orphan boutons, expressing presynaptic markers but lacking either Pak (B) or α-Spectrin (D). wt: w1118; mutant: *dnlg1*^{I960}/*dnlg1*^{H324}.

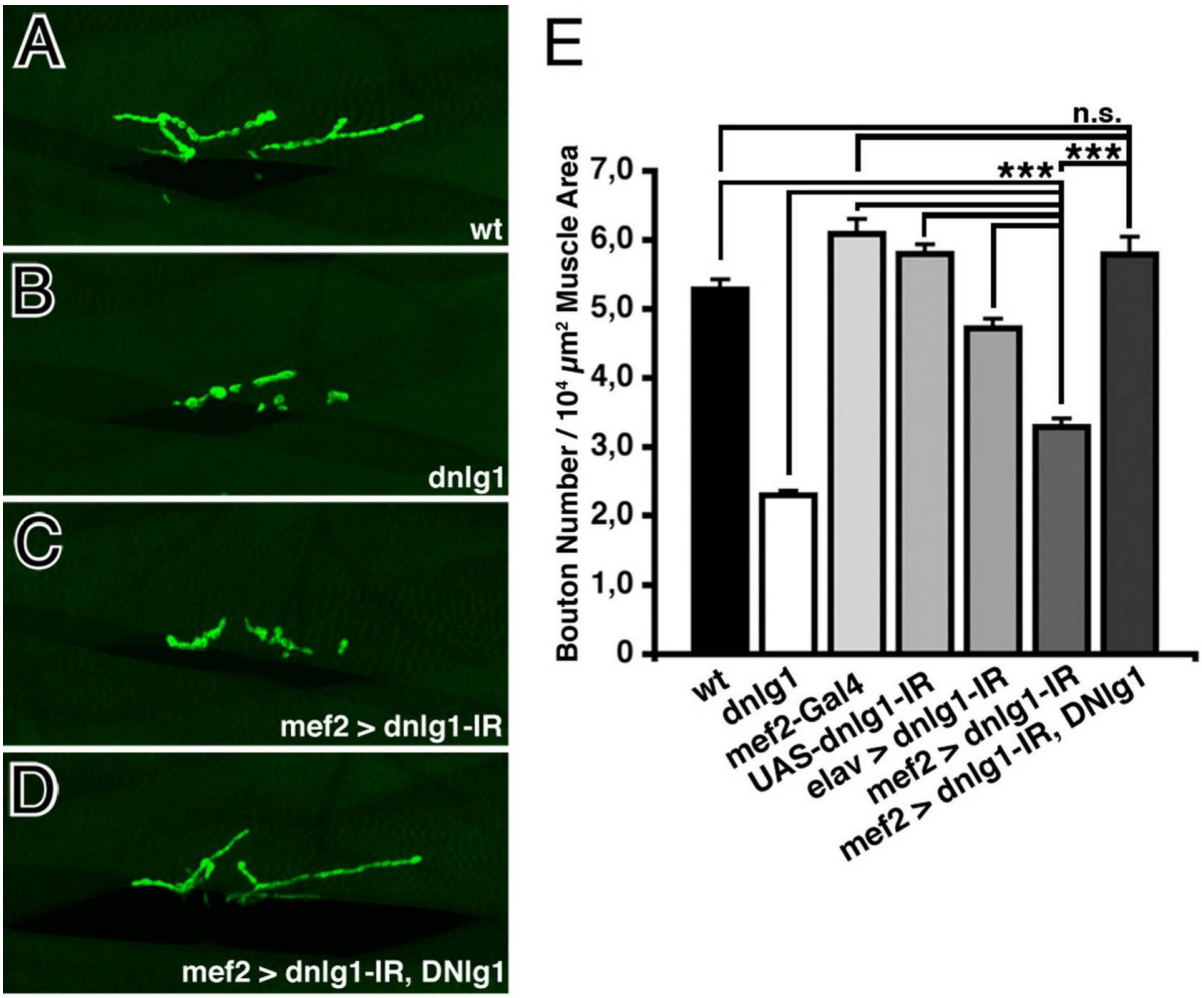

Supplemental Fig. S5

Knock-down of postsynaptic DNlg1 expression phenocopies the NMJ phenotype of *dnlg1* mutants. (A-D) Confocal micrographs of NMJs labeled with the postsynaptic marker CD8-GFP-Sh and imaged through the cuticle of intact third instar larvae. (A) Wild-type NMJs on dorsal muscle pairs 1/9. (B) NMJs on muscles 1/9 are clearly smaller in a $dnlg1^{I960}/dnlg1^{H324}$ mutant larva.

(C) Transgenic RNA interference was expressed tissue-specifically in muscles by expressing double stranded RNA molecules derived from inverted repeats (IR) using mef2-Gal4. Postsynaptic elimination of DNlg1 (as monitored with anti-DNlg1 antibodies) significantly reduces the size of NMJs. (D) Simultaneous expression of a wild-type *dnlg1* cDNA in the background *dnlg1*-specific RNAi inhibits the knock-down of dnlg1 transcripts and rescues the bouton numbers back to wild-type levels.

(E) Quantification of bouton numbers in RNA interference experiments. Postsynaptic elimination of *dnlg1* transcripts significantly reduced bouton numbers. This reduction was prevented by simultaneous expression of a wild-type *dnlg1* cDNA (mef2 > UAS-*dnlg1*-IR, UAS-DNlg1).

Presynaptic RNA interference (elav-Gal4 > UAS-*dnlg1*-IR) caused a slight reduction in bouton numbers. The genetic background of mef2-Gal4 had no effect. n.s.: not significant; asterisks indicate p≤0.001 (Mann-Whitney-U-Test).

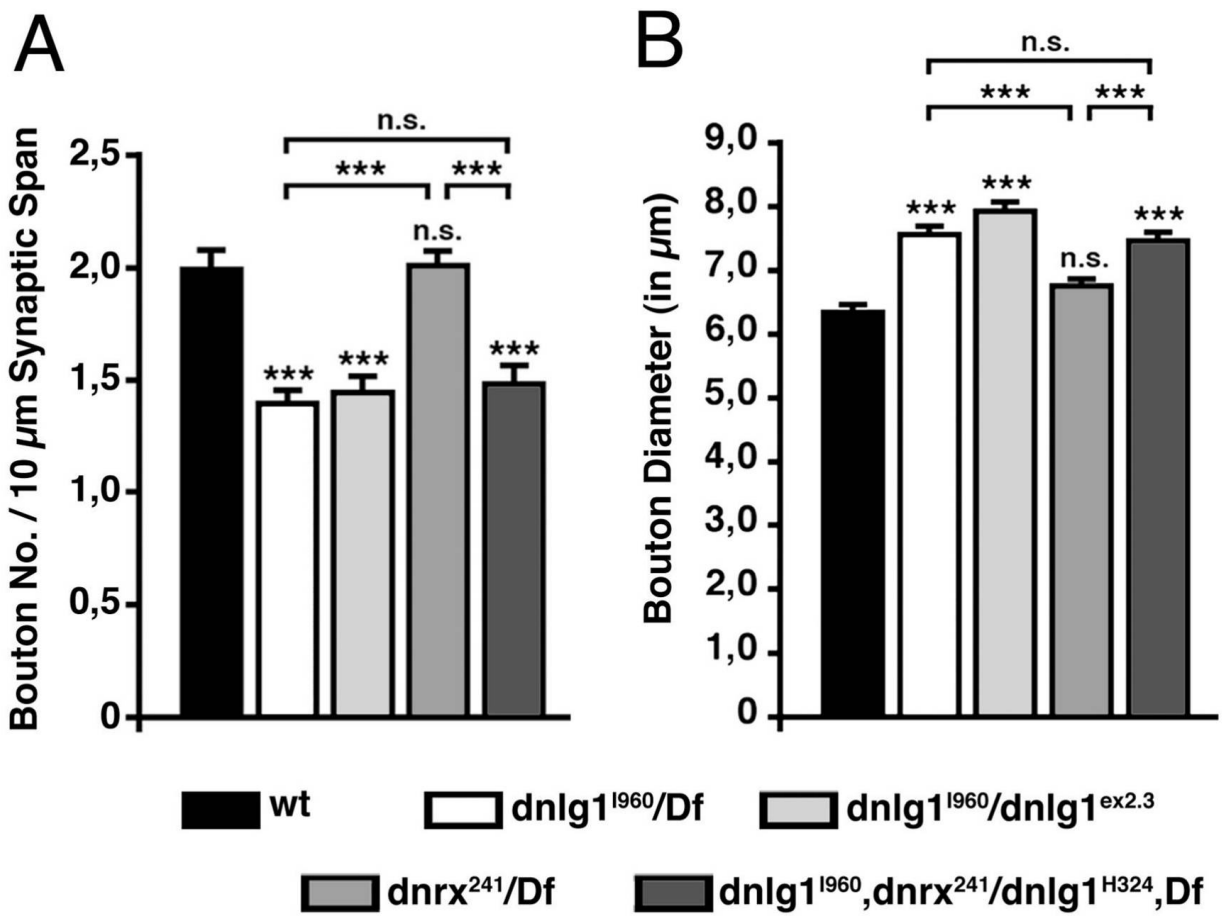

Supplemental Fig. S6

Quantitative comparison of the neuromuscular phenotypes in dnlg1 and dnrx mutants, and double mutant larvae.

(A) Quantification evaluation of the number of boutons per 10 µm synaptic branch length. Compared to wild-type NMJs, the density of synaptic boutons is decreased and the interbouton distance is increase in *dnlg1* but not in *dnrx* mutant genotypes.

(B) Quantification of bouton diameters. The diameter of the largest bouton of a given NMJ is significantly increased in all *dnlg1* mutant phenotypes, irrespective of the alleles used. In contrast, largest bouton size is not significantly altered in *dnrx* mutants. Genotypes are indicated. n.s.: not significant; asterisks indicate p≤0.001 (Mann-Whitney-U-Test).

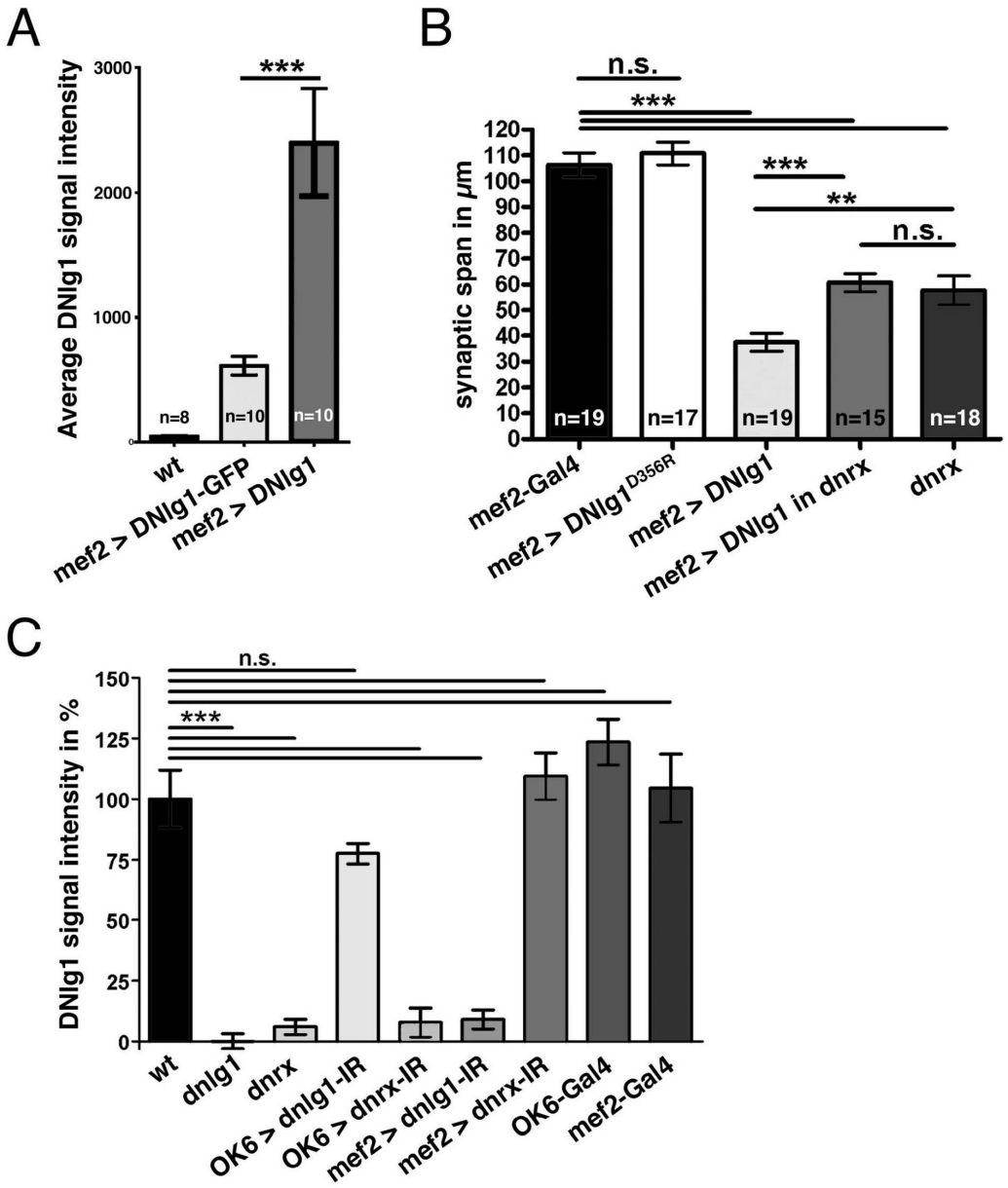

Supplemental Fig. S7

Quantitative and qualitative analysis of the expression levels of endogenous DNlg1 and overexpressed DNlg1 variants.

(A) Evaluation of DNlg1-GFP and DNlg1 signal intensity at NMJs when expressed postsynaptically and stained for DNlg1. Ectopic DNlg1 is expressed at significantly higher levels than DNlg1-GFP or endogenous DNlg1.

(B) Measurements of synaptic span (in µm) on muscle 1 in different genetic backgrounds. Muscle expression of untagged DNlg1 results in strikingly reduced length of NMJs compared to

control (mef2-Gal4/wt) and dnrx mutants (*dnrx*^{241}/Df(3R)Exel6191). When expressed in a *dnrx* mutant background (UAS-*dnlg1*; mef2-Gal4, *dnrx*^{241}/Df(3R)Exel6191) the dominant-negative effect of DNlg1 on NMJ size in a wild-type background is abolished. Expression of DNlg1^{D356R} in muscles of wild-type larvae using mef2-Gal4 does not affect NMJ size.

(C) Quantitative evaluation of the endogenous expression levels of DNlg1 at NMJs of third instar larvae of the indicated genotypes. DNlg1 clustering at NMJs is almost undetectable in *dnlg1* or *dnrx* mutants. Presynaptic downregulation of DNrx, as well as postsynaptic downregulation of DNlg1 by RNA interference, strongly abolishes DNlg1 expression at NMJs. OK6-Gal4 is a motoneuron-specific driver (Aberle et al., 2002). n.s.: not significant; asterisks: p≤0.01 (Mann-Whitney-U-Test).

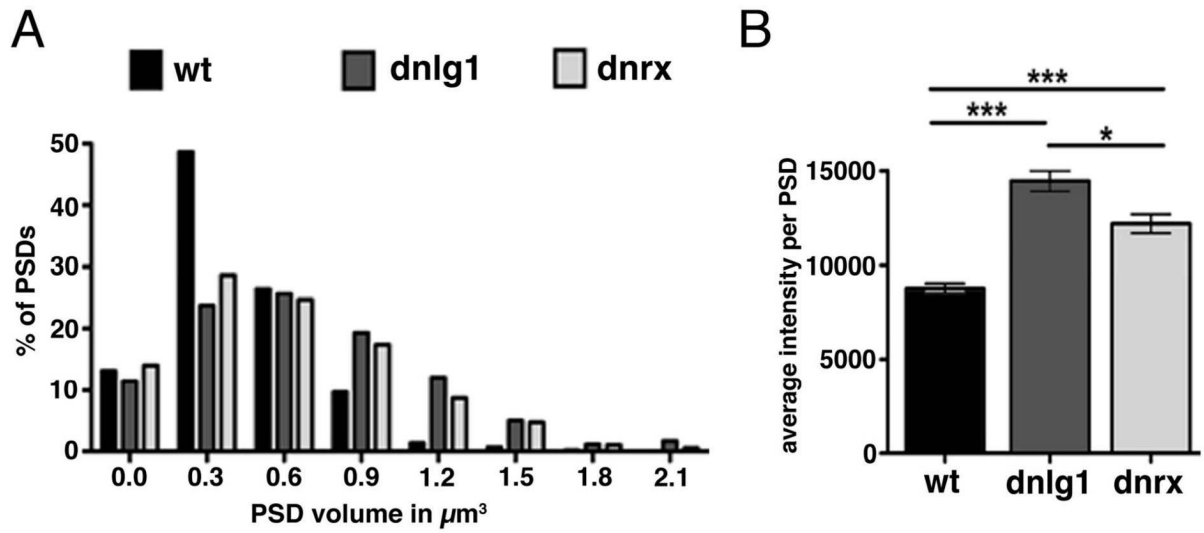

Supplemental Fig. S8

Quantitative evaluation of the postsynaptic GluRIID receptor fields and DNlg1 clusters in *dnrx* and *dnlg1* mutants.

(A) Classification of the 3D reconstituted volume of postsynaptic densities based on GluRIID-positive receptor fields. Postsynaptic densities are increased in dnlg1 and dnrx mutants, and PSDs with volumes larger than 1.5 µm^3 were measured only in mutant boutons.

(B) Quantification of the GluRIID fluorescence intensities showing that the cumulative intensities are increased in both dnlg1 and dnrx mutants compared to wild-type. wt: w1118; *dnrx*: *dnrx*^{241}/Df(3R)Exel6191; *dnlg1*: *dnlg1*^{I960}/*dnlg1*^{H324} . Asterisks: (***) p≤0.001; (*) p≤0.05 (Mann-Whitney-U-Test).

Supplemental Experimental Procedures

Quantification of DNlg1 signal intensities

DNlg1-Signals were quantified by acquiring 16 Bit images of NMJs usings a confocal imaging system (TCS SP5, Leica Mircosystems). Only Ib-terminals on muscle 4 of segment A3 were considered and quantified with ImageJ (http://rsbweb.nih.gov/ij/). Active zone quantification was performed using the spots function of Imaris 6.15 (Bitplane^{TM}) for BRP spot detection. Release sites were defined as BRP positive spots opposed to a GluRIID receptor field. BRP spots lacking a corresponding GluRIID fields were counted as unapposed AZs. Graphpad Prism 4 (Graphpad Software) was used to create the final bar charts.

Analysis of postsynaptic receptor fields

Larval fillet preparations of all genotypes (w1118 , *dnlg1*, *dnrx*) were triple stained with anti-BRP, anti-GluRIID, and anti-HRP antibodies and imaged using a Leica SP5 system. Confocal stacks were taken from type Ib boutons at muscle 4 in segment A3. The GluRIID field size and intensity analysis was performed using ImageJ 1.39t and Bitplane Imaris 6.15. After background correction and normalization (Fuger et al., 2007) the image stacks were further processed in Imaris 6.15. The GluRIID channel was masked by an isosurface (surface area detail level: 0.2 µm) and automatically segmented with a region-growing algorithm. Manual cutting of the resulting surfaces insured correct segmentation of the GluRIID fields in 3D. BRP spots were counted using the internal counting algorithm of the Imaris 6.15 spot function. Final data analysis was performed using Microsoft Exel and Graph rendering was done in GraphPad Prism 4.

Analysis of ultrastructural parameters

To determine vesicle diameters, all synaptic vesicles in a radius of 150 nm surrounding the T-bar

were considered. The diameter was measured using ImageJ software. In order to calculate ratios of bouton/SSR areas, the respective areas were measured in single cross sections using ImageJ. The distribution of membrane ruffles along AZs was analyzed on electron micrographs showing cross sections of T-bar structures. The distance of the highest elevation of the ruffle to the center of the T-bar was measured.

Sequence analysis of the *dnlg1* locus

The QIAamp DNA Mini Kit (Qiagen) was used to isolate genomic DNA. The DNA was amplified by PCR using intron-specific primers and sequenced on both strands using BigDye Terminator Kit (PE Applied Biosystems). Sequences were analyzed using Lasergene (DNAStar). Protein sequences were analyzed using the software tools available at the Expasy website (www.expasy.ch). For the analysis of alternative splicing of dnlg1 transcripts, total RNA of wild-type embryos (stage 1-17) was isolated by phenol/chloroform extraction and reverse transcribed into cDNA using Superscript TM II Reverse Transcriptase and Oligo(dT) 12-18 Primer (Invitrogen). Endogenous dnlg1 transcripts were amplified by PCR using exon-specific primer and subsequently sequenced. Phylogenetic analysis of dnlg1 homologues was conducted using MEGA4 software as described (Tamura et al., 2007; Biswas et al., 2008).

Generation of expression constructs

Full length DNlg1-GFP was generated by inserting GFP between A865 and L866, about 11 aa downstream of the transmembrane domain. These 11 aa are repeated downstream of the GFP to assure a complete intracellular domain, corresponding to the strategy described in (Sheridan et al., 2002; Dresbach et al., 2004). In order to transfer the insert into the gateway vector system (Invitrogen) a PCR product of DNlg1-GFP with flanking KpnI and NotI restriction sites was cloned into the corresponding sites of pENTR4 (Invitrogen), giving rise to pENTR4-dnlg1-GFP. The pUAST-dnlg1-GFP vector was taken as a template for generating the truncated dnlg1-GFP constructs using PCR. *dnlg1*-GFP$^{\Delta cyto}$, *dnlg1*-GFP$^{\Delta extra}$, and in addition full length *dnlg1* and *dnlg1*^{D356R} (both untagged) were inserted into pENTR-D-TOPO (Invitrogen) for transfer into the destination vector pUASTattB by recombination.

For cloning of DNrx-GFP, a 5' fragment of the dnrx cDNA was excised from clone LP14275 (Stapleton et al., 2002) using EcoRI and SphI. A corresponding 3' fragment was generated from LP14275 by PCR using primers 5'ACGACCACCACTCAAGCCACAC and 5'GAGCTCTAGACGACCATGCCGCCTTACACATA. The PCR product was digested with SphI and XbaI. Both fragments were ligated into the EcoRI/XbaI sites of the vector pSL1180, giving raise to pSL-DNrx. The GFP tag was inserted between N1748 and T1749, about 20 amino acids downstream of the transmembrane domain. For this, EGFP was flanked by two linker regions, based on the Tn5 ME linkers described in (Sheridan et al., 2002). The overlapping regions of roughly 30 bps for

each fragment were used to fuse the three fragments in a primer extension reaction (Elongase, Invitrogen). The merged fragments were amplified by PCR, digested with SphI and XbaI, and inserted into the SphI / XbaI sites of pSL-DNrx, giving rise to pSL-Nrx-GFP (8847 bps). Finally, DNrx-GFP was subcloned into pUAST using EcoRI / XbaI.

Mutagenesis of the Neurexin-binding interface was performed using the QuickChange XL Site-Directed Mutagenesis Kit (Stratagene) using pENTR-dnlg1-UTR vector containing the entire 5´- and 3´-UTR sequences. The mutagenesis resulted in an exchange of the amino acid Asp to Arg at

position 356 (DNlg1 D356R) corresponding to the mutation D271R in rat Nlg1 (Reissner et al., 2008). All DNlg1 constructs were cloned into the pUASTattB expression vector using the gateway vector system (Invitrogen).

Supplemental References

Aberle, H., Haghighi, A.P., Fetter, R.D., McCabe, B.D., Magalhaes, T.R., and Goodman, C.S. (2002). wishful thinking encodes a BMP type II receptor that regulates synaptic growth in Drosophila. Neuron 33, 545-558.

Biswas, S., Russell, R.J., Jackson, C.J., Vidovic, M., Ganeshina, O., Oakeshott, J.G., and Claudianos, C. (2008). Bridging the synaptic gap: neuroligins and neurexin I in Apis mellifera. PLoS One 3, e3542.

Dresbach, T., Neeb, A., Meyer, G., Gundelfinger, E.D., and Brose, N. (2004). Synaptic targeting of neuroligin is independent of neurexin and SAP90/PSD95 binding. Mol. Cell. Neurosci. 27, 227-235.

Fuger, P., Behrends, L.B., Mertel, S., Sigrist, S.J., and Rasse, T.M. (2007). Live imaging of synapse development and measuring protein dynamics using two-color fluorescence recovery after photo-bleaching at Drosophila synapses. Nat Protoc 2, 3285-3298.

Reissner, C., Klose, M., Fairless, R., and Missler, M. (2008). Mutational analysis of the neurexin/neuroligin complex reveals essential and regulatory components. Proc. Natl. Acad. Sci. U. S. A. 105, 15124-15129.

Sheridan, D.L., Berlot, C.H., Robert, A., Inglis, F.M., Jakobsdottir, K.B., Howe, J.R., and Hughes, T.E. (2002). A new way to rapidly create functional, fluorescent fusion proteins: random insertion of GFP with an in vitro transposition reaction. BMC Neurosci 3, 7.

Stapleton, M., Liao, G., Brokstein, P., Hong, L., Carninci, P., Shiraki, T., Hayashizaki, Y., Champe, M., Pacleb, J., Wan, K., et al. (2002). The Drosophila gene collection: identification of putative full-length cDNAs for 70% of D. melanogaster genes. Genome Res. 12, 1294-1300.

Tamura, K., Dudley, J., Nei, M., and Kumar, S. (2007). MEGA4: Molecular Evolutionary Genetics Analysis (MEGA) software version 4.0. Mol. Biol. Evol. 24, 1596-1599.

3.1.2 Author contributions

DB, OK, DO, SJS, HA designed research. DB, OK, DO, CW, RT, TR, HA performed experiments.

DB, OK, DO, CW, HA, SJS analyzed data. All authors commented on the paper.

DB, OK, DO, HA, SJS wrote the paper.

Cooperation of Syd-1 with Neurexin synchronizes pre- with postsynaptic assembly

by

David Owald[1,2,*], Omid Khorramshahi[1,2,*], Varun K Gupta[1,2*], Daniel Banovic[3,4], Harald Depner[1,2], Wernher Fouquet[1,2], Carolin Wichmann[1,2], Sara Mertel[1,2], Stefan Eimer[5], Eric Reynolds[1,2], Matthew Holt[1,6], Hermann Aberle[3,4], Stephan J Sigrist[1,2,#]

1 Freie Universität Berlin, Institute for Biology/Genetics, Takustrasse 6, 14195 Berlin, Germany

2 NeuroCure, Charité, Charitéplatz 1, 10117 Berlin, Germany

3 University of Münster, Institute for Neurobiology, Badestrasse 9, 48149 Münster, Germany

4 Heinrich-Heine-University Düsseldorf, Functional Cell Morphology Lab, Universitätsstr. 1, 40225 Düsseldorf, Germany

5. European Neuroscience Institute, Grisebachstr. 5, 37077 Göttingen, Germany

6 VIB Center for the Biology of Disease, Herestraat 49, 3000 Leuven, Belgium

*equal contribution

[#]correspondence: stephan.sigrist@fu-berlin.de

phone: +49-30-450-5390-02/-26

fax: +49-30-450-5769-36

DO, david.owald@cncb.ox.ac.uk; OK, omid-k@gmx.de; VKG, varun_16aug@yahoo.co.in; DB, d.banovic@uni-muenster.de; HD, harald.depner@fu-berlin.de; WF, Wernher.Fouquet@ leica-microsystems.com; CW, cwichma@gwdg.de; SM, s.mertel@fu-berlin.de; SE, seimer@gwdg.de; ER, eric84@twcny.rr.com; MH, Matthew.Holt@cme.vib-kuleuven.be; HA, aberle@uni-duesseldorf.de; SJS, stephan.sigrist@fu-berlin.de.

Running title: Transsynaptic control of synapse assembly in *Drosophila*

Abstract

Synapse formation and maturation requires bidirectional communication across the synaptic cleft. The transsynaptic Neurexin-Neuroligin complex can bridge this gap, and severe synapse assembly deficits are found in *Drosophila neuroligin (dnlg1)* and *neurexin* (*dnrx*) mutants. We show that the presynaptic active zone protein DSyd-1 interacts with DNrx to control synapse formation at the *Drosophila* neuromuscular junction. Mutants in *dsyd-1, dnrx* and *dnlg1* shared active zone-cytomatrix defects, which were non-additive. DSyd-1 and DNrx formed a complex *in vivo*, and DSyd-1 was important for synaptic clustering and immobilization of DNrx. Consequently, postsynaptic clustering of DNlg1 was affected in *dsyd-1*mutants, and *in vivo* glutamate receptor incorporation was changed in *dsyd-1*, *dnrx* and *dnlg1* mutants. *S*tabilization of nascent DSyd-1-DLiprin-α clusters, important to initialize active zone formation, was DNlg1-dependent. Thus, cooperation between DSyd-1 and DNrx-DNlg1 seems to orchestrate early assembly processes between pre- and postsynaptic membranes, promoting avidity of newly forming synaptic scaffolds.

Introduction

Understanding the process of synapse assembly in molecular and cell-biological detail is a prerequisite for understanding neural circuit development and activity-mediated remodeling - and thus important for unraveling learning and memory processes ("structural plasticity")[1-3]. Functional chemical synapses are characterized by two apposed compartments which have to be co-established with high spatiotemporal precision: the presynaptic active zone, where regulated and rapid fusion of neurotransmitter-filled synaptic vesicles takes place, and the postsynaptic density (PSD), which embeds neurotransmitter receptors.

Glutamatergic neuromuscular junction (NMJ) terminals of *Drosophila* larvae grow to meet the requirements of the growing muscle fibers, whereby new synapses are continuously added[4] (synapse: single active zone opposed by a single PSD[1]). Previously, *in vivo* imaging showed that presynaptic DSyd-1 and DLiprin-α clusters initiate active zone formation[5]. On the postsynaptic side, initial PSD growth depends on incorporation of a glutamate receptor (GluR) subunit IIA-containing GluR. Later PSD maturation is marked by the incorporation of GluRIIB-containing receptor complexes[6]. Synapse assembly is concluded at presynaptic active zones, by the incorporation of the active zone scaffold component Bruchpilot (BRP)[5].

Coordinating synapse assembly requires signaling across the synaptic cleft, which separates pre- from postsynaptic membranes. Transsynaptic cell adhesion molecules are obvious candidates for coupling active zone and PSD assembly. *In vitro*, the Neurexin-Neuroligin (Nrx-Nlg) complex can mediate the transsynaptic signaling required for synapse assembly[7, 8]. How this signaling axis integrates with the additional assembly machinery, however, remains largely unclear.

Here, we provide evidence that DSyd-1 plays a dual role in early assembly processes of NMJ synapses. It stalls DLiprin-α clusters at active zones and is important for clustering of presynaptic DNrx, likely via a direct and PDZ-domain-dependent interaction. Consequently, DSyd-1 is also needed for clustering of postsynaptic DNlg1 that organizes postsynaptic assembly. Coincident action of DSyd-1 with DNrx-DNlg1 appears to allow active zone scaffolds to pass through an initial, still fragile assembly phase. We suggest that avidity between DSyd-1 and DNrx-DNlg1 is a means to coordinate pre- with postsynaptic assembly. Our study exemplifies how coincident action of a presynaptic active zone scaffold protein and a transsynaptic cell adhesion protein module can spatiotemporally orchestrate synapse assembly.

Results

Initially described in cell culture systems (for a review see[9]), interaction between mammalian presynaptic Neurexins (Nrxs) and postsynaptic Neuroligins (Nlgs) was proposed to be important for proper synapse assembly. However, genetic ablation of three *nlg* genes in mice[10] does not result in a substantial structural phenotype, potentially reflecting a strong capacity for compensatory processes *in vivo.*

Nonetheless, severe deficits in the *in vivo* assembly of *Drosophila* NMJ synapses[11-13] were reported for mutants of *Drosophila neurexin* (*dnrx*) and *Drosophila neuroligin 1* (*dnlg1*) (for domain organization see Fig. 1a). These findings provided an opportunity for an efficient study of how this transsynaptic signaling complex integrates into synapse assembly in a genetically tractable *in vivo* model.

We started by searching for additional factors involved in the DNlg1-instructed role of DNrx. Previously, we found that muscle (*mef2-Gal4)* expression of DNlg1 lacking its C-terminus (UAS-DNlg1ΔCyto^{GFP} [12], Fig. 1a) results in dramatically undergrown NMJs (Fig. 1b,c). Thus, postsynaptic DNlg1ΔCyto executes a dominant negative effect upon the addition of presynaptic boutons (and thus active zones) throughout terminal expansion. While the mechanism underlying this phenotype is still elusive, we recognized that, after introducing a point mutation interfering with Neurexin-binding[14] (UAS-DNlg1ΔCyto^{D356R}, Fig. 1a), the dominant negative effect of DNlg1ΔCyto was largely suppressed (Fig. 1c). Likewise, expression of DNlg1ΔCyto in the *dnrx* mutant background did not lead to the severe undergrowth DNlg1ΔCyto caused at control junctions. Instead,NMJ structures and bouton numbers were indistinguishable from *dnrx* mutants (Fig. 1b,c). Thus, as the DNlg1ΔCyto phenotype depends on DNrx, testing for suppression of DNlg1ΔCyto might be a way to identify additional presynaptic factors implicated in DNrx signaling.

In both *Drosophila* and *C. elegans*, presynaptic Syd-1/DSyd-1 (for domain organization see Fig. 1a) and Syd-2/DLiprin-α promote presynaptic assembly[5, 15-17]. When we expressed DNlg1ΔCyto in the *dliprin*-α mutant background, NMJ terminals still showed severe undergrowth compared to the mere *dliprin*-α mutant background (Fig. 1b,c). In contrast, the *dsyd-1* mutant background fully suppressed the DNlg1ΔCyto-induced NMJ undergrowth (Fig. 1b,c), implying that DSyd-1 and DNlg1 might operate in the same pathway.

Similar synaptic phenotypes of *dsyd-1*, *dnrx* and *dnlg1*

We previously showed that *dnrx* and *dnlg1* behave non-additively; the reduced NMJ bouton numbers in *dnlg1* mutants are not further diminished in a *dnlg1*, *dnrx* double mutant[12]. In order to test whether *dsyd-1* genetically interacts with *dnrx* or *dnlg1*, we constructed the respective double mutants. NMJ size is reduced in *dnlg1*, *dnrx and dsyd-1,* but also in *dliprin*-α mutants[5, 11, 12, 18]. As expected, all these single mutants showed significantly reduced bouton numbers compared to controls (Fig. 1b,c). Both, *dsyd-1*, *dnrx* as well as *dsyd-1*, *dnlg1* double mutants reached third instar larval stage, allowing for bouton number analysis at mature NMJs (while in contrast, *dsyd-1*, *dliprin*-α double mutants die as embryos[5]). Combinations of *dnrx* or *dnlg1* with the *dsyd-1* mutant did not reduce bouton numbers further than the individual single mutants (Fig. 1b,c).

Apart from reduced NMJ size, all three mutants (*dnlg1*, *dnrx* and *dsyd-1*) show defects in the organization of the remaining active zones[5, 11, 12]. We compared their active zone organization by combining stimulated emission depletion (STED[19]) microscopy at approximately 80 nm resolution (instead of approximately 250 nm of a standard confocal microscope) and electron microscopy. In electron micrographs of controls, active zone dense bodies (T-bars) were properly shaped (Fig. 2a). In contrast, an aberrant "star-shaped" T-bar morphology was regularly observed at the remaining active zones of *dsyd-1* (compare [5]), *dnrx*, and *dnlg1* mutants, but never at control active zones (Fig. 2a-f).

The protein BRP is a direct molecular building block of the electron-dense T-bar[5, 20]. At control NMJs, diffraction-limited BRP spots mark individual active zones[21] that appear as "ring"-shaped structures when imaged at higher resolutions with STED[20, 22] (Fig. 2g,h). We stained *dnrx* (Fig. 2i) and *dnlg1* (Fig. 2j) mutants for BRP and imaged active zones using STED. BRP rings were frequently interconnected and overgrown (Fig. 2i,j). Intriguingly, we had previously observed this phenotype in STED images of *dsyd-1* mutants[5] (Fig. 2k). In fact, BRP ring diameters were increased in all *dsyd-1*(compare[5]), *dnrx* and *dnlg1* single mutants, statistically indistinguishable from each other, and from those of the double mutants (Fig. 2i-o).

DSyd-1 is needed to cluster DNrx and DNlg1 at NMJ synapses

Endogenous DNrx forms distinct clusters at the presynaptic terminal (Fig. 3a)[11, 12]. We performed immunostainings to investigate whether DSyd-1 could influence the distribution of DNrx. Similar to *dnlg1* mutants (Fig. 3a,b), DNrx intensity was significantly reduced in *dsyd-1* mutants (Fig. 3a,b).

DNlg1 normally clusters opposite of presynaptic DNrx. These clusters are no longer detectable in *dnrx* mutants (compare[12]). Consistent with DSyd-1 organizing DNrx clustering, DNlg1 clusters also dropped below the detection limit in *dsyd-1* mutants (Fig. 3c,d).

Both *dsyd-1* and *dnrx* mutant terminals show reduced glutamate release[5, 11]. Thus, lack of DNlg1 clustering could be a mere consequence of reduced synaptic activity. To test this, we quantified DNlg1 intensity levels (as a measure for DNlg1 clustering) in mutants for presynaptic *brp* (*brp*$^{1.3}$)[20]. The *brp* mutant larvae show a more dramatic decrease in presynaptic neurotransmitter release than any of the mutants discussed above[5, 11, 20, 22, 23]. DNlg1 clusters, however, were not reduced in *brp* mutants (Fig. 3c,d), indicating that the observed reduction of DNlg1 levels in *dsyd-1* and *dnrx* mutants was neither due to reduced transmission nor was it a reflection of a general active zone assembly deficit (which is very pronounced in *brp* mutants[22]). Instead, DSyd-1 seems to be specifically involved in clustering postsynaptic DNlg1 adjacent to synapses.

The finding that the cytoplasmic scaffold protein DSyd-1 is needed for both DNrx and DNlg1 clustering is consistent with DNrx directly organizing the synaptic clustering of DNlg1. We also found that muscle-specific DNlg1 expression drastically increased presynaptic DNrx clustering in the control background (Supplementary Fig. 1a), and that there was a trend for motoneuron-driven UAS-DNrx to increase postsynaptic DNlg1 levels (Fig. 3e,f). We reasoned that if DNrx availability was rate-limiting for DNlg1 clustering in *dsyd-1* mutants, over-expression of DNrx in *dsyd-1* mutants might allow restoration of postsynaptic DNlg1 clustering. Indeed, DNlg1 clustering was partially restored when DNrx was overexpressed in the *dsyd-1* mutant background (Fig 3e,f).

Of note, immunostainings for endogenous DSyd-1 showed that the protein was still detectable at both *dnrx* and *dnlg1* mutant NMJs (Supplementary Fig. 2).

Taken together, we show that DSyd-1 is needed to effectively cluster DNrx, which likely impacts the clustering of postsynaptic DNlg1.

DSyd-1 and DNrx form an *in vivo*-complex

These findings motivated us to analyze whether DSyd-1 and DNrx might be part of a common complex. We performed immunoprecipitations from an active zone protein-enriched preparation, derived from *Drosophila* head extracts, using antibodies recognizing DNrx[24]. Robust coimmuno-precipitation of DSyd-1 with DNrx was found, while specificity controls were negative (Fig. 4a).

We next sought to find the molecular link joining DSyd-1 and DNrx. DSyd-1 comprises a PDZ domain, while DNrx has a PDZ-binding motif (Fig. 1a). A large-scale *C. elegans* yeast-two-hybrid screen recently identified a direct interaction of the Syd-1 PDZ domain with *C. elegans* Nrx *in vitro*[25]. We found the same interaction using the corresponding stretches of the highly related fly proteins (Supplementary Fig. 3a). We introduced two point mutations into the DSyd-1 cDNA, resulting in destruction of the ligand binding-essential RxxxxLGL motif within the PDZ domain (DSyd-1 R165A, L170A: DSyd-1^{PDZ}*; compare:[26]). When tested in a yeast two-hybrid assay, binding of the DNrx C-term was largely reduced for the mutated DSyd-1 PDZ domain compared to the unmutated DSyd-1 PDZ domain (Supplementary Fig. 3a).

Expressing DNrx^{GFP} (Fig. 4b) and ^{mStraw}DSyd-1 (Fig. 4c) in larval salivary gland cells we tested this interaction *in vivo*. As expected, when expressed by itself, the transmembrane protein DNrx labeled the plasma membrane (Fig. 4b).In contrast, DSyd-1 or DSyd-1^{PDZ}* expressed on its own showed intracellular distribution (Fig. 4c,d). When co-expressed with DNrx, however, DSyd-1 was clearly recruited to the plasma membrane (Fig.4e), while DSyd-1^{PDZ}* was not (Fig. 4f). In reverse, DNrx lacking its PDZ-binding motif (UAS-DNrx$^{PDB,\ no\text{-}tag}$[24]) failed to recruit ^{mStraw}DSyd-1, while the control,UAS-DNrx$^{no\text{-}tag}$[24], effectively recruited ^{mStraw}DSyd-1 to the plasma membrane (Supplementary Fig. 3b). Thus, DNrx and DSyd-1 can be found in a common complex *in vivo*, apparently mediated via a direct PDZ-domain interaction.

DSyd-1 recruits DNrx to active zones

We next performed *in vivo* live imaging experiments[6] (scheme in Fig. 5a) at NMJs of developing intact larvae. As expected[5], motoneuron-driven UAS-^{mStraw}DSyd-1 invariably marked active zones. UAS-DNrx^{GFP}, when expressed alone, however, distributed more diffusely over the presynaptic terminal membrane (Fig. 5b) and only slightly enriched close to the active zones marked by BRP (not shown). When we co-expressed both proteins under these conditions, DNrx^{GFP} became densely enriched within the DSyd-1 positive active zones (compare Fig. 5b and Fig. 5c). Thus, over-expressed DSyd-1 can obviously direct exogenous DNrx towards active zones. Next, we expressed UAS-DSyd-1^{PDZ}*. UAS-DSyd-1^{PDZ}* still localized at active zones to a good extent (Fig. 5d), while co-expressed DNrx, appeared diffuse (Fig. 5d) and was indistinguishable from the DNrx-distribution in the absence of DSyd-1 co-expression (Fig. 5b). Thus, DSyd-1^{PDZ}* failed to recruit DNrx to active zones. Of note, DLiprin-α overexpression was not sufficient to trigger active zone-enrichment of DNrx^{GFP} (Supplementary Fig. 4a).

We also recognized that endogenous postsynaptic DNlg1 clustering was reduced at terminals that presynaptically overexpressedUAS-DSyd-1^{PDZ}* (Supplementary Fig. 1b). Likely, DSyd-1^{PDZ}* competes

with endogenous DSyd-1 at active zones, impairing DNrx-DSyd-1 interactions and, thereby, DNlg1 clustering.

We next used STED to investigate DNrx localization relative to the active zone-core marker BRP. At approx. 80 nm resolution DSyd-1 puncta surround the BRP core[5]. A good fraction of $DNrx^{GFP}$ puncta also surrounded the BRP core when co-expressed with DSyd-1. This active zone-associated distribution (Fig. 5e) was no longer apparent when co-expressing DNrx and $DSyd\text{-}1^{PDZ}$* (Fig. 5f), where active zone-distal DNrx puncta dominated instead.

DSyd-1 "stalls" DLiprin-α and DNrx at synapses

It appears conceivable that the synapse assembly process should demand continuous trafficking and remodeling. Notably, in the hierarchy of active zone assembly, genetic analysis in *C.elegans* has placed Syd-1 upstream of Syd-2/Liprin-α, a protein linked to long-range transport of vesicular axonal cargo[27, 28].

We previously found that DLiprin-α localization was severely disturbed in *dsyd-1* mutants, and proposed that DSyd-1 might "anchor" clusters of DLiprin-α[5]. To address this, DLiprin-α clusters of control and *dsyd-1* NMJs were imaged *in vivo* in 30-minute increments (Supplementary Fig. 5a), and mobile spots were scored (comparing images taken at 0 and 60 min, see methods section). Numbers of mobile DLiprin-α spots were elevated in the *dsyd-1* mutant background (Supplementary Fig. 5b). Notably, this interaction is not reciprocal, as DSyd-1 mobility appeared unchanged in *dliprin*-α mutants (not shown).

Does DSyd-1 "stall" DNrx in a similar manner? Due to the rather diffuse nature of over-expressed $DNrx^{GFP}$, tracking of individual clusters was problematic here. Instead, we performed fluorescence recovery after photobleaching (FRAP) experiments at $DNrx^{GFP}$-expressing synaptic terminals and measured recovery of the diffuse GFP signal (Fig. 5g,h). We compared NMJs expressing $DNrx^{GFP}$ in *dsyd-1* mutants, in a "rescue situation" (DSyd-1 re-expressed in the *dsyd-1* mutant background), and with $DSyd\text{-}1^{PDZ}$* re-expressed in the *dsyd-1* mutant background (Fig. 5g,h). The *dsyd-1* mutants showed higher $DNrx^{GFP}$ mobility in comparison to rescue controls. Notably, UAS-$DSyd\text{-}1^{PDZ}$* expression in the *dsyd-1* mutant background also resulted in a very high recovery of bleached $DNrx^{GFP}$ signal. In contrast, $DNrx^{GFP}$ recovery appeared unchanged in both *dliprin*-α mutants and in a DLiprin-α over-expressing background (Supplementary Fig. 4b). These findings suggest that DSyd-1, but not DLiprin-α, is able to stall DNrx.

During these live imaging experiments, we observed that $DNrx^{GFP}$ levels were reduced in *dsyd-1* mutants, when compared to the control background. In reverse, a trend towards increased DNrx

levels was observed when over-expressing DSyd-1 in the *dsyd-1* mutant background (Supplementary Fig. 6). Thus, it appears likely that complex formation with DSyd-1 not only stalls but also stabilizes DNrx.

Collectively, these data suggest that, as expected, DSyd-1 promotes the anchoring of DLiprin-α clusters. DSyd-1 also actively recruits and keeps DNrx levels high at active zone-near compartments.

Evidence for a spatially retrograde function of DNlg1

In vivo NMJ synapse assembly is a protracted process of roughly ten hours at 25°C, and finally reaches a "mature" steady state. DLiprin-α and DSyd-1 mark places of synapse formation first. Postsynaptic GluRIIA follows next, and finally BRP is incorporated[5]. To re-address this "early" assembly process, we imaged DSyd-1 and DLiprin-α at 30-minute intervals in living *Drosophila* larvae (Fig. 6a). As expected[5], DLiprin-α and DSyd-1 were tightly co-clustered (Fig. 6b). We, however, noticed that such DLiprin-α/DSyd-1 clusters often dissolved again (Fig. 6c). In contrast, such disassembly events were hardly ever observed for GluRIIA ([6], not shown). Apparently not all "early" DLiprin-α/DSyd-1 clusters entered the irreversible assembly phase marked by GluRIIA accumulation.

To address the influence of postsynaptic DNlg1 on presynaptic assembly, we imaged DLiprin-α/DSyd-1 clusters in *dnlg1* mutants (Fig. 6d). Notably, the distribution of DSyd-1 (Supplementary Fig. 7) and DLiprin-α (not shown) seemed to rapidly change over time at individual *dnlg1* mutant active zones. Likewise, DLiprin-α/DSyd-1clusters appeared highly mobile (Fig. 6e,f). We scored all mobile clusters, evaluating each channel (DSyd-1 and DLiprin-α) separately, as well as a merge of the two channels, finding that the overall mobility of all, DSyd-1 spots, DLiprin-α spots, and DSyd-1/DLiprin-α clusters, was significantly elevated in *dnlg1* mutants (see legend Fig. 6). Consistent with DNlg1 and DSyd-1 converging on DNrx, we also found a tendency towards increased mobility of DLiprin-α clusters in *dnrx* mutants (Supplementary Fig. 5).

Together, these data suggest that DNlg1 is important for DLiprin-α/DSyd-1-cluster stabilization in a spatially retrograde fashion. Lack of postsynaptic DNlg1 seems to destabilize the corresponding presynaptic complex. Most likely this is due to deficits in the transsynaptic promotion of DNrx clustering in *dnlg1* mutants (Fig. 3c,d), which ultimately leads to aberrant presynaptic active zones (Fig. 2).

Defective GluR incorporation in *dnrx*, *dnlg1* and *dsyd-1*

Drosophila NMJ PSDs incorporate glutamate receptors containing either the GluRIIA or the GluRIIB subunit. Normally, the majority of immature, young PSDs form by preferentially incorporating the GluRIIA complex, later followed by GluRIIB during subsequent PSD maturation[6]. Would presynaptic DNrx and DSyd-1 also influence postsynaptic assembly?

We addressed postsynaptic assembly at *dsyd-1*, *dnrx* and *dnlg1* single mutant NMJs (Fig. 7a) by co-expressing fluorescently-tagged GluRIIA and GluRIIB from genomic constructs[6, 29]. Identified NMJs were re-imaged after 24h and PSDs were tracked over time in 3D. This method allowed us to identify newly formed PSDs (Fig. 7a, arrows). As expected, new PSDs in controls were predominantly rich in GluRIIA (Fig. 7a,b). On the contrary, in *dsyd-1*, *dnrx* and *dnlg1* single mutants, novel PSDs were rich in GluRIIB (Fig. 7a,b). The early incorporation of GluRIIA, but not GluRIIB, is a rate-limiting major driving force for PSD assembly and thus for synapse formation at growing NMJs[6, 29, 30]. This deficit in early GluRIIA incorporation might contribute to less synapses forming in these mutants (Fig. 1c,d).

GluRIIA incorporation appearsto be nearly irreversible[6]. As a result, PSDs often show a GluRIIA-rich core surrounded by a GluRIIB-rich edge (Fig. 7c). Notably, this concentric arrangement was regularly inverted in all three -*dnlg1*, *dnrx,* and *dsyd-1* - mutants (Fig. 7c), reflecting GluRIIB-rich PSDs, which eventually incorporate GluRIIA (Supplementary Fig. 8a). As this suggests that a lack of DNlg1 is ultimately responsible here, we tested whether receptor organization in *dnrx* mutants would profit from DNlg1 overexpression. In fact, the receptor distribution largely normalized after DNlg1 overexpression (not shown), indicating that in fact lack of DNlg1 is responsible for the PSD assembly deficits of *dnrx* (and by extension also for *dsyd-1* defects).

Of note, a fraction of PSDs finally overgrew in all three mutants (Supplementary Fig. 8b,c).
In summary, *dnlg1*, *dnrx,* and *dsyd-1* mutants share a specific deficit in the early, PSD growth-promoting GluRIIA incorporation, and are likely directly responsible for this specific assembly deficit in the subcellular PSD distribution of GluR subunits. In our model, DSyd-1 supports the aggregation of DNrx, which in turn clusters postsynaptic DNlg1, in effect coupling pre- to postsynaptic assembly (Supplementary Fig. 9).

Discussion

Nrx and Nlg family proteins are autism susceptibility genes[31, 32] and needed for proper synapse formation during circuit development. It so far, however, remains largely unclear how they molecularly integrate into the synapse formation process, particularly in regard to the assembly of the presynaptic active zone scaffold. Thus, identifying proteins coupling Nrx-Nlg to the very assembly process and defining where in the sequence of events Nrx-Nlg acts is critical for a deeper understanding of synapse formation and remodeling.

Independent work in model organisms has identified and characterized proteins steering active zone assembly, with Syd-1 proteins functioning upstream of Syd-2/Liprin-α[5, 15, 16]. *In vivo* imaging demonstrated that both DSyd-1 and DLiprin-α accumulate very early during synapse assembly (Supplementary Fig. 9) – earlier than postsynaptic GluRs, and much earlier than presynaptic BRP[5]. *In vivo* FRAP analysis now suggests that DSyd-1 increases the ”dwell time” of DNrx close to active zones and can actively recruit DNrx in a PDZ-dependent manner (Supplementary Fig. 9). Likewise, DLiprin-α cluster mobility is largely elevated in the *dsyd-1* mutant background, implying a stalling function of DSyd-1 for both proteins at assembling active zones. This study also proposes that the assembly of initially forming DSyd-1 and DLiprin-α scaffolds is reversible (Supplementary Fig. 9). The “success rate” of establishing stable DSyd-1/DLiprin-α scaffolds drops in the absence of DNlg1 (Fig. 6d-f). As postsynaptic overexpression of DNlg1 increases the expression level of presynaptic DNrx (Supplementary Fig. 1a), interaction of these initial active zone scaffolds is likely to be directly dependent on local DNrx interacting with DSyd-1. Our data suggest that spatiotemporal coincidence of DSyd-1 and DNrx-DNlg1 is integrated into a cooperative scenario (Supplementary Fig. 9). It is tempting to speculate that the DNrx-DSyd-1 interaction provides avidity at newly forming active zones to drive DLiprin-α scaffolds[33, 34] “over a critical point”, to enter an essentially irreversible maturation process (characterized by the onset of GluRIIA incorporation). Such a cooperative scheme might be optimized for the integration of regulatory elements and protect the system from untimely and aberrant assembly. In fact, the active zone component BRP was shown to be under tonic phosphorylation in order to avoid premature assembly[35, 36].

We here find that mutants for *dnlg1* and *dnrx* show aberrant active zone organization reflected in overgrown (“star-shaped”) T-bars (Fig. 2). We previously observed these phenotypes in *dsyd-1* mutants[5]. All three mutants (*dsyd-1, dnrx, dnlg1*) assemble less active zones per NMJ[5, 11, 12]. Consequently, levels of “unused” active zone scaffold components, such as BRP, might locally accumulate along their NMJ terminals. This increase in building blocks in turn might result in

overgrowth of the remaining active zone scaffolds. On the other hand, DSyd-1, DNrx and DNlg1 might define an assembly sequence, which in turn could be a precondition to properly terminate assembly. One could speculate that an improper assembled scaffold might keep free "valences" and that the scaffold might outgrow improperly. As active zone localization of DSyd-1 clustering did not gravely depend on either DNrx or DNlg1, we suspect that a complex of DSyd-1 with DNrx might be important for the regulation of BRP incorporation. Potentially, binding to DNrx (in a transsynaptic complex with DNlg1) might unmask additional domains of DSyd-1 for assembly, and thereby allow for the effective stabilization of DLiprin-α scaffolds. Importantly, mammalian Nlg1 was also implicated in induction and maturation of the presynaptic terminal[37,38].

DNrx[11]and DSyd-1[5] are both expressed throughout the CNS, while DNlg1 is not [12]. It is likely that other DNlgs (see[12]) substitute for DNlg1 at central synapses. Of note, we found star-shaped T-bars at adult CNS synapses of *dsyd-1* mutants as well (not shown), suggesting that similar mechanisms as here described for NMJ synapses apply to CNS synapses.

While DSyd-1 remains cytoplasmic and depends on the presence of DNrx to localize to the plasma membrane in "naïve cells" (salivary gland epithelial cells, Fig. 4b-f), DSyd-1 can localize to active zones also in the absence of DNrx. Consistently, DSyd-1 mutated in its PDZ-domain (*Gal4/UAS* expressed) still localized to active zones, at least to a good extent. Thus, nascent active zones seemingly contain additional proteins providing binding sites for DSyd-1 (that also may be needed to stabilize a complex of DSyd-1 and DNrx). Binding sites are still present after deletion of either DLiprin-α or BRP–despite a direct interaction of DSyd-1 withBRP[5]. Additional proteins representing potential upstream functions are prime candidates for the localization of DSyd-1, such as the adaptor protein Neurabin that was shown to recruit *C. elegans* Syd-1 and Syd-2 to F-actin foci[39].

In contrast to endogenous DSyd-1, levels of *Gal4/UAS*-expressed DSyd-1 depended on the presence of DNrx (Supplementary Fig. 6). Thus "uncomplexed", excessive DSyd-1 might be subjected to degradation. Of note, DLiprin-α is a downstream effector and possible substrate of the E3 ubiquitin ligase APC/C[40].

We found that early and rapid GluRIIA-mediated growth of nascent PSDs (younger than 24 h) is selectively impaired in *dsyd-1*, *dnrx* and *dnlg1* mutants, where young PSDs are characterized by a high GluRIIB content. Mutants for *gluRIIA*, but not for *gluRIIB*, fail to grow sufficient synapses per terminal when challenged by high temperature rearing[41]. In addition, terminals of *dsyd-1*, *dnrx* and *dnlg1* all suffer from undergrown synaptic terminals[5, 11, 12]. Thus, this undergrowth might partially be a consequence of reduced initial GluRIIA incorporation. However, this leaves the question on how DNlg1 dictates GluRIIA incorporation. DNlg1 clusters, functionally associated with proteins regulating

initial synapse assembly, might take a direct role inselectively promoting GluRIIA incorporation (Supplementary Fig. 9). Notably, Nrx-Nlg complexes have been associated with GluR subunit-specific recruitment into PSDs in mammals. Here, overexpression of Nlg1 selectively decreased the surface mobility of GluA2 containing AMPA-type glutamate receptors, mediated by a PSD95-Nlg1 interaction, while having no effect on GluA1 homomers[42, 43]. Indeed, DNlg1 is able to recruit the PSD95 ortholog Dlg to the *Drosophila* NMJ[12]. DSyd-1 and DNrx-instructed DNlg1 clustering might mediate a seed for GluRIIA clustering via Dlg and other scaffold proteins. It should be noted, however, that GluRIIA receptors still incorporate at *dnlg1*-mutant PSDs, although at a later time point of assembly, with PSDs also overshooting in size (Supplemental Fig8c). Thus, DNlg1 seems particularly important to provide avidity for GluRIIA complexes during "early assembly", and choosing the right temporal sequence also seems important for the assembly process to come to a proper end.

Acknowledgements

We would like to thank Christine Quentin and Anastasia Stawrakakis for excellent technical assistance, and Dr Reinhard Jahn for the use of equipment. Till Andlauer and Dr Ulrich Thomas critically read the manuscript. We further thank Dr Manzoor Bhat and Dr Wei Xie for generously sharing reagents. This work was supported by grants from the Deutsche Forschungsgemeinschaft to SJS (Exc 257, SI849/2-1 and 2-2, TP A16/SFB 551, TP B23/SFB581) and HA (AB 116/3-2). MH is funded by an ERC Starting Grant (Astrofunc).

Abbreviation list

FRAP, fluorescence recovery after photobleach; mStraw, mStrawberry; NMJ, neuromuscular junction; PSD, postsynaptic density; STED, stimulated emission depletion microscopy

Methods

Genetics and Molecular Cloning:

Fly strains were reared under standard laboratory conditions. For all experiments both male and female larva were used for analysis. All mutations were kept in the *w1118* genetic background. Double mutant combinations were verified via genomic PCR[5, 11, 12] or, where possible, by complementation analysis. Mutants for *dsyd-1* (*dsyd-1*$^{ex1.2}$/*dsyd-1*$^{ex3.4}$)[5], *dnrx* (*dnrx*^{241}/*dnrxDf*)[11], *dnlg1* (*dnlg1*$^{ex1.9}$/*dnlg1*$^{ex2.3}$ or *dnlg1*^{l960}/*dnlg1*^{H324})[12], *dliprin*-a (*dliprin*- α ^{EPexR60}/*dliprin*- α ^{F3ex15})[18] and *brp* (*brp*$^{1.3}$/*Df(2)BSC29*)[20] were described previously. Flies carrying UAS-GFP-tagged DNrx[12], UAS-untagged-DNrx[24], UAS-untagged-DNrx^{PDB}*[24],UAS-GFP or -mStraw-tagged DSyd-1[5], UAS-GFP-tagged DLiprin-α[20], UAS-GFP-tagged-DNlg1[12] and UAS-GFP-tagged-DNlg1ΔCyto[12] were described previously. mStrawberry tagged UAS-DLiprin-α was obtained using the Gateway vector pTWmStrawberry and *pENTR4/DLiprin*- a [20]. The D358R point mutation was introduced to GFP-tagged-DNlg1ΔCyto as previously described[12]. UAS-DSyd-1^{PDZ}* was constructed based on the UAS-DSyd-1cDNA (also referred to as DSyd-1 Rescue)[5]. Two fragments were obtained via PCR using (1) 5'-GAGCGCGGCCGCGATGACG -3', and 5'-AGCCCGCCGTCTGGCCCGGCGCCTTGACTA-3', and (2) 5'-TAGTCAAGGCGCCGGGCCAGACGGCGGGCTTGT-3', and 5'-CCGTTGACATTCTTCTCGAGGGACCCA-3' and joined using elongation PCR to create PDZ*. *UAS-DSyd-1cDNA* and *-PDZ** were digested using NotI and XhoI and ligated. *pTmStrawberryW/DSyd-1*^{PDZ}* was obtained using the Gateway system (Invitrogen). Point mutations were confirmed via double strand sequencing. For the yeast two-hybrid bait vector a region encoding the cytoplasmic C-term of DNrx was obtained via PCR on the *UAS-DNrx-cDNA*[12] using 5'-GATGCCATGGAGTCGAATGGCGATCGTGGCT-3' and 5'-GTCTATGAATTCGTTTACACATACCACTCCTTGACGTCCT-3'. The product was digested using NcoI and EcoRI and ligated into *pGADT7-IIB* (modified *pGADT7*, with NcoI as single cutter). For the yeast two-hybrid prey vectors a region encoding the DSyd-1 PDZ domain was obtained via PCR on *UAS-DSyd-1cDNA* and *UAS-DSyd-1*^{PDZ}*cDNA* respectively using 5'-GTCTATGAATTCCTGGTAGAAATAGTCAAG-3' and 5'-GTCTATGGATCCCTACGTTGGCGGTCCAGGAG-3'.The products were digested using EcoRI and BamHI and ligated into *pGBKT7*.

Immunostainings and imaging:

The relative number of synaptic boutons (type Ib + Is) was quantified on dorsal muscles 1/9 in abdominal segment A3 of intact CD8-GFP-Sh third-instar larvae expressing UAS-DNlg1ΔCyto^{GFP} (*mef2*-

Gal4) in various genetic backgrounds. The relative number of synaptic boutons was calculated by adjusting the absolute bouton number to the approximate muscle surface areas.

Larval filets were dissected and stained as described previously[5]. The following primary antibodies were used: RbαGluRIID (1:500), MαNc82 (1:100) (provided by E. Buchner, Universität Würzburg), RbαDNlg1 (1:500), and GpαDNrx (1:500) (provided by M. Bath, UNC School of Medicine, University of North Carolina)[12]. Secondary antibodies were diluted 1:500. For STED we used GαM Alexa488 (Molecular Probes, Germany).

DNlg1 and DNrx clusters were quantified from confocal stacks of NMJs converted to maximal projections. The signal of a Cy5αHRP antibody (1:250) was used as template for a mask, restricting the quantified area to the shape of the NMJ. After subtraction of background signals (where indicated), the absolute intensity per NMJ-area was acquired using ImageJ and converted to the relative intensity in Microsoft Excel.

In vivo imaging: All UAS-constructs (except for DNlg1 constructs (*mef2-Gal4*, see above)) were driven in motoneurons using *ok6-Gal4*[44]. NMJs on muscles 26 and 27 were recorded. Salivary glands were also imaged from living larvae. All live imaging was performed as previously described[5, 6, 20]. Briefly, different genotypes were mounted in the imaging chamber and single confocal sections were acquired. For FRAP experiments (all performed in the synaptic area of the NMJ), intense laser light was applied to a region of interest, bleaching green or/and red fluorescent-fusion tags. The "after photobleach" image was taken approximately 1-2 minutes after the t=0 min image. After an incubation time of 30 minutes, the junctions were re-imaged and compared with the images taken before bleaching. For 30-minute time-course experiments, larvae were wakened by applying fresh air, but remained in the imaging chamber between the acquisition points. For 24h imaging intervals, the larvae were reared in an incubator at 25°C in between acquisition.

FRAP analysis was done following a previously described protocol[20].

Quantification of mobile DLiprin-α and DSyd-1 spots was performed on a time series of three confocal stacks of individual junctions which were sequentially acquired in an 30 minutes interval (t=0min/t=30min/t=60min). These images were deconvolved using Autoquant X 2.1.1 from MediaCybernetics. Confocal stacks were merged into a single plane by using the maximum projection function of ImageJ. Subsequently, a Gaussian blur filter was applied (blur radius: 0.5 pixels) and the highest signal intensity was scaled to 255. Only spots with a mean intensity 2.5 times higher than the background intensity were counted. The spots were classified as mobile spots or immobile spots. Spots were considered as 'immobile' spots if they remained at their initial position (relative to the

surrounding spots) during all three time points whereas 'mobile' spots were defined as spots, which appeared and/or disappeared during the time interval of 60 minutes. All spots were manually counted, and the number of spots was normalized to the length of the junction (estimated using the line function in ImageJ).

For quantitative analysis of GluR fields the following genotypes were produced: [Df(2L)^{h4},GluRIIB-GFP/A22,GluRIIA-mRFP] for control animals, [Df(2L)^{h4},GluRIIB-GFP/A22,GluRIIA-mRFP ; *dsyd-1*$^{ex1.2}$/ *dsyd-1*$^{ex3.4}$] for *dsyd-1*, [Df(2L)^{h4},GluRIIB-GFP/A22,GluRIIA-mRFP ; *dnrx*^{241}/*dnrx*^{241}] for *dnrx*, &[Df(2L)^{h4},GluRIIB-GFP/A22,GluRIIA-mRFP ; *dnlg1*$^{ex2.3}$/*dnlg1*$^{ex1.9}$] for *dnlg1* mutants.

The *gluRIIA/IIB* (Df(2L)^{h4}/A22) double mutation was rescued by the expression of fluorescently-tagged genomic constructs of GluRIIA and IIB under the control of their endogenous promoters[6].

Confocal image stacks were analyzed using ImageJ and Imaris 6.15. 3D-surface masks were generated after background subtraction, scaling to the highest pixel intensity and application of Gaussian blur filters. These stacks were further analyzed in Imaris and single receptor fields (PSDs) were detected using the seed point detection algorithm combined with manual segmentation. Pixel intensities of unprocessed GluRIIA and GluRIIB channels in single PSDs were transferred to Microsoft Excel for further processing, as previously described[6, 12].

Receptor topology at individual PSDs and GluRIIA intensities in Control, *dnrx*, *dsyd-1*, and *dnlg1* animals were evaluated in images acquired from muscle 4 of fixed preparations and analyzed as described previously[12].

All confocal images were acquired on a Leica TCS-SP5 (Leica) microscope with a 63x magnification, NA 1.4 oil objective using Application Suite Advanced Fluorescence (LAS AF; Leica) software. Confocal stacks were processed with ImageJ software (http://rsbweb.nih.gov/ij/), Imaris 6.15 (Bitplane), and Autoquant X 2.1.1 (MediaCybernetics).

STED and Electron Microscopy:

STED images were acquired on a Leica TCS STED CW. Images were deconvolved using the built-in deconvolution algorithms of the Leica LAS-AF software. The PSF was generated by using a 2D Lorentz function with the full-width half-maximum set to 80nm (as calculated on the image using the Wiener Filter algorithm (Regulation Parameter: 0.05)). For illustration, a Gaussian blur filter of 0.5 was applied to the images.

Measurement of BRP ring diameters: deconvolved STED images of BRP stained NMJs (muscle 4) of 3rd instar larvae were processed in ImageJ. The diameters of planar oriented BRP rings were measured utilizing the line tool of ImageJ. The distance from intensity maximum to intensity maximum was acquired in the plot window of individual hand-drawn lines and transferred to Microsoft Excel. 5-7 images per genotype were analyzed resulting in 36-56 measurements per group.

Electron microscopy: Conventional transmission electron microscopy and 3D-serial reconstructions were conducted as described[5].

Co-Immunoprecipitation and Yeast two-hybrid

For protein extracts used in co-immunoprecipitation experiments a *Drosophila* head fractionation was carried out, based on protocols from mammalian subcellular preparations[45]. In brief, in the absence of detergents, *Drosophila* wild-type heads were sheared mechanically and differential centrifugation was applied to separate particles according to their size and density. Recovered membranes were finally solubilized in aqueous immunoprecipitation buffer containing 20 mM HEPES pH 7.4, 200 mM KCl, 2 mM $MgCl_2$, 1% Triton X-100. Precleared protein extract was incubated for 10 h at 4° C with either MαDNrx (mAb4, provided by W. Xie, Nanjing, China,[24]) or murine IgGs (Sigma-Aldrich) coupled to Protein A Sepharose-beads (Bio-rad). After washing four times with immunoprecipitation buffer, proteins were eluted with 50µL 2x SDS-PAGE sample buffer. For immunoblot analysis, 4% of input and 10µL of the eluate were loaded. Membranes were probed with MαDNrx[24] and RbαDSyd-1[5].

For the yeast two-hybrid assay, *Saccharomyces cerevisiae* reporter strain Y187 (Clontech) was cotransformed with the DNrx bait vector and prey vectors containing the unmutated PDZ domain or the mutated domain (PDZ*) of DSyd-1. Clontech´s control vectors (pGBKT7-Lam, pGBKT7-53 and pGADT7-T) were used to obtain the negative and positive controls. Liquid cultures were assayed for β-galactosidase using ONPG (o-nitrophenyl β-D-galactopyranoside) to compare for relative strength of the protein-protein interaction. The assay was performed as described in the Yeast Protocols Handbook (Clontech) with the exceptions that cells were permeabilized with SDS/chloroform[46] and that OD_{405} was measured. Clones showing β -galactosidase activity twice that of the negative control values were analyzed.

Statistics: Data were analyzed with Prism (GraphPad Software). Asterisks are used to denote significance. To compare two groups non-parametric Mann-Whitney U-tests were used for all data sets. For comparison of more than two groups non-parametric Kruskal-Wallis tests were used,

followed by a Dunn's multiple comparison test. P-Values, 'n's, and U- or K-statistic are denoted in the figure legends.

References

1. Owald, D. & Sigrist, S.J. Assembling the presynaptic active zone. *Curr Opin Neurobiol***19**, 311-318 (2009).

2. Fejtova, A. & Gundelfinger, E.D. Molecular organization and assembly of the presynaptic active zone of neurotransmitter release. *Results Probl Cell Differ***43**, 49-68 (2006).

3. Jin, Y. & Garner, C.C. Molecular Mechanisms of Presynaptic Differentiation. *Annu Rev Cell Dev Biol* (2008).

4. Collins, C.A. & DiAntonio, A. Synaptic development: insights from Drosophila. *Curr Opin Neurobiol***17**, 35-42 (2007).

5. Owald, D. *et al.* A Syd-1 homologue regulates pre- and postsynaptic maturation in Drosophila. *J Cell Biol***188**, 565-579 (2010).

6. Schmid, A. *et al.* Activity-dependent site-specific changes of glutamate receptor composition in vivo. *Nat Neurosci***11**, 659-666 (2008).

7. Scheiffele, P., Fan, J., Choih, J., Fetter, R. & Serafini, T. Neuroligin expressed in nonneuronal cells triggers presynaptic development in contacting axons. *Cell***101**, 657-669 (2000).

8. Graf, E.R., Zhang, X., Jin, S.X., Linhoff, M.W. & Craig, A.M. Neurexins induce differentiation of GABA and glutamate postsynaptic specializations via neuroligins. *Cell***119**, 1013-1026 (2004).

9. Sudhof, T.C. Neuroligins and neurexins link synaptic function to cognitive disease. *Nature***455**, 903-911 (2008).

10. Varoqueaux, F. *et al.* Neuroligins determine synapse maturation and function. *Neuron***51**, 741-754 (2006).

11. Li, J., Ashley, J., Budnik, V. & Bhat, M.A. Crucial role of Drosophila neurexin in proper active zone apposition to postsynaptic densities, synaptic growth, and synaptic transmission. *Neuron***55**, 741-755 (2007).

12. Banovic, D. *et al.* Drosophila neuroligin 1 promotes growth and postsynaptic differentiation at glutamatergic neuromuscular junctions. *Neuron***66**, 724-738 (2010).

13. Sun, M. *et al.* Neuroligin 2 is required for synapse development and function at the Drosophila neuromuscular junction. *J Neurosci***31**, 687-699 (2011).

14. Fairless, R. *et al.* Polarized targeting of neurexins to synapses is regulated by their C-terminal sequences. *J Neurosci***28**, 12969-12981 (2008).

15. Dai, Y. *et al.* SYD-2 Liprin-alpha organizes presynaptic active zone formation through ELKS. *Nat Neurosci***9**, 1479-1487 (2006).

16. Patel, M.R. *et al.* Hierarchical assembly of presynaptic components in defined C. elegans synapses. *Nat Neurosci***9**, 1488-1498 (2006).

17. Patel, M.R. & Shen, K. RSY-1 is a local inhibitor of presynaptic assembly in C. elegans. *Science***323**, 1500-1503 (2009).

18. Kaufmann, N., DeProto, J., Ranjan, R., Wan, H. & Van Vactor, D. Drosophila liprin-alpha and the receptor phosphatase Dlar control synapse morphogenesis. *Neuron***34**, 27-38 (2002).
19. Hell, S.W. Far-field optical nanoscopy. *Science***316**, 1153-1158 (2007).
20. Fouquet, W. *et al.* Maturation of active zone assembly by Drosophila Bruchpilot. *J Cell Biol***186**, 129-145 (2009).

21. Marrus, S.B. & DiAntonio, A. Preferential localization of glutamate receptors opposite sites of high presynaptic release. *Curr Biol***14**, 924-931 (2004).

22. Kittel, R.J. *et al.* Bruchpilot promotes active zone assembly, Ca2+ channel clustering, and vesicle release. *Science***312**, 1051-1054 (2006).

23. Hallermann, S. *et al.* Naked dense bodies provoke depression. *J Neurosci***30**, 14340-14345 (2010).

24. Sun, M. *et al.* Genetic interaction between Neurexin and CAKI/CMG is important for synaptic function in Drosophila neuromuscular junction. *Neurosci Res***64**, 362-371 (2009).

25. Lenfant, N. *et al.* A genome-wide study of PDZ-domain interactions in C. elegans reveals a high frequency of non-canonical binding. *BMC Genomics***11**, 671 (2010).

26. Swan, L.E. *et al.* Complex interaction of Drosophila GRIP PDZ domains and Echinoid during muscle morphogenesis. *EMBO J***25**, 3640-3651 (2006).

27. Miller, K.E. *et al.* Direct observation demonstrates that Liprin-alpha is required for trafficking of synaptic vesicles. *Curr Biol***15**, 684-689 (2005).

28. Spangler, S.A. & Hoogenraad, C.C. Liprin-alpha proteins: scaffold molecules for synapse maturation. *Biochem Soc Trans***35**, 1278-1282 (2007).

29. Rasse, T.M. *et al.* Glutamate receptor dynamics organizing synapse formation in vivo. *Nat Neurosci***8**, 898-905 (2005).

30. Sigrist, S.J., Thiel, P.R., Reiff, D.F. & Schuster, C.M. The postsynaptic glutamate receptor subunit DGluR-IIA mediates long-term plasticity in Drosophila. *J Neurosci***22**, 7362-7372 (2002).

31. Lise, M.F. & El-Husseini, A. The neuroligin and neurexin families: from structure to function at the synapse. *Cell Mol Life Sci***63**, 1833-1849 (2006).

32. Jamain, S. *et al.* Reduced social interaction and ultrasonic communication in a mouse model of monogenic heritable autism. *Proc Natl Acad Sci U S A***105**, 1710-1715 (2008).

33. Taru, H. & Jin, Y. The Liprin homology domain is essential for the homomeric interaction of SYD-2/Liprin-alpha protein in presynaptic assembly. *J Neurosci***31**, 16261-16268 (2011).

34. Wei, Z. *et al.* Liprin-mediated large signaling complex organization revealed by the liprin-alpha/CASK and liprin-alpha/liprin-beta complex structures. *Mol Cell***43**, 586-598 (2011).

35. Nieratschker, V. *et al.* Bruchpilot in Ribbon-Like Axonal Agglomerates, Behavioral Defects, and Early Death in SRPK79D Kinase Mutants of Drosophila. *PLoS Genet***5**, e1000700 (2009).

36. Johnson, E.L., 3rd, Fetter, R.D. & Davis, G.W. Negative regulation of active zone assembly by a newly identified SR protein kinase. *PLoS Biol***7**, e1000193 (2009).

37. Futai, K. *et al.* Retrograde modulation of presynaptic release probability through signaling mediated by PSD-95-neuroligin. *Nat Neurosci***10**, 186-195 (2007).

38. Wittenmayer, N. *et al.* Postsynaptic Neuroligin1 regulates presynaptic maturation. *Proc Natl Acad Sci U S A***106**, 13564-13569 (2009).

39. Chia, P.H., Patel, M.R. & Shen, K. NAB-1 instructs synapse assembly by linking adhesion molecules and F-actin to active zone proteins. *Nat Neurosci***15**, 234-242 (2012).

40. van Roessel, P., Elliott, D.A., Robinson, I.M., Prokop, A. & Brand, A.H. Independent regulation of synaptic size and activity by the anaphase-promoting complex. *Cell***119**, 707-718 (2004).

41. Schmid, A. *et al.* Non-NMDA-type glutamate receptors are essential for maturation but not for initial assembly of synapses at Drosophila neuromuscular junctions. *J Neurosci***26**, 11267-11277 (2006).

42. Mondin, M. *et al.* Neurexin-neuroligin adhesions capture surface-diffusing AMPA receptors through PSD-95 scaffolds. *J Neurosci***31**, 13500-13515 (2011).

43. Heine, M. *et al.* Activity-independent and subunit-specific recruitment of functional AMPA receptors at neurexin/neuroligin contacts. *Proc Natl Acad Sci U S A***105**, 20947-20952 (2008).

44. Aberle, H. *et al.* wishful thinking encodes a BMP type II receptor that regulates synaptic growth in Drosophila. *Neuron***33**, 545-558 (2002).

45. Huttner, W.B., Schiebler, W., Greengard, P. & De Camilli, P. Synapsin I (protein I), a nerve terminal-specific phosphoprotein. III. Its association with synaptic vesicles studied in a highly purified synaptic vesicle preparation. *J Cell Biol***96**, 1374-1388 (1983).

46. Guarente, L. Yeast promoters and lacZ fusions designed to study expression of cloned genes in yeast. *Methods Enzymol***101**, 181-191 (1983).

Fig. 1: Double mutants analysis of *dnrx*, *dnlg1*, and *dsyd-1*

a) Schematic representation of the domain structures of DNrx, DNlg1 and DSyd-1. DNrx is comprised of extracellular Lam G and EGF-3domains. The short intracellular domain has a PDZ-binding domain (PDZ bind). The extracellular part of DNlg1 comprises an acetylcholinesterase-like (Ach-E) domain, while the cytoplasmic part has a PDZ-binding domain (PDZ bind). The D356R point mutation in the Ach-E domain interferes with DNrx binding. The cytoplasmic part is deleted in DNlg1ΔCyto constructs. TM = transmembrane domain.DSyd-1 comprises a PDZ domain, a C2 domain and a putative RhoGAP domain. The DSyd-1 R165A, L170A point mutations are indicated by PDZ* (DSyd-1^{PDZ}*). b) CD8-GFP-Sh expressing NMJs 1/9. Scale bar: 20µm. c) Quantification of bouton numbers on NMJ 1/9 relative to muscle area. (Control: 5.185±0.171, n=20; UAS-DNlg1ΔCyto: 0.850±0.205, n=20; UAS-DNlg1ΔCyto^{D356R}: 3.84±0.22, n=20; *dnrx:* 3.23±0.18, n=20; *dnrx*, UAS-DNlg1ΔCyto: 3.20±0.21, n=20; *dliprin-α:* 3.93±0.16, n=20; *dliprin-* α, UAS-DNlg1ΔCyto: 1.37±0.27, n=20; *dsyd-1:* 3.95±0.20, n=20; *dsyd-1*, UAS-DNlg1ΔCyto: 3.54±0.21, n=20; *dnlg1*: 3.11±0.17, n=19; *dsyd-1,dnrx*: 3.51±0.23, n=20; *dsyd-1,dnlg1*: 3.20±0.25, n=18. All single and double mutants were analyzed using the Kruskal-Wallis test with Dunn's multiple comparison test (K=48.77). Each single mutant was compared to UAS-DNlg1ΔCyto expressed in the mutant background using the Mann-Whitney U-test, p(*dnrx x dnrx*, UAS-DNlg1ΔCyto)=0.59, U=179.5; p(*dliprin-* α *x dliprin-* α, UAS-DNlg1ΔCyto)<0.001, U=15.0; p(*dsyd-1 x dsyd-1*, UAS-DNlg1ΔCyto)=0.22, U=138.0. Control, UAS-DNlg1ΔCyto′ and UAS-DNlg1ΔCyto^{D356R} were analyzed using the Kruskal-Wallis test with Dunn's multiple comparison test (black, K=44.73). *:p<0.05; **:p<0.01; ***:p<0.001, ns: p>0.05, not significant; all values are mean ± s.e.m.

Fig. 2: Comparison of active zone ultrastructure for *dnrx*, *dnlg1*and *dsyd*-1mutants

a) Electron micrograph showing a regular presynaptic electron-dense projection (T-bar) of a control bouton. c) Serial reconstruction of the T-bar shown in (a). T-bars of (b) *dsyd-1*, (d) *dnrx*, and (e) *dnlg1* mutant active zones often show star-like shapes. Aberrant T-bar morphology is indicated by arrows. f) Serial reconstruction of a *dnlg1* mutant T-bar. Scale bar: 100nm. Examples of confocal (g) and STED (h) images of BRP spots at a control NMJ (muscle 4). i-n) BRP rings are irregular and interconnected (see arrows) in (i) *dnrx*, (j) *dnlg1*, (k) *dsyd-1,* and *dsyd-1, dnlg1* (l), *dnrx, dnlg1* (m) *as well as dsyd-1, dnlg1* (n) double mutant animals (l-n). STED images were deconvolved with a Lorentz point spread function of 80 nm using a Wiener filter (0.05 regulation parameter). Scale bar: 500nm. (o) Quantification of BRP ring diameter. Control: 0.233±0.012, n=34; *dnlg1*: 0.305±0.015, n=43; *dsyd-1*: 0.301±0.011, n=47; *dnrx*: 0.322±0.013, n=54; *dnrx,dnlg1*: 0.315±0.013, n=52; *dsyd-1*,*dnlg1*: 0.321±0.013, n=46; *dsyd-1*,*dnrx*:

0.328±0.017, n=43. Data was analyzed using the Kruskal-Wallis test with Dunn's multiple comparison test (K=29.2). *:p<0.05; **:p<0.01; ***:p<0.001, ns: not significant; all values are mean ± s.e.m.

Fig. 3: Absence of endogenous DNrx and DNlg1 clusters at *dsyd-1* mutant NMJ

a) Muscle 4 boutons of Control, *dnlg1*, *dsyd-1* and *dnrx* larvae immunostained for DNrx (green) and BRP (red). b) Quantification of DNrx signal intensities from Ib NMJs on muscle 4 normalized to control levels. Residual background (mean intensity of *dnrx* mutants) was subtracted for all genotypes and then data sets were normalized to the Control. (Control: 100.0±12.40, n=21; *dsyd-1*: 29.44±6.58, n=19; *dnlg1*: 34.46±5.06, n=18; *dnrx*: 0.00±1.43, n=18; p(Control x *dsyd-1*)<0.001; p(Control x *dnlg1*)<0.01; p(Control x *dnrx*)<0.001; p(*dsyd-1* x *dnlg1*)>0.05; Kruskal-Wallis test with Dunn's multiple comparison test (K=52.6). c) Muscle 4 boutons of Control, *dnlg1*, *dsyd-1*, and *brp* larvae immunostained for DNlg1 (green) and BRP (red). d) DNlg1 signal intensity quantification of Ib NMJs on muscle 4. Residual background (mean intensity of *dnlg1* mutants) was subtracted for all genotypes (hence the negative values for *dsyd-1* mutants) and then data sets were normalized to Control. (Control: 100.0±14.61, n=14; *dsyd-1*: -20.8±7.34, n=9; *dnlg1*: 0.0±19.36, n=8; *brp*: 90.1±38.95, n=7; p(Control x *dsyd-1*)<0.001; p(Control x *dnlg1*)<0.01; p(Control x *brp*)>0.05; Kruskal-Wallis test with Dunn's multiple comparison test (K=22.4). e) Muscle 4 boutons of Control, and UAS-DNrx^{GFP} driven in motoneurons of Control and *dsyd-1* animals. f) Quantification of DNlg1 signal intensities normalized to control levels. (Control: 100.0±10.40, n=12; DNrx^{GFP}: 195.0±45.59, n=13; *dsyd-1*: 8.505±1.390, n=13; DNrx^{GFP};*dsyd-1*: 36.43±4.202; n=12; p(Control x DNrx^{GFP})>0.05; Mann-Whitney U-test (U=55.0); p(*dsyd-1* x DNrx^{GFP}; *dsyd-1*)<0.001; Mann-Whitney U-test(U=0.0). ns: p>0.05 (not significant), **: p<0.01, ***:p<0.001, all values are mean ± s.e.m.). Scale bars: 2µm.

Fig. 4: Biochemical and cell biological analysis of DSyd-1-DNrx complex formation

a) Immunoblot of DNrx pull-down from a *Drosophila* active zone protein-enriched preparation. DSyd-1 co-precipitates with DNrx, but is not detected in the random mouse IgG control, for the full blots see Supplementary Fig. 10. b) UAS-DNrx^{GFP} localizes to the cell membrane of salivary gland cells, while both UAS-^{mStraw}DSyd-1 or UAS-^{mStraw}DSyd-1^{PDZ}* (c-d) when expressed alone distribute diffusely throughout the cytoplasm. Co-expression of UAS-^{mStraw}DSyd-1 and UAS-DNrx^{GFP}, directs UAS-^{mStraw}DSyd-1 to the plasma membrane (e). In contrast, localization of UAS-^{mStraw}DSyd-1^{PDZ}*(f) co-expressed with UAS-DNrx^{GFP} remains diffuse. Scale bar: 25µm.

Fig. 5: DSyd-1 influences localization and FRAP of DNrx at NMJ

a) Schematic representation of the *in vivo* imaging procedure at *Drosophila* larval NMJs. Identified synapses get re-imaged at defined time intervals in an intact animal. b) Junctional localization of UAS-DNrx^{GFP} driven in motoneurons (muscle 26/27). c) Junctional localization of UAS-DNrx^{GFP}, when co-expressed with UAS-^{mStraw}DSyd-1. Arrows indicate active zone-near clusters of DSyd-1 and DNrx. (d) Junctional localization of UAS-DNrx^{GFP}, when co-expressed with UAS-^{mStraw}DSyd-1^{PDZ}*. Arrow indicates missing overlap of DSyd-1 and DNrx at active zone-near zones. Scale bar: 2µm**.** (e-f) Single confocal slices of triple labeled boutons for endogenous BRP, UAS-DNrx^{GFP}, and ^{mStraw}DSyd-1 (e), or ^{mStraw}DSyd-1^{PDZ}* (f) respectively. STED images of UAS-DNrx^{GFP} reveal the sub-synaptic distribution of DNrx. When co-expressed with DSyd-1, DNrx clusters localize adjacent to active zones labeled by BRP. When co-expressed with DSyd-1^{PDZ}* the distribution of UAS-DNrx appears randomized, and not enriched near active zones. Scale bar: 500nm. (g) FRAP of UAS-DNrx^{GFP} driven in motoneurons of *dsyd-1* mutant, *dsyd-1*, UAS-DSyd-1 (*dsyd-1* R) rescue, and *dsyd-1*, UAS-DSyd-1^{PDZ*} (*dsyd-1^{PDZ*}*) animals. The middle panel ("photobleached") was taken approx. 1-2 minutes after the time point 0. Scale bar: 2µm. (h) Quantification of the DNrx recovery signal. DNrx FRAP is normalized to the recovery of DNrx in *dsyd-1* mutants. (*dsyd-1*: 1.000±0.087, n=15; *dsyd-1*, UAS-DSyd-1(*dsyd-1* R): 0.320±0.070, n=12; *dsyd-1*, UAS-DSyd-1^{PDZ}* (*dsyd-1* PDZ*): 1.171±0.063 , n=13; p(*dsyd-1* x *dsyd-1 R*)<0.001; p(*dsyd-1 R* x *dsyd-1 PDZ**)<0.001, Kruskal-Wallis test with Dunn's multiple comparison test (K=23.5), ***: p<0.001, all values are mean ± s.e.m.).

Fig. 6: *In vivo* imaging of DLiprin-α/DSyd-1 cluster dynamics at *dnlg1* mutant NMJs

a) *In vivo* imaged NMJ boutons from a UAS-^{GFP}DSyd-1 and UAS-DLiprin-α^{mStraw} expressing animal (muscle 26/27). Junctions were reimaged after 30 and 60 minutes. b) A novel DLiprin-α (red, arrow heads) and DSyd-1 (green, arrows) positive site emerges at 60 minutes (as expected[5]). c) A nascent site disassembling again. d) *In vivo* imaged NMJ boutons from a UAS-^{GFP}DSyd-1 and UAS-DLiprin-α^{mStraw} expressing *dnlg1* mutant animal. Novel DLiprin-α (red, arrows) and DSyd-1 (green, arrows) positive sites can readily be observed assembling (e), disassembling (f) and moving. We scored all mobile clusters, evaluating each channel (DSyd-1 and DLiprin-α) separately, as well as a merge of the two channels. Quantification over 60 minutes shows that the mobile population of DLiprin-α (Control: 0.080±0.007, n=8; *dnlg1*: 0.189±0.021, n=8; p(Control x *dnlg1*)<0.001, Mann-Whitney U-Test, U=1.0), DSyd-1 (Control: 0.079±0.006, n=8; *dnlg1*: 0.176±0.013, n=8; p(Control x *dnlg1*)<0.001, Mann-Whitney U-Test, U=0.0), and DLiprin-α/DSyd-1 clusters is significantly elevated in *dnlg1* mutants (Control: 0.052±0.009, n=8; *dnlg1*: 0.155±0.017, n=8, p(Control x *dnlg1*)<0.001, Mann-

Whitney U-Test, U=1.0). All values are mean ± s.e.m.. Scale bar (a) and (d): 5µm. Scale bar (b, c, e, f): 1µm.

Fig. 7: Analysis of *in vivo* glutamate receptor incorporation in *dnlg1*, *dnrx* and *dsyd-1* mutants

a) 24h time-lapse experiments of growing NMJs at muscles 26/27 allow for the determination of GluR content of newly forming PSDs. At control NMJs, most of the young PSDs (arrows) are rich in GluRIIA with few exceptions (asterisk). Young PSDs in *dnrx*, *dsyd-1* and *dnlg1* show an inversed trend in GluRIIA-IIB composition (arrows). b) The GluRIIB-IIA ratio in newly formed PSDs is significantly shifted towards GluRIIB, in comparison to control PSDs for all *dnrx*, *dsyd-1* and *dnlg1* mutants. (Control: -0.283±0.038, n=23; *dnrx*: -0.019±0.038, n=20; *dsyd-1*: 0.064±0.035, n=16; *dnlg1*: 0.114±0.026, n=30; p(Control x *dnrx*)<0.01; p(Control x *dsyd-1*)<0.001; p(Control x *dnlg1*)<0.001; Kruskal-Wallis test with Dunn's multiple comparison test (K=39.1)**:p<0.01, ***:p<0.001, all values are mean ± s.e.m.). c) Sub-synaptic localization of GluRIIA- and GluRIIB-type glutamate receptor subunits at individual PSDs on muscle 4of 3rd instar larvae (fixed preparation). GluRIIB localizes to the edge of a GluRIIA-rich core in most control PSDs. Examples of PSDs in *dnrx*, *dsyd-1* and *dnlg1* mutant NMJs where this distinct localization is reversed. Scale bars: 5µm.

Figure 1.) Owald et al., 2012

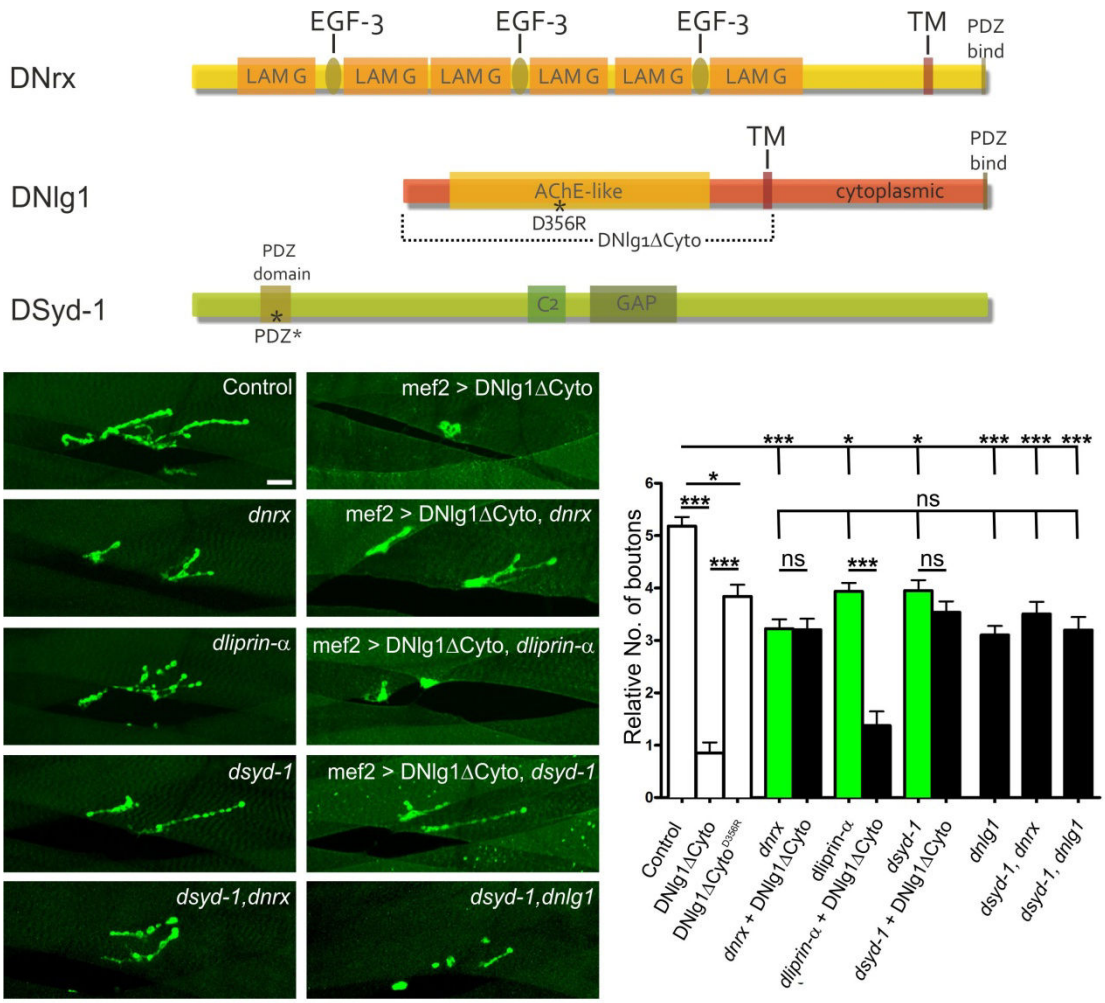

Figure 2.) Owald et al., 2012

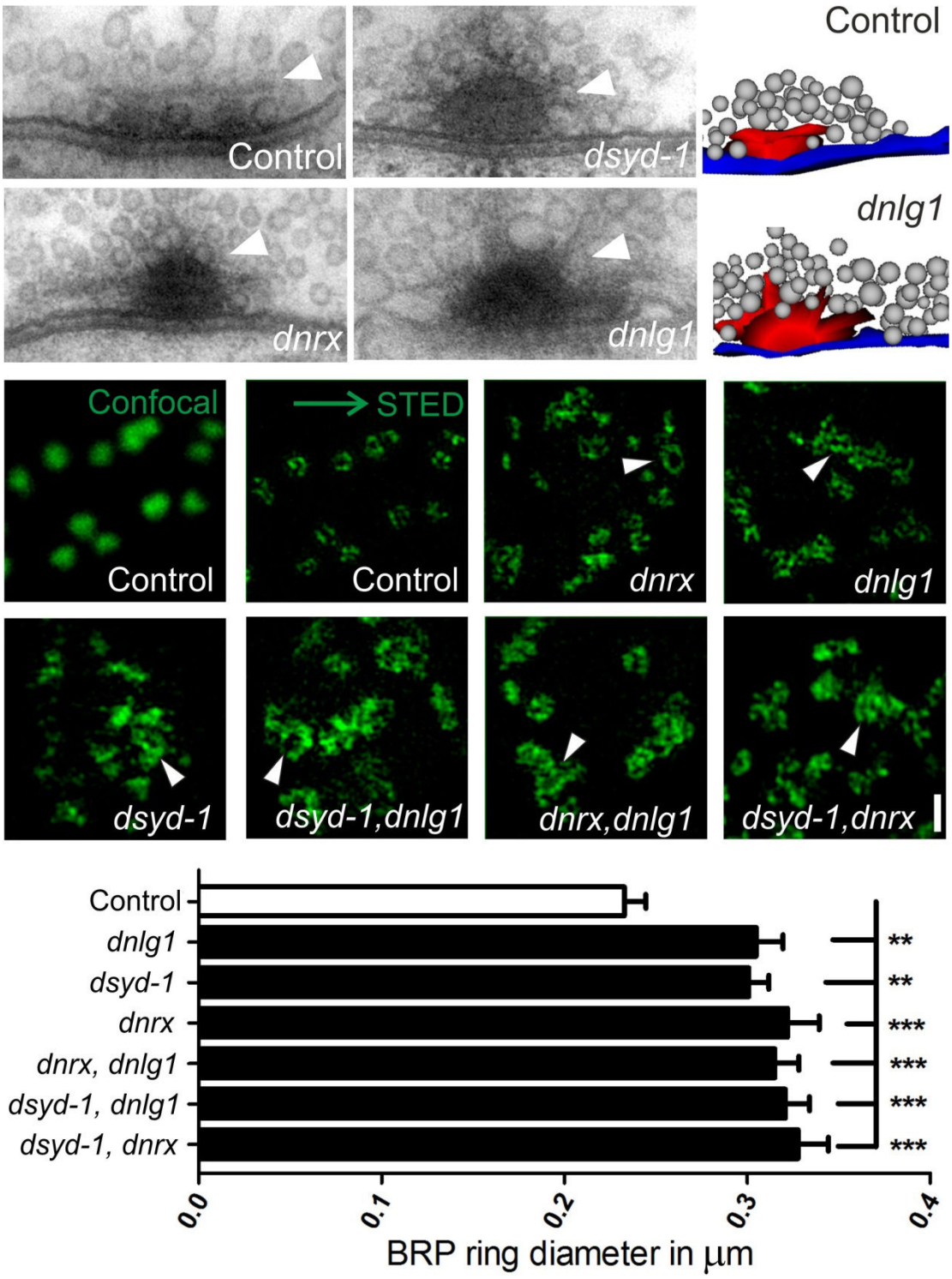

Figure 3.) Owald et al., 2012

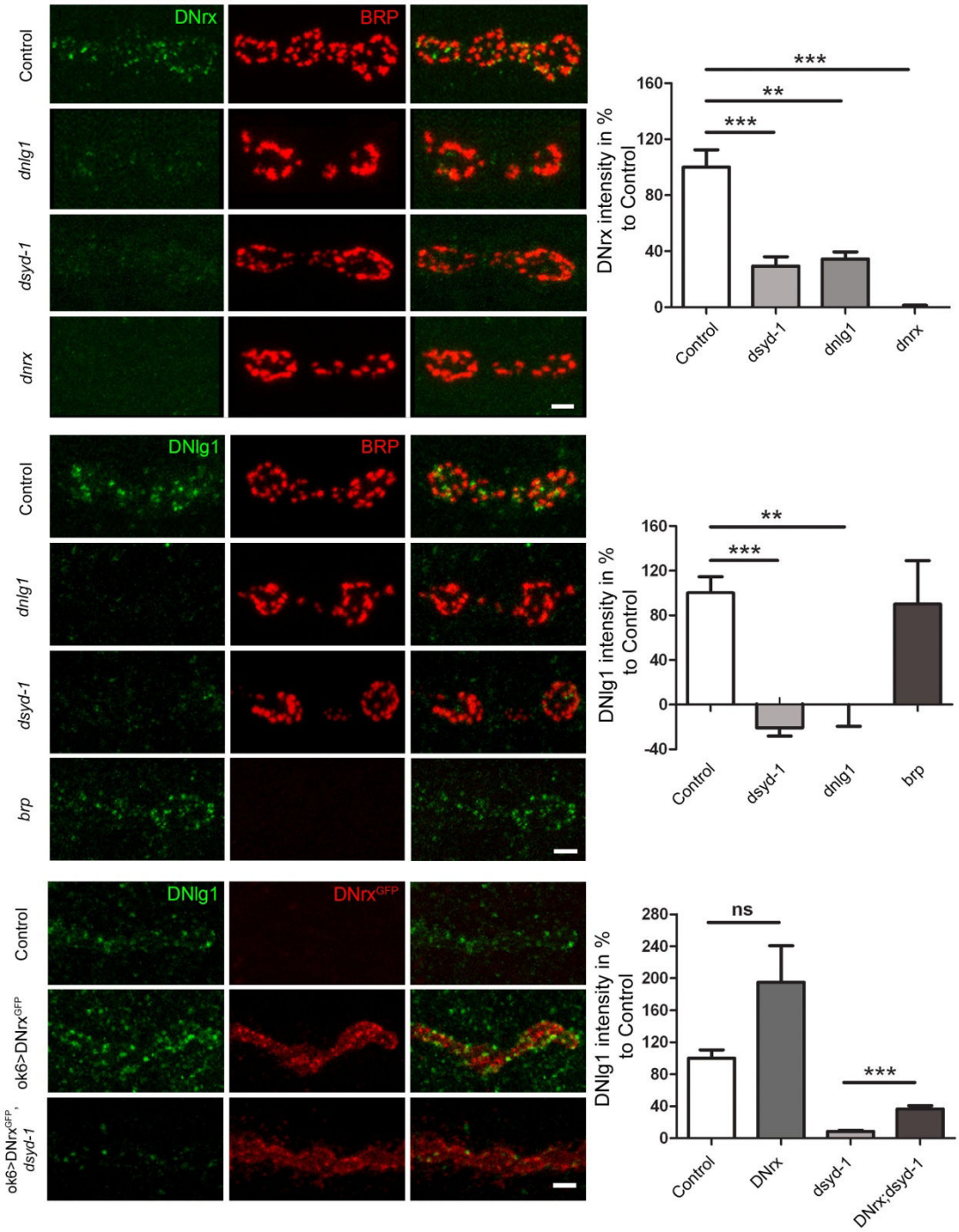

Figure 4.) Owald et al., 2012

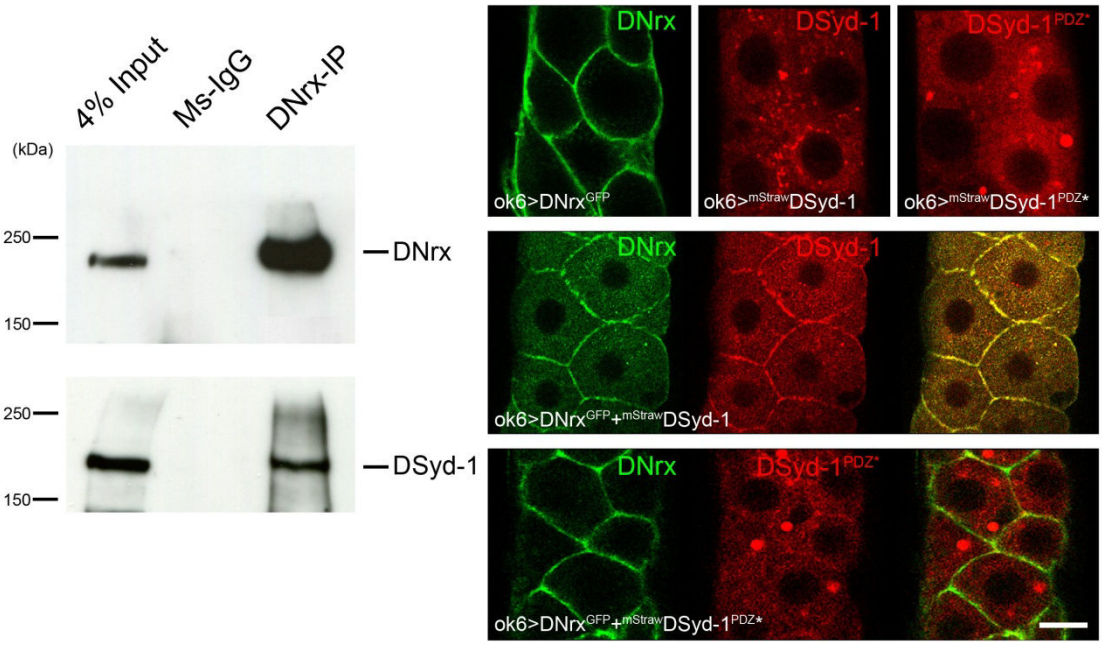

Figure 5.) Owald et al., 2012

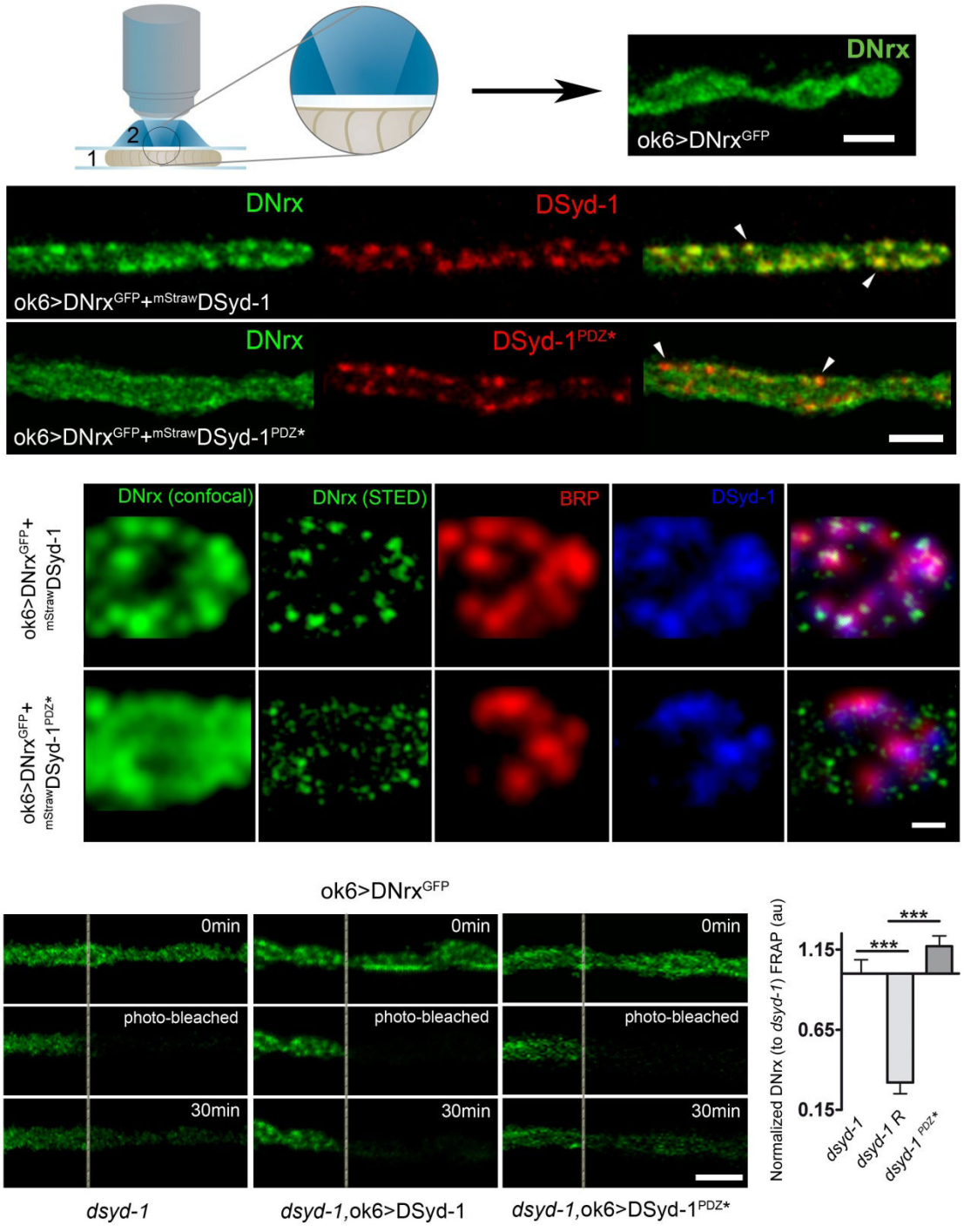

Figure 6.) Owald et al., 2012

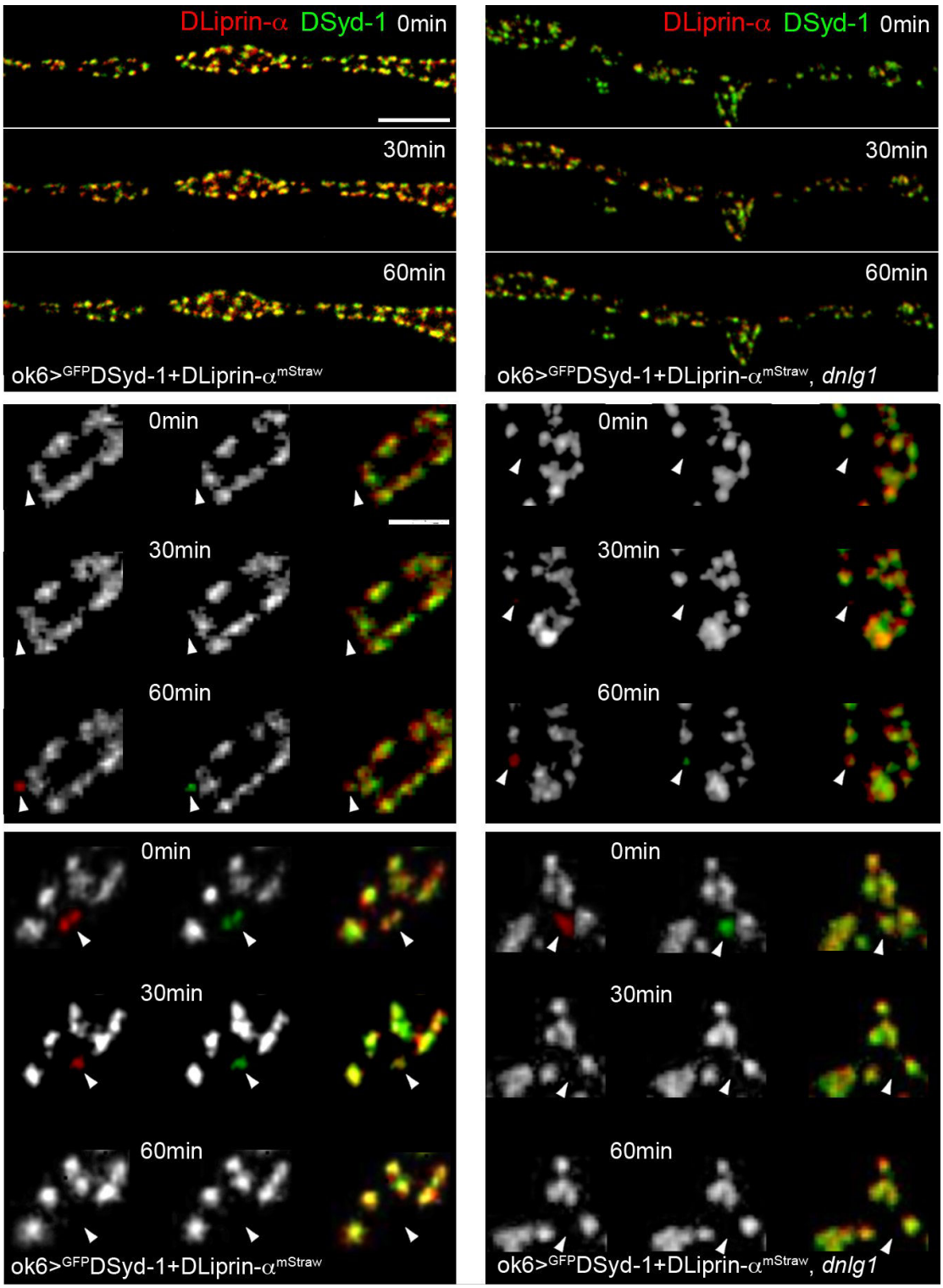

Figure 7.) Owald et al., 2012

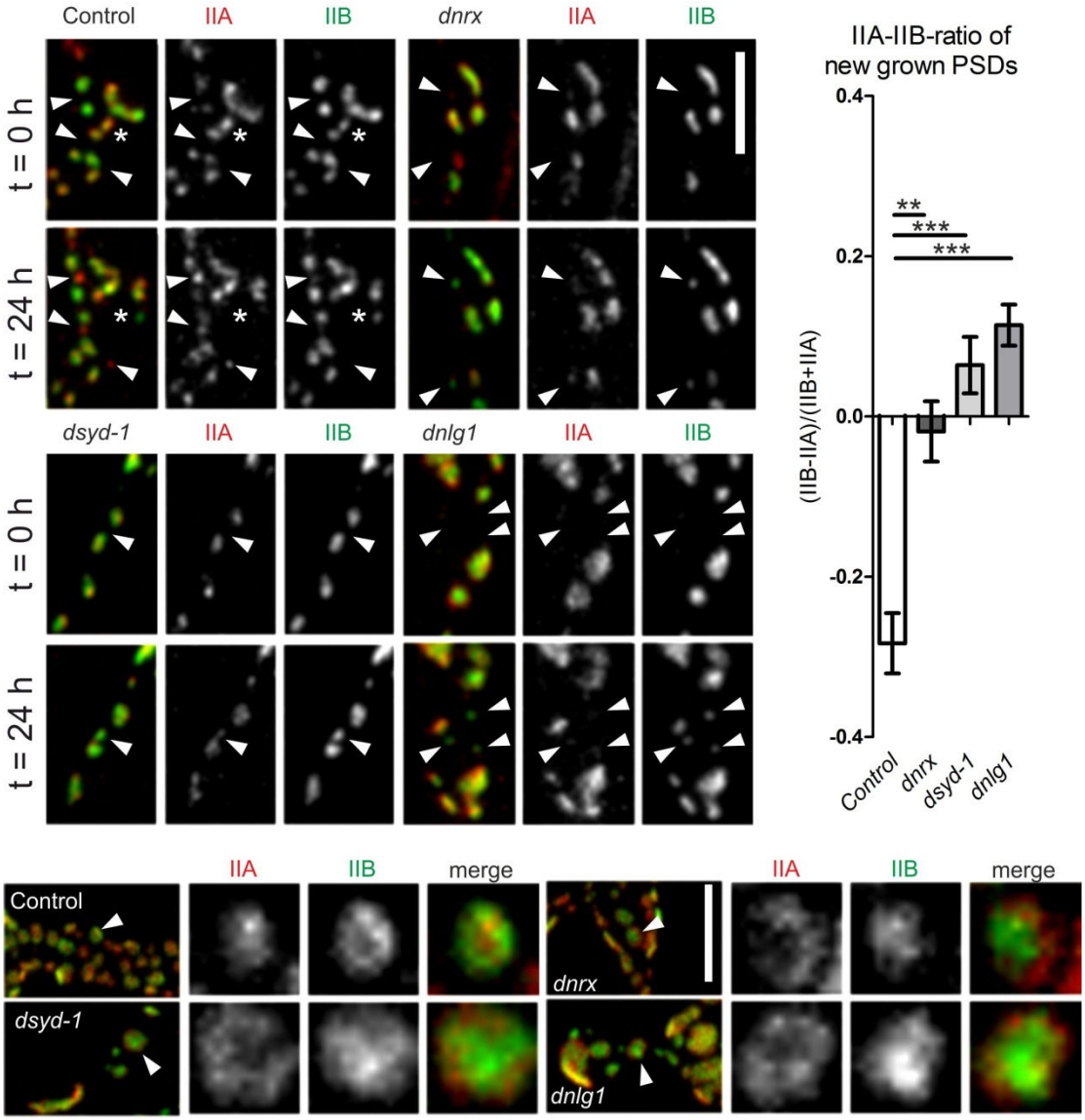

Supplemental Information

Supplemental Figures

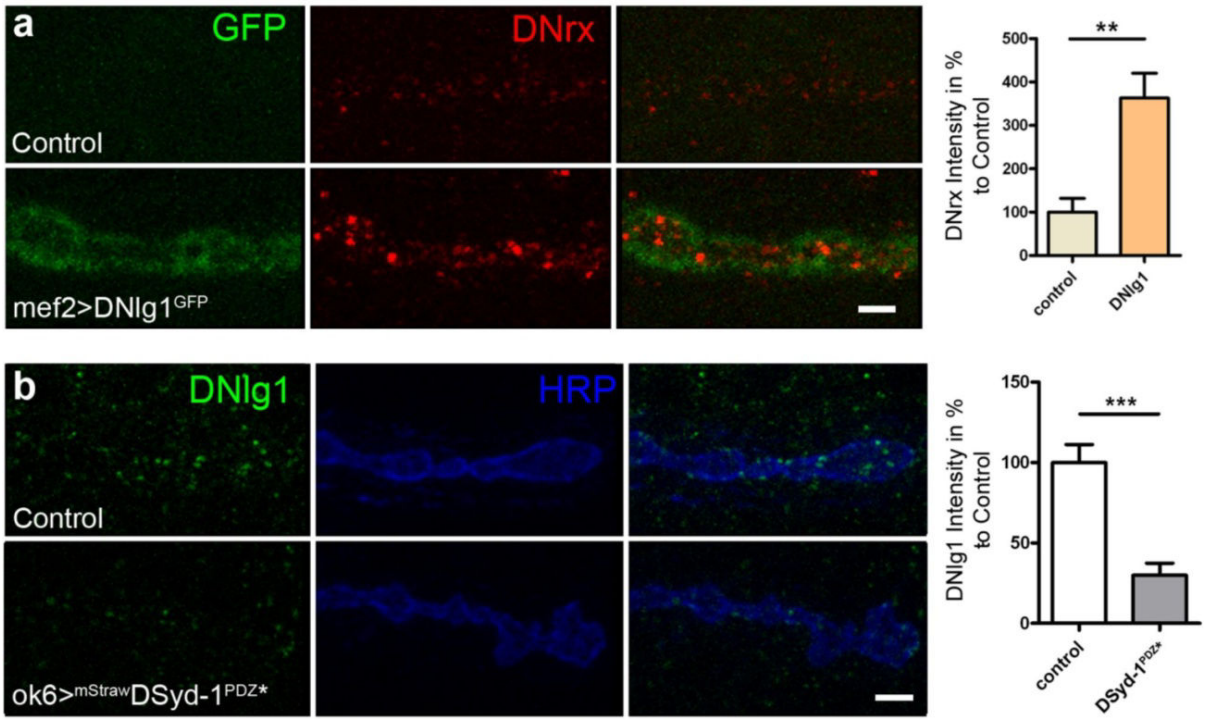

Supplementary Fig. 1: Analysis of DNlg1 localization

a) Muscle 4 boutons of a Control (upper panels), and UAS-DNlg1^{GFP} driven in muscles (lower panels) and immunostained for GFP and DNrx. Quantification of DNrx signal intensities normalized to control levels. (Control: 100.0±31.71, n=5; DNlg1: 362.9±56.81, n=10; p(Control x DNlg1)<0.01; Mann-Whitney U-test, U=1.0, **: p<0.01; all values are mean ± s.e.m.). Scale bar: 2µm. b) Muscle 4 boutons of Control (upper panels) and UAS-^{mStraw}DSyd-1^{PDZ*} driven in motoneurons (lower panels), co-stained for DNlg1 (green) and HRP (blue) that labels neuronal plasma membranes. Quantification of absolute DNlg1 signal intensities normalized to control levels. (Control: 100.0±11.26, n=11; DSyd-1^{PDZ*}: 29.93±7.52, n=12; p(Control x DSyd-1^{PDZ*})<0.001; Mann-Whitney U-test, U=1.0. ***: p<0.001; all values are mean ± s.e.m.). Scale bar: 2µm.

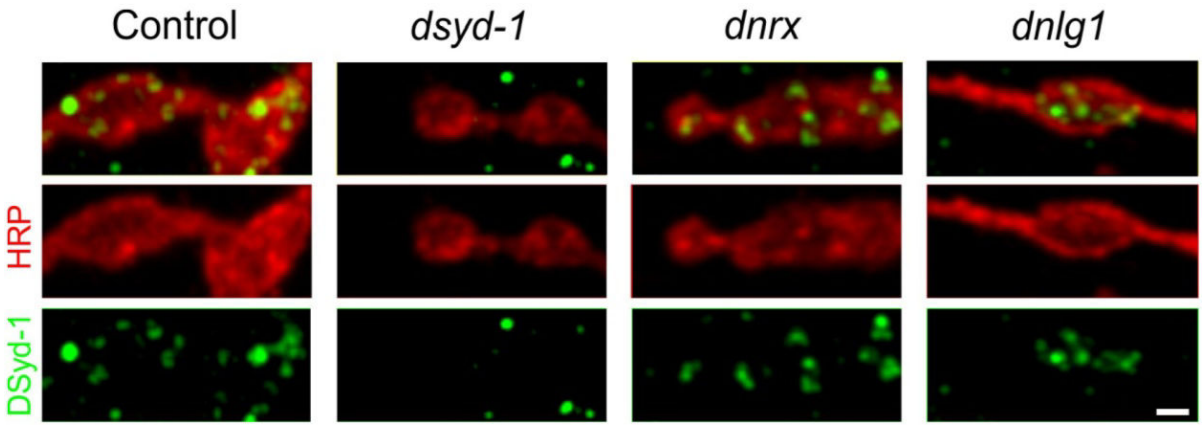

Supplementary Fig. 2: DSyd-1 persists at active zones of dnrx and dnlg1 larvae

Muscle 4 boutons from Control, *dsyd-1*, *dnrx* and *dnlg1* larvae immunostained for DSyd-1 (green) and HRP (red). Background reactivity of the DSyd-1 antibody at NMJs is indicated by asterisks.

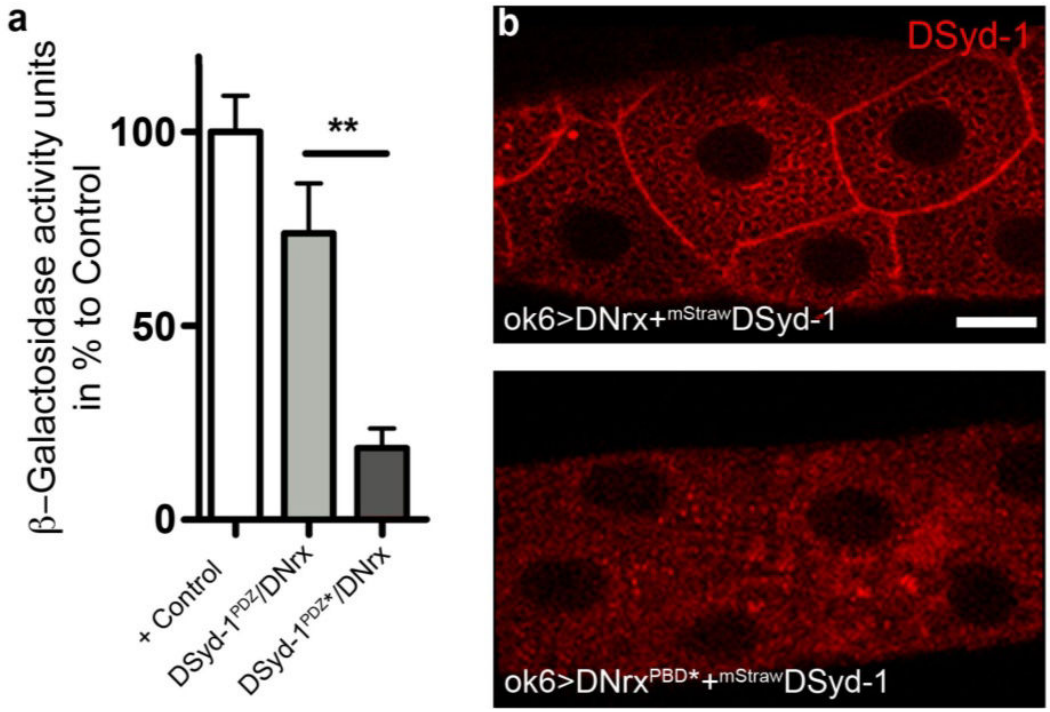

Supplementary Fig. 3: PDZ-mediated binding of DSyd-1 and DNrx

a) Liquid yeast two-hybrid assay. Binding of the unmutated PDZ (n=6 clones, 73.8±12.9), and the mutated PDZ domain (n=10 clones, 18.4±5.1), normalized to the positive Control (n=8 clones, p53/largeT, 100.0±9.4). p(mutated PDZ x unmutated PDZ)=0.003, Mann-Whitney U-Test, U=4.0.

b) UAS-^{mStraw}DSyd-1 is recruited to the plasma membrane of salivary glands when co-expressed with untagged UAS-DNrx, but not when co-expressed with untagged UAS-DNrx^{PDB} . Scale bar: 25µm.

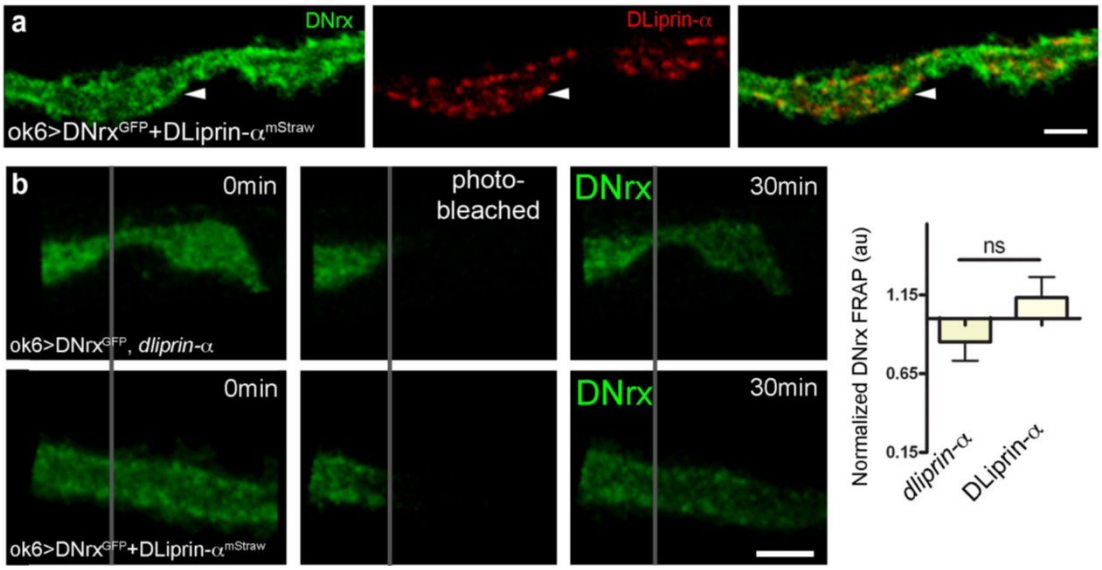

Supplementary Fig. 4: DLiprin-α is not sufficient to recruit DNrx to the active zone

a) Motoneuron-expression of UAS-DNrx^{GFP} with UAS-DLiprin-α^{mStraw}. DNrx does not co-localize with DLiprin-α (arrow). b) FRAP of UAS-DNrx^{GFP} driven in motoneurons of dliprin-α mutants, or together with UAS-DLiprin-α^{mStraw}. Quantification of DNrx recovery normalized to Control (dliprin-α: 0.850±0.117, n=13; DLiprin-α: 1.133±0.131, n=13; p(dliprin-α x DLiprin-α)>0.05; Mann-Whitney U-Test, U=53. ns: not significant; all values are mean ± s.e.m.). Scale bar: 2µm.

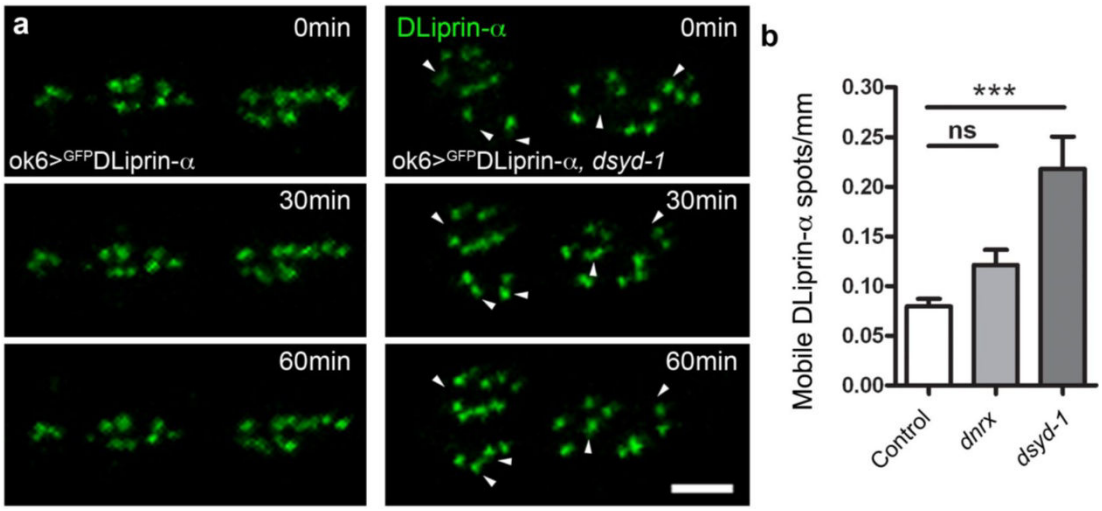

Supplementary Fig. 5: DLiprin-α is stalled by DSyd-1

a) Boutons of UAS-DLiprin-α animals imaged at 30 min intervals in Control and *dsyd-1* mutant animals. Arrows indicate mobile DLiprin-α spots in *dsyd-1*. Scale bar: 2µm. b) Quantification of mobile DLiprin-α and DSyd-1 clusters (over 60 minutes) normalized to the junction length (Control: 0.080±0.007, n=8; *dnrx*: 0.121±0.015, n=8; dsyd-1: 0.218± 0.032, n=8; p(Control x dnrx)>0.05, p(Control x *dsyd-1*)<0.001; Kruskal-Wallis test with Dunn's multiple comparison test (K=14.86).ns: not significant; ***: p<0.001; all values are mean ± s.e.m.). DLiprin-α mobility is significantly increased in *dsyd-1* mutants.

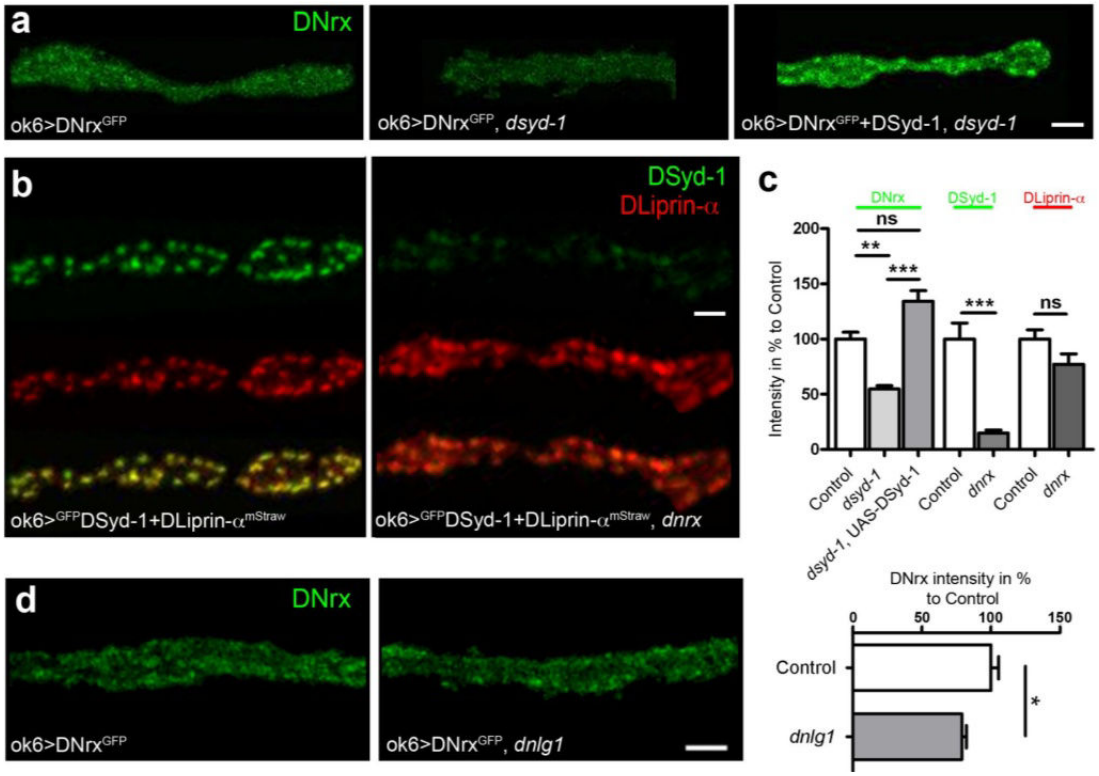

Supplementary Fig. 6: Expression levels of Gal4/UAS-expressed DNrx and DSyd-1

a) Muscle 26/27 junctional levels of UAS-DNrx^{GFP} driven in motoneurons of Control, *dsyd-1*, and *dsyd-1*, UAS-DSyd-1 (*dsyd-1* R) animals.

b) UAS-^{GFP}DSyd-1 and UAS-DLiprin-α^{mStraw} driven in motoneurons of Control and *dnrx* animals (muscle 26/27). Scale bar: 2µm.

c) Quantification of signal intensities normalized to control levels. (Control: 100.0±6.2, n=13; dsyd-1: 54.7±3.0, n=15; *dsyd-1*, UAS-DSyd-1 (dsyd-1 R): 134.2±9.6, n=12; p(Control x dsyd-1)<0.01, p(Control x *dsyd-1*, UAS-DSyd-1)>0.05, p(*dsyd-1* x *dsyd-1*, UAS-DSyd-1 (*dsyd-1* R))<0.001, Kruskal-Wallis test with Dunn's multiple comparison test (K=28.76). Control: 100.0±14.5, n=9; *dnrx*: 14.7±2.9, n=11; p (Control x *dnrx*)<0.001, Mann-Whitney U-Test, U=0.0. Control: 100.0±8.4, n=9; *dnrx*: 77.2±9.3, n=11; p(Control x *dnrx*)>0.05, Mann-Whitney U-Test, U=27. ns: p>0.05 (not significant), ***:p<0.001, all values are mean ± s.e.m.). The overexpressed DSyd-1 signal is reduced in *dnrx* mutants. Likely as a consequence of this, the overexpressed (excess) DLiprin-α appears diffuse in *dnrx* mutants (compare Supplementary Fig. 5).

d) Muscle 26/27 junctional levels of UAS-DNrx^{GFP} driven in motoneurons of Control and *dnlg1* animals. Quantification of signal intensities normalized to control levels. (Control: 100.0±5.5, n=13; *dnlg1*: 79.0±3.2, n=10; p(Control x *dnlg1*)<0.05; Mann-Whitney U-test, U=26.0. *: p<0.05; all values are mean ± s.e.m.). Scale bar: 2µm.

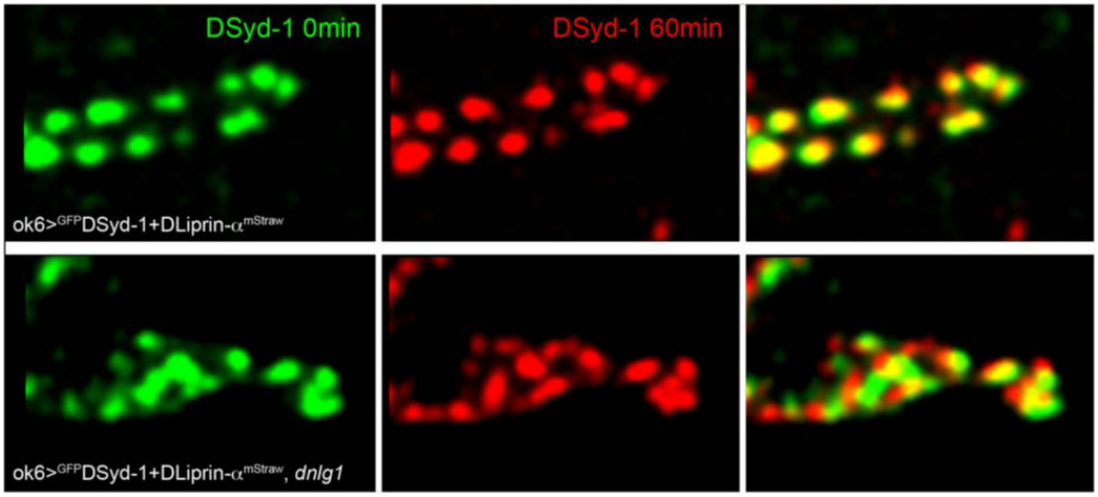

Supplementary Fig. 7: DSyd-1 fluctuates at dnlg1 mutant NMJs

DSyd-1 channel in Control and *dnlg1* mutant synapses (see Fig. 6) at time point t=0 min (green) and t=60 min (red). The DSyd-1 pattern strongly fluctuates in *dnlg1* mutants.

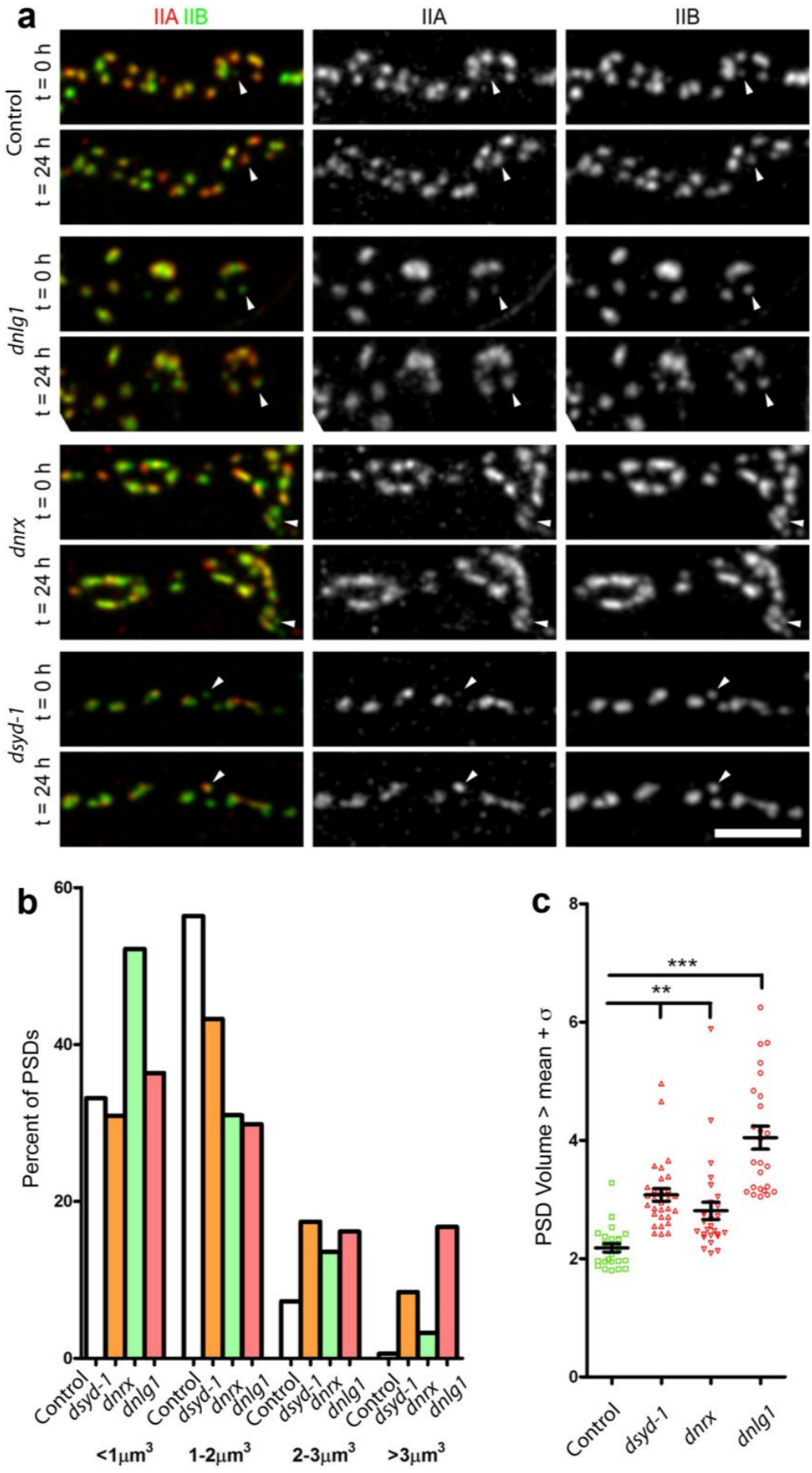
a
IIA IIB
IIA
IIB
Control
t = 0 h
t = 24 h
dnlg1
dnrx
dsyd-1
b
Percent of PSDs
60
40
20
0
Control
dsyd-1
dnrx
dnlg1
<1μm3
1-2μm3
2-3μm3
>3μm3
c
PSD Volume > mean + σ
8
6
4
2
0
***
**
Control
dsyd-1
dnrx
dnlg1

Supplementary Fig. 8: GluRIIA incorporation and PSD size distribution at *dnlg1*, *dnrx*, and *dsyd-1* NMJs

a) Examples of nascent, IIB-rich PSDs in Control, *dnlg1*, *dnrx*, and *dsyd-1* NMJs (arrows at t=0h) which incorporate IIB and major amounts of IIA after 24 hours (arrows at t=24h). Scale bar: 5µm.

b) Frequency distribution (in %) of the PSD size (in µm 3) for Control, *dsyd-1*, *dnrx*, and *dnlg1*. There is a strong shift towards big PSDs (2-3 μm^3 and >3 μm^3) in all three mutants. However, PSD volumes also differ between mutants.

c) Quantification of PSDs larger than the mean + σ of an individual group shows a significant shift in all three mutants towards larger PSDs compared to Controls. (Control: 2.18±0.07, n=24; *dsyd-1*: 3.08±0.11, n=30; *dnrx*: 2.81±0.15, n=28; *dnlg1*: 4.05±0.19, n=25; p(Control x *dsyd-1*)<0.01; p(Control x *dnrx*)<0.01; p(Control x *dnlg1*)<0.001; Kruskal-Wallis test with Dunn's multiple comparison test (K=64.07). **: p<0.01; ***: p<0.001; all values are mean ± s.e.m.).

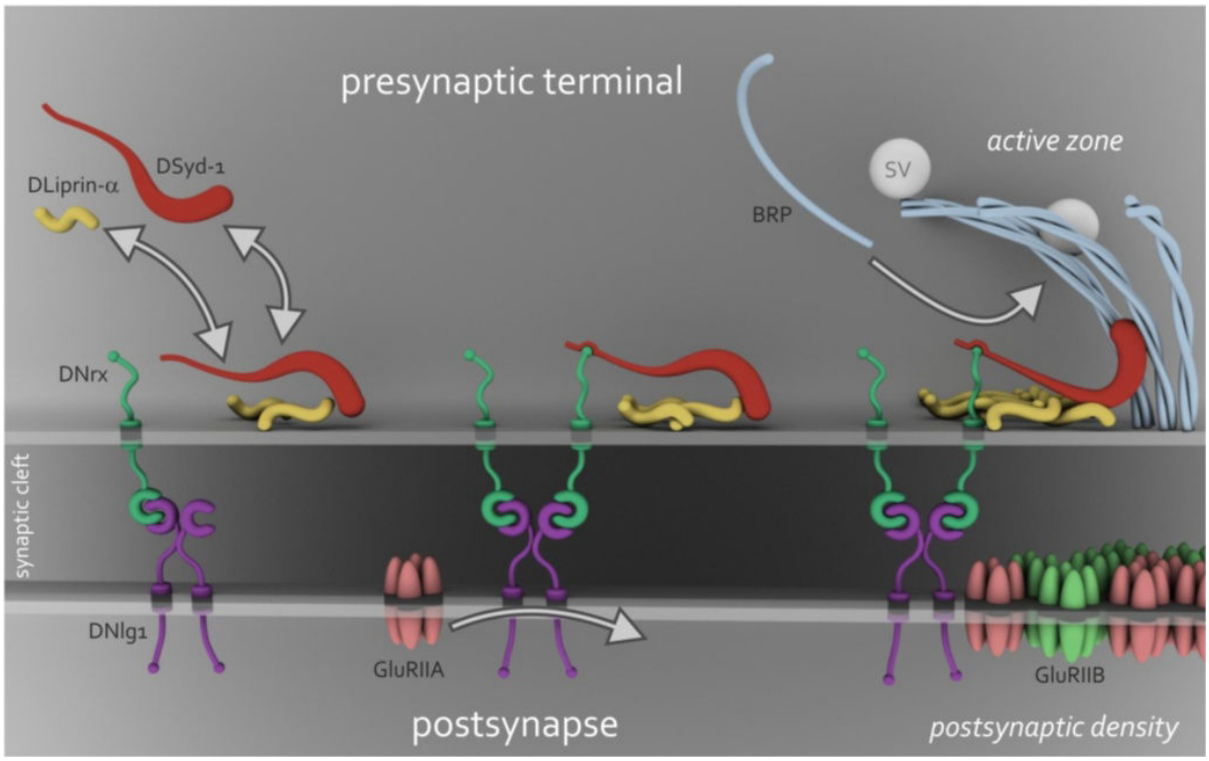

Supplementary Fig. 9: Model of transsynaptic regulation of synapse assembly

Clusters of DLiprin-α and DSyd-1 undergo rounds of assembly and disassembly at the presynaptic membrane (left). Coincident presence of DNrx (interacting with postsynaptic DNlg1) and DSyd-1 via a PDZ-motif interaction defines the sites where novel synapses form. DSyd-1 stalls DNrx and DLiprin-α, and DNlg1 keeps DSyd-1 in place (middle). On the postsynaptic side, the PSD localization of DNlg1 is dependent on presynaptic DSyd-1 and on DNrx. DNlg1 is instructive for early rapid incorporation of the growth promoting IIA-type GluR. As the synapse matures (right), DSyd-1 regulates the incorporation of BRP to the presynaptic active zone. This also appears to be

dependent on DNrx and DNlg1. On the postsynaptic side, receptor incorporation switches to the GluRIIB containing complex.

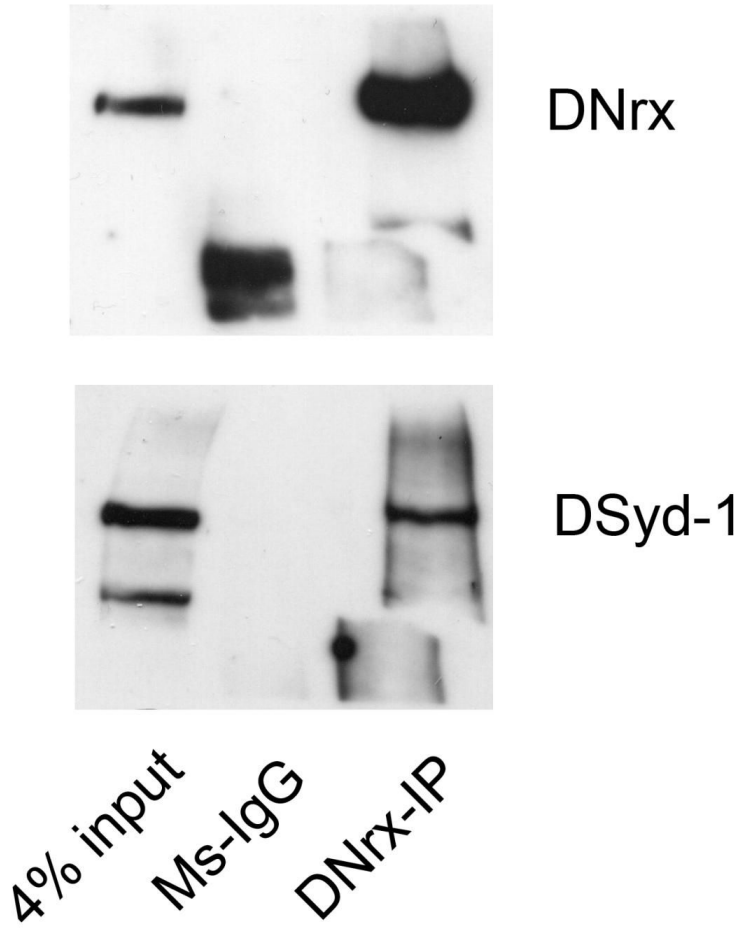

Supplementary Fig. 10: Co-Immunoprecipitation of DNrx and DSyd-1

Full blot of data shown in Fig. 4a.

3.22 Author contributions

DO, OK, SJS designed research.

DO, OK, VKG, DB, HD, WF, CW, SM, ER performed experiments.

DO, OK, VKG, DB, HD, WF, CW, SM, HA, SJS analyzed data.

MH and SE shared protocols/reagents/advice.

All authors commented on the paper.

DO, OK, SJS wrote the paper.

4 Discussion

Neuroligins (Nlg) are generally considered to play an important role in the establishment of fully functional neuronal circuits. In addition, mutations in human *nlg* genes have been linked to cognitive diseases such as autism (Dean & Dresbach, 2006). In previous experiments utilizing cultured cells, it has been shown that the binding of postsynaptic Nlg to presynaptic Neurexin (Nrx) is sufficient to induce synapse formation (Scheiffele et al., 2000). These were the first findings that suggested a synaptogenic role for the Nlg-Nrx complex. Further studies in mice, however, were hampered by the fact that rhodents posses 3 Nlg genes and single-gene knockout animals seem compensate for their loss with a redundant gene set. In addition, the characterization of the synaptic role of Nlgs in the mouse CNS is further complicated by the amount of synaptic connections in the brain (trillions). To unravel the mechanisms of synapse formation in an *in vivo* situation, we turned to the extensively studied NMJ of *Drosophila* to dissect Nlg function. The work presented here summarizes our attempts to unravel the function of postsynaptic *Drosophila* Neuroligin 1 (DNlg1) in synapse assembly (Banovic et al., 2010). Moreover, we addressed the role of presynaptic proteins DNrx and DSyd-1 in organizing synapse assembly via a transsynaptic complex (Owald et al., 2012).

4.1 *Drosophila* Neuroligin 1: new insights on a NMJ exclusive Nlg

4.1.1 NMJs of *dnlg1* mutants show severe morphological defects

DNlg1 was initially identified in an unbiased mutagenesis screen as *dnlg1* mutants feature significantly undergrown synaptic terminals in *Drosophila* larvae (Banovic et al., 2010; Fig. 1). Taking this as a starting point, we further dissected the *dnlg1* phenotype at the level of individual synaptic sites (synapses) to mechanistically study DNlg1's role in synapse assembly. We defined an individual prototypic synapse as one unit being build of a single presynaptic release site (AZ) which is apposed by a postsynaptic density (PSD). We analyzed NMJs of *dnlg1* mutants by staining for presynaptic BRP, demarking individual AZs (Marrus et al., 2004), and by labeling postsynaptic GluR fields (Qin et al., 2005). Stained NMJs were subjected to light-microscopic image acquisition and subsequent image analysis. Our data revealed severe miss-alignments of pre- and postsynaptic structures in *dnlg1* mutants. At NMJs of *dnlg1* mutants, a subset of AZs appeared to be un-apposed by postsynaptic GluRs; such missalignments occured in control NMJs only very rarely (Banovic et al., 2010; Fig. 4). Occasionally, we also found whole mutant boutons which completely lacked any postsynaptic GluR signal. TEM micrographs of mutant NMJs revealed that these boutons were missing any postsynaptic

specializations (*subsynaptic reticulum*, *SSR*) (Banovic et al., 2010; Fig. 5B-C). These boutons were thus termed *orphan boutons* (Banovic et al., 2010; arrows in Fig. 4B,D & E). However, the remaining postsynapses that harbored postsynaptic GluR fields were apposed by AZs. At the same time, the size of these GluR fields was significantly increased compared to controls (Banovic et al., 2010; Fig. S8).

We wondered whether the smaller NMJs of *dnlg1* mutants also harbor less synapses. Thus, we quantified the total number of synapses per NMJ – only synapses with a correct alignment of BRP and GluRs were counted – which revealed a reduction of about 50% in mutants (Banovic et al., 2010; Fig. 2A). This reduction seems proportional to the reduction in evoked excitatory junctional currents (eEJC) we measured using intracellular recordings (Banovic et al., 2010; Fig. 2B-C). We therefore concluded that the remaining synapses in *dnlg1* mutants are apparently functional, and their decrease in number is likely fully responsible for the reduction in transmitter release.

4.1.2 *In vivo* imaging reveals assembly of *orphan boutons*

The occurrence of *orphan boutons* in *dnlg1* mutants could be either the consequence of a postsynaptic assembly defect or of a mechanical detachment event of established synapses due to a lack of proper cell adhesion. The latter has been described for mutants of the Dynactin complex (Eaton & Davis, 2005; Eaton et al., 2002), which show an excess of retraction events of matured synaptic contacts. The remaining of these contacts can be detected on the muscle membrane as so called *footprints*, which contain postsynaptic proteins but lack presynaptic AZ differentiation. Although we did not detect any *footprints* in *dnlg1* mutants, we still wanted to rule out any postsynaptic retraction events as a cause for *orphan boutons*. To tackle this question we turned to intravital imaging (Andlauer & Sigrist, 2012; Rasse et al., 2005) of mutant larvae to follow the synapse assembly process at the NMJ during development. In the animals examined, presynaptic AZ-material was labeled by a BRP fragment fused to RFP (BRP_{short}-Straw; Schmid et al., 2008) and the SSR by the postsynaptic marker CD8-GFP-Sh (Zito et al., 1999). However, we were unable to detect a single synaptic detachment process in the 9 mutant terminals we imaged within 24 hours time intervals. Instead, we witnessed the accumulation of presynaptic material in the absence of any postsynaptic compartments during several occasions (Banovic et al., 2010; Fig. 3E-F). These findings suggest that *dnlg1* mutant terminals do not suffer from detachment defects, but instead accumulate AZ material independent of the postsynaptic maturation status. Altogether, we concluded that DNlg1 is responsible for the correct alignment of pre- and postsynaptic material, and the lack of DNlg1 causes the formation of *orphan boutons*.

4.1.3 DNlg1 localizes adjacent to glutamate receptor fields

Hereafter, we produced a DNlg1 antibody (AB) to investigate the synaptic location of endogenous DNlg1 at the NMJ. We found endogenous DNlg1 to localizing in a punctuate pattern at NMJ terminals adjacent but distinct from postsynaptic GluRs (Banovic et al., 2010; Fig. 6K-N). The DNlg1 antibody staining was no longer visible in *dnlg1* mutant NMJs (Banovic et al., 2010 Fig. 6E-F). To test whether DNlg1 is solely localized to the postsynaptic compartments of the NMJ we started to eliminate *dnlg1* expression in selected tissues using RNA interference (RNAi). Presynaptic knockdown of DNlg1 (using elav-Gal4 and ok6-Gal4) did not alter the staining of DNlg1 at NMJs (Banovic et al., 2010; Fig. 6G-H; S7C). In contrast, RNAi-suppression of *dnlg1* expression in muscles, utilizing the *mef2-gal4* driver, strongly reduced DNlg1 specific stainings (Banovic et al., 2010; Fig. 6I-J; S7C). These findings support the conclusion that DNlg1 is exclusively localized at postsynaptic compartments. This is in line with studies on vertebrate Neuroligins (Südhof, 2008).

We also generated a fluorescently labeled DNlg1 construct with GFP fused to a juxta-membrane position (DNlg1-GFP), as this location is predicted not to interfere with protein function (Dean & Dresbach, 2006; Wittenmayer et al., 2009; Banovic et al., 2010; Fig. 7A). The DNlg1 antibody staining was sensitive to the overexpression of DNlg1-GFP in the muscle, which resulted in a more than 100-fold increase of staining signal compared to *wildtype* NMJs (Banovic et al., 2010; Fig. S7A). Thus, our DNlg1 antibody was specific for endogenous DNlg1 and our DNlg1-GFP construct.

4.1.4 Presynaptic *Drosophila* Neurexin is required for effective localization of postsynaptic DNlg1

With these tools at hand, we were able to investigate the dependence of DNlg1 on its prime binding partner candidate: *Drosophila* Neurexin (DNrx). In many vertebrate studies it has been evaluated that Nrx is a major ligand for Nlg (Dean & Dresbach, 2006; Südhof, 2008). Therefore, we expected that this would hold also true for the conserved *Drosophila* homologues: DNrx and DNlg1. DNrx has been previously reported to be present at presynaptic NMJ terminals (Li et al., 2007). Intriguingly, *dnrx* mutants share similar phenotypes with *dngl1* mutant animals such as membrane ruffles at AZs and smaller NMJs with a reduced number of boutons (Li, Ashley, Budnik, & Bhat, 2007 ; Banovic et al., 2010; Fig. 8 A-E). In addition, quantification after 3D-reconstruction of postsynaptic receptor fields of mutant NMJs revealed that the integrated GluR intensities per PSD were significantly increased in *dnlg1* and *dnrx* mutants (Banovic et al., 2010; Fig. S8). Interestingly, NMJs of the *dnrx*, *dnlg1* double mutants were not significantly different from the *dnlg1* single mutant. Thus, further loss of synaptic DNrx does not add to the NMJ growth defects already present in *dnlg1* single mutants. This suggests that DNlg1 and DNrx act in the same pathway to promote terminal growth.

To study the relationship between DNlg1 and DNrx localization we visualized the distribution of DNrx and DNlg1 at the NMJ by performing co-labeling experiments. Herefore, we created a GFP-tagged cDNA construct of DNrx (DNrx-GFP), which we expressed in presynaptic motoneurons of *dnrx* mutants. Subsequently, these NMJs were counter-stained for DNlg1. Endogenous DNlg1 and DNrx-GFP were frequently found in apposing spots localizing adjacent to the synapse (Banovic et al., 2010; Fig. 8L).

Next, we tested if presynaptic DNrx is needed for effective clustering of postsynaptic DNlg1 by staining *dnrx* mutant NMJs for DNlg1. Interestingly, DNlg1 clusters were drastically reduced in *dnrx* mutant terminals (Banovic et al., 2010; Fig. 8N). Furthermore, presynaptic down-regulation of DNrx (using ok6-Gal4) significantly decreased endogenous DNlg1 levels, whereas the postsynaptic expression of *dnrx*-RNAi did not affect the DNlg1 signal (Banovic et al., 2010; Fig. S8C). These experiments showed that presynaptic DNrx is required for effective accumulation of apposed DNlg1 in compartments close to individual synapses.

4.1.5 Overexpression of DNlg1 results in a NMJs with decreased size

During our studies on DNlg1 a peculiar phenomenon drew our attention. We observed a significant undergrowth of *wildtype* NMJs (Banovic et al., 2010; Fig. 8F-K) when overexpressing untagged DNlg1 in muscles, at levels significantly higher than DNlg1-GFP (Banovic et al., 2010; Fig. S7A). The ecto-domain of DNlg1 was crucial for this effect, since overexpression of a truncated version of DNlg1, which is lacking the n-terminal part (Banovic et al., 2010, Fig. 7A) (DNlg1-Δextra), did not affect NMJ size. We further tested, if this effect of full-length DNlg1 overexpression depends on the binding of DNlg1's ecto-domain to DNrx. Therefore, we introduced a point mutation into the ligand-binding domain of DNlg1, DNlg1^{D356R}, which has been reported to abolish the binding of Nlg to Nrx in mammals (Reissner et al., 2008). In contrast to the unmodified version, DNlg1^{D356R} overexpression in *wildtype* muscles did not visibly alter the structure of NMJs (Banovic et al., 2010; Fig. 8G). Thus, the dominant-negative effect of overexpressed DNlg1 obviously depends on its ability to directly interact with DNrx. Interestingly, overexpression of a DNlg1 construct lacking the cytosolic C-terminus (DNlg1-cyto) resulted in the most dramatic reduction of NMJ size (Banovic et al., 2010; Fig. 7E-L).

While the mechanism underlying this phenotype remains elusive so far, we utilized DNlg1-cyto overexpression for a small candidate suppressor screen to score for potential candidates involved in the DNlg1-DNrx pathway. In the following report, we started out to test if mutants for our candidate genes would suppress the strong DNlg1-Δcyto-overexpression phenotype.

4.2 A transsynaptic complex regulates pre- and postsynaptic maturation

4.2.1 Phenotypic similarities between *dsyd-1*, *dnrx*, and *dnlg1* mutant NMJs

One prime candidate for we wanted to test for its involvement in the DNrx-DNlg1 pathway was DSyd-1. *Drosophila* mutants of *dsyd-1* share many phenotypic similarities with mutants for *dnrx* and *dnlg1*. For example, NMJs mutant for *dsyd-1* feature a reduction in NMJ size, neuronal membrane rufflings, abnormally shaped T-bars and ectopic accumulation of AZ material (Owald et al., 2010). All these phenotypes can be also observed in mutants for *dnrx* and *dnlg1* (Li et al., 2007; Banovic et al., 2010).

Intriguingly, *dsyd-1* mutant background completely suppressed the strong DNlg1-cyto phenotype (Owald et al., 2012 Fig. 1b-c). This implies that DSyd-1 might act in the same pathway as DNrx and DNlg1. In the following, we started a detailed comparison of the mutant phenotypes of *dnlg1*, *dnrx*, and *dsyd-1* mutants to review this finding.

Quantification of NMJ size showed that all three mutants (*dnlg1*, *dnrx*, and *dsyd-1*) feature comparable defects in terminal growth (Owald et al., 2012; Fig. 1b-c). When we extended this analysis to the double-mutant combinations of all three mutants, we found that they behaved non-additive, meaning that the NMJ size of double mutants was not significantly different from the respective single mutants (Owald et al., 2012; Fig. 1b,-c).

Hereafter, we focused our attention to defects of individual synapses and started out to analyze the AZ morphology of all mutants with *stimulated emission depletion* (STED) microscopy (Hell et al., 1994; Klar et al., 2000). In traditional fluorescence microscopes, the spatial resolution depends on the size of the excitation spot. The spot size, in turn, depends on the microscopes parameters and is limited by about half the wavelength of the fluorescent light. However, in STED microscopes most of the excited fluorophores inside the excitation spot get quenched to their ground state by stimulated emission. This effect allows to shrink the emission volume and increases hereby the optical resolution (Hell & Wichmann, 1994). In contrast to traditional electron microscopy, STED technique allowed us to quickly and effectively quantify changes of the T-bar morphology on a nanometer scale in a great number of genotypes.

The samples we analyzed with STED were stained with antibodies against *Bruchpilot* (BRP). As mentioned already in the introduction (*Synaptic proteins at the Drosophila NMJ*), BRP is a direct molecular building block of the electron-dense T-bar (Fouquet et al., 2009), and BRP assembly was previously linked to overgrown T-bars in *dsyd-1* mutants (Owald et al., 2010). At control NMJs, diffraction-limited BRP spots appear as “ring”-shaped structures when imaged at higher resolutions with STED (Kittel et al., 2006). Intriguingly, BRP rings were frequently interconnected and overgrown

in all mutants (Owald et al., 2012; Fig. 2h-i). In fact, quantification of STED images showed BRP ring diameters to be similarly increased in all *dsyd-1*, *dnrx* and *dnlg1* single mutants, and double mutants (Owald et al., 2012; Fig. 2n). This strongly supports the hypothesis that all three proteins, DSyd-1, DNrx, and DNlg1, act in a common pathway. Although vertebrates share homologues with all three proteins (Haucke et al., 2011; Owald & Sigrist, 2009), a functional connection between Syd-1 and Nrx has not been described so far. This encouraged us to investigate the potential involvement of DSyd-1 in the transsynaptic DNrx-DNlg1 pathway.

4.2.2 Direct interaction between DSyd-1 and DNrx

To explore the relationship of DSyd-1 and the transsynaptic DNrx-DNlg1 complex, we utilized antibodies against DNrx and DNlg1 (Li et al., 2007; Banovic et al., 2010). At *wildtype* NMJs, endogenous DNrx forms clusters at the presynaptic terminal (Li et al., 2007; Owald et al.; 2012; Fig. 3a) opposite to the postsynaptic localization of endogenous DNlg1 (Banovic et al., 2010; Fig. 8L). In *dsyd-1* mutants however, the signals of DNrx and DNlg1 at the NMJ are completely abolished (Owald et al., 2012; Fig. 3c-d). Thus, DSyd-1 is involved in clustering presynaptic DNrx and postsynaptic DNlg1 adjacent to synapses. However, DSyd-1 itself did not fail to cluster in *dnrx* and *dnlg1* mutant NMJs (Owald et al., 2012; Fig. S2) suggesting an involvement of other, DNrx-DNlg1-independent pathways in synaptic DSyd-1 clustering.

In a previous report the *C. elegans* homologues of Syd-1 and Nrx were found to interact in yeast-to-hybrid screens (Lenfant et al., 2010). Therefore, we tested if this direct binding is conserved in *Drosophila* Syd-1 and Nrx. Harald Depner (AG Sigrist) performed immunoprecipitations from an AZ protein-enriched preparation using antibodies recognizing endogenous DNrx (Sun et al., 2009). Thus, we were able to show that DSyd-1 and DNrx are part of a common complex under *in vivo* conditions (Owald et al., 2012; Fig. 4a).

4.2.3 The PDZ binding domain of DSyd-1 is crucial for synaptic DNrx localization

Next, our aim was to find the molecular link joining DSyd-1 and DNrx. Lenfant et al. (2010) identified a direct interaction of the Syd-1 PDZ-domain with Nrx under *in vitro* settings (Lenfant et al., 2010). To test this potential interaction with *Drosophila* homologues and under *in vivo* settings, mutations were introduced into the PDZ-domain of a fluorescently labeled DSyd-1 fusion construct (DSyd-1 ^{PDZ*}-Straw) with the aim to disrupt the ligand binding motif (Owald et al., 2012; Fig. 1a).

This construct was utilized in an series of *in vivo* imaging experiments (Rasse et al., 2005) to test for PDZ dependent interactions at the NMJ of intact animals. First, we expressed *wildtype* cDNA constructs of DSyd-1 (Dsyd-1-Straw) and DNrx (DNrx-GFP) in motoneurons. While DSyd-1-Straw localized to AZs (Owald et al., 2010), DNrx-GFP, when solely expressed, was distributed more diffusely over the presynaptic terminal membrane (Owald et al., 2012; Fig. 5b). However, in NMJs co-expressing both constructs, DNrx-GFP became clearly enriched within the Dsyd-1-Straw positive AZs (Owald et al., 2012; Fig. 5c). Thus, over-expressed DSyd-1 is sufficient to direct over-expressed DNrx towards AZs. Next, we expressed DSyd-1^{PDZ}*-Straw together with DNrx-GFP. DSyd-1 ^{PDZ*}-Straw still localized at AZs to a good extent, whereas DNrx-GFP appeared diffuse in this situation and was indistinguishable from the DNrx-distribution in the absence of DSyd-1 co-expression (Owald et al., 2012; Fig. 5d). Thus, DSyd-1^{PDZ}*-Straw failed to recruit DNrx-GFP to AZs.

We also used STED-microscopy to investigate DNrx localization relative to the AZ marker BRP. At approximately 80 nm resolution DSyd-1 puncta surrounded the BRP core (Owald et al., 2010). When co-expressed with DSyd-1-Straw, a fraction of UAS-DNrx-GFP puncta also surrounded the BRP core. As expected, this AZ-associated fraction (Owald et al., 2012; Fig. 5e) was no longer apparent when co-expressing DNrx-GFP together with DSyd-1^{PDZ}*-Straw. Under this condition, DNrx-GFP distributed randomly and distal from AZs (Owald et al., 2012; Fig. 5f). Taken together, DSyd-1 and DNrx can not only be found biochemically in one complex, but DSyd-1 can also change the distribution of overexpressed DNrx from a more diffuse distribution towards a more synaptic localization.

4.2.4 NMJs mutant for *dsyd-1*, *dnrx*, or *dnlg1* share the same GluR assembly defects

We finally turned our attention to the postsynapse to examine the consequences of a disrupted DNrx-DNlg1 complex on GluR clustering. As mentioned above (Rasse et al., 2005; Schmid et al., 2008) the majority of young PSDs are composed of GluRIIA in control NMJs (Owald et al., 2012; Fig. 7a). In contrast, all three single mutants (*dnlg1*, *dnrx*, and *dsyd-1*) featured young PSDs with a significant shift towards a more GluRIIB-rich composition (Owald et al., 2012; Fig. 7a-b). Therefore, all three mutants show an obvious inability to effectively cluster GluRIIA containing complexes in early synapse assembly. The early incorporation of GluRIIA is a major driving force for PSD assembly and thus for synapse formation at growing NMJ terminals (Rasse et al., 2005; Schmid et al., 2008; Sigrist, et al., 2002). This deficit in early GluRIIA incorporation might contribute to the reduced number of synapses forming in these mutants (Banovic et al., 2010; Fig. 2A; Owald et al., 2012; Fig. 1c-d).

GluRIIA incorporation appears to be nearly irreversible as photo-activation experiments have previously shown (Rasse et al., 2005). In these experiments, early incorporated GluRIIA remained at the PSD core after the incorporation of other GluRs during subsequent PSD growth. As a result, PSDs of *wildtype* NMJs often show a GluRIIA-rich core surrounded by a GluRIIB-rich edge (Owald et al., 2012; Fig. 7c). Notably, this "concentric arrangement" was regularly inverted in *dnlg1*, *dnrx,* and *dsyd-1* single mutants (Owald et al., 2012; Fig. 7c), reflecting GluRIIB-rich PSDs, which eventually incorporate GluRIIA (Owald et al., 2012; Fig. S8a). Finally, a fraction of PSDs overgrew in all three mutants (Owald et al., 2012; Fig. S8b-c).

In summary, all three mutants share a specific deficit in the early, PSD growth-promoting GluRIIA incorporation. DSyd-1 and DNrx1 are likely directly responsible for specific assembly of the synaptic distribution of GluR subunits, by enabling proper postsynaptic clustering of DNlg1. In our model, DSyd-1 supports the aggregation of DNrx, which in turn clusters postsynaptic DNlg1, thus resulting in a coupling of pre- to postsynaptic assembly (Owald et al., 2012; Fig. 7d). The function of DNlg1 appears to be to provide avidity for GluRIIA complexes during "early assembly", and choosing the right temporal sequence seems important for the GluR clustering process to come to a proper end (proper PSD size).

It is most likely that the GluR clustering defect, which is present in all three mutants, is the result of an interrupted interaction between GluRs and an interacting protein. Intriguingly, all three single mutants did not only feature defective segregation of GluRs inside individual PSDs, but were also lacking proper DNlg1 clustering at NMJs. If DNlg1 itself interacts directly with GluRs remains still unclear. In vertebrates however, the functional interactions between Neuroligin and AMPARs was shown to involve indirect binding of both proteins. At the mouse postsynapse, PSD-95 binds to the c terminus of Neuroligin via PDZ mediated interaction and the auxiliary AMPAR subunit Stargazin (Mondin et al., 2011; Opazo et al., 2010). Intriguingly, there are *Drosophila* homologues for PSD-95 (Dlg) and Stargazin (DSTG; see thesis T. Schwarz) present at the NMJ (Knight, Xie, & Boulianne, 2011; Owald et al., 2010).

Neuroligins and TARPs share common features in their domain structure. Both feature trans-membrane- and extracellular ecto-domains that could, in principle, interact with the ecto-domains of GluRs. At their c terminus Nlgs (Nlg1-4) posses a PDZ binding motif –*TTRV*, which is close to the terminal motif of TARPs (-*TTPV*). Synaptic scaffolding proteins, such as PSD-95 and MAGI-2, are able to cluster both, Neuroligins (Iida et al., 2004; Irie et al., 1997) and TARPs (Deng et al., 2006; Funke et al., 2005), via these PDZ binding motifs.

5 Outlook

5.1 Desensitization kinetics modulates synaptic incorporation dynamics of GluRs

The data presented above reveal a stereotypic pattern of subunit specific GluR clustering in PSD-subdomains at *wildtype* synapses. However, this pattern of GluRIIA and GluRIIB clustering is inverted in *dsyd-1*, *dnrx,* and *dnlg1* mutants. This suggests the involvement of the transsynaptic DNlg1-DNrx pathway to actively steer GluR incorporation.

A previous report has shown that neuronal activity itself can also regulate GluR localization at PSDs. In 2000, Sigrist et al. enhanced locomotor activity of 3rd instar larvae by increasing the rearing temperature from 18°C (25°C) to 29°C. As a result, NMJs increased in size, featured a higher synapse density, and a higher GluRIIA immunoreactivity at PSDs. It can therefore be concluded that the regulation of GluR incorporation at the *Drosophila* NMJ is enabled by interplay of activity regulated mechanisms (Sigrist et al., 2002) and transsynaptic CAM-mediated control (Owald et al., 2012). Whether there is an intersection of these two regulatory pathways, and how these convey their effect on the GluRs remains elusive. To shed more light on these missing details of GluR control, we focused our attention on the intrinsic properties of the GluR itself to examine how these affect GluR localization. All results shown derive from unpublished datasets.

5.2 Regulation of two different types of GluRs enables postsynaptic plasticity at the *Drosophila* NMJ

At the *Drosophila* NMJ there are two GluR complexes present containing either the GluRIIA or GluRIIB subunit. Here, these complexes are referred to as GluRIIA and GluRIIB (DiAntonio et al., 1999; Petersen et al., 1997). Both receptor complexes differ in their synaptic localization, trafficking behavior (Rasse et al., 2005; Schmid et al., 2008), and bio-physiological properties (DiAntonio et al., 1999; Petersen et al., 1997; see table 1). Recent *in vivo* imaging studies from our lab dissected the differences of subunit-specific GluR incorporation into synapses with fluorescence recovery after photobleaching (FRAP) experiments (Rasse et al., 2005; Schmid et al., 2008). Here, significant differences in the incorporation dynamics of GluRIIA and GluRIIB into PSDs were shown. Moreover, the experiments revealed that GluRIIB incorporates more uniform over all PSDs, whereas the incorporation of GluRIIA is typical for newly forming PSDs and is therefore often different between individual synapses (Schmid et al., 2008; see 2.4 Ionotropic glutamate receptors at the *Drosophila* NMJ*)* and table **1**.

Table 1.) Reported findings on GluRIIA and GluRIIB complexes and *gluRIIA*^{null} and *gluRIIB*^{null} mutants

	GluRIIA	GluRIIB	published in
quantal size in mutants:	4x smaller in *glurRIIA*^{null}	as in *gluRIIB*^{nul} mutants	DiAntonio et al., 1999
change in quantal size by overexpression:	33-59% increase	68% decrease	Petersen et al., 1997 & DiAntonio et al.,1999
desensitization time constant:	18.8ms	2.0ms	DiAntonio et al., 1999
single channel current amplitude:	9.2pA	8.1pA	DiAntonio et al., 1999
bouton number in mutant NMJs:	not significatly changed	increased	Sigrist et al., 2002
overexpression NMJ phenotype:	higher n of synapses	no change to controls	Sigrist et al., 2002
PSD incorporation behaviour:	varies among synapses	uniformly	Schmid et al., 2008

for more informations on GluRIIA & GluRIIB see:: 2.4 Ionotropic glutamate receptors at the *Drosophila* NMJ

In Schmid et al., (2008) we tested for the role of neuronal activity on postsynaptic GluR localization by expressing *tetanus toxin light chain* (TNT) in motor neurons, which effectively suppresses evoked glutamate release (Sweeney et al., 1995). This resulted in increased incorporation of GluRIIA into PSDs. FRAP experiments under these conditions showed that the number of newly incorporated GluRIIA complexes increased, whereas the number of newly incorporated GluRIIB complexes decreased (Schmid et al., 2008). As a result, NMJs expressing TNT featured more IIA-rich PSDs as compared to control NMJs (Schmid et al., 2008). Therefore, we asked which interactions might effectively account for the change in GluR localization under activity suppression.

From here, we went on to test if the intracellular C-terminal domains (CTDs) of the GluRs are the substrate for activity dependent modifications. Furthermore, our motivation was to test if these modifications might effectively account for the change in GluR localization under activity suppression.

In vertebrates, the intracellular C-terminal domains (CTDs) of GluRs have been implicated in the subunit-specific target behavior of GluRs (Barry & Ziff, 2002; Bredt & Nicoll, 2003; Malinow & Malenka, 2002). Therefore, we decided to test if the intracellular C-terminal domains (CTDs) of *Drosophila* GluRs are affecting the individual FRAP behaviors. For this purpose, chimeric GluRIIA and GluRIIB constructs with exchanged CTDs were generated (GluRIIA$_B$ and GluRIIB$_A$). However, FRAP analysis of GluRIIA$_B$ and GluRIIB$_A$ revealed that swopping the CTDs between GluRIIA and GluRIIB did not switch the incorporation behavior of both GluR types (Schmid et al., 2008). Hence, other mechanisms involving the extracellular ecto- or transmembrane domains (TMDs) have to be involved in the subunit specific incorporation of GluR complexes into PSDs.

To test for further mechanisms controlling synaptic GluR dynamics we turned to the biophysical properties of the receptor. In physiological terms, the most striking difference of both GluR complexes is the difference in desensitization kinetics. Based on single channel recordings, GluRIIB was suggested to desensitize about 10 times more rapidly than GluRIIA (DiAntonio et al., 1999). Desensitization is a long-lasting conformational state of receptors in which they are bound to ligands while the channel pore remains closed. In the next step we tested if the difference in desensitization kinetics between GluRIIA and GluRIIB conveys directly into the difference of synaptic trafficking behavior. Hence, we developed a system to perturb the desensitization characteristics of our genomic GluRIIA construct (Rasse et al., 2005).

5.3 Structural basis of desensitization /gating behavior of GluRs

The most straightforward approach to perturb specific protein functions is to replace specific Amino Acids (AAs). This is achieved by the introduction of point mutations into the DNA sequence. Hereby, it is possible to convert the triplet code of one specific AA into that of another. The GluRs expressed at the NMJ of *Drosophila* are closely related to mammalian GluRs, namely AMPA and even more Kainate (KA) receptors, with a high degree of conservation at the ligand binding domains (LBDs) (Fig. 1). The structure-function relationship of channel-gating in GluRs has been extensively analyzed in heterologuos expression systems where directed mutagenesis of AMPARs was combined with electro-physiological characterizations (Madden, 2002). These reports enabled a detailed understanding of the intra-molecular mechanisms that accompany the gating events of GluRs.

In the following I will discuss the mechanisms of GluR desensitization in more detail.

Typically, ligand gated ion channels are closed in the resting state, open in response to the binding of agonist (activation), and close spontaneously even in the continuing presence of agonist (desensitization). After agonist binding, channels undergo conformational changes to permit gating of the ion pore. Thus, the free binding energy provided by the agonist stabilized LBD-closure conveyed into a movement of the transmembrane domains (TMDs) that form the ion channel pore and enable the ion-flux through this pore (Fig. 1a.) (Armstrong & Gouaux, 2000; Mayer et al., 2001; Sun et al., 2002). The dimer interface between a pair of LBDs has been shown to be crucial for this, as both LBDs are required to be held in a fixed position while the ion channels move (Madden, 2002). It has been further proposed that during desensitization the agonist binding energy is used to disrupt the dimer interface, allowing the pore to close with the LDBs remaining in the closed-cleft conformation (Sun et al., 2002).

Figure 1.) Mutations in conserved GluR domains affecting desensitization kinetics

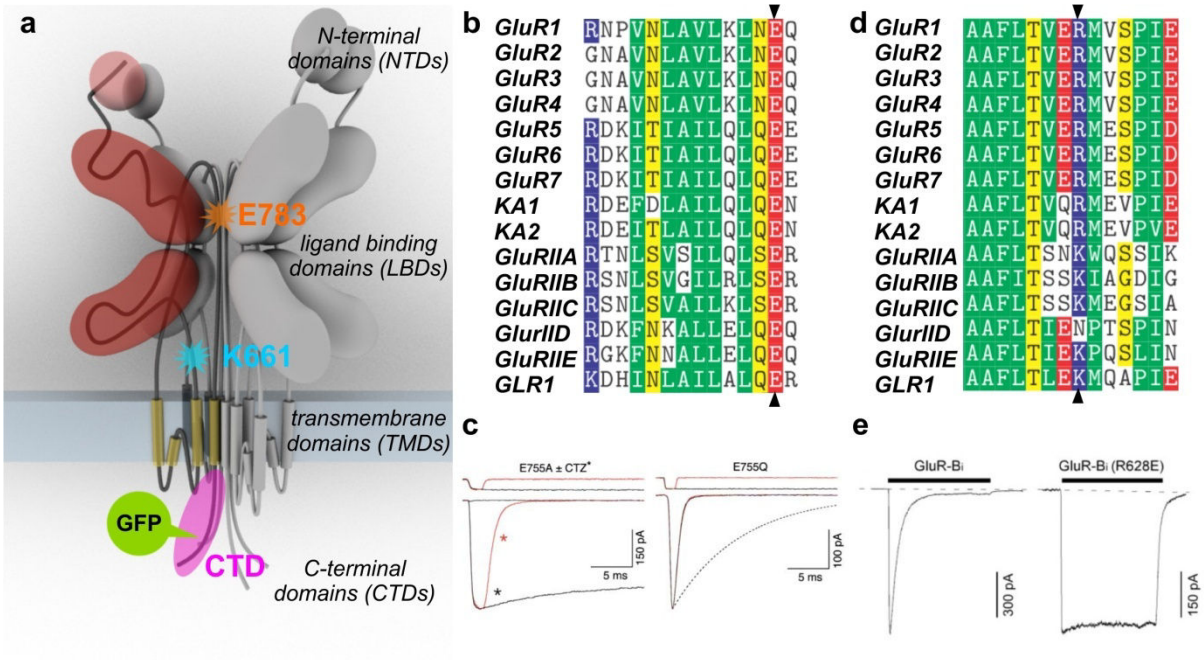

(**a**) Simplified sketch of the secondary structure of GluRIIA subunit in a tetrameric complex. Modified positions are highlighted in colored overlays. Glutamate 783 (E783 in orange) at the dimer interface and Lysine 661 (K661 in cyan) in the M3–S2linker are targets of site directed mutagenesis. GuRIIAtransgenes harbor a GFP in their CTD, which has been replaced with the CTD of GluRIIB in chimeric constructs (see list 1). (**b**) Blast alignment of the amino acid sequence of helix J reveals conserved positions in rat AMPARs, KARs, Drosophila GluRs and C. elegans GLR1 at amino acid E755 (e.g. E783)(see arrow heads). (**c**) Superimposed responses to 1 and 500 ms pulses of 10 mM glutamate are shown for two mutants. The mutant E755A displayed no response to glutamate; however, after prior application of cyclothiazide, glutamate-evoked currents were recorded, as indicated by *. In contrast, E755Q responded to glutamate in the absence of cyclothiazide with a rapidly desensitizing response. Modified from *Horning and Mayer* (2004) (**d**) BLAST alignment of the amino acid sequence of the M3–S2linker shows functionally conserved positions various GluRs at amino acid R628 (see arrow heads). (**e**) Effect of the R to E charge reversal in the M3–S2 linker on glutamate-activated currents in AMPAR channels. Glutamate-activated currents in outside-out patches isolated from HEK 293 cells expressing *wildtype* (left traces) or mutant GluR-Bi channels (right traces). Currents were elicited by a 100 msec application of glutamate (3 mM; filled bar) at a holding potential of–60 mV. Dashed lines show zero current level. The time scale is the same for both panels. Modified from (Yelshansky et al., 2004).

In a recent report, M. S. Horning and M. L. Mayer targeted contacts between adjacent LBDs of GluR2 homomers to define the mechanism responsible for activation of ion channel gating by agonists. The most dramatic effect on LBD-interface was achieved by the substitution of glutamate *755* with alanine (GluR2^{E755A}). Receptors harboring this mutation did not respond to the application of glutamate. However, weakly desensitizing glutamate-evoked currents could be recorded after the application of 100□M cyclothiazide. Cyclothiazide is an allosteric modulator which reduces desensitization of AMPA receptors (Sun et al., 2002). M. S. Horning and M. L. Mayer proposed two models to explain the inability of the mutant GluR2^{E755A} to gate under physiological conditions. Either GluR2^{E755A} desensitizes faster than it activates, or this mutant receptor is already in a desensitized conformation in the absence of agonist (Horning & Mayer, 2004).

5.4 Bioengineering approach to modulate desensitization behaviour of GluRIIA

Intriguingly, E755 is not only conserved across all mammalian AMPA and Kainate GluR subunits, but also in all five muscle expressed *Drosophila* GluR subunits (Fig. 1b; arrow heads). Thus, we could introduce a homologous mutation in GluRIIA (GluRIIA^{E783A}) to study the synaptic trafficking and incorporation characteristics of this 'hyper-desensitized'GluRIIA^{E783A} mutant (Fig. 1a and table 2). GluRIIA^{E783A} is based on a single point mutation in the genomic GluRIIA-GFP construct (GluRIIA^{GFP}) (Rasse et al., 2005), which includes the endogenous *glurIIA* promoter that drives expression. In its unmutated "*wildtype*" version, GluRIIA^{GFP} rescues the otherwise embryonic lethal *gluRIIA^{null}*, *gluRIIB^{null}* background (Rasse et al., 2005). The GluRIIA^{E783A} mutant is expected to be unable to gate under physiological conditions and thus rendered non-functional. Consequently, we found GluRIIA^{E783A} to be unable to rescue the embryonic lethality of *gluRIIA^{null}*, *gluRIIB^{null}* mutants (Schmid et al., 2006). Since we wanted to conduct all experiments in the *glurIIA^{null}*, *gluRIIB^{null}* background, we paired the expression of a functional copy of GluRIIA^{RFP} (e.g. GluRIIB^{RFP}) with GluRIIA^{E783A} in the *gluRIIA^{null}*, *gluRIIB^{null}*-mutant background, denominated IIA/IIA* (expression of GluRIIA^{RFP} and GluRIIA^{E783A} in *glurIIA^{null}*, *gluRIIB^{null}*) and IIB/IIA*(GluRIIB^{RFP} instead of GluRIIA^{RFP}) respectively. The corresponding controls were named IIA/IIA (GluRIIA^{RFP} and GluRIIA^{GFP} in *glurIIA^{null}*, *gluRIIB^{null}*) and IIB/IIA. All following experiments were carried out in this genetic background.

Table 2.) Newly engineered transgenic genomic GluRIIA constructs

name	*description*
GluRIIA-GFP	wildtype GluRIIA (fused to EGFP)
GluRIIA-mEOS	wildtype GluRIIA tagged with photoswitchable FP
GluRIIA$_B$-GFP	chimeric GluRIIA with GluRIIB-CTD ('c terminus swap')
GluRIIA^{E783A}-GFP	hyperfast desensitizing GluRIIA (E>A conversion)
GluRIIA^{E783Q}-GFP	fast desensitizing GluRIIA (E>Q conversion)
GluRIIA$_B^{E783A}$-GFP	hyperfast desensitizing GluRIIA with GluRIIB-CTD
GluRIIA$_B^{E783Q}$-GFP	fast desensitizing GluRIIA with GluRIIB-CTD
GluRIIA^{K661E}-GFP	slow desensitizing GluRIIA

All listed GluRIIA constructs are based on the genomic GluRIIA-GFP construct published in Rasse et la., 2005 and were cloned into the pGenattB vector for site-specific integration into ϕC31 compatible landing sites (Fig. 4).

5.5 The E783A mutation affects synaptic localization of GluRIIA

We first studied the synaptic localization of the E783A mutant (IIA*). Herefore, confocal micrographs of IIA/IIA* NMJs in intact larvae were acquired with an *in vivo* imaging setup (Andlauer & Sigrist, 2012; Rasse et al., 2005). Interestingly, IIA* localizes at PSDs (Fig. 2b and Fig. 3a) suggesting that the inability of IIA* to rescue the IIA^{null}/IIB^{null} background does not derive from fundamental perturbations in surface trafficking or synaptic localization, but rather from functional defects of the receptor. This implies that despite its severe gating defect, IIA* is able to pass through the control mechanism at the *endoplasmic reticulum* (ER), which test GluRs for proper glutamate binding before exit (Greger et al., 2002). In summary, this genetic constellation (IIA/IIA*) allows for the analysis of both GluR species at the same NMJ.

Figure 2.) The E783A mutation changes localization of IIA

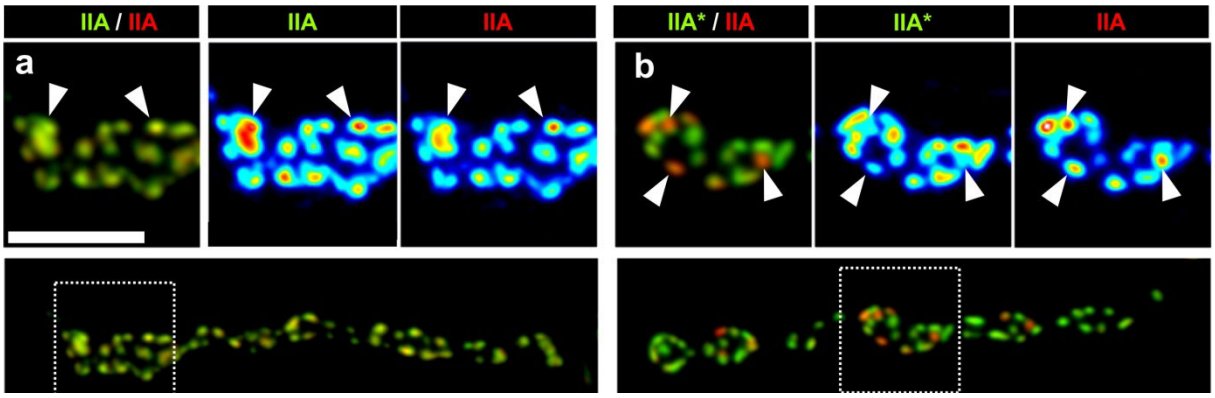

Junctional localization of co-expressed GluRIIAs at the NMJ. (**a**) Confocal images of GFP/RFP labeled GluRs at NMJs of intact animals (in vivo imaging) at NMJs of muscle 27 (m27). Two copies of *wildtype* IIA (GluRIIA/GluRIIA) constructs tagged with GFP/RFP perfectly co-localize at individual PSDs (arrow heads). (**b**) $GluRIIA^{E783A}$ paired with GluRIIA (IIA*/IIA). PSDs with highest IIA levels often feature low IIA* levels as demarked with arrow heads. Scale bar is 5 µm.

In the next step, we analyzed co-localization of the RFP- and GFP-signals on the level of individual PSDs in a qualitative manner (Fig. 2a-b; blow-ups). In the IIA/IIA-control situation the overall distribution of the RFP/GFP-signal appears uniform over the entire NMJ (Fig. 2a). Furthermore, individual PSDs which feature a strong RFP-signal do also show increased GFP-signals (Fig. 2a; arrow heads). The striking co-localization in this IIA/IIA-situation was expected as both IIA receptors differ only in the fluorophore they are carrying. In addition, we have previously shown that the choice of fluorophore has no apparent effect on GluR localization or physiology (Schmid et al., 2008).

In contrast, the GFP-signal of IIA* differs strongly from the co-expressed '*wildtype*' IIA in the IIA/IIA* constellation (Fig. 2b). Here, the PSDs with the highest IIA and IIA* signals are distributed in a salt-and-pepper like fashion and do not converge at PSDs that show high signals for both GluRs (Fig. 2b). From here on I will refer to this behavior as *segregation*. What stands out is that PSDs which show particular high levels of '*wildtype*' IIA (Fig. 2b; arrow heads) have mostly low levels of IIA*.

5.6 Suppression of activity has a differential effect on GluRIIA and GluRIIA-E783A levels

In our recent work (Schmid et al., 2008), we discovered differences in the localization and FRAP dynamics of IIA and IIB complexes at the level of individual PSDs depending on their level of maturation (PSD size) (see **2.4** ' Ionotropic glutamate receptors at the *Drosophila* NMJ' and table **1.**). Taking these findings as a starting point, we tested if these differences were linked to the maturation status of individual AZs. Herefore, we conducted *in vivo* experiments with transgenic larvae expressing fluorescently labeled IIA and IIB receptors, together with a CFP tagged BRP construct (BRP^{short}). This combination of transgenes allowed experiments, in which presynaptic BRP spots were monitored together with the corresponding postsynaptic FRAP signals of IIA and IIB (Fig. 3a). The data acquired in these experiments showed that single synapses featuring high BRP signals, a reliable indicator for T-bar assembly (Fouquet et al., 2009), did incorporate less IIA (at t= 8h) than synapses with lower BRP intensity (Schmid et al., 2008). From these results we suggested that individual presynaptic AZs differ in their release status, based on varying BRP levels, which in turn regulate postsynaptic GluR incorporation (Fig. 3b). In fact, a very recent study showed that there is a great variety of release probability and amplitude among individual release sites at the *Drosophila* NMJ (Peled & Isacoff, 2011) further supporting our model from 2008. However, if this grade of release is sufficient to induce such effects on GluR localization remains elusive.

It is tempting to speculated that the segregation phenotype in the IIA*/IIA situation (Fig. 2a) is caused by an activity dependent mechanism. If this mechanism acts different on IIA and IIA*, it could explain the distinctive localization of both GluRIIA complexes. In preliminary experiments I tested this hypothesis by correlating the level of presynaptic BRP and the corresponding IIA/IIA* ratio at individual synapses. To this end, antibody stainings for BRP in fixed larval filets expressing IIA/IIA* were performed and confocal images acquired (data not shown). However, we did not observe a correlation between BRP and GluR (IIA or IIA*) levels.

To further investigate the influence of neuronal activity on the IIA*/IIA-segregation phenotype, we went on to alter synaptic release to reveal differences in activity dependent regulation of IIA and IIA*localization. We tested for this by silencing presynaptic activity by expressing TNT (Sweeney et al., 1995) in a subset of motoneurons. TNT suppresses evoked glutamate release and should hereby, on one hand, strongly alter presynaptic activity and, on the other hand, largely abolish differences in "presynaptic activity" (i.e. presynaptic glutamate release) between individual release sites.

Strikingly, we did not observe TNT-expressing NMJs with a strong segregation phenotype of IIA* and IIA as in control NMJs (compare Fig. 4a with 4d). Moreover, quantitative analysis of junctional GluR signals revealed a significant shift in the GluR composition between these two conditions. In NMJs that exhibit undisturbed activity, mutated IIA* dominates over IIA (Fig. 2e; left bar). This situation is reversed under tonic TNT expression (Fig. 4e**;** right bar). Therefore, activity suppression results in elevated IIA levels at the NMJ (Fig. 2f) in conjunction with a decrease of IIA* levels (Fig. 2g).

Figure 3.) Site-specific regulation of GluR trafficking through BRP dependent release component

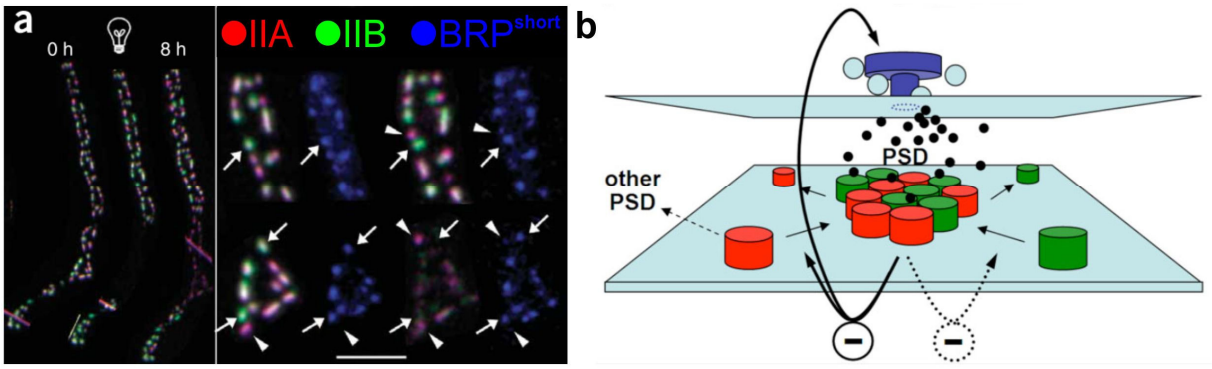

(**a**) In vivo imaging of IIA-RFP (red), IIB-GFP (green), and BRP-short-CFP (blue). Left, images of the whole NMJ at 0 h, before, and after specifically bleaching IIA-RFP and IIB-GFP, and at 8 h. Right, blow-up of unbleached area and FRAP in bleached area. Arrows indicate mature synapses, characterized by large IIB and large BRP signals. Arrowheads show synapses characterized by large IIA and small BRP signals. Scale bar, 5 µm. (**b**) Model connecting activity-dependent GluR dynamics at single PSDs with the rate of PSD formation via the amount of GluRIIA available for the maturation of new PSDs. Green, IIB; Red, IIA. Modified from *Schmid et al.,* (2008).

Our results suggest that the activity-dependent mechanism, which enhances IIA incorporation into PSDs under low activity (Schmid et al., 2008) are unable to increase the synaptic levels of IIA*. This could explain the segregation between IIA* and IIA at the level of individual PSDs in control NMJs. Under physiological conditions the varying levels of presynaptic release (Peled & Isacoff, 2011) could translate into PSDs with different levels of IIA and IIA*. This hypothesis would predict that PSDs with high levels of IIA and low levels of IIA* (Fig. 2b; arrow heads) would have low release probabilities.

Figure 4.) Postsynaptic IIA* localization depends on presynaptic activity

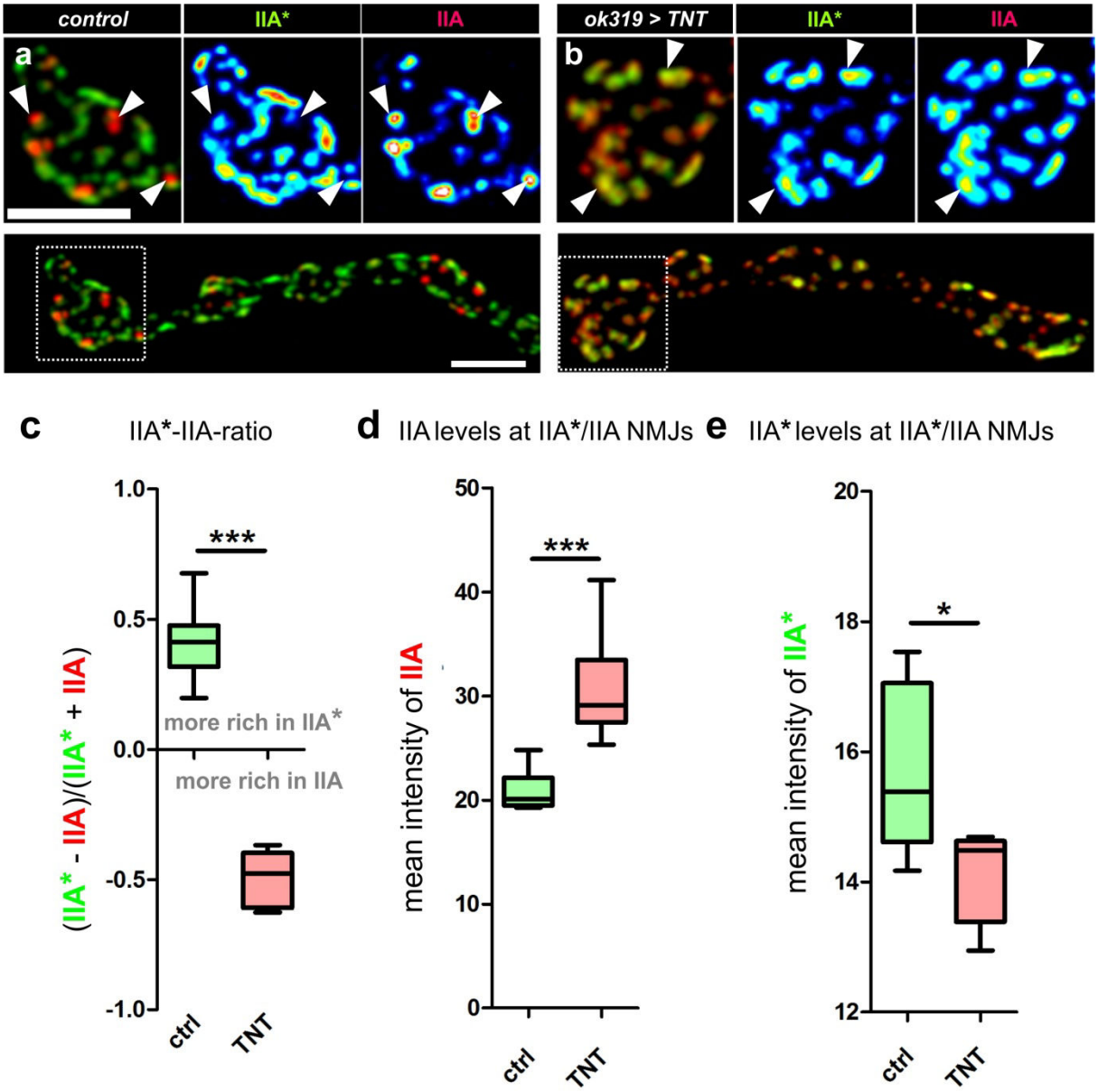

(**a**) NMJ, expressing GluRIIA^{E783A}-GFP (IIA*) and GluRIIA-RFP (IIA). Arrowheads indicate PSDs with high IIA intensity and low IIA* levels. (**b**) TNT expressing NMJs display decreased IIA* levels (**e**) and an increase in IIA signal (**c**). Under this condition, the intensity of both GluRs correlates on most PSDs (**b**; arrowheads). (**d**) The ratio of both GluR complexes is significant shifted from IIA* rich towards IIA under activity suppression. This is due to increased IIA (**d**) and decreased IIA*levels (**e**) in TNT expressing NMJs. Scale bar is 5 µm

Although the TNT experiments (Fig. 4) did discover that activity dependent mechanisms are at least partially responsible for the segregation of IIA and IIA*, they did not shed light on the nature of the mechanisms itself. Nevertheless, it would be of great interest to elucidate the mechanisms and involved regulatory proteins, since segregation of two different GluRs into two populations of PSDs appears to occur in *wildtype* NMJs as well. During embryonic development, IIA and IIB containing receptor complexes cluster to the first forming PSDs in an exclusive manner, strongly resembling the

IIA/IIA* segregation phenotype (Dave Featherstone, *personal communications*). It is possible that the segregation phenomenon is regulated by pathways, which ensure the exclusive localization of GluRs to distinct PSDs early on in synaptic development to ensure the availability of postsynapses with different response dynamics.

In principle, this differential synaptic localization of IIA and IIB could be mediated by their distinct CTDs. These harbor phosphorylation motifs, which are able to regulate junctional levels of IIA and IIB. Namely, a recent report states that increased activity of postsynaptic CAMKII increases IIB and decreases IIA levels at the NMJ (Morimoto et al., 2010), an effect which is most likely mediated by specific CTD-phosphorylation. It could be assumed that the E783A mutation of IIA* changes the availability of specific phosphorylation motifs at its CTD which translates into the different localizations of IIA and IIA*. Hence, we generated IIA and IIA* constructs, which contain the CTD of IIB (table **2.**). In future experiments, these chimeras ($GluRIIA_B$ and $GluRIIA_B^{E783A}$) will enable us to test if the segregation phenotype is mediated by the IIA-CDT. Furthermore, TNT experiments combined with these constructs will allow for conclusions about the impact of activity dependent mechanisms on GluR segregation.

5.7 E783A mutation increases speed of GluRIIA incorporation into PSDs

The mechanism that enables GluRIIA to outcompete its mutated version remains elusive but might be dependent on the abundance of these complexes at the PSD. Differences in synaptic abundance between IIA and IIA* could have an effect on the respective dwell time of both receptor complexes at synapses. In turn, this would result in different incorporation dynamics of IIA and IIA*into PSDs. Since FRAP experiments allow to measure incorporation rates of XFP-labelled proteins, we went on to apply this technique to determine the incorporation rate of IIA*. Since all tested GluR constructs (table **2.**) are fluorescently labeled, we were able to apply the established *In vivo* protocols from our lab (Andlauer & Sigrist, 2012; Rasse et al., 2005; Schmid et al., 2008).

The way we chose to do these experiments, was to bleach part of the GluR-signal of an NMJ by continuous laser stimulation and subsequently re-image and quantify this particular NMJ (Fig. 5A**-**B) after time intervals of 8 and 24 hours. These experiments were carried out to determine alterations of IIA* incorporation compared to non-mutated IIA (IIA*/IIA) and, in a second set of experiments, IIA* in comparison to IIB (IIA*/IIB). NMJs expressing IIA/IIA (*glurIIB*^{null}) and IIA/IIB (*wildtype*), respectively served as controls.

Figure 5.) Highly increased FRAP IIA* after 8h interval

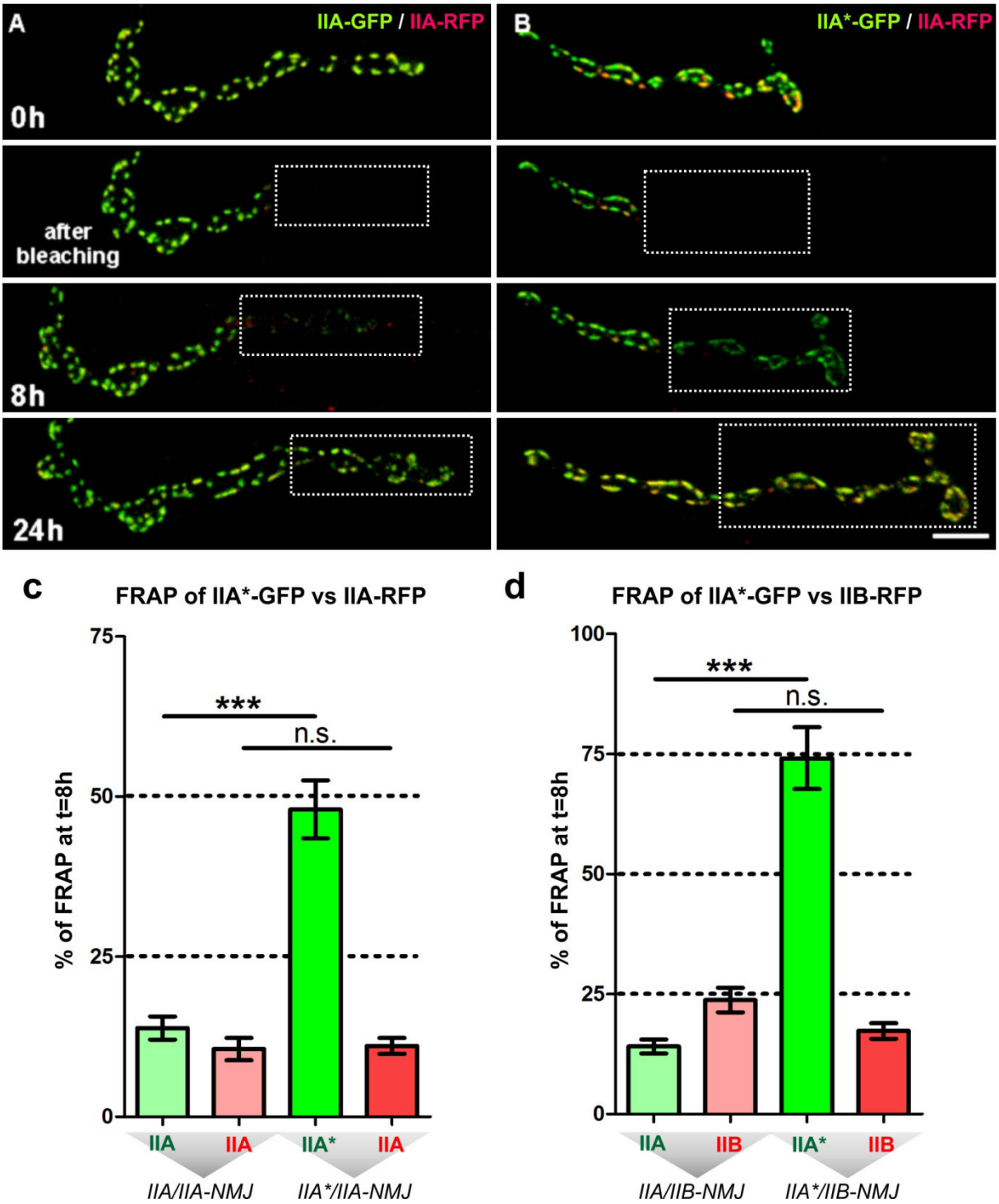

FRAP experiments in intact larvae reveal an increased PSD incorporation rate of GluRIIA^{E783A}-GFP (IIA*) compared to GluRIIA-RFP (IIA) and GluRIIB-RFP (IIB). (**a**) Control NMJ expressing IIA-GFP and IIA-RFP. Both GluRs co-localize at the PSDs as the fluorophore does not have any effect on synaptic localization. (**b**) FRAP signal is highly elevated in NMJs expressing IIA*(**a** and **b**; compare areas at t=8h) (**c**) Quantification of signal intensities of single PSDs reveals a significant increase of FRAP signal after 8 hours of IIA* compared to non-mutated IIA. (**d**) FRAP of IIA*is even stronger when co-expressed with IIB. Bar height = Mean FRAP; Error bar = SEM; n.s.: not significant; ***p ≤ 0.0001 (Mann-Whitney U-Test). Scale bar is 5µm.

Quantification of IIA-GFP FRAP signals showed a recovery of about 10% after 8 hours (Fig. 5c; green bar at IIA/IIA-NMJ; IIA-GFP: Median= 10,21±1.81(n=57)). Surprisingly however, IIA* recovered up to 50% of their initial signal in 8 hours in the IIA*/IIA situation (Fig. 5c**;** IIA*/IIA-NMJ; IIA*: Median= 38.58±4.54). This is an almost 4-fold increase in incorporation speed compared to IIA.

Subsequently, we expressed our mutated IIA subunit (IIA*) together with IIB to test if the increase in IIA* recovery is linked to a competition with non-mutated IIA. However, these experiments show that IIA* FRAP is still high in the IIA*/IIB situation, which shows that the presence of IIB does not slow down IIA* incorporation dynamic. When co-expressed with IIB, IIA* recovers more than 5-fold faster than the *wildtype* IIA (IIA: Median= 11.97± 1.45 (n=60) vs IIA*: Median= 64.38±6.46 (n=75)). This is an about 25% faster recovery of IIA* in the IIA*/IIB situation compared to the IIA*/IIA situation (compare Fig. 5c and 5d). This difference might be explained with an occupation of IIA specific '*slots*' (Kennedy & Ehlers, 2006; Opazo et al., 2011; Introduction: '*the postsynaptic density'*). The competition of two different IIA complexes might slow down the incorporation rate of IIA* and therefore mask its potential incorporation dynamic.

In conclusion, FRAP of IIA* was increased in both genetic conditions, IIA*/IIA and IIA*/IIB. Therefore, we can state that the *in-rate* of IIA* is significantly increased compared to IIA. However, the steady state signals of IIA* (Fig. 5b; unbleached area) did not rise substantially higher than the levels of IIA (data not shown). Altogether, both findings, high *in-rate* at bleached PSDs but stable *steady state* levels at unbleached PSDs, show that the overall dynamic of IIA* is highly increased. We can therefore deduce that the *out-rate* of IIA* must be high as well. But to directly measure the *out-rate* one would have to 'tag' a set of GluRs at one time point and measure the levels of these receptors after a certain time interval. In fact, photo-switchable fluorophores allow these experiments. Therefore, we will test our hypothesis in future experiments by determining the precise *out-rate* with a newly generated IIA-mEosFP fusion construct (Nienhaus et al., 2006) (table **2**).

The high mobility of IIA* is most likely associated with a weak abundance at the PSD. The best candidates to mediate the synaptic abundance are interacting proteins that co-cluster with GluRs themselves, such as auxiliary subunits, or proteins that are part of the postsynaptic scaffold. These proteins could in principle bind directly to the GluRs, e.g. via the cytosolic CTD, or interact with the CTD of another protein that is tightly bound to the GluR as an auxiliary subunit (Opazo et al., 2010). Interestingly, the functional defect of IIA*, a continuous state of '*hyper*'-desensitization, appears to mediate a conformational change of the GluR itself and inhibits interactions which enables synaptic targeting of IIA in an activity dependent manner.

It is possible to imagine that the conformation of desensitized GluRs alters the CTD-structure in such a way that it is not as accessible to interacting scaffold proteins anymore. However, desensitization is much more likely to affect binding of auxiliary subunits, which could read out the conformation of the LBDs and TM domains of the receptor (Milstein & Nicoll, 2009; Nakagawa, 2010; Tomita et al., 2007). In fact, several studies have recently reported that ligand binding of AMPARs, followed by desensitization, can induce a rapid dissociation of TARP/AMPAR binding (Morimoto-tomita et al., 2009; Shi et al., 2009; Tomita et al., 2004).

5.8 Concluding remarks and future experiments

The presented data shed new light on how the conformational states of GluRs might influence their synaptic trafficking. Ultimately, this could help to identify interacting proteins, which control synaptic GluR localization dependent on the conformational status of the receptor. But prior to this, more points need to be addressed.

First of all, the E783A mutation of IIA needs to be analyzed in more detail.

1) Precise dissection of the out-rate of GluRs at individual PSDs using photoswitchable fluorescent proteins (e.g. mEosFP).

2) An electro-physiological characterization of desensitization kinetics of all generated GluRIIA mutants (see table **2.**). In first experiments, we have been applying two-electrode voltage clamp recordings to larval NMJs expressing IIB together with IIA* (IIB/IIA*) to study the effects of the E783A-mutation in *Drosophila* GluRs. As glutamate E783 is highly conserved (Fig. 1b), we expect the E783A mutation in GluRIIA (IIA*) to speed up of the desensitization in a similar manner as described for GluR2 (Horning and Mayer 2004). This change in desensitization speed is expected to manifest in the decay kinetics of miniature events and evoked junctional currents (EJCs) (Pawlu, DiAntonio, & Heckmann, 2004). Since IIB desensitizes 10x faster than *wildtype* IIA, our measurements will be able to determine an up-to 10x increase in desensitization speed of IIA* before the shape of the postsynaptic currents will be 'masked' by the IIB response.

In the end, electrophysiological analysis of all IIA mutants (table **2.**) is the best way to verify if the homologous mutations in *Drosophilas* GluRIIA affect desensitization properties as in vertebrate AMPARs.

Figure 6.) Scheme of site-directed genomic integration of GluRIIA-GFP transgenes

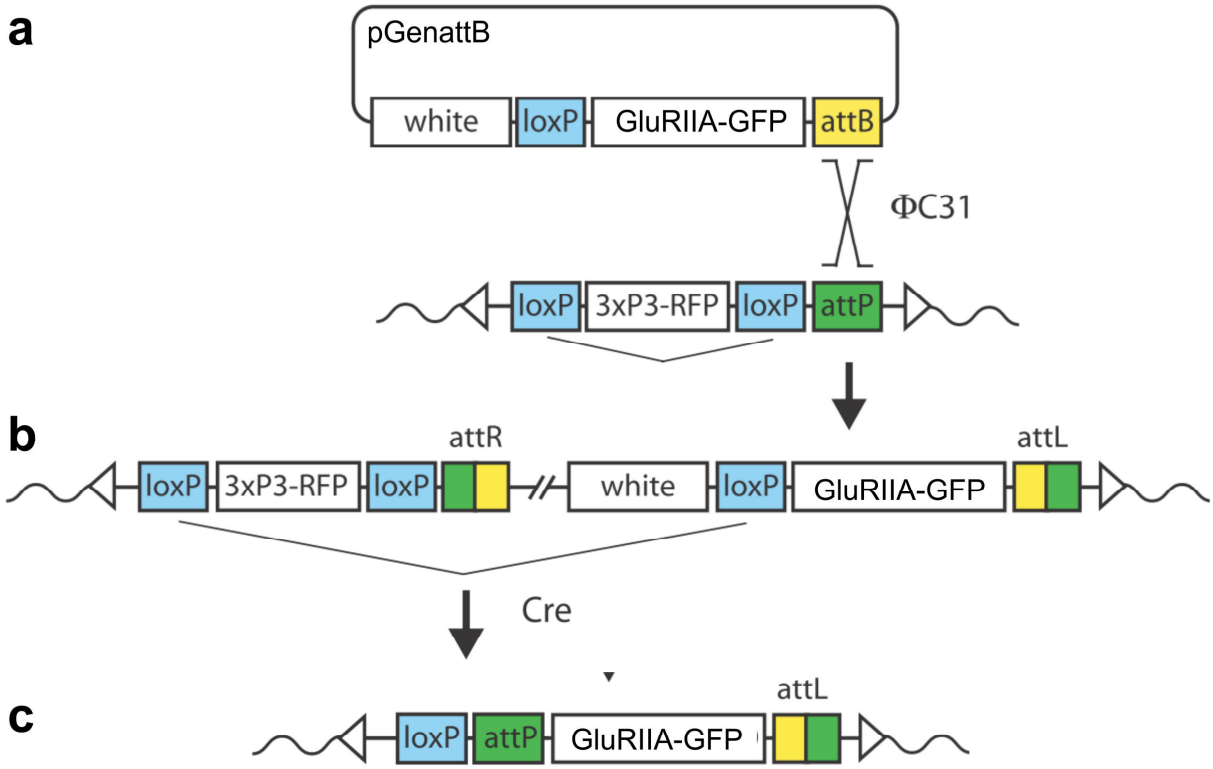

(**a**) All genomic GluRIIA constructs were created, starting from a GluRIIA-GFP fusion construct that includes the whole genomic *glurIIa* locus including 2KBps (1KBps) of the upstream (downstream) region (Rasse et al., 2005). Finally, these constructs were all cloned into the pGenattB vector (kind gift from Alf Herzel). The pGenattB vector contains a 285-bp attB fragment, the white^{+} selectable marker, and a single loxPsite. (**b**) The ϕC31 integrase mediates recombination between *attB* and *attP*sites, resulting in the integration of pGenattB into the landing site, thereby creating the two hybrid sites *attL* and *attR*, which are refractory to the ϕC31 integrase. (**c**) The *loxP* sites allow elimination of intervening sequences before or after integration of pGenattB (indicatedwithflatarrowheads). In all injections we used the pGenattB vector; it contained a 3xp3 driven RFP and a multiple cloning site. Modified from Bischof et al., 2006.

All presented data derive from experiments with GluRIIA harboring a single amino acid exchange, namely E783A. It will be important to compare the effects of this mutation with mutations that speed up the desensitization in a less 'drastic' manner, or, in contrast, slow down desensitization. In the paper by Horning and Mayer that reported the effect of the E755A mutation in GluR2 AMPARs (Horning & Mayer, 2004) a similar mutation was analyzed. The E755Q mutation did not disrupt the LBD dimer interface formation as severe and therefore allowed for recordings without the use of cyclothiazide. The desensitization rate of E755Q mutants was reported to be increased 18-fold. Since this mutation does not appear to render the GluR subunit non-functional and still speeds up GluR desensitization significantly, we engineered a corresponding GluRIIA mutant, called GluRIIA^{E783Q}. It will be interesting to test if the IIA^{E783Q} mutant that should exhibit a less dramatic desensitization phenotype, also features a less severe segregation phenotype when compared to IIA^{E783A}. It is also reasonable to speculate that IIA^{E783Q} will show an effect in its synaptic incorporation dynamic as

observable in IIA^{E783A}. To exclude the possibility that this effect is caused by specific GluRIIA-CTD interactions we applied the E783Q and E783A mutations to chimeric IIA constructs, harboring the CTD sequence of IIB (Andreas Schmid's PhD thesis). These were termed $GluRIIA_B^{E783Q}$ and $GluRIIA_B^{E783A}$.

Finally, we also plan to analyze the effect of slowed down desensitization on synaptic localization of GluRs. Therefore, a mutation in the linker sequence located between the pore-forming M3 segment and the S2 lobe was applied to GluRIIA. This R to E substitution (R624E) mutation results in an approximately twofold slowdown of desensitization in AMPARs (Yelshansky et al., 2004). The corresponding mutant (K611E) was introduced in *Drosophila* ($GluRIIA^{K611E}$).

In future experiments, these mutants of IIA-GFP (Fig. 4a) will be co-expressed with *wildtype* IIA-RFP and their synaptic localization and trafficking compared. To exclude differences in expression strength of these transgenes, which might be caused by differences in their genomic location, we utilized the □C31 system (Bischof et al., 2007; Groth et al., 2004). In the presented data, P-element based transformations of the IIA constructs were used, which create random (sometimes multiple) insertions in the genome. Transgenes introduced with this technique might disrupt essential genes and might not insert on the chromosome of choice. In contrast, the □C31 integration system is a site-specific integration approach, which applies bacteriophage□C31 integrase to mediate the sequence-specific recombination between two largely different attachment sites (attB and attP) (Groth et al., 2000; Thorpe & Smith, 1998). All GluRIIA constructs were therefore cloned into appropriate pGenattB vectors (kind gift of Dr. Alf Herzig) and injected in flies harboring the same landing site: E68 (Fig. 6) (Bischof et al., 2007).

All together, the presented data above and the variety of newly created tools should make it feasible to build on these findings and produce new results in the near future that expand the knowledge about the correlation of GluR desensitization and synaptic clustering. Hopefully, these experiments will then unravel new mechanisms or expand the details on already described pathways (DNlg1 dependent/ activity dependent) which orchestrate the incorporation of GluRs into PSDs.

6 References

Akins, M. R., & Biederer, T. (2006). Cell-cell interactions in synaptogenesis. *Current opinion in neurobiology*, *16*(1), 83-9.

Andlauer, T. F. M., & Sigrist, S. J. (2012). In vivo imaging of the Drosophila larval neuromuscular junction. *Cold Spring Harbor protocols*, *2012*(4).

Araç, D., Boucard, A. a, Ozkan, E., Strop, P., Newell, E., Südhof, T. C., & Brunger, A. T. (2007). Structures of neuroligin-1 and the neuroligin-1/neurexin-1 beta complex reveal specific protein-protein and protein-Ca2+ interactions. *Neuron*, *56*(6), 992-1003.

Armstrong, N., & Gouaux, E. (2000). Mechanisms for activation and antagonism of an AMPA-sensitive glutamate receptor: crystal structures of the GluR2 ligand binding core. *Neuron*, *28*(1), 165-181.

Atwood, H L, Govind, C. K., & Wu, C. F. (1993). Differential ultrastructure of synaptic terminals on ventral longitudinal abdominal muscles in Drosophila larvae. *Journal of Neurobiology*, *24*(8), 1008-1024.

Atwood, Harold L, & Karunanithi, S. (2002). Diversification of synaptic strength: presynaptic elements. *Nature reviews. Neuroscience*, *3*(7), 497-516.

Augustine, G. J., & Neher, E. (1992). Neuronal Ca2+ signalling takes the local route. *Current Opinion in Neurobiology*, *2*(3), 302-307.

Banovic, D., Khorramshahi, O., Owald, D., Wichmann, C., Riedt, T., Fouquet, W., Tian, R., et al. (2010). Drosophila neuroligin 1 promotes growth and postsynaptic differentiation at glutamatergic neuromuscular junctions. *Neuron*, *66*(5), 724-38.

Barry, M. F., & Ziff, E. B. (2002). Receptor trafficking and the plasticity of excitatory synapses. *Science*, 279-286.

Bate, M., Landgraf, M., & Ruiz Gómez Bate, M. (1999). Development of larval body wall muscles. *International review of neurobiology*, *43*, 25-44.

Bats, C., Groc, L., & Choquet, D. (2007). The interaction between Stargazin and PSD-95 regulates AMPA receptor surface trafficking. *Neuron*, *53*(5), 719-34.

Bischof, J., Maeda, R. K., Hediger, M., Karch, F., & Basler, K. (2007). An optimized transgenesis system for Drosophila using germ-line-specific phiC31 integrases. *Proceedings of the National Academy of Sciences of the United States of America*, *104*(9), 3312-7.

Blomberg, F., Cohen, R. S., & Siekevitz, P. (1977). The structure of postsynaptic densities isolated from dog cerebral cortex. II. Characterization and arrangement of some of the major proteins within the structure. *The Journal of cell biology*, *74*(1), 204-25.

Brand, a H., & Perrimon, N. (1993). Targeted gene expression as a means of altering cell fates and generating dominant phenotypes. *Development* , *118*(2), 401-15.

Bredt, D. S., & Nicoll, R. A. (2003). AMPA Receptor Trafficking at Excitatory Synapses. *Neuron*, *40*(2), 361-379.

Broadie, K., & Bate, M. (1993). Activity-dependent development of the neuromuscular synapse during Drosophila embryogenesis. *Neuron*, *11*(4), 607-19.

Budnik, V. (1996). Synapse maturation and structural plasticity at Drosophila neuromuscular junctions. *Current opinion in neurobiology*, *6*(6), 858-67.

Budnik, Vivian, Zhong, Y., & Wu, C.-F. (1990). Morphological Plasticity Altered Excitability of Motor Axons in Drosophila Mutants with, J Neuroscience, 10(11), 3754-3768.

Chen, L., Chetkovich, D. M., Petralia, R. S., Sweeney, N. T., Kawasaki, Y., Wenthold, R. J., Bredt, D. S., et al. (2000). Stargazin regulates synaptic targeting of AMPA receptors by two distinct mechanisms. *Nature*, *408*(6815), 936-43.

Chen, Xiaoyan, Liu, H., Shim, A. H. R., Focia, P. J., & He, X. (2008). Structural basis for synaptic adhesion mediated by neuroligin-neurexin interactions. *Nature structural & molecular biology*, *15*(1), 50-6.

Chen, Xiaobing, Winters, C., Azzam, R., Li, X., Galbraith, J. a, Leapman, R. D., & Reese, T. S. (2008). Organization of the core structure of the postsynaptic density. *Proceedings of the National Academy of Sciences of the United States of America*, *105*(11), 4453-8.

Choquet, D., & Triller, A. (2003). The role of receptor diffusion in the organization of the postsynaptic membrane. *Nature reviews. Neuroscience*, *4*(4), 251-65.

Chubykin, A. a, Atasoy, D., Etherton, M. R., Brose, N., Kavalali, E. T., Gibson, J. R., & Südhof, T. C. (2007). Activity-dependent validation of excitatory versus inhibitory synapses by neuroligin-1 versus neuroligin-2. *Neuron*, *54*(6), 919-31.

Chung, H. J., Xia, J., Scannevin, R. H., Zhang, X., & Huganir, R. L. (2000). Phosphorylation of the AMPA receptor subunit GluR2 differentially regulates its interaction with PDZ domain-containing proteins. *J Neurosci*, *20*(19), 7258-67.

Cohen, R. S., Blomberg, F., Berzins, K., & Siekevitz, P. (1977). STRUCTURE FROM OF POSTSYNAPTIC DOG CEREBRAL DENSITIES ISOLATED CORTEX I . O v e r a l l M o r p h o l o g y a n d P r o t e i n C o m p o s i t i o n. *The Journal of Cell Biology*, *74*, 181-203.

Dai, Y., Taru, H., Deken, S. L., Grill, B., Ackley, B., Nonet, M. L., & Jin, Y. (2006). SYD-2 Liprin-alpha organizes presynaptic active zone formation through ELKS. *Nat Neuroscience*, *9*(12), 1479-87.

Davis, G. W., Diantonio, A., Petersen, S. A., & Goodman, C. S. (1998). and Reveals a Retrograde Signal that Regulates Presynaptic Transmitter Release in Drosophila, *20*, 305-315.

Dean, C., & Dresbach, T. (2006). Neuroligins and neurexins: linking cell adhesion, synapse formation and cognitive function. *Trends in neurosciences*, *29*(1), 21-9.

Deng, F., Price, M. G., Davis, C. F., Mori, M., & Burgess, D. L. (2006). Stargazin and other transmembrane AMPA receptor regulating proteins interact with synaptic scaffolding protein MAGI-2 in brain. *J Neurosci*, *26*(30), 7875-84.

Derkach, V, Barria, a, & Soderling, T. R. (1999). Ca2+/calmodulin-kinase II enhances channel conductance of alpha-amino-3-hydroxy-5-methyl-4-isoxazolepropionate type glutamate receptors. *Proceedings of the National Academy of Sciences of the United States of America*, *96*(6), 3269-74.

Derkach, Victor a, Oh, M. C., Guire, E. S., & Soderling, T. R. (2007). Regulatory mechanisms of AMPA receptors in synaptic plasticity. *Nature reviews. Neuroscience*, *8*(2), 101-13.

DiAntonio, a, Petersen, S. a, Heckmann, M., & Goodman, C. S. (1999). Glutamate receptor expression regulates quantal size and quantal content at the Drosophila neuromuscular junction. *J Neurosci*, *19*(8), 3023-32.

Diantonio, A. (2006). Glutamate receptors at the Drosophila neuromuscular junction. *International Review of Neurobiology*, *75*(5), 165-179.

Eaton, B. a, & Davis, G. W. (2005). LIM Kinase1 controls synaptic stability downstream of the type II BMP receptor. *Neuron*, *47*(5), 695-708.

Eaton, B. a, Fetter, R. D., & Davis, G. W. (2002). Dynactin is necessary for synapse stabilization. *Neuron*, *34*(5), 729-41.

Elias, G. M., Funke, L., Stein, V., Grant, S. G., Bredt, D. S., & Nicoll, R. a. (2006). Synapse-specific and developmentally regulated targeting of AMPA receptors by a family of MAGUK scaffolding proteins. *Neuron*, *52*(2), 307-20.

Esteban, J. a, Shi, S.-H., Wilson, C., Nuriya, M., Huganir, R. L., & Malinow, R. (2003). PKA phosphorylation of AMPA receptor subunits controls synaptic trafficking underlying plasticity. *Nat Neuroscience*, *6*(2), 136-43.

Fabrichny, I. P., Leone, P., Sulzenbacher, G., Comoletti, D., Miller, M. T., Taylor, P., Bourne, Y., et al. (2007). Structural analysis of the synaptic protein neuroligin and its beta-neurexin complex: determinants for folding and cell adhesion. *Neuron*, *56*(6), 979-91.

Featherstone, D. E., Rushton, E., & Broadie, K. (2002). Developmental regulation of glutamate receptor field size by nonvesicular glutamate release. *Nat Neuroscience*, *5*(2), 141-6.

Feng, W., Shi, Y., Li, M., & Zhang, M. (2003). Tandem PDZ repeats in glutamate receptor-interacting proteins have a novel mode of PDZ domain-mediated target binding. *Nature structural biology*, *10*(11), 972-8.

Fouquet, W., Owald, D., Wichmann, C., Mertel, S., Depner, H., Dyba, M., Hallermann, S., et al. (2009). Maturation of active zone assembly by Drosophila Bruchpilot. *The Journal of cell biology*, *186*(1), 129-45.

Funke, L., Dakoji, S., & Bredt, D. S. (2005). Membrane-associated guanylate kinases regulate adhesion and plasticity at cell junctions. *Annual review of biochemistry*, *74*, 219-45.

Gramates, L. S., & Budnik, V. (1999). Assembly and maturation of the Drosophila larval neuromuscular junction. *International Review of Neurobiology*, *43*, 93-117.

Greger, I. H., Khatri, L., & Ziff, E. B. (2002). RNA editing at arg607 controls AMPA receptor exit from the endoplasmic reticulum. *Neuron*, *34*(5), 759-72.

Groc, L., & Choquet, D. (2006). AMPA and NMDA glutamate receptor trafficking: multiple roads for reaching and leaving the synapse. *Cell and tissue research*, *326*(2), 423-38.

Groth, A. C., Fish, M., Nusse, R., & Calos, M. P. (2004). Construction of transgenic Drosophila by using the site-specific integrase from phage phiC31. *Genetics*, *166*(4), 1775-82.

Groth, A. C., Olivares, E. C., Thyagarajan, B., & Calos, M. P. (2000). A phage integrase directs efficient site-specific integration in human cells. *Proceedings of the National Academy of Sciences of the United States of America*, *97*(11), 5995-6000.

Hallermann, S., Kittel, R. J., Wichmann, C., Weyhersmüller, A., Fouquet, W., Mertel, S., Owald, D., et al. (2010). Naked dense bodies provoke depression. *J Neurosci*, *30*(43), 14340-5.

Halpern, E., Johansen, M., & Keshishian, H. (1989). Stereotypic Morphology of Glutamatergic Muscle Cells of Drosophila Larvae Synapses on Identified. *Soc Neuroscience. 9*(2), 710-725.

Haucke, V., Neher, E., & Sigrist, S. J. (2011). Protein scaffolds in the coupling of synaptic exocytosis and endocytosis. *Nature reviews. Neuroscience*, *12*(3), 127-38. Nature Publishing Group.

Heckmann, M., & Dudel, J. (1997). Desensitization and resensitization kinetics of glutamate receptor channels from Drosophila larval muscle. *Biophysical journal*, *72*(5), 2160-9.

Hell, S. W., & Wichmann, J. (1994). Breaking the diffraction resolution limit by stimulated emission: stimulated-emission-depletion fluorescence microscopy. *Optics Letters*, *19*(11), 780-782.

Heuser, J. E., & Reese, T. S. (1973). Evidence for recycling of synaptic vesicle membrane during transmitter release at the frog neuromuscular junction. *The Journal of cell biology*, *57*(2), 315-44.

Hoang, B., & Chiba, a. (2001). Single-cell analysis of Drosophila larval neuromuscular synapses. *Developmental biology*, *229*(1), 55-70.

Hormuzdi, S. G., Filippov, M. a, Mitropoulou, G., Monyer, H., & Bruzzone, R. (2004). Electrical synapses: a dynamic signaling system that shapes the activity of neuronal networks. *Biochimica et biophysica acta*, *1662*(1-2), 113-37.

Horning, M. S., & Mayer, M. L. (2004). Regulation of AMPA receptor gating by ligand binding core dimers. *Neuron*, *41*(3), 379-88.

Ichtchenko, K., Hata, Y., Nguyen, T., Ullrich, B., Missler, M., Moomaw, C., & Südhof, T. C. (1995). Neuroligin 1: a splice site-specific ligand for beta-neurexins. *Cell*, *81*(3), 435-43.

Iida, J., Hirabayashi, S., Sato, Y., & Hata, Y. (2004). Synaptic scaffolding molecule is involved in the synaptic clustering of neuroligin. *Molecular And Cellular Neurosciences*, *27*(4), 497-508.

Irie, M., Hata, Y., Takeuchi, M., Ichtchenko, K., Toyoda, A., Hirao, K., Takai, Y., et al. (1997). Binding of neuroligins to PSD-95. *Science*, *277*(5331), 1511-1515.

Jahn, R., Lang, T., & Südhof, T. C. (2003). Membrane fusion. *Cell, 112*(3), 519-533.

Jan, Y.-N., & Jan, L. (1976). PROPERTIES OF THE LARVAL NEUROMUSCULAR JUNCTION IN DROSOPHILA MELANOGASTER. *The Journal of Physiology*, 189-214.

Jia, X. X., Gorczyca, M., & Budnik, V. (1993). Ultrastructure of neuromuscular junctions in Drosophila: comparison of wild type and mutants with increased excitability. *Journal of Neurobiology*, *24*(8), 1025-1044.

Kato, A. S., Siuda, E. R., Nisenbaum, E. S., & Bredt, D. S. (2008). AMPA receptor subunit-specific regulation by a distinct family of type II TARPs. *Neuron*, *59*(6), 986-96.

Katz, B. (1971). Quantal mechanism of neural transmitter release. *Science*, *173*(3992), 123-6.

Kaufmann, N., Deproto, J., Ranjan, R., Wan, H., Vactor, D. V., & Francisco, S. S. (2002). and the Receptor Phosphatase Dlar Control Synapse Morphogenesis, *34*, 27-38.

Kennedy, M. B. (1998). Signal transduction molecules at the glutamatergic postsynaptic membrane. *Brain research Brain research reviews*, *26*(2-3), 243-257.

Kennedy, M. J., & Ehlers, M. D. (2006). Organelles and trafficking machinery for postsynaptic plasticity. *Annual review of neuroscience*, *29*, 325-62.

Kim, E., & Sheng, M. (2004). PDZ domain proteins of synapses. *Nature reviews. Neuroscience*, *5*(10), 771-81.

Kittel, R. J., Wichmann, C., Rasse, T. M., Fouquet, W., Schmidt, M., Schmid, A., Wagh, D. a, et al. (2006). Bruchpilot promotes active zone assembly, Ca2+ channel clustering, and vesicle release. *Science*, *312*(5776), 1051-4.

Klar, T. A., Jakobs, S., Dyba, M., Egner, A., & Hell, S. W. (2000). Fluorescence microscopy with diffraction resolution barrier broken by stimulated emission, *Proceedings of the National Academy of Sciences of the United States of America*, *97*(15), 8206-8210.

Klein, R. (2009). Bidirectional modulation of synaptic functions by Eph/ephrin signaling. *Nat Neuroscience*, *12*(1), 15-20.

Knight, D., Xie, W., & Boulianne, G. L. (2011). Neurexins and Neuroligins: Recent Insights from Invertebrates. *Molecular neurobiology*, 426-440.

Kumar, J., Schuck, P., & Mayer, M. L. (2011). Structure and assembly mechanism for heteromeric kainate receptors. *Neuron*, *71*(2), 319-31.

Köhr, G. (2006). NMDA receptor function: subunit composition versus spatial distribution. *Cell and tissue research*, *326*(2), 439-46.

Landgraf, M., Bossing, T., Technau, G. M., & Bate, M. (1997). The origin, location, and projections of the embryonic abdominal motorneurons of Drosophila. *J Neurosci*, *17*(24), 9642-55.

Lenfant, N., Polanowska, J., Bamps, S., Omi, S., Borg, J.-P., & Reboul, J. (2010). A genome-wide study of PDZ-domain interactions in C. elegans reveals a high frequency of non-canonical binding. *BMC genomics*, *11*(1), 671.

Li, J., Ashley, J., Budnik, V., & Bhat, M. a. (2007). Crucial role of Drosophila neurexin in proper active zone apposition to postsynaptic densities, synaptic growth, and synaptic transmission. *Neuron*, *55*(5), 741-55.

Li, P., Kerchner, G. a, Sala, C., Wei, F., Huettner, J. E., Sheng, M., & Zhuo, M. (1999). AMPA receptor-PDZ interactions in facilitation of spinal sensory synapses. *Nat Neuroscience*, *2*(11), 972-7.

Lisman, J. E., & McIntyre, C. C. (2001). Synaptic plasticity: a molecular memory switch. *Current biology : CB*, *11*(19), R788-91.

Long, J. (2003). Supramodular structure and synergistic target binding of the N-terminal tandem PDZ domains of PSD-95. *Journal of Molecular Biology*, *327*(1), 203-214.

Madden, D. R. (2002). THE STRUCTURE AND FUNCTION OF GLUTAMATE RECEPTOR ION CHANNELS. *Neuroscience*, *3*(February).

Malinow, R., & Malenka, R. C. (2002). AMPA receptor trafficking and synaptic plasticity. *Annual review of neuroscience*, *25*, 103-26.

Marrus, S. B., Diantonio, A., & Louis, S. (2004). Preferential Localization of Glutamate Receptors Opposite Sites of High Presynaptic Release. *Current*, *14*, 924-931.

Mayer, M. L., Olson, R., & Gouaux, E. (2001). Mechanisms for ligand binding to GluR0 ion channels: crystal structures of the glutamate and serine complexes and a closed apo state. *Journal of Molecular Biology*, *311*(4), 815-836.

Milstein, A. D., & Nicoll, R. A. (2009). TARP modulation of synaptic AMPA receptor trafficking and gating depends on multiple intracellular domains, *106*(27).

Missler, M., Zhang, W., Rohlmann, A., Kattenstroth, G., Hammer, R. E., Gottmann, K., & Südhof, T. C. (2003). Alpha-neurexins couple Ca2+ channels to synaptic vesicle exocytosis. *Nature*, *423*(6943), 939-48.

Mondin, M., Labrousse, V., Hosy, E., Heine, M., Tessier, B., Levet, F., Poujol, C., et al. (2011). Neurexin-Neuroligin Adhesions Capture Surface-Diffusing AMPA Receptors through PSD-95 Scaffolds. *Journal of Neuroscience*, *31*(38), 13500-13515.

Monyer, H., Seeburg, P. H., & Wisden, W. (1991). Glutamate-operated channels: developmentally early and mature forms arise by alternative splicing. *Neuron*, *6*(5), 799-810.

Morimoto, T., Nobechi, M., Komatsu, a, Miyakawa, H., & Nose, a. (2010). Subunit-specific and homeostatic regulation of glutamate receptor localization by CaMKII in Drosophila neuromuscular junctions. *Neuroscience*, *165*(4), 1284-92. IBRO.

Morimoto-tomita, M., Zhang, W., Straub, C., Cho, C.-hoon, Kim, K. S., & Howe, J. R. (2009). Article Autoinactivation of Neuronal AMPA Receptors via Glutamate-Regulated TARP Interaction. *Neuron*, *61*(1), 101-112.

Mosbacher, J., Schoepfer, R., Monyer, H., Burnashev, N., Seeburg, P. H., & Ruppersberg, J. P. (1994). A molecular determinant for submillisecond desensitization in glutamate receptors. *Science*, *266*(5187), 1059-62.

Nakagawa, T. (2010). The biochemistry, ultrastructure, and subunit assembly mechanism of AMPA receptors. *Molecular neurobiology*, *42*(3), 161-84.

Ng, D., Pitcher, G. M., Szilard, R. K., Sertié, A., Kanisek, M., Clapcote, S. J., Lipina, T., et al. (2009). Neto1 is a novel CUB-domain NMDA receptor-interacting protein required for synaptic plasticity and learning. *PLoS biology*, *7*(2), e41.

Nicoll, R. a, Tomita, S., & Bredt, D. S. (2006). Auxiliary subunits assist AMPA-type glutamate receptors. *Science*, *311*(5765), 1253-6.

Nienhaus, G. U., Nienhaus, K., Hölzle, A., Ivanchenko, S., Renzi, F., Oswald, F., Wolff, M., et al. (2006). Photoconvertible fluorescent protein EosFP: biophysical properties and cell biology applications. *Photochemistry and photobiology*, *82*(2), 351-8.

Okabe, S. (2007). Molecular anatomy of the postsynaptic density. *Molecular and cellular neurosciences*, *34*(4), 503-18.

Opazo, P., Labrecque, S., Tigaret, C. M., Frouin, A., Wiseman, P. W., De Koninck, P., & Choquet, D. (2010). CaMKII triggers the diffusional trapping of surface AMPARs through phosphorylation of stargazin. *Neuron*, *67*(2), 239-52. Elsevier Ltd.

Opazo, P., Sainlos, M., & Choquet, D. (2011). Regulation of AMPA receptor surface diffusion by PSD-95 slots. *Current opinion in neurobiology*. *22*(1), 1-8.

Owald, D., Fouquet, W., Schmidt, M., Wichmann, C., Mertel, S., Depner, H., Christiansen, F., et al. (2010). A Syd-1 homologue regulates pre- and postsynaptic maturation in Drosophila. *The Journal of cell biology*, *188*(4), 565-79.

Owald, D., & Sigrist, S. J. (2009). Assembling the presynaptic active zone. *Current opinion in neurobiology*, *19*(3), 311-8.

Patel, M. R., Lehrman, E. K., Poon, V. Y., Crump, J. G., Zhen, M., Bargmann, C. I., & Shen, K. (2006). Hierarchical assembly of presynaptic components in defined C. elegans synapses. *Nat Neuroscience*, *9*(12), 1488-98.

Pawlu, C., DiAntonio, A., & Heckmann, M. (2004). Postfusional control of quantal current shape. *Neuron*, *42*(4), 607-18.

Peled, E. S., & Isacoff, E. Y. (2011). Optical quantal analysis of synaptic transmission in wild-type and rab3-mutant Drosophila motor axons. *Nat Neuroscience*, *14*(4), 519-526.

Peters, A., Palay, S. L., & Webster, H. D. (1991). The Fine Structure of the Nervous System. *3rd ed New York Oxford University Press 1991*.

Petersen, S. a, Fetter, R. D., Noordermeer, J. N., Goodman, C. S., & DiAntonio, a. (1997). Genetic analysis of glutamate receptors in Drosophila reveals a retrograde signal regulating presynaptic transmitter release. *Neuron*, *19*(6), 1237-48.

Prakash, S., McLendon, H. M., Dubreuil, C. I., Ghose, A., Hwa, J., Dennehy, K. a, Tomalty, K. M. H., et al. (2009). Complex interactions amongst N-cadherin, DLAR, and Liprin-alpha regulate Drosophila photoreceptor axon targeting. *Developmental biology*, *336*(1), 10-9.

Pumplin, D. W., Reese, T. S., & Llinás, R. (1981). Are the presynaptic membrane particles the calcium channels? *Proceedings of the National Academy of Sciences of the United States of America*, *78*(11), 7210-3.

Qin, G., Schwarz, T., Kittel, R. J., Schmid, A., Rasse, T. M., Kappei, D., Ponimaskin, E., et al. (2005). Four different subunits are essential for expressing the synaptic glutamate receptor at neuromuscular junctions of Drosophila. *J Neurosci*, *25*(12), 3209-18.

Rasse, T. M., Fouquet, W., Schmid, A., Kittel, R. J., Mertel, S., Sigrist, C. B., Schmidt, M., et al. (2005). Glutamate receptor dynamics organizing synapse formation in vivo. *Nat Neuroscience*, *8*(7), 898-905.

Reiff, D. F., Thiel, P. R., & Schuster, C. M. (2002). Differential regulation of active zone density during long-term strengthening of Drosophila neuromuscular junctions. *J Neurosci*, *22*(21), 9399-409.

Reissner, C., Klose, M., Fairless, R., & Missler, M. (2008). Mutational analysis of the neurexin/neuroligin complex reveals essential and regulatory components. *Proceedings of the National Academy of Sciences of the United States of America*, *105*(39), 15124-9.

Rizzoli, S. O., & Jahn, R. (2007). Kiss-and-run, collapse and "readily retrievable" vesicles. *Traffic*, *8*(9), 1137-44.

Robert, A., Armstrong, N., Gouaux, J. E., & Howe, J. R. (2005). AMPA Receptor Binding Cleft Mutations That Alter Affinity , Efficacy , and Recovery from Desensitization. *J Neuroscience*, *25*(15), 3752-3762.

Rodesch, C. K., & Broadie, K. (2000). Genetic studies in Drosophila: vesicle pools and cytoskeleton-based regulation of synaptic transmission. *NeuroReport*, *11*(18), R45-R53.

Rouach, N., Byrd, K., Petralia, R. S., Elias, G. M., Adesnik, H., Tomita, S., Karimzadegan, S., et al. (2005). TARP γ-8 controls hippocampal AMPA receptor number, distribution and synaptic plasticity. *Nat Neuroscience*, *8*(11), 1525-1533.

Scheiffele, P., Fan, J., Choih, J., Fetter, R., & Serafini, T. (2000). Neuroligin expressed in nonneuronal cells triggers presynaptic development in contacting axons. *Cell*, *101*(6), 657-69.

Schmid, A., Hallermann, S., Kittel, R. J., Khorramshahi, O., Frölich, A. M. J., Quentin, C., Rasse, T. M., et al. (2008). Activity-dependent site-specific changes of glutamate receptor composition in vivo. *Nat Neuroscience*, *11*(6), 659-66. Nature Publishing Group.

Schnell, E., Sizemore, M., Karimzadegan, S., Chen, L., Bredt, D. S., & Nicoll, R. a. (2002). Direct interactions between PSD-95 and stargazin control synaptic AMPA receptor number. *Proceedings of the National Academy of Sciences of the United States of America*, *99*(21), 13902-7.

Schoch, S., & Gundelfinger, E. D. (2006). Molecular organization of the presynaptic active zone. *Cell and tissue research*, *326*(2), 379-91.

Schwenk, J., Harmel, N., Zolles, G., Bildl, W., Kulik, A., Heimrich, B., Chisak, O., et al. (2009). Science, (March), 1313-1319.

Sheng, M., & Hoogenraad, C. C. (2007). The postsynaptic architecture of excitatory synapses: a more quantitative view. *Annual review of biochemistry*, *76*, 823-47.

Shi, Y., Lu, W., Milstein, A. D., & Nicoll, R. A. (2009). The stoichiometry of AMPA receptors and TARPs varies by neuronal cell type. *Neuron*, *62*(5), 633-640.

Sigrist, S. J., & Schmitz, D. (2011). Structural and functional plasticity of the cytoplasmic active zone. *Current opinion in neurobiology*, *21*(1), 144-50.

Sigrist, S. J., Thiel, P. R., Reiff, D. F., & Schuster, C. M. (2002). The postsynaptic glutamate receptor subunit DGluR-IIA mediates long-term plasticity in Drosophila. *J Neurosci*, *22*(17), 7362-72.

Sommer, B., Keinänen, K., Verdoorn, T. a, Wisden, W., Burnashev, N., Herb, a, Köhler, M., et al. (1990). Flip and flop: a cell-specific functional switch in glutamate-operated channels of the CNS. *Science*, *249*(4976), 1580-5.

Song, J. Y., Ichtchenko, K., Südhof, T. C., & Brose, N. (1999). Neuroligin 1 is a postsynaptic cell-adhesion molecule of excitatory synapses. *Proceedings of the National Academy of Sciences of the United States of America*, *96*(3), 1100-5.

Soto, D., Coombs, I. D., Renzi, M., Zonouzi, M., Farrant, M., & Cull-Candy, S. G. (2009). Selective regulation of long-form calcium-permeable AMPA receptors by an atypical TARP, gamma-5. *Nat Neuroscience*, *12*(3), 277-85.

Spangler, S. a, & Hoogenraad, C. C. (2007). Liprin-alpha proteins: scaffold molecules for synapse maturation. *Biochemical Society transactions*, *35*(Pt 5), 1278-82.

Stern-Bach, Y., Russo, S., Neuman, M., & Rosenmund, C. (1998). A point mutation in the glutamate binding site blocks desensitization of AMPA receptors. *Neuron*, *21*(4), 907-18.

Sudhof, T. C. (2004). The synaptic vesicle cycle. *Annual review of neuroscience*, *27*, 509-47.

Sun, Y., Olson, R., Horning, M., Armstrong, N., Mayer, M., & Gouaux, E. (2002). Mechanism of glutamate receptor desensitization. *Nature communications*, *2*(6886), 245-253.

Sweeney, S. T., Broadie, K., Keane, J., Niemann, H., & O'Kane, C. J. (1995). Targeted expression of tetanus toxin light chain in Drosophila specifically eliminates synaptic transmission and causes behavioral defects. *Neuron*, *14*(2), 341-51.

Südhof, T. C. (2008). Neuroligins and neurexins link synaptic function to cognitive disease. *Nature*, *455*(7215), 903-11.

Takamori, S., Holt, M., Stenius, K., Lemke, E. a, Grønborg, M., Riedel, D., Urlaub, H., et al. (2006). Molecular anatomy of a trafficking organelle. *Cell*, *127*(4), 831-46.

Thompson, V. (1977). Recombination and response, 125-140.

Thorpe, H. M., & Smith, M. C. M. (1998). In vitro site-specific integration of bacteriophage DNA catalyzed by a recombinase of the resolvase/invertase family. *Proceedings of the National Academy of Sciences of the United States of America*, *95*(10), 5505-5510.

Tomita, S., Chen, L., Kawasaki, Y., Petralia, R. S., Wenthold, R. J., Nicoll, R. a, & Bredt, D. S. (2003). Functional studies and distribution define a family of transmembrane AMPA receptor regulatory proteins. *The Journal of cell biology*, *161*(4), 805-16.

Tomita, S., Fukata, M., Nicoll, R. A., & Bredt, D. S. (2004). Dynamic interaction of stargazin-like TARPs with cycling AMPA receptors at synapses. *Science*, *303*(5663), 1508-1511.

Tomita, S., Shenoy, A., Fukata, Y., Nicoll, R. a, & Bredt, D. S. (2007). Stargazin interacts functionally with the AMPA receptor glutamate-binding module. *Neuropharmacology*, *52*(1), 87-91.

Tomita, S., Stein, V., Stocker, T. J., Nicoll, R. a, & Bredt, D. S. (2005). Bidirectional synaptic plasticity regulated by phosphorylation of stargazin-like TARPs. *Neuron*, *45*(2), 269-77.

Triller, A., & Choquet, D. (2005). Surface trafficking of receptors between synaptic and extrasynaptic membranes: and yet they do move! *Trends in neurosciences*, *28*(3), 133-9.

Varoqueaux, F., Aramuni, G., Rawson, R. L., Mohrmann, R., Missler, M., Gottmann, K., Zhang, W., et al. (2006). Neuroligins determine synapse maturation and function. *Neuron*, *51*(6), 741-54.

Vinade, L., Chang, M., Schlief, M. L., Petersen, J. D., Reese, T. S., Tao-Cheng, J.-H., & Dosemeci, A. (2003). Affinity purification of PSD-95-containing postsynaptic complexes. *Journal of Neurochemistry*, *87*(5), 1255-1261.

Wagh, D. a, Rasse, T. M., Asan, E., Hofbauer, A., Schwenkert, I., Dürrbeck, H., Buchner, S., et al. (2006). Bruchpilot, a protein with homology to ELKS/CAST, is required for structural integrity and function of synaptic active zones in Drosophila. *Neuron*, *49*(6), 833-44.

Walikonis, R. S., Jensen, O. N., Mann, M., Provance, D. W., Mercer, J. a, & Kennedy, M. B. (2000). Identification of proteins in the postsynaptic density fraction by mass spectrometry. *J Neurosci* , *20*(11), 4069-80.

Wang, X., Hu, B., Zieba, A., Neumann, N. G., Kasper-Sonnenberg, M., Honsbein, A., Hultqvist, G., et al. (2009). A protein interaction node at the neurotransmitter release site: domains of Aczonin/Piccolo, Bassoon, CAST, and rim converge on the N-terminal domain of Munc13-1. *J Neurosci*, *29*(40), 12584-96.

Wittenmayer, N., Körber, C., Liu, H., Kremer, T., Varoqueaux, F., Chapman, E. R., Brose, N., et al. (2009). Postsynaptic Neuroligin1 regulates presynaptic maturation. *Proceedings of the National Academy of Sciences of the United States of America*, *106*(32), 13564-9.

Yelshansky, M. V., Sobolevsky, A. I., Jatzke, C., & Wollmuth, L. P. (2004). Block of AMPA receptor desensitization by a point mutation outside the ligand-binding domain. *J Neurosci*, *24*(20), 4728-36.

Zhai, R. G., & Bellen, H. J. (2004). The architecture of the active zone in the presynaptic nerve terminal. *Physiology (Bethesda, Md.)*, *19*(5), 262-70. American Physiological Society.

Zhang, M., & Wang, W. (2003). Organization of Signaling Complexes by PDZ-Domain Scaffold Proteins, *36*(7), 530-538.

Zhang, W., St-Gelais, F., Grabner, C. P., Trinidad, J. C., Sumioka, A., Morimoto-Tomita, M., Kim, K. S., et al. (2009). A transmembrane accessory subunit that modulates kainate-type glutamate receptors. *Neuron*, *61*(3), 385-96.

Zheng, Y., Mellem, J. E., Brockie, P. J., Madsen, D. M., & Maricq, A. V. (2004). SOL-1 is a CUB-domain protein required for GLR-1 glutamate receptor function in C . elegans, *1*, 451-457.

Zito, K., Parnas, D., Fetter, R. D., Isacoff, E. Y., Goodman, C. S., & Hughes, H. (1999). Watching a Synapse Grow : Noninvasive Confocal Imaging of Synaptic Growth in Drosophila,Neuron, *22*, 719-729.

Ziv, N. E., & Garner, C. C. (2001). Principles of glutamatergic synapse formation : seeing the forest for the trees. *Current Opinion in Neurobiology*, 536-543.

von Engelhardt, J., Mack, V., Sprengel, R., Kavenstock, N., Li, K. W., Stern-Bach, Y., Smit, A. B., et al. (2010). CKAMP44: a brain-specific protein attenuating short-term synaptic plasticity in the dentate gyrus. *Science*, *327*(5972), 1518-22.

7 Appendix

7.1 Summary

Chemical synapses are cell-cell contacts, which play a central role in neuronal communication. These cell-cell contacts rely on a precise alignment of pre- and postsynaptic domains. The formation and maturation of synapses requires therefore bidirectional communication across the synaptic cleft. Recent *in vitro* studies suggest that the transsynaptic Neurexin-Neuroligin (Nrx-Nlg) complex is a key component in this process. The data presented in this work derive from studies that aimed at untangling the function of the Nrx-Nlg complex at the *Drosophila* neuromuscular junction (NMJ).

In a genetic screen several mutant alleles of *Drosophila neuroligin 1* (*dnlg1*) were recovered causing severe assembly defects at NMJs. *In situ* hybridization experiments showed that DNlg1 is exclusively expressed in muscle fibres, and subsequent immunohistological labeling revealed that DNlg1 forms discrete clusters adjacent to postsynaptic densities (PSDs). Formation of these clusters depends on presynaptic *Drosophila* Neurexin (DNrx). A second study showed that sufficient localization of DNlg1 depends further on *Drosophila* synapse defective 1 (DSyd-1), as DSyd-1 interacts with DNrx to control synapse formation at the NMJ. Mutants of *dsyd-1, dnrx,* and *dnlg1* share active zone-cytomatrix defects, which behave non-additive in double mutant combinations. DSyd-1 and DNrx form a complex *in vivo*, and the PDZ domain-binding motif of DSyd-1 is important for synaptic clustering and immobilization of DNrx. Consequently, glutamate receptor (GluR) incorporation into newly forming PSDs is altered in *dsyd-1*, *dnrx,* and *dnlg1* mutants. Thus, cooperation between DSyd-1 and DNrx-DNlg1 seems to orchestrate early assembly processes between pre- and postsynaptic membranes, promoting seed-points for newly forming synaptic scaffolds. Finally, a novel mechanism for regulating synaptic GluR clustering is discussed. Unpublished results from a mutated GluR show that altered bio-physical properties of GluRs result in increased mobility and changes in the distinct localization pattern at PSDs. These findings could shed new light on mechanisms which regulate GluR trafficking depending on their physiological properties.

7.2 Zusammenfassung

Chemische Synapsen sind Zell-Zell-Kontakte, welche eine zentrale Rolles in neuronalen Netzen spielen. Diese Zell-Zell Kontakte sind auf eine präzise Anordnung von prä- und postsynaptischen Strukturen angewiesen sind. Daher ist für die Entstehung und Entwicklung von Synapsen eine bidirektionale Kommunikation über den synaptischen Spalt unerlässlich. Frühere *in vitro* Experimente ließen vermuten, dass der trans-synaptische Neurexin-Neuroligin (Nrx-Nlg) Komplex eine zentrale Rolle bei diesem Prozess spielt. Die hier präsentierte Arbeit befasst sich mit der Funktion des Nrx-Nlg Komplexes an der neuromuskulären *junction* (NMJs) von *Drosophila melanogaster*.

Bei einem genetischen Screen wurden mehrere Fliegen mit Mutationen im *Drosophila* neuroligin 1 (*dnlg1*) Gen gefunden, welche starke Assemblierungsdefekte an den NMJs aufwiesen. In anschließenden *In-situ*-Hybridisierungs- und immunohistochemischen Markierungsexperimenten konnte gezeigt werden,dass DNlg1 ausschließlich in Muskelzellen exprimiert wird und in der Nähe von postsynaptic densities (PSDs) clustert. Zur Bildung dieser Cluster benötigt es die Präsenz von präsynaptischem Drosophila Neurexin (DNrx). In einer weiteren Studie stellte sich heraus, dass Drosophila synapse defective 1 (DSyd-1) ebenfalls einen Einfluss auf die Lokalisierung von DNlg1 hat. Darüber hinaus zeigten weitere Experimente, dass DSyd-1 über die Interaktion mit DNrx die Bildung von Synapsen an der NMJ kontrollieren kann: Einzelmutanten für *dsyd-1, dnrx* und *dnlg1* weisen Defekte in der Morphologie ihrer Aktiven Zonen-Cytomatrix auf, welche sich in den Doppelmutanten nicht verstärkten. DSyd-1 und DNrx bilden einen Komplex *in vivo*, wobei das PDZ-Bindungsmotiv von DSyd-1 eine wichtige Rolle für das synaptische Clustern von DNrx spielt. Desweiteren ist die postsynaptische Anreicherung von Glutamatrezeptoren (GluRs) an neu entstandenen PSDs in *dsyd-1, dnrx* und *dnlg1* Mutanten stark verändert. Somit kann geschlußfolgert werden, dass das Zusammenspiel von DSyd-1 mit dem DNrx-DNlg1 Komplex die frühen Anlagerungsprozesse an der prä- und postsynaptischen Membran dirigiert und hierdurch die Neuentstehung des synaptischen Gerüsts unterstützt. Der letzte Abschnitt dieser Arbeit befasst sich mit einem bisher unbekannten Mechanismus, der das Clustern von GluRs an Synapsen reguliert. Untersucht wurde ein mutierter GluR, der veränderte bio-physikalischen Eigenschaften aufweist, welche sich auf seine synaptische Mobilität und Lokalisierung auswirken. Diese Befunde könnten zu neuen Hypothesen führen, die erklären, warum GluRs mit unterschiedlichen physiologischen Eigenschaften sich in Ihrem synaptischen *targeting* unterscheiden.

7.3 Curriculum vitae

For reasons of data protection,
the curriculum vitae is not included in the online version

7.4 Publications

Undergraduate studies:

Omid Khorramshahi, J. Marcus Schartau, Ronald H.H. Kröger (2008). A complex system of ligaments and a muscle keep the crystalline lens in place in the eyes of bony fishes (teleosts). Vision Research 48, 1503–1508

Diploma:

Schmid A, Hallermann A, Kittel RJ, Khorramshahi O, Frölich A, Quentin C, Rasse TM, Mertel S, Heckmann M & Sigrist SJ (2008). Activity-dependent site-specific changes of glutamate receptor composition *in vivo.* Nature Neuroscience 11, 659 - 666

PhD work:

Banovic D*, Khorramshahi O*, Owald D, Wichmann C, Riedt T, Fouquet W, Tian R, Sigrist SJ, Aberle H. (2010). Drosophila neuroligin 1 promotes growth and postsynaptic differentiation at glutamatergic neuromuscular junctions. Neuron. 66, 724-38.
**equal contribution*

Owald D*, Khorramshahi O*, Gupta VK*, Banovic D, Depner H, Fouquet W, Wichmann C, Mertel S, Eimer S, Reynolds E, Holt M, Aberle H, Sigrist SJ (2012). Cooperation of Syd-1 with Neurexin synchronizes pre- with postsynaptic assembly. Nature Neuroscience. *accepted*
**equal contribution*

7.5 Acknowledgements

First of all I would like to thank my instructor Prof. Dr. Stephan Sigrist for his friendly support and scientific guidance. I am also grateful to Prof. Hermann Aberle for his valuable and welcome support and to Dr. Andrew Plastid for his critical comments on the manuscript. Furthermore, I thank Dr. David Owald for lively discussions and successfull collaborations, Dr. Daniel Banovic for being such a great collaborateur, and Dr. Andreas Schmid for his kind introduction to *Drosophila*, imaging, and his GluR constructs.

Dear Dr. Astrid Petzold, thank you very much for proofreading and Schockolade.

Thanks to all current and former members of the Sigrist lab who supported and entertained me throughout my lab time. I am honoured to have been part of this excellent research group!

Special thanks to:

Matthias Siebert (‘*Matze*’), Harald Depner (‘*Halli*’), Till Andlauer (‘*Boy*’), Elena Knoche, Dr. Wernher Fouquet, Frauke Cristiansen-Engelhardt, Peter Engerer, Sara Mertel, Christina Zube, Franziska Zehe, Christine Quentin, Anastasia Stawrakakis, Dr. Carolin Wichmann, Madeleine Brünner, Dr. Tobias Schwarz, Karen Liu, Rui Tian, Tanja Matkovic, Karzan Muhamad, Varun Gupta, Dr. Suneel Reddy, and of course Christoph, Husam, Stefanie, Heidi, Marta.

I am greatly indebted to my family, who endowed me with loving (and spiritual) support throughout my whole university education and the rest of my life.

Last but not least, I truly thank my girlfriend Julia for her great support and endless patience and my son Carlo for being my greatest source of joy.

7.6 Selbstständigkeitserklärung

Hiermit erkläre ich, dass ich diese Arbeit selbst verfasst habe sowie keine anderen als die angegebenen Quellen und Hilfsmittel in Anspruch genommen habe. Ich versichere, dass diese Arbeit in dieser oder anderer Form keiner anderen Prüfungsbehörde vorgelegt wurde.

Omid Florian Khorramshahi Berlin, Juli 2012